

WIND-INDUCED EFFECTS ON HIGH-RISE BUILDINGS WITH VARIED CROSS-SECTIONAL SHAPES

A DISSERTATION

SUBMITTED IN PARTIAL FULFILLMENT OF THE REQUIREMENTS

FOR THE AWARD OF THE DEGREE

OF

MASTER OF TECHNOLOGY

IN

STRUCTURAL ENGINEERING

Submitted by:

PAWAN PRAKASH

(2K21/STE/16)

Under the supervision of

DR. RITU RAJ



DEPARTMENT OF CIVIL ENGINEERING

DELHI TECHNOLOGICAL UNIVERSITY

(Formerly Delhi college of Engineering)

Bawana Road, Delhi-110042

MAY, 2023

DELHI TECHNOLOGICAL UNIVERSITY

(Formerly Delhi college of Engineering)

Bawana Road, Delhi-110042

CANDIDATE'S DECLARATION

I, Pawan Prakash, 2K21/STE/16, student of M.Tech Structural Engineering, hereby declare that the project Dissertation titled “WIND-INDUCED EFFECTS ON HIGH-RISE BUILDINGS WITH VARIED CROSS-SECTIONAL SHAPES” which is submitted by me to the Department of Civil Engineering, Delhi Technological University, Delhi in partial fulfillment of the requirement for the award of the degree of Master of Technology, is original and not copied from any source without proper citation . This work has not previously formed the basis for the award of any Degree, Diploma Associateship, Fellowship or other similar title or recognition.



Place: Delhi

PAWAN PRAKASH

Date:

DEPARTMENT OF CIVIL ENGINEERING
DELHI TECHNOLOGICAL UNIVERSITY

(Formerly Delhi college of Engineering)

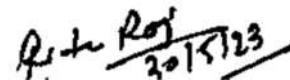
Bawana Road, Delhi-110042

CERTIFICATE

I hereby certify that the Project Dissertation titled “WIND-INDUCED EFFECTS ON HIGH-RISE BUILDINGS WITH VARIED CROSS-SECTIONAL SHAPES” which is submitted by Pawan Prakash, 2K21/STE/16 Department of Civil Engineering, Delhi Technological University, Delhi in partial fulfillment of the requirement for the award of the degree of Master of Technology, is a record of the project work carried out by the students under my supervision. To the best of my knowledge this work has not been submitted in part or full for any Degree or Diploma to this University or elsewhere.

Place: Delhi

Date:

Handwritten signature of Dr. Ritu Raj, dated 20/5/23.

Dr. RITU RAJ
Assistant Professor
Department of Civil Engineering
Delhi Technological University

ABSTRACT

High-rise structures are susceptible to dynamic wind effects, which can significantly impact their safety and serviceability. Predicting wind loads on tall buildings is a complex problem that involves numerous variables, such as wind speed, direction, turbulence, and the building's shape, size, and orientation. Additionally, interference effects between adjacent buildings can further complicate the problem. While some research efforts have been made to address this issue, there is still a lack of data available in international standards for predicting wind loads on complex building shapes and interference situations.

This study focuses on the analysis of wind effects and interference on an asymmetrical building with varying dimensions but the same height and width of 60m. Using computational fluid dynamics (CFD) simulations in ANSYS CFX 2022 R2 and AutoCAD, we compute the wind effects for wind incidence angles ranging from 0 to 180 degrees with a 15-degree interval, using a mesh size of 0.005mm and 100 iterations. The Power Law equation is used to determine the wind speed profile within the atmospheric boundary layer. The pressure contours on the building's surface are analyzed to determine the pressure distribution, and we observe that the shape and size of the face are independent of the pressure distribution.

We compare graphs of drag force, drag moment, lift force, and lift moment to identify critical faces for different wind incidence angles.

The present study establishes blockage by placing twin-building models in various orientations at a distance of 10% of the model's height, i.e., 60 mm. The study provides valuable insights into dynamic wind effects and can inform the design of safe and efficient high-rise structures. This research project is crucial in helping architects and engineers better understand the dynamic wind effects on high-rise structures, which is an essential factor in designing safe and sustainable buildings.

This study contributes to the field of wind engineering by providing a comprehensive analysis of the along-wind effects and interference on high-rise structures. The results can be used to improve the design of tall buildings, ensuring their safety and serviceability in the face of dynamic wind effects.

ACKNOWLEDGEMENT

I would like to express my sincere appreciation and gratitude to everyone who has contributed to the successful completion of this project. Although it may not be possible to name everyone who has helped me along the way, I would like to recognize some individuals for their exceptional support and guidance.

First and foremost, I would like to express my sincere gratitude to my project supervisor, Dr. Ritu Raj, for their unwavering support and guidance throughout my project. Their expertise, feedback, and insightful comments have been invaluable in shaping the direction and scope of this study. I am grateful for their patience, dedication, and mentorship throughout my research journey.

I would also like to acknowledge and thank my Ph.D. guide, Mr. Deepak Sharma, for their invaluable contributions to this project. Their extensive knowledge, insights, and guidance have been critical in developing my research skills and advancing my academic pursuits.

Furthermore, I would like to extend my gratitude to the faculty and staff of the department for providing me with access to necessary resources and facilities. I am thankful for their support and encouragement.

Finally, I would like to express my heartfelt appreciation to my family, friends, and colleagues for their constant encouragement and motivation. Their unwavering support has been instrumental in helping me achieve my academic goals.

I am grateful to everyone who has contributed to the successful completion of this project. I am humbled and honored by their support and guidance, and I will cherish these experiences for a lifetime.

Pawan Prakash
(2K21/STE/16)

TABLE OF CONTENTS

CANDIADTE’S DECLARATION.....	ii
CERTIFICATE.....	iii
ABSTRACT.....	iv
ACKNOWLEDGEMENT.....	v
TABLE OF CONTENTS.....	vi
LIST OF TABLES.....	ix
LIST OF FIGURES.....	xii
CHAPTER 1 - INTRODUCTION	xiii
1.1 BACKGROUND AND MOTIVATION	3
1.2 CHALLENGES AND PROPOSED METHODOLOGY	4
1.3 OBJECTIVES AND RESEARCH QUESTIONS	5
1.4 SCOPE AND LIMITATIONS.....	7
1.5 CONTRIBUTION OF THE THESIS	7
CHAPTER 2 - LITERATURE REVIEW	9
2.1 EXPERIMENTAL INVESTIGATIONS.....	9
2.2 STUDY ON HIGH-RISE BUILDINGS OF ASYMMETRICAL C/S.....	10
2.3 WIND EFFECTS ON BUILDINGS HAVING VARYING C/S SHAPE.....	11
2.4 TURBULENCE MODEL	12
CHAPTER 3 - METHODOLOGY	14
3.1 NUMERICAL METHODS FOR WIND LOAD ANALYSIS	14
3.2 GEOMETRY.....	15
3.3 MESHING.....	15
3.4 SETUP.....	18
3.5 BOUNDARY CONDITION.....	19
3.6 LINE CO-ORDINATES	20
3.7 SOLUTION.....	21
3.8 RESULT.....	21

CHAPTER 4 - ISOLATED BUILDING SIMULATION	21
4.1 WIND-INDUCED RESPONSES OF ISOLATED BUILDING	22
4.2 RESULTS & VALIDATION FOR ISOLATED MODEL.....	22
4.3 PRESSURE COEFFICIENT CALCULATION.....	23
4.4 PRESSURE CONTOURS	24
4.5 VALIDATION OF CFD RESULTS WITH INTERNATIONAL CODES.....	43
4.6 VELOCITY STREAMLINES	46
4.6.1 Horizontal streamlines.....	47
4.6.2 Vertical Streamline	53
4.7 LIFT/ DRAG AND MOMENT FORCES	56
4.8 AVERAGE PRESSURE COEFFICIENT (C_p).....	63
CHAPTER 5 - INTERFERENCE STUDY SIMULATION	68
5.1 WIND EFFECTS ON INTERFERENCE OF HIGH-RISE BUILDINGS	68
5.2 NUMERICAL MODEL DEVELOPMENT	71
CHAPTER 6 - RESULTS & DISCUSSION FOR INTEFERENCE STUDY	78
6.1 PRESSURE CONTOURS	78
6.1.1 Back to Back Interference Condition	78
6.1.2 Back to Front Interference Condition	94
6.1.3 Front to Back Interference Condition	104
6.1.4 Front to Front Interference Condition.....	112
6.2 VALIDATION WITH INTERNATIONAL CODES.....	121
6.3 INTERFERENCE FACTOR	123
6.4 VELOCITY STREAMLINES	125
6.5 HORIZONTAL STREAMLINES	125
6.5.1 Back-to-Back Interference Condition.....	125
6.5.2 Back to Front Interference Condition	127
6.5.3 Front-to-Back Interference Condition	130
6.5.4 Front-to-Front Interference Condition.....	132
6.6 VERTICAL STREAMLINE.....	134
6.6.1 Back-to-Back Interference Condition.....	134
6.6.2 Back to Front Interference Condition	137

6.6.3	Front-to-Back Interference Condition	138
6.6.4	Front-to-Front Interference Condition	139
CHAPTER 7	- RESULTS AND ANALYSIS	141
7.1	COMPARISON OF THE RESULTS FROM ISOLATED AND INTERFERENCE STUDY SIMULATION.....	141
7.2	DISCUSSION OF THE IMPLICATIONS OF THE FINDINGS ON BUILDING DESIGN	142
CHAPTER 8	- CONCLUSION AND RECOMMENDATIONS	144
8.1	RECOMMENDATIONS FOR FUTURE RESEARCH.....	144
9	REFERENCES	146

LIST OF TABLES

Table 3.1:	Co-Ordinates of the Lines on Windward side.....	20
Table 4.1:	Pressure contour of faces at 0 degree wind inclination.....	24
Table 4.2:	Pressure and Cp values for each face at wind incidence of 0 degree	25
Table 4.3:	Pressure and Cp values for each face at wind incidence of 15 degree	26
Table 4.4 :	Pressure contour of faces at 15 degree wind inclination.....	26
Table 4.5:	Pressure contour of faces at 30 degree wind inclination.....	27
Table 4.6:	Pressure and Cp values for each face at wind incidence of 30 degree	28
Table 4.7:	Pressure and Cp values for each face at wind incidence of 45 degree	29
Table 4.8:	Pressure contour of faces at 45 degree wind inclination.....	29
Table 4.9:	Pressure contour of faces at 60 degree wind inclination.....	30
Table 4.10:	Pressure and Cp values for each face at wind incidence of 60 degree	31
Table 4.11:	Pressure and Cp values for each face at wind incidence of 75 degree	32
Table 4.12:	Pressure contour of faces at 75 degree wind inclination.....	32
Table 4.13:	Pressure and Cp values for each face at wind incidence of 90 degree	33
Table 4.14:	Pressure contour of faces at 90 degree wind inclination.....	34
Table 4.15:	Pressure contour of faces at 105 degree wind inclination.....	34
Table 4.16:	Pressure and Cp values for each face at wind incidence of 105 degree	35
Table 4.17:	Pressure and Cp values for each face at wind incidence of 120 degree	36
Table 4.18:	Pressure and Cp values for each face at wind incidence of 120 degree	36
Table 4.19:	Pressure and Cp values for each face at wind incidence of 135 degree	37
Table 4.20:	Pressure and Cp values for each face at wind incidence of 135 degree	38
Table 4.21:	Pressure and Cp values for each face at wind incidence of 150 degree	39
Table 4.22:	Pressure and Cp values for each face at wind incidence of 150 degree	39
Table 4.23:	Pressure and Cp values for each face at wind incidence of 165 degree	40
Table 4.24:	Pressure and Cp values for each face at wind incidence of 165 degree	41
Table 4.25:	Pressure and Cp values for each face at wind incidence of 180 degree	41
Table 4.26:	Pressure and Cp values for each face at wind incidence of 180 degree	42
Table 4.27:	Pressure contours for Square model	43
Table 4.28:	Comparison of (Cp) on the Square plan shape tall building.....	44
Table 4.29:	Comparing Cp values in accordance with IS: 875 (Part III) – 2015.....	46
Table 4.30:	Horizontal velocity streamlines for Wind incidence angle 0 to 180.....	47
Table 4.31:	Vertical velocity streamlines for Wind incidence angle 0 to 120.....	53
Table 4.32:	Vertical velocity streamlines for Wind incidence angle 135 to 180.....	55
Table 4.33:	Lift/ Drag and Moment Force calculation	58
Table 4.34:	Projected/Reference area at each wind incidence angle	61

Table 4.35:	Average Cp for wind angle 0 to 180.....	67
Table 6.1:	Pressure contour at 0 degree wind inclination for Model A and B.....	79
Table 6.2:	Average Cp value for wind inclination 0 degree	80
Table 6.3:	Pressure contour at 30 degree wind inclination for Model A and B.....	81
Table 6.4:	Average Cp value for wind inclination 30 degree	82
Table 6.5:	Pressure contour at 60 degree wind inclination for Model A and B.....	83
Table 6.6:	Average Cp value for wind inclination 60 degree	84
Table 6.7:	Pressure contour at 90 degree wind inclination for Model A and B.....	85
Table 6.8:	Average Cp value for wind inclination 90 degree	86
Table 6.9:	Pressure contour at 120 degree wind inclination for Model A and B.....	87
Table 6.10:	Average Cp value for wind inclination 120 degree	88
Table 6.11:	Pressure contour at 150 degree wind inclination for Model A and B.....	89
Table 6.12:	Table 38: Average Cp value for wind inclination 150 degree	90
Table 6.13:	Pressure contour at 180 degree wind inclination for Model A and B.....	91
Table 6.14:	Table 38: Average Cp value for wind inclination 180 degree	92
Table 6.15:	Average Cp value for wind inclination 0 to 180 degrees.....	93
Table 6.16:	Pressure contour at 0 degree wind inclination for Model A and B.....	94
Table 6.17:	Average Cp value for wind inclination 0 degree	95
Table 6.18:	Pressure contour at 60 degree wind inclination for Model A and B.....	96
Table 6.19:	Average Cp value for wind inclination 60 degree	97
Table 6.20:	Pressure contour at 120 degree wind inclination for Model A and B.....	98
Table 6.21:	Average Cp value for wind inclination 120 degree	99
Table 6.22:	Pressure contour o at 180 degree wind inclination for Model A and B.....	100
Table 6.23:	Average Cp value for wind inclination 180 degree	101
Table 6.24:	Average Cp value for wind inclination 30, 90 and 150 degrees.....	102
Table 6.25:	Average Cp value for wind inclination 0 to 180 degrees.....	103
Table 6.26:	Pressure contour at 0 degree wind inclination for Model A and B.....	104
Table 6.27:	Average Cp value for wind inclination 0 degree	105
Table 6.28:	Pressure contour at 60 degree wind inclination for Model A and B.....	106
Table 6.29:	Average Cp value for wind inclination 90 degree	107
Table 6.30:	Pressure contour at 180 degree wind inclination for Model A and B.....	108
Table 6.31:	Average Cp value for wind inclination 180 degree	109
Table 6.32:	Average Cp value for wind inclination 30, 60, 120 and 150 degrees.....	110
Table 6.33:	Average Cp value for wind inclination 0 to 180 degrees.....	112
Table 6.34:	Pressure contour at 0 degree wind inclination for Model A and B.....	113
Table 6.35:	Average Cp value for wind inclination 0 degree	114
Table 6.36:	Pressure contour at 60 degree wind inclination for Model A and B.....	114
Table 6.37:	Average Cp value for wind inclination 90 degree	116
Table 6.38:	Pressure contour at 180 degree wind inclination for Model A and B.....	116
Table 6.39:	Average Cp value for wind inclination 180 degree	118
Table 6.40:	Average Cp value for wind inclination 30, 60, 120 and 150 degrees.....	119

Table 6.41: Average C_p value for wind inclination 0 to 180 degrees.....	121
Table 6.42: Pressure and C_p variation on the faces of Square Model	122
Table 6.43: Comparison of (C_p) on the Square plan shape tall building	123
Table 6.44: Maximum and minimum C_p at face for different interference conditions	123
Table 6.45: Interference factor for Square and Fish Shape Model	124
Table 6.46: Horizontal velocity streamlines for Back to back interference.....	126
Table 6.47: Horizontal velocity streamlines for Back to front interference	128
Table 6.48: Horizontal velocity streamlines for Front to back interference	131
Table 6.49: Horizontal velocity streamlines for Front to front interference	133
Table 6.50: Vertical velocity streamlines for Back to back interference	134
Table 6.51: Vertical velocity streamlines for Back to front interference.....	137
Table 6.52: Vertical velocity streamlines for Front to back interference	138
Table 6.53: Vertical velocity streamlines for Front to front interference	140

LIST OF FIGURES

Figure 1.1:	Flow around a body and Low-pressure region on the leeward side	4
Figure 1.2:	Vortices formation on the opposite side of a building	5
Figure 3.1:	Geometry of Fish shape model with co-ordinates	15
Figure 3.2:	Meshing of the Geometry	16
Figure 3.3:	Face sizing, Face sizing 2, Inflation and Automatic method	17
Figure 3.4:	Material properties and Solver control in setup	18
Figure 3.5:	A reproduction of the domain used by Franke (2007)	19
Figure 3.6:	Nomenclature of the Model, Windward and Leeward faces	21
Figure 4.1:	Geometry & model description	22
Figure 4.2:	Geometry of the model when the inclination is 0 degree	24
Figure 4.3:	Square Model Shape for Validation	43
Figure 4.4:	Results validation with international standards for wind angle 0 degree	45
Figure 4.5:	Results validation with international standards when for angle 90 degree	45
Figure 4.6:	Comparative CFx graph for Fish model at various wind incidence angle	58
Figure 4.7:	Comparative CFz graph for Fish model at various wind incidence angle	59
Figure 4.8:	Comparative CFr graph for Fish model at various wind incidence angle	59
Figure 4.9:	Comparative CMx graph for Fish model at various wind incidence angle	60
Figure 4.10:	Comparative CMz graph for Fish model at various wind incidence angle	60
Figure 4.11:	Comparative CMr graph for Fish model at various wind incidence angle	60
Figure 4.12:	Variation of Cp on faces at 0 to 180 degree	67
Figure 5.1:	Isolated Fish Plan Shape Model	70
Figure 5.2:	Back to Back, Back to Front, Front to Back and Front to Front	70
Figure 5.3:	Full Blockage interference condition of Square-Plan shape building model ..	71
Figure 5.4:	Back to Back interference condition	72
Figure 5.5:	Nomenclature of the Model Windward and Leeward faces	72
Figure 5.6:	Back to Front interference condition	73
Figure 5.7:	Nomenclature of the Model Windward and Leeward faces	73
Figure 5.8:	Front-to-back interference condition	74
Figure 5.9:	Nomenclature of the Model Windward and Leeward faces	74
Figure 5.10:	Front-to-front interference condition	75
Figure 5.11:	Nomenclature of the Model Windward and Leeward faces	75
Figure 5.12:	Geometry for back-to-back interference condition	76
Figure 5.13:	Meshing	76
Figure 5.14:	Setup in ANSYS 2022 R1	77
Figure 5.15:	Solver control, Material properties and Expressions as per Power Law	77
Figure 6.1:	Geometry and Pressure contour when the inclination is 0 degree	78

Figure 6.2: Graphical representation of Average Cp value	94
Figure 6.3: Graphical representation of Average Cp value	104
Figure 6.4: Graphical representation of Average Cp value	111
Figure 6.5: Graphical representation of Average Cp value	120
Figure 6.6: Square Plan Shape Model for validation and Nomenclature of the model	122
Figure 6.7: Graphical representation of the variation of Cp for Square Model.....	122

CHAPTER 1 - INTRODUCTION

Wind is a crucial element that architects and engineers must carefully consider when designing tall buildings. Despite the seemingly solid and rigid nature of skyscrapers, all tall structures are actually designed with flexibility in mind. This is primarily because the increasing height of a building introduces wind forces, commonly referred to as "wind loads," that exert significant influence on its stability and performance. Being one of the principal loads acting on above-ground, accurately determining design wind loads is important in achieving safety consistent with the construction economy. In professional practice worldwide, design wind loads for most structures are evaluated based on wind load provisions specified in standards and codes.

Today, advanced changes in building construction techniques have tended to make tall and more flexible structures for wind action, so wind loading is more significant along with other forces acting on the structure, which is considered in the design of low and flexible structures. We need to analyse the high-rise building by considering all parameters of wind, which are given as per codal provisions. As one ascends higher, the force of the wind tends to amplify significantly.

The safety and serviceability of tall buildings depend on various factors, including damping, mass, natural frequency, and structure stiffness, which can impact their response to wind loads. Therefore, it is crucial to incorporate these factors into the design process to ensure the buildings' stability and functionality in the face of wind loads. Considering wind loads and their consequences is of utmost importance as they can pose a significant threat to both the structure and human lives. This research aims to gain a comprehensive understanding of how wind affects tall buildings with different cross-sectional shapes throughout their height. Unlike previous studies that primarily focused on a single cross-sectional shape, this study investigates the impact of asymmetrical structures, resembling a fish shape.

This approach allows for a more realistic representation of real-world buildings and provides insights into the wind effects on different building parts. The wind incidence

angles considered in the study range from 0° to 180° degree at an interval of 15° . This range covers a broad spectrum of wind directions and enables evaluating the building's response to wind from different directions.

As per **(Xu Y. L., 2014) [1]** tall buildings are more susceptible to wind-induced vibrations and dynamic loads due to their height and slender shape. Wind can cause the building to sway, which can cause discomfort to occupants and potentially lead to structural damage; as mentioned by **(Farouk F. , 2016) [2]** to mitigate these effects, the cross-section of the building can be optimized to improve its wind resistance. Using advanced modelling and simulation techniques, architects and engineers can analyse different cross-section designs and determine which offers the best wind resistance and overall structural stability performance. The high wind turbulence can contribute to the variation in wind-induced loads on the building, making it difficult to accurately predict and measure these forces.

Predicting wind loads on tall buildings is complex and involves many variables, such as wind speed, direction, turbulence, and the building's shape, size, and orientation. Additionally, interference effects between adjacent buildings can further complicate the problem. While there have been some research efforts to address this issue, such as wind tunnel tests and computational fluid dynamics simulations, there is still a lack of data available in International standards such as **(IS 875 (Part 3), 2015 [3])**, **(AS/NZS: 1170.2, 2011) [4]**, **(EN 1991-1-4, 2005) [5]**, **(BS 6399 – 2, 1997) [6]** and **(GB 50009, 2001) [7]**, for predicting wind loads on complex building shapes and interference situations. This highlights the need for continued research in this area to improve the safety and comfort of occupants in tall buildings.

The presence of adjacent structures can greatly influence the wind loads encountered by a tall building. Nearby buildings can introduce alterations in wind speed, turbulence, and direction, causing variations in the pressure distribution on the monitored building. The impact of interference on wind loads is intricate and relies on various factors, including the separation between the buildings, their configurations and orientations, and the prevailing wind speed and direction. At times, the proximity of nearby buildings can amplify the wind

loads on the monitored building, while in other instances; it can result in a reduction of wind loads.

(Raj, 2020) [8] emphasized the importance of accurate wind load estimation in the design of tall buildings. They noted that underestimating wind loads could have drastic consequences, such as structural failure or damage, and could lead to safety hazards for building occupants and the public. To avoid underestimating wind loads, the authors suggested using analytical and experimental studies to evaluate realistic wind-induced conditions. This includes using advanced computational fluid dynamics simulations and wind tunnel tests to analyse the wind loads on the building under different scenarios, including the effect of interference from nearby buildings.

The findings of studies on wind-induced loads and vibrations in tall buildings can be very useful for structural designers in developing innovative solutions to meet both collapse and serviceability requirements in extreme wind conditions. For example, one such solution could be using advanced cross-sectional shapes to enhance the building's wind resistance and reduce wind-induced vibrations. The findings can also help structural designers optimize the design of tall buildings to account for interference effects from nearby buildings and to ensure that the building can withstand a wide range of wind conditions while maintaining the safety and comfort of occupants.

1.1 BACKGROUND AND MOTIVATION

Computational fluid dynamics (CFD) simulation has emerged as a powerful tool for predicting and analysing the flow of fluids around complex geometries, such as high-rise buildings, to study their response to wind loads. This technology enables researchers to analyse the effects of wind pressure on buildings and structures without relying on expensive and time-consuming physical experiments. In recent years, with the increasing demand for taller and more complex building designs, it has become imperative to analyse the effects of wind on these structures, which can cause significant damage and even collapse if not adequately designed to withstand wind loads. Thus, the motivation for this research is to utilize CFD simulation to evaluate the wind effects on high-rise structures

with utilizing diverse cross-sectional configuration to provide valuable insights into the design of buildings that are more resilient to wind loads.

1.2 CHALLENGES AND PROPOSED METHODOLOGY

The wind study of high-rise buildings using Computational Fluid Dynamics (CFD) is necessary due to various challenges in predicting the wind effects on such structures. Some of the challenges include:

- The intricate and unpredictable patterns of wind movement around tall structures, along with the fluctuations in wind attributes like direction, speed, turbulence, and atmospheric stability.
- The correlation among wind and the configuration of the structure, encompassing the form, dimensions, and alignment of the building.
- The impact of surrounding buildings and terrain on the wind streamlines around the building leads to interference and vortex shedding.
- Accurately predicting wind-induced loads and dynamic response is necessary to ensure the building's structural integrity and occupant comfort.

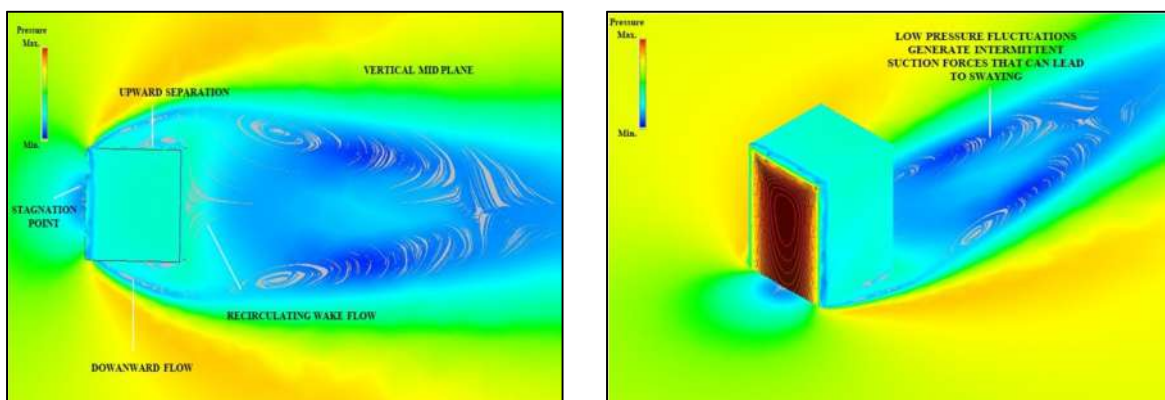


Figure 1.1: Flow around a body and Low-pressure region on the leeward side

When the wind encounters a solid structure such as a square building, it undergoes a phenomenon called flow separation at the corners, leading to the formation of vortices and a region of reduced airflow known as a wake. This flow pattern generates fluctuating pressures that result in unsteady loads (**Figure 1.1**) in both the cross-flow and wind

directions. Upon encountering solid-walled buildings, the wind flow is disrupted, creating obstructions. This disruption leads to the formation of low-pressure areas (as depicted in **Figure 1.2**) on the opposing side, generating suction forces that pull the buildings and induce swaying motion. While the initial movement may be minimal, in high wind conditions, vortices may arise, aligning with the building's inherent frequency and resulting in noticeable swaying and shaking sensations experienced by occupants inside.

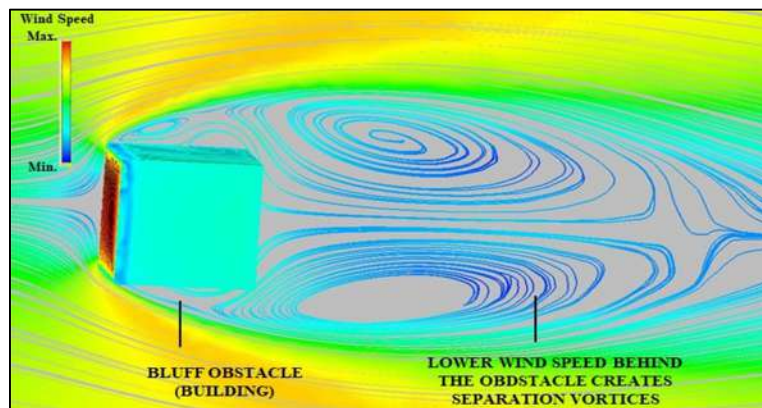


Figure 1.2: Vortices formation on the opposite side of a building

One effective and straightforward method to mitigate the influence of strong winds on tall buildings is by employing a corner-softening technique. Additionally, enhancing the porosity of the structure is another approach to minimize the effects of high winds on these buildings. This involves strategically removing sections of the building and creating spaces that allow air to circulate through and around the mass of the structure..

1.3 OBJECTIVES AND RESEARCH QUESTIONS

This project aims to investigate the wind-induced effects on high-rise buildings with varying cross-sectional shapes using CFD simulations. The primary objectives are:

- To conduct numerical investigations using ANSYS 2022 R1 software to obtain precise and accurate data on the pressure and drag coefficients for a particular building shape.
- To investigate wind effects at different angles ranging from 0° to 180° and obtain more realistic wind flow conditions through CFD simulations.

- To investigate the interference effects between adjacent buildings under 100% (full blockage) wind interference conditions and provide more accurate and reliable data that can be used in international standards.
- To assess the movement of air currents around the building using CFD and identify areas of high turbulence and interference.
- To evaluate the building's wind-induced loads and dynamic response for different cross-sectional shapes, including the impact of interference from surrounding buildings.
- To investigate the effectiveness of different mitigation strategies, such as aerodynamic modifications and passive damping systems, to reduce wind-induced vibrations and improve the building's wind resistance.
- To provide recommendations for optimizing the building's cross-section to improve its wind resistance and overall structural stability, leading to more comfortable and safer living and working environments.

These objectives represent the main goals of the research thesis and provide a clear outline of the work that will be undertaken.

Research Question: How can the winds effects on a building structure be accurately and reliably investigated using CFD simulations, and what mitigation strategies can be employed to improve the building's wind resistance and overall structural stability?

This study's research question focuses on investigating how wind effects on a building structure can be accurately and reliably investigated using CFD simulations and identifying effective mitigation strategies to improve the building's wind resistance and overall structural stability. This will involve conducting numerical investigations using ANSYS 2022 R1 software, investigating wind effects at different angles, analysing wind flow around the building, evaluating wind-induced loads and dynamic response of the building, and investigating the effectiveness of different mitigation strategies such as aerodynamic modifications and passive damping systems. The aim is to provide recommendations for optimizing the building's cross-section to improve its wind resistance and overall structural stability, leading to safer and more comfortable living and working environments.

1.4 SCOPE AND LIMITATIONS

This research study aims to investigate the wind induced effects on a building structure using Computational Fluid Dynamics (CFD) simulations and identify effective mitigation strategies to improve the building's wind resistance and overall structural stability. The study will focus on a particular building shape and investigate wind effects at different angles ranging from 0° to 180° . Interference effects between adjacent buildings under 100% (full blockage) wind interference conditions will also be analysed. The wind flows around the building will be analysed to identify areas of high turbulence and interference and the wind-induced loads and response of the building under dynamic conditions will be evaluated for different cross-sectional shapes, including the impact of interference from surrounding buildings. This study recommends optimizing the building's cross-section to improve its wind resistance and overall structural stability, leading to safer and more comfortable living and working environments.

However, it is important to acknowledge certain limitations in this study. To begin with, the simulations will rely on assumptions and simplifications, which may not comprehensively encompass the intricate nature of wind impacts on structures in the real world. Secondly, the study will only focus on a specific building shape, and the results may not be generalizable to other building shapes or configurations. Thirdly, the study will only consider wind effects at a single location and may not fully capture the variability of wind effects in different regions or climates. Fourthly, the effectiveness of the identified mitigation strategies may depend on specific building and environmental factors and may not apply to all situations. Finally, this study will not consider the economic feasibility of implementing the identified mitigation strategies, which may be a key consideration in real-world applications. These limitations will be acknowledged and discussed in the research report to ensure that the conclusions drawn from this study are accurate and reliable.

1.5 CONTRIBUTION OF THE THESIS

This research paper makes several contributions to the field of civil engineering. Firstly, it investigates the impact of wind effects on specific building structure using ANSYS 2022 R1 software and CFD simulations, providing valuable insights into the pressure coefficient

and drag coefficient under different wind angles. The implications of these discoveries are significant for the development and construction of structures capable of enduring wind-induced pressures and dynamic reactions. This ultimately results in the creation of living and working spaces that are both safer and more comfortable.

Secondly, the research paper investigates the interference effects between adjacent buildings under 100% (full blockage) wind interference conditions, providing more accurate and reliable data that can be used in international standards. This is achieved through CFD simulations, which can identify areas of high turbulence and interference. The findings have significant implications for the design and development of structures in densely populated urban areas, where wind obstruction is a prevalent obstacle.

Thirdly, the research paper evaluates the effectiveness of different mitigation strategies, such as aerodynamic modifications and passive damping systems, to reduce wind-induced vibrations and improve the building's wind resistance. This is achieved through ANSYS 2022 R1 software and CFD simulations, which can identify areas of high turbulence and interference. The discoveries carry significant implications for the development and design of buildings capable of withstanding wind-induced forces and dynamic reactions, resulting in the creation of safer and more comfortable living and working spaces.

CHAPTER 2 - LITERATURE REVIEW

Studying the wind angle and wind patterns around buildings can help identify areas where air can enter or exit the building and where ventilation systems should be placed to ensure optimal airflow. This analysis is particularly important in high-rise buildings, where wind speeds can be and greater at higher elevations and where the building's shape can create the low pressure or high turbulence areas.

The standards provide information on wind loads, the response of the building to wind, and other relevant factors that can affect the structural design of the building. However, designing irregularly shaped tall buildings requires additional considerations beyond the international standards for regular-shaped buildings. In these cases, either wind tunnel testing or CFD simulations can be used to evaluate the wind-induced effects on the structure and inform the design process.

Ensuring the safety and comfort of occupants is crucial when estimating wind loads on buildings. Computational fluid dynamics (CFD) simulations are extensively employed for examining the impact of wind on architectural designs. This literature review aims to provide an overview of previous studies related to the CFD simulation of wind loads on buildings, particularly those with irregular shapes. In this review, we focus on studies that investigate the interference of a fish-shaped building with the surrounding flow.

2.1 EXPERIMENTAL INVESTIGATIONS

Wind loads on tall buildings are a crucial aspect to consider during their design and construction. Numerous research studies have utilized diverse experimental techniques to examine these loads. Specifically, several investigations have employed field measurements and wind tunnel experiments to assess the wind-induced pressures, torques, and acceleration responses on various types of tall structures. One study by **(Xu Y. H., 2014) [9]** focused on super-tall buildings and used field measurements to evaluate wind loads. The acceleration response data of the Shanghai Tower, one of the world's tallest buildings, was collected using a measurement system. The study revealed that the

building's geometry and wind direction significantly influenced the wind-induced acceleration response.

Another study by (Mallick, 2019) [10] examined wind-induced pressures on C-shaped buildings using an experimental investigation. Using pressure sensors, wind-induced pressures on a reduced-scale model of a C-shaped structure were measured within a wind tunnel. The findings indicated that the building's configuration had a notable impact on the wind-induced pressures, with the C-shaped building encountering greater wind loads in comparison to rectangular structures.

A study by (Li, 2017) [11] investigated wind-induced torques on L-shaped tall buildings using wind tunnel experiments. The investigation utilized a reduced-scale replica of a building with an L-shape and assessed the wind-induced torques on the structure at varying wind speeds and angles of impact. The research concluded that the wind-induced torques were significantly influenced by the configuration of the building, with L-shaped structures encountering greater wind loads compared to rectangular buildings.

2.2 STUDY ON HIGH-RISE BUILDINGS OF ASYMMETRICAL C/S

(El-Heweity, 2019) [12] conducted a numerical simulation to investigate buffeting longitudinal wind forces on buildings. The investigation employed ANSYS Fluent software for simulating the airflow around a rectangular structure and verified the outcomes through experimental data. The findings revealed that the computational simulation effectively anticipated the wind-driven pressures on the building, highlighting the practicality of computational fluid dynamics (CFD) in forecasting the response of structures to wind loads.

The work by (Xu Y. L., 2014) [13] evaluated wind loads on super-tall buildings using a finite element model to simulate the response of the building to wind loads. The study compared the findings with data obtained from on-site measurements of wind-induced acceleration response. The research demonstrated the accurate prediction of wind-induced response for the building using the finite element model. This underscores the significance

of employing numerical simulations in optimizing the design of exceptionally tall structures and ensuring their stability during high wind conditions.

The study by **(Zheng, 2018)** [14] investigated the wind-induced responses of tall buildings under combined aerodynamic control using a coupled fluid-structure interaction model. The study simulated the flow over a tall building and the response of the building to wind loads, taking into account the effect of various control strategies such as external damping devices and internal mass dampers. The study found that these control strategies could significantly reduce the wind-induced responses of the building, demonstrating the potential of numerical simulations in optimizing the design of buildings for improved wind resistance.

Similarly **(Aly, 2013)** [15] proposed a pressure integration technique for predicting wind-induced response in high-rise buildings. They used the technique to simulate the flow over a tall building and validated the results with experimental data. The simulation work by **(Farouk B. A., 2016)** [16] studied the comfort of occupants in high-rise buildings using CFD. They used ANSYS Fluent to simulate the flow over a tall building and investigated indoor air quality and thermal comfort. The study showed that the ventilation and thermal comfort in the building were affected by the wind.

2.3 WIND EFFECTS ON BUILDINGS HAVING VARYING CROSS-SECTIONAL SHAPE

Several researchers have also investigated wind-induced pressures on buildings of various shapes. **(Chakraborty, 2014)** [17] investigated wind load on an irregularly-shaped tall building using CFD simulations. They used the ANSYS Fluent software to simulate the flow over the building and studied the effect of building shape on the wind loads. **(Cheng, 2015)** [18] used proper orthogonal decomposition (POD) analysis to study crosswind forces on a tall building with square and H-shaped cross sections. They used CFD simulations to compute the flow over the building and the resulting forces. **(Paul, 2016)** [19] investigated wind effects on ‘Z’ plan-shaped tall building: a case study.

(Gomes, 2005) [20] studied the experimental and numerical study of wind pressures on irregular-plan shapes. **(Amin R. &, 2011)** [21] performed an experimental study of wind-

induced pressures on buildings of various geometries. (**Bhattacharyya R. &, 2020**) [22] conducted an experimental and numerical study of wind-pressure distribution on irregular-plan-shaped buildings, while (**Bhattacharyya R. D., 2014**) [23] studied wind-induced pressure on ‘E’ plan-shaped tall buildings.

Several studies have investigated wind loads on buildings using CFD simulations and validated the results with experimental data. Codes and standards provide guidelines for wind loads on buildings in different countries. However, to our knowledge, no previous study has specifically investigated the interference of a fish-shaped building. Previous research has mainly focused on CFD simulation of isolated building models, with limited work on interference effects.

(**Telrandhe, 2019**) [24] studied the dynamic wind effects on high-rise buildings with varying dimensions and heights. (**Ashok, 2018**) [25] used CFD to investigate wind effects on buildings. (**Pal A. K., 2021**) [26] conducted a wind tunnel study to examine the impact of wind incidence on a Fish-plan building model.

2.4 TURBULENCE MODEL

In the study, the (k- ϵ) model is employed, which is widely utilized in computational fluid dynamics (CFD) to simulate the average flow characteristics under turbulent flow conditions. This particular model is a commonly used two-equation approach that provides a comprehensive representation of turbulence by utilizing a pair of transport equations (partial differential equations).

The turbulent kinetic energy (k) **Eq. (1)** is the primary variable that is transported , followed by the dissipation rate of turbulent kinetic energy (ϵ) **Eq. (2)**.

In this study, it is assumed that the turbulent viscosity of the wind, which is considered to be 10 m/s, exhibits isotropic characteristics.

- **For turbulent kinetic energy (k)**

$$\frac{\partial(\rho k)}{\partial t} + \frac{\partial(\rho k u_i)}{\partial x_i} = \frac{\partial}{\partial x_j} \left[\frac{\mu_t}{\sigma_k} \frac{\partial k}{\partial x_j} \right] + 2\mu_t E_{ij} E_{ij} - \rho \varepsilon \quad \text{Eq. (3)}$$

- **For dissipation (ε)**

$$\frac{\partial(\rho \varepsilon)}{\partial t} + \frac{\partial(\rho \varepsilon u_i)}{\partial x_i} = \frac{\partial}{\partial x_j} \left[\frac{\mu_t}{\sigma_\varepsilon} \frac{\partial \varepsilon}{\partial x_j} \right] + C_{1\varepsilon} \frac{\varepsilon}{k} 2\mu_t E_{ij} E_{ij} - C_{2\varepsilon} \rho \frac{\varepsilon^2}{k} \quad \text{Eq. (4)}$$

The (k- ε) model is a commonly employed computational fluid dynamics (CFD) model utilized to simulate turbulent flow situations. This model, consisting of two equations, provides a description of the turbulence properties of a flow by solving for the transport equations of turbulent kinetic energy (k) and the dissipation rate of turbulent kinetic energy (ε). In this model, the turbulent viscosity of the flow is assumed to be uniform in all directions.

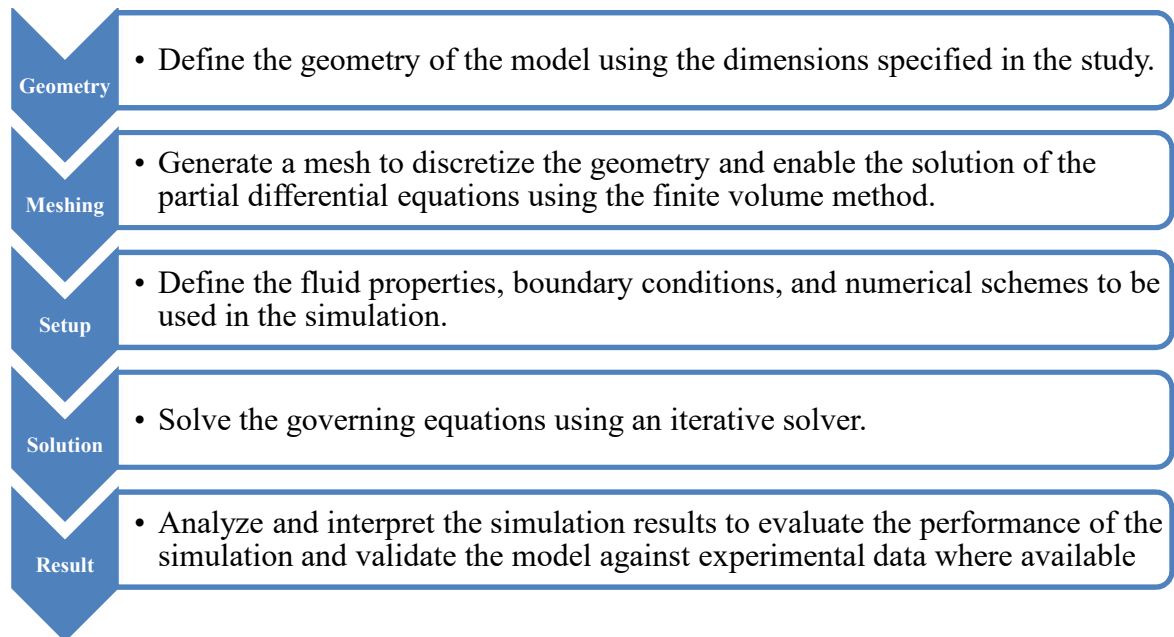
The (k- ε) model serves as a valuable tool for simulating intricate and turbulent flow conditions by offering a comprehensive depiction of turbulence in a flow. By solving the transport equations associated with the variables k and ε , this model enables the prediction of significant turbulence quantities like velocity fluctuations, turbulent kinetic energy, and energy dissipation rate. Employing the (k- ε) model in CFD simulations offers several advantages. It facilitates the analysis of intricate flow phenomena, including flow separation, turbulence-induced noise, and vortex shedding. Additionally, it presents a cost-effective alternative to expensive and time-consuming physical experiments.

The (k- ε) model is a valuable tool for CFD simulation of turbulent flow conditions. It allows for predicting important turbulence quantities and enables the analysis of complex flow phenomena, making it useful for a wide range of engineering applications.

CHAPTER 3 - METHODOLOGY

The utilization of computational fluid dynamics (CFD) simulation methodology has experienced a growing popularity in diverse engineering applications, enabling the prediction of fluid flows. This approach involves defining numerical techniques to solve the governing equations that describe fluid motion, commonly through finite volume or finite element methods. The accuracy and dependability of CFD simulations rely on several factors, such as the selection of turbulence model, numerical scheme, and boundary conditions. ANSYS software is widely utilized for CFD simulations and encompasses five sequential steps: geometry, meshing, setup, solution, and result. The geometry and mesh are defined during the geometry and meshing steps, respectively. In the setup step, the fluid properties, boundary conditions, and numerical schemes are specified for the simulation. The solution step involves solving the governing equations, and the result step entails analysing and interpreting the obtained simulation results. In this particular study, the (k-epsilon) turbulence model in ANSYS software is employed within the CFD simulation methodology to predict the average flow characteristics of turbulent flow conditions.

3.1 NUMERICAL METHODS FOR WIND LOAD ANALYSIS



3.2 GEOMETRY

In this step, model's geometry is defined (**Figure 3.1**) using the dimensions specified in the study. This can be done using 3D CAD software or importing an existing model. The geometry should be defined with a high level of accuracy, as any errors or inaccuracies can significantly affect the accuracy of the simulation results.

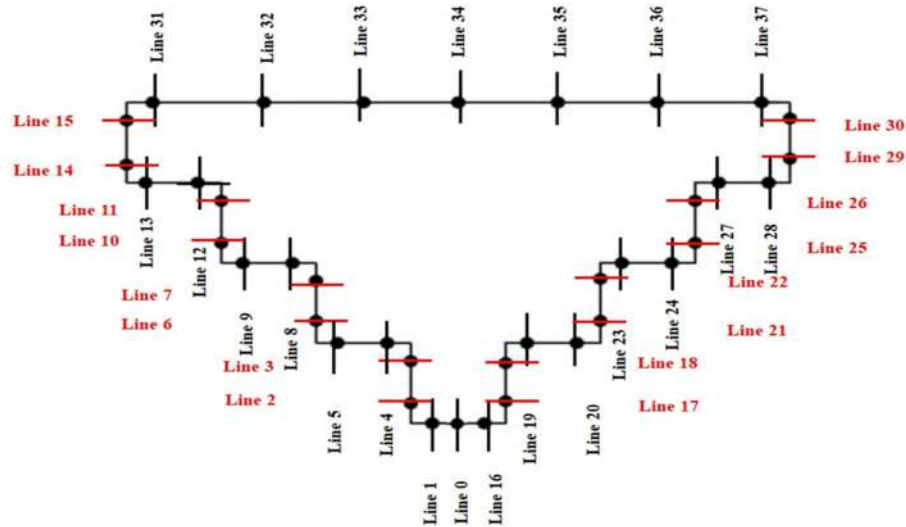


Figure 3.1: Geometry of Fish shape model with co-ordinates

3.3 MESHING

ANSYS software is used for the analysis, which involves creating a 3D model in the geometry step, defining boundary conditions to represent the air current around the building accurately, and meshing the computational domain with tetrahedral elements of size 0.2 meters.

The mesh should be generated with sufficient detail, as a coarse mesh can result in inaccurate or unstable simulation results. The mesh should also be free from inconsistencies or errors, as these can lead to numerical instabilities during the solution phase. The mesh quality is critical for accuracy and efficiency in the simulation, and two types of meshing are utilized: meshing of the domain and meshing with inflation around the model. The

study aims to provide insight into the impact of building shape on wind flow and could inform the design of high-rise buildings in the future. (See **Figure 3.2**)

The meshing of the domain is necessary to divide the computational domain into small cells or elements to solve the governing equations of fluid motion for each cell separately. Meshing with inflation is used to resolve the boundary layer around the object being simulated, capturing the gradient in velocity and turbulence parameters near the object's surface for accurate prediction of aerodynamic forces.

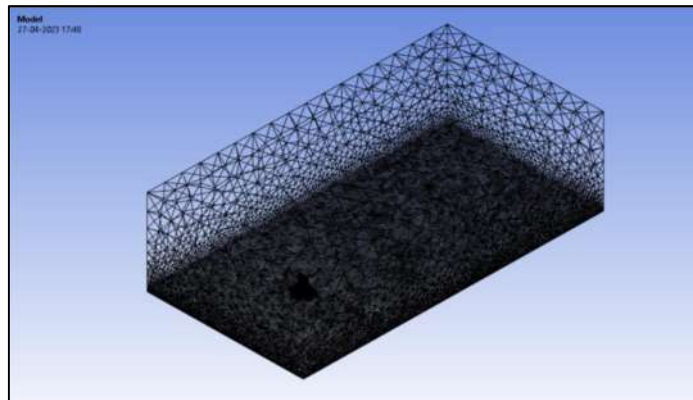


Figure 3.2: Meshing of the Geometry

Meshing is the process of discretizing the continuous geometry of a model into a finite number of smaller elements or cells. This is a critical step in CFD simulation as it directly affects the accuracy and computational efficiency of the analysis. The mesh should be generated to represent the model's geometry and resolves the details of the flow while being coarse enough to minimize computational cost. Here is a detailed description of the meshing procedure in CFD simulation

1. The first step in meshing is to generate a surface mesh of the geometry. This involves dividing the model's surface into smaller elements or triangles, which are used to define the model's geometry. The surface mesh should be carefully designed to accurately capture the model's geometry.
2. Once the surface mesh is generated, a volume mesh is created by extruding the surface mesh into the volume of the model. The volume mesh should be fine

enough to capture flow details while being coarse enough to minimize computational cost.

3. After generating the mesh, its quality should be carefully checked. Mesh quality can be evaluated based on skewness, aspect ratio, and volume ratio. Meshes with poor quality can lead to numerical instabilities and inaccuracies in the results.
4. If the mesh quality is poor or the results are inaccurate, the mesh should be refined. Mesh refinement involves increasing the number of elements in regions of interest to resolve the flow field better. This process can be repeated until the desired level of accuracy is achieved.

Finally, the mesh can be exported to the simulation software for analysis. It is important to note that the accuracy of the simulation results depends strongly on the mesh quality mesh's quality; therefore, the meshing procedure should be performed with care and attention to detail. (See **Figure 3.3**)

Scope	
Scoping Method	Geometry Selection
Geometry	17 Faces
Definition	
Suppressed	No
Type	Element Size
<input type="checkbox"/> Element Size	8.e-003 m
Advanced	
<input type="checkbox"/> Defeature Size	Default (3.5542e-003 m)
Influence Volume	No
Behavior	Soft
<input type="checkbox"/> Growth Rate	Default (1.2)
Capture Curvature	No
Capture Proximity	No

Scope	
Scoping Method	Geometry Selection
Geometry	1 Face
Definition	
Suppressed	No
Type	Element Size
<input type="checkbox"/> Element Size	8.e-002 m
Advanced	
<input type="checkbox"/> Defeature Size	Default (3.5542e-003 m)
Influence Volume	No
Behavior	Soft
<input type="checkbox"/> Growth Rate	Default (1.2)
Capture Curvature	No
Capture Proximity	No

Scope	
Scoping Method	Geometry Selection
Geometry	1 Body
Definition	
Suppressed	No
Boundary Scoping Method	Geometry Selection
Boundary	17 Faces
Inflation Option	Smooth Transition
<input type="checkbox"/> Transition Ratio	Default (0.77)
<input type="checkbox"/> Maximum Layers	5
<input type="checkbox"/> Growth Rate	1.2
Inflation Algorithm	Pre

Scope	
Scoping Method	Geometry Selection
Geometry	1 Body
Definition	
Suppressed	No
Method	Automatic
Element Order	Use Global Setting

Figure 3.3: Face sizing, Face sizing 2, Inflation and Automatic method

3.4 SETUP

The initial steps of a CFD simulation involve establishing the boundary conditions, defining the fluid properties, and selecting an appropriate turbulence model. The accuracy of the simulation outcomes greatly relies on the setup quality, as it directly influences the behaviour of the flow field:

Boundary conditions define the interactions between the model and the external environment. They can be physical (e.g. inflow velocity, pressure, temperature) or numerical (e.g. wall functions, symmetry planes). The selection of the boundary conditions should be based on the physical phenomena of the problem being studied.

The fluid properties of the flow, such as density, viscosity, and thermal conductivity, must be specified (See **Figure 3.4**). These properties can be temperature-dependent and may vary depending on the composition of the fluid. The accuracy of the results is sensitive to the accuracy of these properties. The turbulence model accounts for the effects of turbulence in the flow.

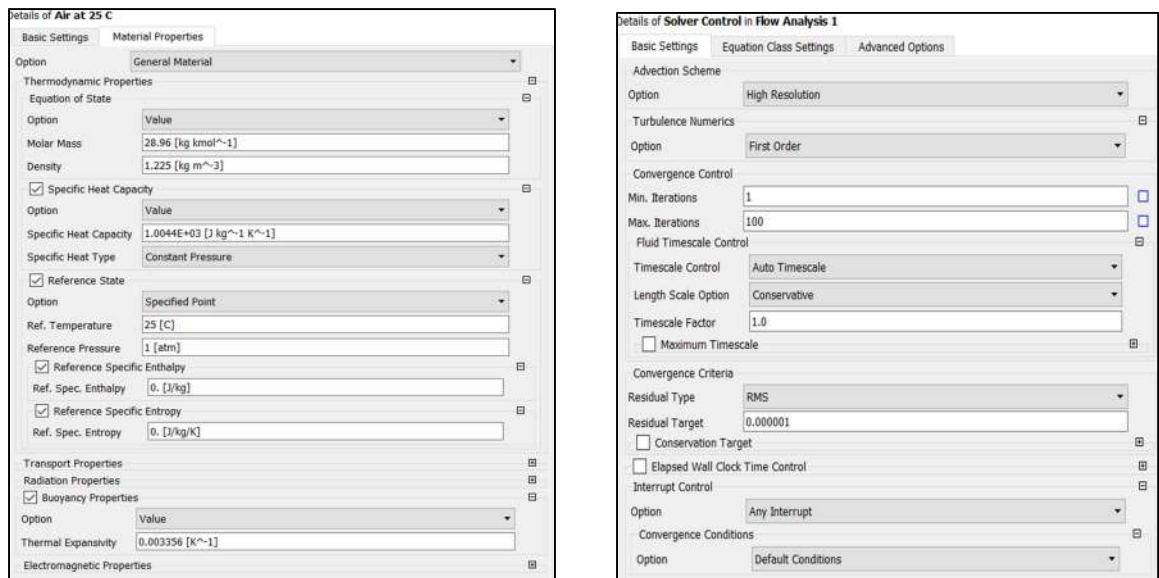


Figure 3.4: Material properties and Solver control in setup

The choice of a turbulence model depends on the flow characteristics and Reynolds number, as it characterizes the dissipation rate of turbulent kinetic energy. Common

turbulence models include the K-epsilon, K-omega, and SST models. Once the boundary conditions, fluid properties, and turbulence model have been specified, the numerical solver can be set up. The numerical solver discretizes the equations governing the flow field and solves them iteratively over a time domain. The accuracy of the solver depends on the time step, convergence criteria, and numerical scheme. After the numerical solver is set up, the simulation can be run. The simulation output can be visualized and analysed to obtain insights into the flow field. It is important to note that the accuracy of the simulation results depends heavily on the setup's quality; therefore, the setup procedure should be performed with care and attention to detail.

3.5 BOUNDARY CONDITION

To effectively address simulation problems, it is crucial to establish precise boundary conditions using numerical simulation. The utilization of extensive dimensions in the virtual wind tunnel guarantees an unrestricted applied domain. Inside this virtual wind tunnel, the building is positioned on the ground, and its model is accurately scaled to fulfill particular specifications.

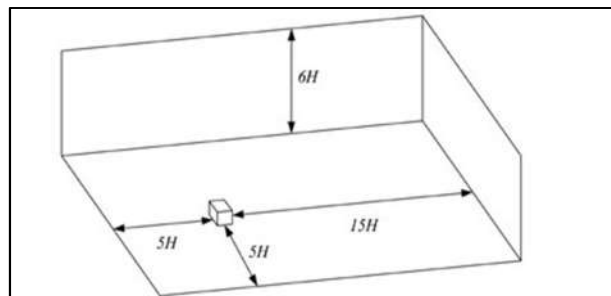


Figure 3.5: A reproduction of the domain used by Franke (2007)

The size of the domain has a notable impact on pressure coefficients and velocity fields. The use of a large domain is preferred as it yields the most reliable and accurate results, simulating infinitely distant boundaries. Conversely, the small domain lacks the capacity to provide precise outcomes. **Figure 3.5** depicts the domain employed by Franke (2007) during the modeling of the Silsoe cube.

3.6 LINE CO-ORDINATES

In computational fluid dynamics (CFD) simulations, lines are often drawn at the coordinates of each face to represent the pressure coefficient (C_p) distribution along the surface of the object being studied. These lines are typically drawn with height to represent the magnitude of the C_p values at each point along the surface. In general, a positive C_p value signifies a low-pressure zone, whereas a negative C_p value signifies a high-pressure zone. Engineers can visually assess the pressure distribution across the object's surface by drawing lines on each face, enabling them to identify regions of high and low pressure. Drawing lines with height allows for a more intuitive and informative representation of the C_p distribution, as it provides a three-dimensional visualization of the data. It also allows engineers to quickly identify regions of interest or concern, such as areas of high pressure that could result in structural failure or areas of low pressure that could lead to aerodynamic instability. Co-ordinate of line for each face of the fish shape is shown below in **Table 3.1**.

Table 3.1: Co-Ordinates of the Lines on Windward side

Co-Ordinates for the Left side of the building			Co-Ordinates for the Right side of the building		
Line Number	Ground Co-Ordinates	Top Co-Ordinates	Line Number	Ground Co-Ordinates	Top Co-Ordinates
Line 0	(0,0,0.1)	(0,0.6,0.1)	Line 17	(0.025,0,0.09)	(0.025,0.6,0.09)
Line 1	(-0.015,0,0.1)	(-0.015,0.6,0.1)	Line 18	(0.025,0,0.06)	(0.025,0.6,0.06)
Line 2	(-0.025,0,0.09)	(-0.025,0.6,0.09)	Line 19	(0.035,0,0.05)	(0.035,0.6,0.05)
Line 3	(-0.025,0,0.06)	(-0.025,0.6,0.06)	Line 20	(0.065,0,0.05)	(0.065,0.6,0.05)
Line 4	(-0.035,0,0.05)	(-0.035,0.6,0.05)	Line 21	(0.075,0,0.04)	(0.075,0.6,0.04)
Line 5	(-0.065,0,0.05)	(-0.065,0.6,0.05)	Line 22	(0.075,0,0.01)	(0.075,0.6,0.01)
Line 6	(-0.075,0,0.04)	(-0.075,0.6,0.04)	Line 23	(0.085,0,0)	(0.085,0.6,0)
Line 7	(-0.075,0,0.01)	(-0.075,0.6,0.01)	Line 24	(0.115,0,0)	(0.115,0.6,0)
Line 8	(-0.085,0,0)	(-0.085,0.6,0)	Line 25	(0.125,0,-0.01)	(0.125,0.6,-0.01)
Line 9	(-0.115,0,0)	(-0.115,0.6,0)	Line 26	(0.125,0,-0.04)	(0.125,0.6,-0.04)
Line 10	(-0.125,0,-0.01)	(-0.125,0.6,-0.01)	Line 27	(0.125,0,-0.05)	(0.125,0.6,-0.05)
Line 11	(-0.125,0,-0.04)	(-0.125,0.6,-0.04)	Line 28	(0.165,0,-0.05)	(0.165,0.6,-0.05)
Line 12	(-0.125,0,-0.05)	(-0.125,0.6,-0.05)	Line 29	(0.175,0,-0.06)	(0.175,0.6,-0.06)
Line 13	(-0.165,0,-0.05)	(-0.165,0.6,-0.05)	Line 30	(0.175,0,-0.09)	(0.175,0.6,-0.09)
Line 14	(-0.175,0,-0.06)	(-0.175,0.6,-0.06)	Co-Ordinate for the Leeward side of the building		
Line 15	(-0.175,0,-0.09)	(-0.175,0.6,-0.09)	Line Number	Ground Co-Ordinates	Top Co-Ordinates
Line 16	(0.015,0,0.1)	(0.015,0.6,0.1)	Line 31	(-0.165,0,-0.1)	(-0.165,0.6,-0.1)

Line 32	(-0.110,0,-0.1)	(-0.110,0.6,-0.1)
Line 33	(-0.055,0,-0.1)	(-0.055,0.6,-0.1)
Line 34	(0,0,-0.1)	(0,0.6,-0.1)
Line 35	(0.055,0,-0.1)	(0.055,0.6,-0.1)
Line 36	(0.110,0,-0.1)	(0.110,0.6,-0.1)
Line 37	(0.165,0,-0.1)	(0.165,0.6,-0.1)

3.7 SOLUTION

After defining the setup, the governing equations are solved using an iterative solver. The solution can be performed using either steady-state or time-dependent methods, depending on the problem being studied. The solution phase can be computationally expensive, and the convergence criteria must be carefully selected to ensure accurate and stable results.

Figure 3.6 shows the name of the windward and leeward faces of the model.

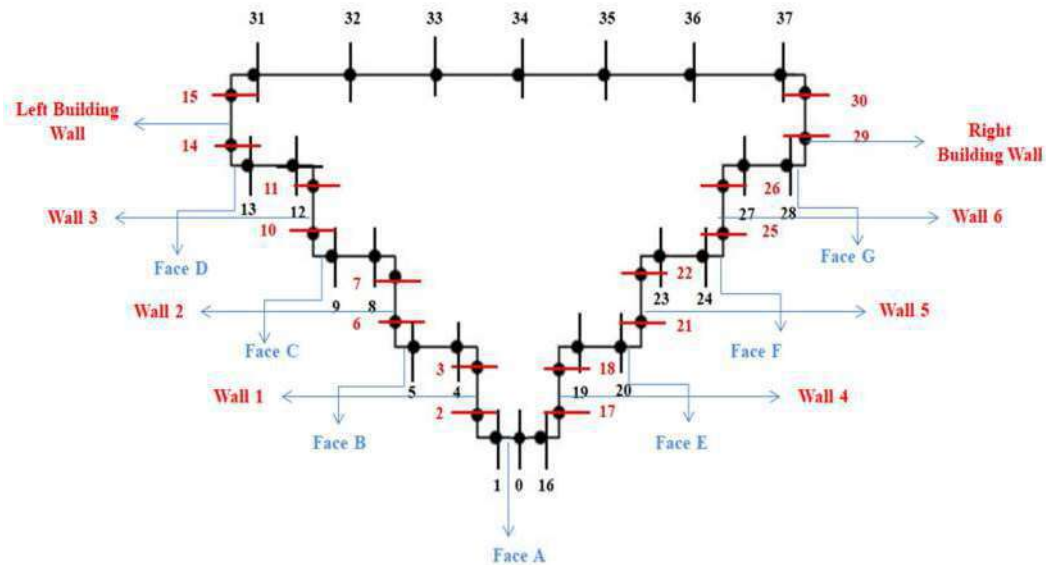


Figure 3.6: Nomenclature of the Model, Windward and Leeward faces

3.8 RESULT

Finally, the simulation results are analysed and interpreted to evaluate the performance of the simulation and validate the model against experimental data where available. This involves post-processing the results to generate visualizations of the flow field and calculating relevant metrics such as pressure drop, velocity profiles, and other parameters of interest. The results should be carefully analysed to ensure they are accurate and reliable and can be used to draw meaningful conclusions.

CHAPTER 4 - ISOLATED BUILDING SIMULATION

4.1 WIND-INDUCED RESPONSES OF ISOLATED BUILDING

In this study, we conducted a CFD simulation of the flow field over a given geometry (fish shape) **Figure 4.1**. The simulation results provided valuable insights into the flow characteristics, including pressure contours, vertical and horizontal streamlines, and pressure coefficients at various angles ranging from 0 to 180 degrees at an interval of 15 degrees.

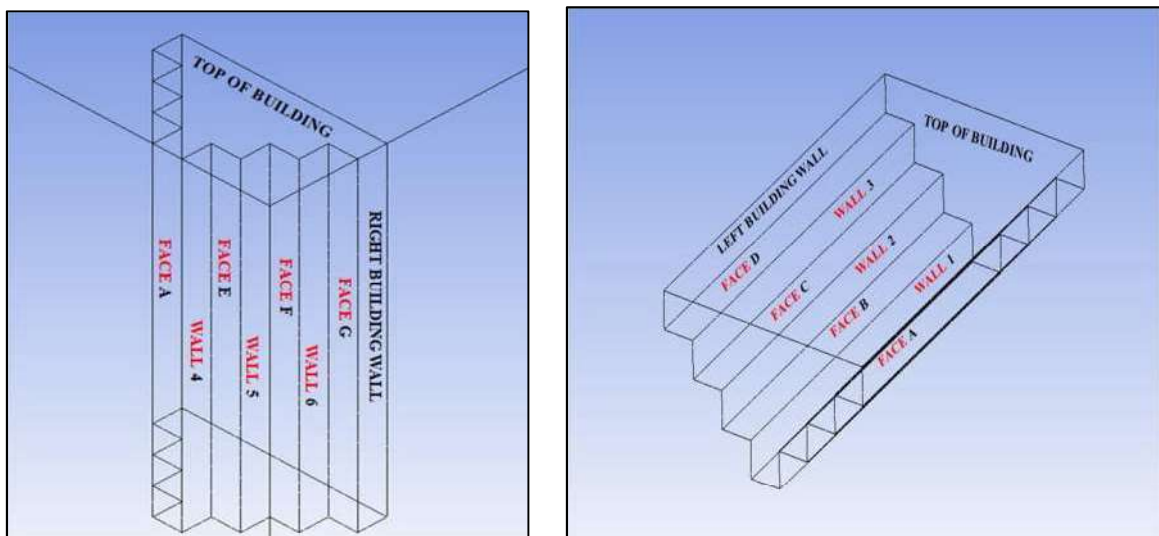


Figure 4.1: Geometry & model description

4.2 RESULTS & VALIDATION FOR ISOLATED MODEL

The pressure contours reveal high and low pressure areas, providing insights into the flow separation, recirculation zones, and pressure distribution over the geometry. The vertical and horizontal streamlines show the flow paths and direction, providing information on the fluid behavior and any potential flow separation or turbulence.

The pressure coefficient is a dimensionless quantity widely used to describe the pressure distribution over a surface. The pressure coefficient results obtained from the simulation provide valuable information on the aerodynamic performance of the geometry and can be used to optimize its design.

By comparing our simulation results with existing experimental data from various sources in the literature, we were able to validate them. This comparison revealed a strong correlation between the simulated and experimental outcomes, instilling confidence in the precision and reliability of our simulation results. The wind speed profile within the atmospheric boundary layer is determined by an equation known as the "**Power Law equation.**" In this equation, v_{Ref} represents the wind speed at the reference height, which is 10 m/s. The parameter α accounts for the ground roughness, which can vary, while z_{Ref} is set at a value of 1.0.

$$\frac{v}{v_{Ref}} = \left(\frac{z}{z_{Ref}} \right)^\alpha \quad Eq. (3)$$

4.3 PRESSURE COEFFICIENT CALCULATION

The pressure coefficient is a unit less measure commonly used to describe how the pressure is distributed over a surface. It quantifies the difference between the local pressure and a reference pressure, relative to the dynamic pressure of the flow. Pressure coefficient (C_p) is given as:

$$C_p = \frac{\text{Average pressure } (P)}{0.5 * \rho * V^2} \quad Eq. (4)$$

Where P is the local average pressure, ρ is the density of the air which is 1.225 kg/m^3 , and V is the velocity of the air which is 10 m/s .

$$C_p = \frac{\text{Average pressure } (P)}{0.5 * 1.225 * 10^2}$$

$$C_p = \frac{P}{61.25} = 0.02P \quad Eq. (5)$$

The pressure coefficient is useful in aerodynamics as it provides information about the pressure distribution over a surface. It is commonly used to design and optimize aircraft wings, turbine blades, and other aerodynamic structures. By analyzing the pressure coefficient distribution over a surface, engineers can identify areas of high and low

pressure, flow separation, and other flow phenomena that can affect the performance and efficiency of the structure.

Therefore, obtaining accurate pressure coefficient data through CFD simulations can provide valuable insights for designing and optimizing aerodynamic structures.

4.4 PRESSURE CONTOURS

Pressure contours are acquired through analysis using ANSYS: CFX mode. These contours serve the purpose of visually representing variations in pressure values across a given surface. The pressure contours shown below show a comparative difference in pressure impact at wind inclination varying from 0° to 180° at an interval of 15° . The pressure contours of each face are determined for various wind angles.

- Case 1 – The incident wind angle is 0°

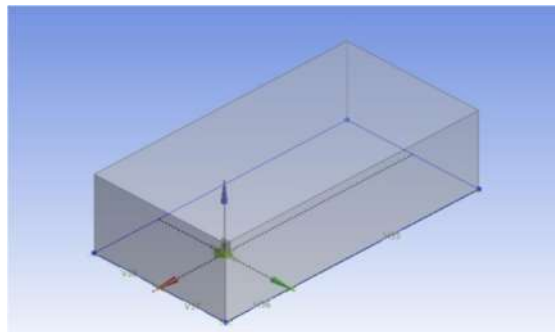
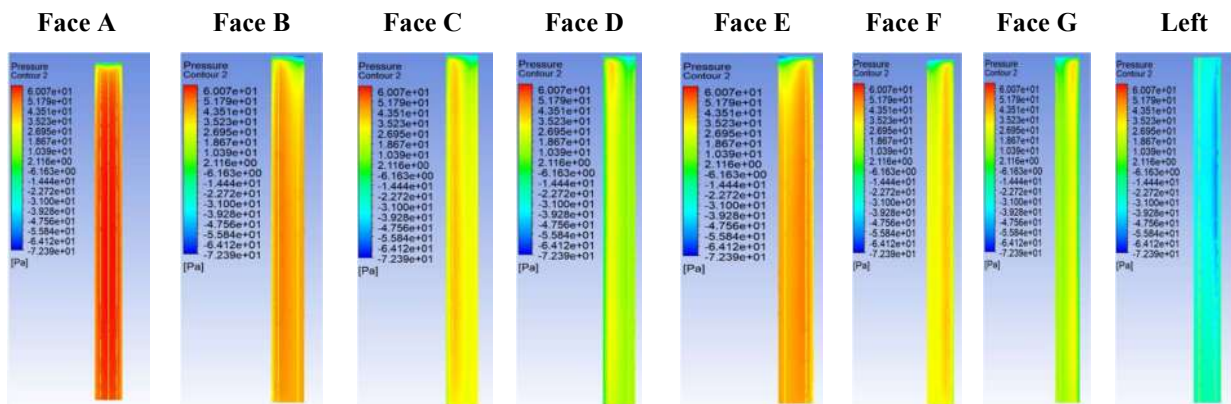


Figure 4.2: Geometry of the model when the inclination is 0 degree

Table 4.1: Pressure contour of faces at 0-degree wind inclination



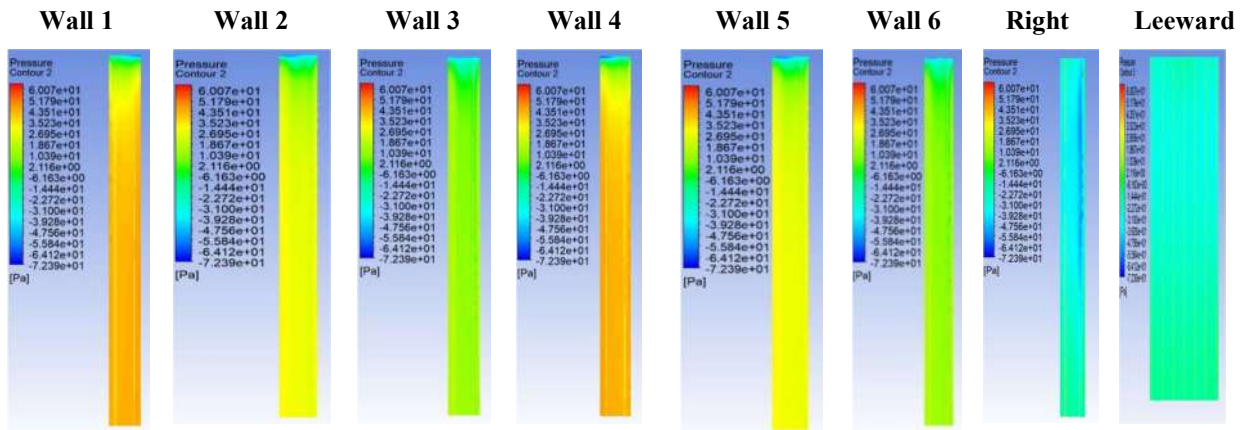


Table 4.2: Pressure and Cp values for each face of the Model at wind incidence of 0 degree

Wind Inclination Angle 0									
Faces/Wall	Line	Range of Pressure	Average value of Pressure	Range of Cp	Average Value of Cp	Fx	Fz	Mx	Mz
Face A	Line 0	(64.12,-29.07)	60.20	(1.05,-0.47)	0.98	-1.47795E-05	-1.69324	-0.491499	4.79E-06
	Line 1	(60.02,-28.76)	57.34	(0.99,-0.47)	0.94				
	Line 16	(60.93,-12.27)	57.45	(0.99,-0.20)	0.94				
Wall 1	Line 2	(43.65,-27.20)	36.01	(0.71,-0.44)	0.59	1.1621	0.00103474	0.00027308	-0.31107
	Line 3	(45.50,-58.25)	39.66	(0.74,-0.95)	0.65				
Face B	Line 4	(44.82,-62.67)	38.33	(0.73,-1.02)	0.63	9.01771E-05	-1.28084	-0.359948	-0.000144205
	Line 5	(51.68,-36.97)	48.12	(0.84,-0.60)	0.79				
Wall 2	Line 6	(30.30,-57.10)	25.52	(0.49,-0.93)	0.42	0.720703	0.00140734	0.000462499	-0.184221
	Line 7	(30.30,-57.10)	25.52	(0.49,-0.93)	0.42				
Face C	Line 8	(29.46,-47.59)	23.27	(0.48,-0.78)	0.38	0.00048523	-0.888516	-0.2502	-0.000337754
	Line 9	(41.54,-30.22)	38.89	(0.68,-0.49)	0.63				
Wall 3	Line 10	(11.30,-34.55)	3.37	(0.18,-0.56)	0.05	0.249809	0.00154338	0.000560668	-0.0520828
	Line 11	(14.25,-44.21)	10.44	(0.23,-0.72)	0.17				
Face D	Line 12	(13.13,-42.50)	7.52	(0.21,-0.69)	0.12	-0.000156953	-0.439623	-0.124656	-0.000194537
	Line 13	(37.61,-20.68)	27.19	(0.61,-0.34)	0.44				
Left Building Wall	Line 14	(-23.63,-54.46)	-43.38	(-0.39,0.89)	-0.71	-0.991739	0.00112846	0.000582311	0.323564
	Line 15	(-20.30,-39.66)	-32.56	(-0.33,-0.65)	-0.53				
Wall 4	Line 17	(43.51,-30.53)	35.92	(0.71,-0.50)	0.59	-1.16042	0.00103796	0.00027521	0.310261
	Line 18	(45.36,-61.12)	39.63	(0.74,-1.00)	0.65				
Face E	Line 19	(44.76,-58.23)	38.39	(0.73,-0.95)	0.63	-9.87554E-05	-1.28021	-0.359859	0.000147235
	Line 20	(51.57,-43.31)	48.03	(0.84,-0.71)	0.78				
Wall 5	Line 21	(27.87,-39.71)	20.34	(0.46,-0.65)	0.33	-0.721723	0.00138995	0.000454826	0.184441
	Line 22	(30.28,-57.33)	25.58	(0.49,-0.94)	0.42				
Face F	Line 23	(29.71,-46.16)	23.45	(0.49,-0.75)	0.38	-0.000469138	-0.889508	-0.250818	0.000325766
	Line 24	(40.88,-28.59)	38.80	(0.67,-0.47)	0.63				
Wall 6	Line 25	(12.09,-35.45)	3.42	(0.20,-0.58)	0.06	-0.249359	0.00152944	0.000553989	0.0506555
	Line 26	(14.75,-47.15)	10.45	(0.24,-0.77)	0.17				
Face G	Line 27	(13.52,-43.86)	7.60	(0.22,-0.72)	0.12	0.000186615	-0.439856	-0.123225	0.000189288
	Line 28	(37.69,-20.68)	27.12	(0.62,-0.34)	0.44				
Right Building Wall	Line 29	(-22.48,-53.54)	-43.21	(-0.37,-0.87)	-0.71	0.988738	0.00116246	0.000605345	-0.325358
	Line 30	(-19.03,-39.46)	-32.37	(-0.31,-0.46)	-0.53				
	Line 31	(-17.07,-32.81)	-26.49	(-0.28,-0.54)	-0.43				
Leeward Face	Line 32	(-16.85,-32.43)	-26.23	(-0.28,-0.53)	-0.43	-0.000949786	-5.53956	-1.82856	0.000312152
	Line 33	(-16.92,-32.02)	-25.83	(-0.28,-0.52)	-0.42				
	Line 34	(-16.90,-31.99)	-25.62	(-0.28,-0.52)	-0.42				
	Line 35	(-16.54,-32.23)	-25.90	(-0.27,-0.53)	-0.42				
	Line 36	(-15.97,-32.66)	-26.19	(-0.26,-0.53)	-0.43				
	Line 37	(-16.11,-32.97)	-26.26	(-0.26,-0.54)	-0.43				

The range of average pressure values for the wind inclination angle of 0° (Figure 4.1) is between [-43.38, 60.20] (Table 4.1). The maximum positive and negative pressure values of 60.20 and -43.38, respectively, occur on Face A and the left building wall. The range of pressure coefficient Cp lies in the range ε [-0.71, 0.98] (Table 4.2). The maximum positive

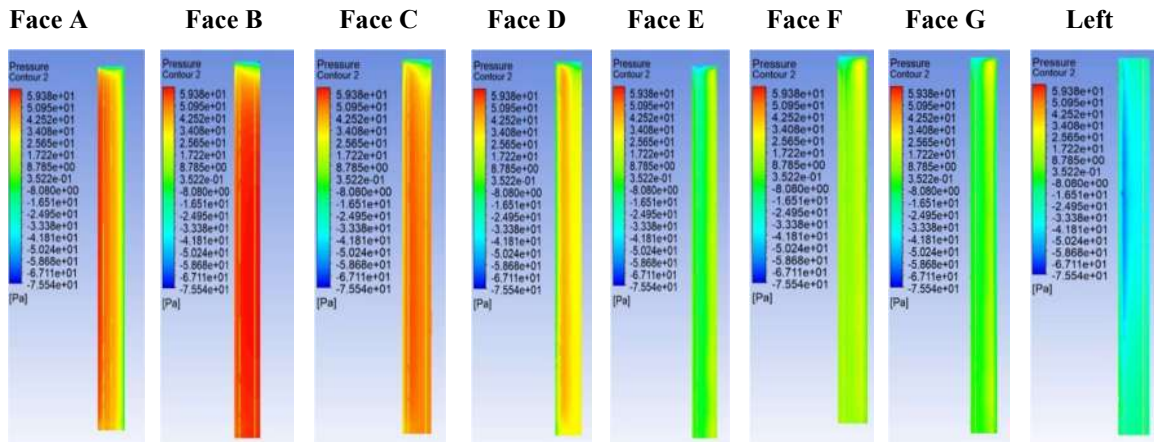
and negative values of 0.98 and -0.71 occur on **Face A** and **Left Building walls**, indicating the areas of the building that will experience the highest wind load.

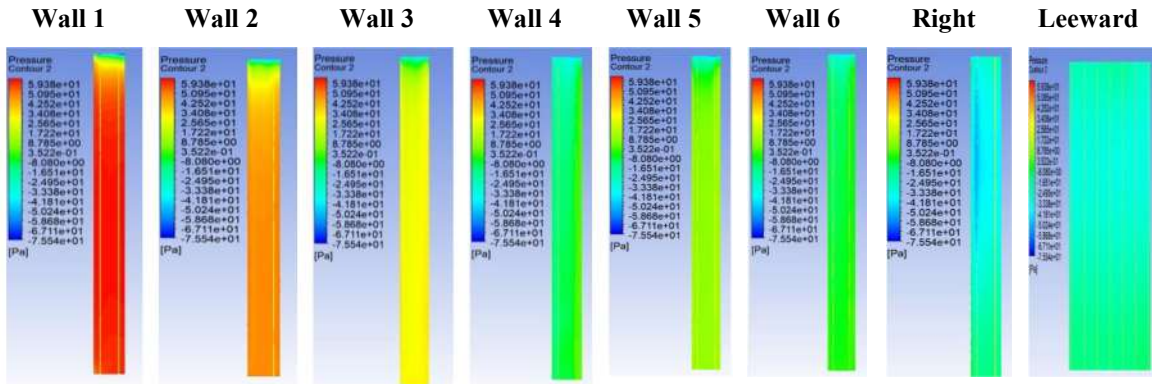
- Case 2 – The incident wind angle is 15°

Table 4.3: Pressure and Cp values for each face of the Model at wind incidence of 15 degree

Wind Inclination Angle 15 deg						Force(N)		Moment(N-m)	
Faces/Wall	Line	Range of Pressure	Average value of Pressure	Range of Cp	Average Value of Cp	Fx	Fz	Mx	Mz
Face A	Line 0	(48.10,-30.35)	45.21	(0.79,-0.50)	0.74	0.00363662	-1.2	-0.354211	-0.00104035
	Line 1	(55.44,-53.80)	51.98	(0.91,-0.88)	0.85				
	Line 16	(32.60,-40.49)	30.32	(0.53,-0.66)	0.49				
Wall 1	Line 2	(63.53,-57.60)	58.03	(1.04,-0.94)	0.95	1.74542	-0.000245044	-0.000189982	-0.495245
	Line 3	(63.05,-60.28)	57.32	(1.03,-0.98)	0.94				
Face B	Line 4	(63.21,-50.33)	57.63	(1.03,-0.82)	0.94	-0.000857059	-1.70754	-0.485006	0.000208177
	Line 5	(60.65,-32.25)	56.17	(0.99,-0.53)	0.92				
Wall 2	Line 6	(50.22,-47.01)	44.77	(0.82,-0.77)	0.73	1.32286	0.000876092	0.000278793	-0.361391
	Line 7	(50.22,-47.01)	44.77	(0.82,-0.77)	0.73				
Face C	Line 8	(49.50,-47.68)	43.73	(0.81,-0.78)	0.71	-0.00010636	-1.40642	-0.398464	-0.0001317
	Line 9	(54.70,-38.14)	51.03	(0.89,-0.62)	0.83				
Wall 3	Line 10	(29.95,-36.90)	21.71	(0.49,-0.60)	0.35	0.778791	0.00131703	0.000471952	-0.208417
	Line 11	(31.69,-42.29)	27.60	(0.52,-0.69)	0.45				
Face D	Line 12	(31.24,-38.44)	25.67	(0.51,-0.63)	0.42	-0.000779255	-0.891119	-0.256168	2.12E-05
	Line 13	(43.83,-21.49)	38.94	(0.72,-0.35)	0.64				
Left Building Wall	Line 14	(-21.14,-58.34)	-46.60	(-0.35,-0.95)	-0.76	-1.00987	0.00132003	0.000677407	0.329169
	Line 15	(-18,-41.27)	-32.33	(-0.29,-0.67)	-0.53				
Wall 4	Line 17	(-8.49,-37.34)	17.91	(-0.14,-0.61)	-0.29	0.333498	0.00273621	-0.120542	-0.120542
	Line 18	(-1.40,-51.13)	-5.88	(-0.02,-0.83)	-0.10				
Face E	Line 19	(-4.92,-49.40)	-10.84	(-0.08,-0.81)	-0.18	-0.00261269	0.0277979	0.0187557	0.000880015
	Line 20	(21.49,-29.33)	13.86	(0.35,-0.48)	0.23				
Wall 5	Line 21	(8.52,-37.25)	3.40	(0.14,-0.61)	0.06	-0.18532	0.000849912	0.000295289	0.0349311
	Line 22	(10.23,-51.90)	7.04	(0.17,-0.85)	0.12				
Face F	Line 23	(9.98,-44.28)	5.50	(0.16,-0.72)	0.09	-0.000353773	0.000849912	-0.0833277	0.000293687
	Line 24	(31.38,-34.42)	18.03	(0.51,-0.56)	0.29				
Wall 6	Line 25	(-4.23,-39.02)	-13.43	(-0.07,-0.64)	-0.22	0.256493	0.0014217	0.000519848	-0.0955433
	Line 26	(-2.30,-39.20)	-6.35	(-0.04,-0.64)	-0.10				
Face G	Line 27	(-3.64,-0.06)	-9.34	(-0.38,-0.62)	-0.15	-0.000312765	0.0628869	0.0243111	0.000321017
	Line 28	(32.01,-18.15)	10.63	(0.52,-0.30)	0.17				
Right Building Wall	Line 29	(-17.18,-52.40)	-40.76	(-0.28,-0.86)	-0.67	0.963144	0.00100016	0.000585628	-0.324231
	Line 30	(-15.20,-41.24)	-31.58	(-0.25,-0.67)	-0.52				
Leeward Face	Line 31	(-14.79,-34.07)	-25.88	(-0.24,-0.56)	-0.42	-0.00313413	-5.57473	-1.85128	0.000992619
	Line 32	(-15.02,-33.40)	-26.08	(-0.25,-0.55)	-0.43				
	Line 33	(-15.42,-33.35)	-25.96	(-0.25,-0.54)	-0.42				
	Line 34	(-15.34,-33.65)	-25.94	(-0.25,-0.55)	-0.42				
	Line 35	(-14.86,-34.07)	-25.74	(-0.24,-0.56)	-0.42				
	Line 36	(-13.79,-34.23)	-26.42	(-0.23,-0.56)	-0.43				
	Line 37	(-12.97,-34.21)	-25.65	(-0.21,-0.56)	-0.42				

Table 4.4 : Pressure contour of faces at 15-degree wind inclination





The range of average pressure values for the wind inclination angle of 15° (Table 4.3). is between [-46.60, 58.03] The maximum positive and negative pressure values of 58.03 and -46.60, respectively, occur on Wall 1 and the left building wall. The range of pressure coefficient C_p lies in the range of ϵ [-0.76, 0.95] The maximum positive and negative values of 0.95 and -0.76 occur on Wall 1 and the Left Building wall, indicating the areas of the building that will experience the highest wind load (Table 4.4).

- Case 3 – The incident wind angle is 30°

Table 4.5: Pressure contour of faces at 30-degree wind inclination

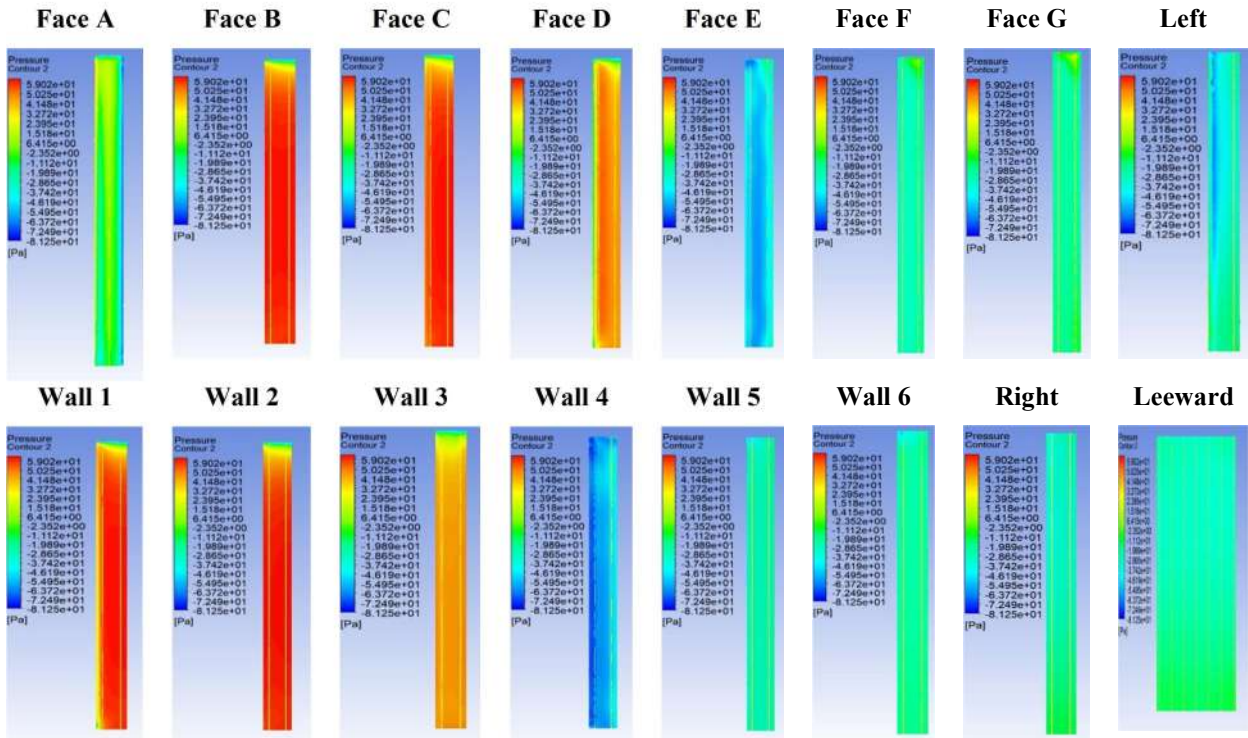


Table 4.6: Pressure and Cp values for each face of the Model at wind incidence of 30 degree

Wind Inclination Angle 30 deg						Force(N)		Moment(N-m)	
Faces/Wall	Line	Range of Pressure	Average value of Pressure	Range of Cp	Average Value of Cp	Fx	Fz	Mx	Mz
Face A	Line 0	(15.69,-30.41)	4.49	0.26,-0.50	0.07	0.00536828	0.314425	0.0644289	-0.00161638
	Line 1	(9.17,-48.53)	-19.78	(0.15,-0.79)	-0.32				
	Line 16	(-2.97,-46.51)	-13.64	(-0.05,-0.76)	-0.22				
Wall 1	Line 2	(60.01,-60.25)	55.80	(0.98,-0.98)	0.91	1.64983	0.00155788	0.000315461	-0.477794
	Line 3	(63.27,-60.42)	57.54	(1.03,-0.99)	0.94				
Face B	Line 4	(63.13,-47.01)	-57.53	(1.03,-0.77)	0.94	0.000222171	-1.75133	-0.499836	-0.00010677
	Line 5	(63.29,-37.39)	58.53	(1.03,-0.61)	0.96				
Wall 2	Line 6	(62.84,-54.12)	56.75	(1.03,-0.88)	0.93	1.71776	-0.000360391	-0.00014867	-0.483954
	Line 7	(62.84,-54.12)	56.75	(1.03,-0.88)	0.93				
Face C	Line 8	(62.98,-45.33)	57.05	(1.03,-0.74)	0.93	-0.00088001	-1.68822	-0.478953	0.000153575
	Line 9	(60.12,-33.13)	55.61	(0.98,-0.54)	0.91				
Wall 3	Line 10	(45.40,-54.71)	38.65	(0.74,-0.89)	0.63	1.24817	0.000873911	0.000308878	-0.346033
	Line 11	(47.00,-57.35)	42.27	(0.77,-0.94)	0.69				
Face D	Line 12	(46.86,-45.00)	41.55	(0.77,-0.33)	0.68	-0.0012999	-1.24574	-0.357086	0.000202858
	Line 13	(50.09,-34.03)	46.66	(0.82,-0.56)	0.76				
Left Building Wall	Line 14	(-28.16,-63.30)	-52.52	(-0.46,-1.03)	-0.86	-1.06351	0.00165284	0.000763806	0.349539
	Line 15	(-15.67,-38.49)	-30.72	(-0.26,-0.63)	-0.50				
Wall 4	Line 17	(-58.27,-70.48)	-67.39	(-0.95,-1.15)	-1.10	1.72332	0.00336801	0.00104358	-0.509066
	Line 18	(-42.54,-61.00)	-49.47	(-0.69,-1.00)	-0.81				
Face E	Line 19	(-44.58,-70.33)	-53.50	(-0.73,-1.15)	-0.87	-0.00478162	1.51523	0.441343	0.00128899
	Line 20	(-17.72,-52.07)	-44.81	(-0.29,-0.85)	-0.73				
Wall 5	Line 21	(-27.26,-48.30)	-29.98	(-0.45,-0.79)	-0.49	0.891338	0.891338	0.000437712	-0.268997
	Line 22	(-25.54,-29.90)	-28.45	(-0.42,-0.49)	-0.46				
Face F	Line 23	(-23.30,-30.00)	-29.33	(-0.39,-0.49)	-0.48	-0.00148891	0.81966	0.23992	0.000351204
	Line 24	(3.79,-28.33)	-23.93	(0.06,-0.46)	-0.39				
Wall 6	Line 25	(-18.77,-46.42)	-24.27	(-0.31,-0.76)	-0.40	0.706066	0.000487351	0.000167912	-0.222438
	Line 26	(-18.17,-28.58)	-22.84	(-0.30,-0.47)	-0.37				
Face G	Line 27	(-10.15,-26.27)	-23.23	(-0.17,-0.43)	-0.38	-9.25E-05	0.649531	0.198975	-3.60E-05
	Line 28	(9.99,-24.60)	-17.89	(0.16,-0.40)	-0.29				
Right Building Wall	Line 29	(-12.96,-42.22)	-31.82	(-0.21,-0.69)	-0.52	0.867324	0.000330422	0.000315439	-0.294959
	Line 30	(-13.45,-35.83)	-28.51	(-0.22,-0.58)	-0.47				
Leeward Face	Line 31	(-12.71,-32.40)	-24.73	(-0.21,-0.53)	-0.40	-0.00394239	-5.4978	-1.86105	0.00113491
	Line 32	(-13.38,-36.69)	-25.77	(-0.22,-0.60)	-0.42				
	Line 33	(-18.80,-36.70)	-26.26	(-0.23,-0.60)	-0.43				
	Line 34	(-14.14,-36.92)	-26.77	(-0.23,-0.60)	-0.44				
	Line 35	(-14.03,-34.28)	-26.75	(-0.23,-0.56)	-0.44				
	Line 36	(-13.30,-33.41)	-25.87	(-0.22,-0.55)	-0.42				
	Line 37	(-12.17,-33.35)	-25.46	(-0.20,-0.54)	-0.42				

The range of average pressure values for the wind inclination angle of 30° (**Table 4.5**) is between [-67.39, 58.53]. The maximum positive and negative pressure values of 58.53 and -67.39, respectively, occur on Face B and wall 4. The range of pressure coefficient Cp lies in the range ϵ [-1.10, 0.96]. The maximum positive and negative values of 0.96 and -1.10 occur on Face B and wall 4. As the wind inclination angle increases, the Cp value changes, which reflect the change in pressure distribution on the objects, surface (**Table 4.6**). In some cases, the Cp values may increase, indicating an increase in pressure differences between the surface of the object and the surrounding wind.

- Case 4 – The incident wind angle is 45°

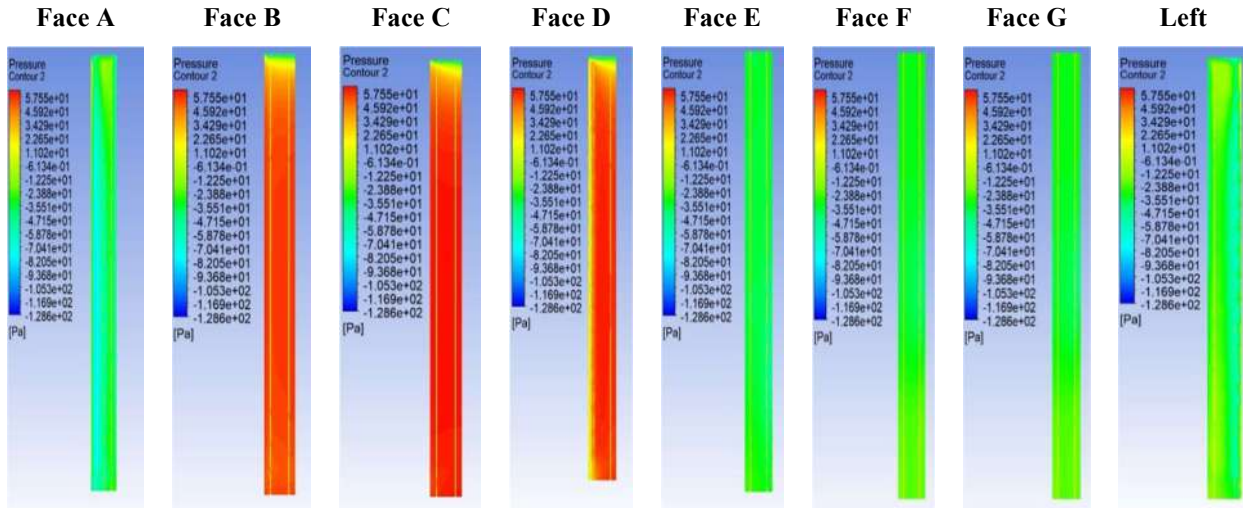
The range of average pressure values for the wind inclination angle of 45° (**Table 4.7**) is between [-74.31, 58.28]. The maximum positive and negative pressure values of 58.28 and -74.31, respectively, occur on **Face A** and **Face C**. The range of pressure coefficient Cp lies

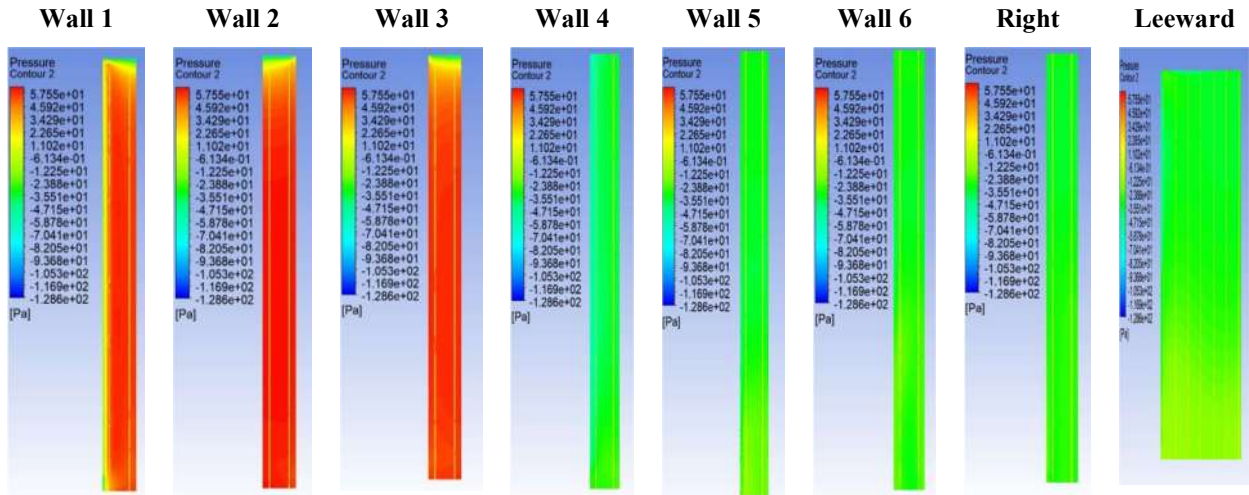
in the range ε [-1.21, 0.95]. The maximum positive and negative values of 0.95 and -1.21 occur on Face A and Face C (Table 4.8).

Table 4.7: Pressure and Cp values for each face of the Model at wind incidence of 45 degree

Wind Inclination Angle 45 deg						Force(N)		Moment(N-m)	
Faces/Wall	Line	Range of Pressure	Average value of Pressure	Range of Cp	Average Value of Cp	Fx	Fz	Mx	Mz
Face A	Line 0	(-14.90,-49.57)	-42.74	(-0.24,-0.81)	-0.7	0.001571	1.40751	0.396871	-0.000609564
	Line 1	(-41.37,-84.48)	-74.31	(-0.68,-1.38)	-1.21				
	Line 16	(-19.44,-45.25)	-32.29	(-0.32,-0.74)	-0.53				
Wall 1	Line 2	(53.47,-33.57)	49.70	(0.87,-0.55)	0.81	1.43657	0.00217324	0.000514987	-0.418656
	Line 3	(57.12,-51.14)	52.14	(0.93,-0.83)	0.85				
Face B	Line 4	(57.12,-47.91)	52.15	(0.93,-0.78)	0.85	-0.000253673	-1.56553	-0.446098	2.67E-05
	Line 5	(55.40,-64.33)	50.43	(0.90,-1.05)	0.82				
Wall 2	Line 6	(63.21,-48.37)	57.19	(1.03,-0.79)	0.93	1.73404	0.000287355	-2.80E-05	-0.491106
	Line 7	(63.21,-48.37)	57.19	(1.03,-0.79)	0.93				
Face C	Line 8	(63.19,-50.89)	57.20	(1.03,-0.83)	0.93	-0.000145076	-1.74156	-0.493487	-6.82E-05
	Line 9	(63.27,-42.97)	58.28	(1.03,-0.70)	0.95				
Wall 3	Line 10	(57.66,-46.32)	52.56	(0.94,-0.76)	0.86	1.62683	7.25E-05	2.48E-05	-0.460601
	Line 11	(59.28,-61.32)	53.86	(0.97,-1.00)	0.88				
Face D	Line 12	(59.56,-53.21)	54.21	(0.97,-0.87)	0.89	-0.0020189	-1.49897	-0.430666	0.000416889
	Line 13	(54.49,-56.17)	50.33	(0.89,-0.92)	0.82				
Left Building Wall	Line 14	(-33.33,-70.35)	-54.23	(-0.54,-1.15)	-0.88	-0.930997	-0.00173821	-0.000616088	0.282738
	Line 15	(-12.65,-35.79)	-20.70	(-0.21,-0.58)	-0.34				
Wall 4	Line 17	(-28.12,-49.58)	-44.52	(-0.46,-0.81)	-0.73	1.172	0.0013383	0.000277911	-0.363039
	Line 18	(-24.75,-37.23)	-34.26	(-0.40,-0.61)	-0.56				
Face E	Line 19	(-26.60,-37.56)	-34.84	(-0.43,-0.61)	-0.57	-0.000613903	1.10794	0.332732	0.000253104
	Line 20	(-33.09,-45.30)	-39.30	(-0.54,-0.74)	-0.64				
Wall 5	Line 21	(-17.02,-36.22)	-30.37	(-0.28,-0.59)	-0.50	0.936177	0.000690747	0.000142054	-0.297661
	Line 22	(-20.73,-36.06)	-30.46	(-0.34,-0.59)	-0.50				
Face F	Line 23	(-20.66,-36.30)	-30.63	(-0.34,-0.59)	-0.50	-0.000134595	0.950421	0.300462	0.000248959
	Line 24	(-20.55,-42.68)	-32.33	(-0.34,-0.70)	-0.53				
Wall 6	Line 25	(-19.67,-34.28)	-28.25	(-0.32,-0.56)	-0.46	0.926054	-0.00068744	1.26E-05	-0.283044
	Line 26	(-25.82,-34.46)	-30.07	(-0.42,-0.56)	-0.49				
Face G	Line 27	(-23.93,-34.41)	-29.24	(-0.39,-0.53)	-0.48	0.000975853	0.963581	0.290693	2.03E-05
	Line 28	(-27.95,-35.92)	-31.44	(-0.46,-0.59)	-0.51				
Right Building Wall	Line 29	(-25.86,-34.42)	-29.94	(-0.42,-0.56)	-0.49	0.952805	0.00172952	0.000381414	-0.293945
	Line 30	(-30.30,-35.45)	-32.41	(-0.49,-0.58)	-0.53				
Leeward Face	Line 31	(-12.16,-44.55)	-30.69	(-0.20,-0.73)	-0.50	-0.00496921	-5.57507	-1.91784	0.00122862
	Line 32	(-11.55,-45.06)	-25.81	(-0.19,-0.74)	-0.42				
	Line 33	(-12.36,-42.52)	-26.11	(-0.20,-0.69)	-0.43				
	Line 34	(-14.12,-41.51)	-27.30	(-0.23,-0.68)	-0.45				
	Line 35	(-14.71,-38.02)	-27.81	(-0.24,-0.62)	-0.45				
	Line 36	(-13.70,-35.10)	-27.41	(-0.22,-0.57)	-0.45				
	Line 37	(-11.80,-35.37)	-26.07	(-0.19,-0.58)	-0.43				

Table 4.8: Pressure contour of faces at 45-degree wind inclination

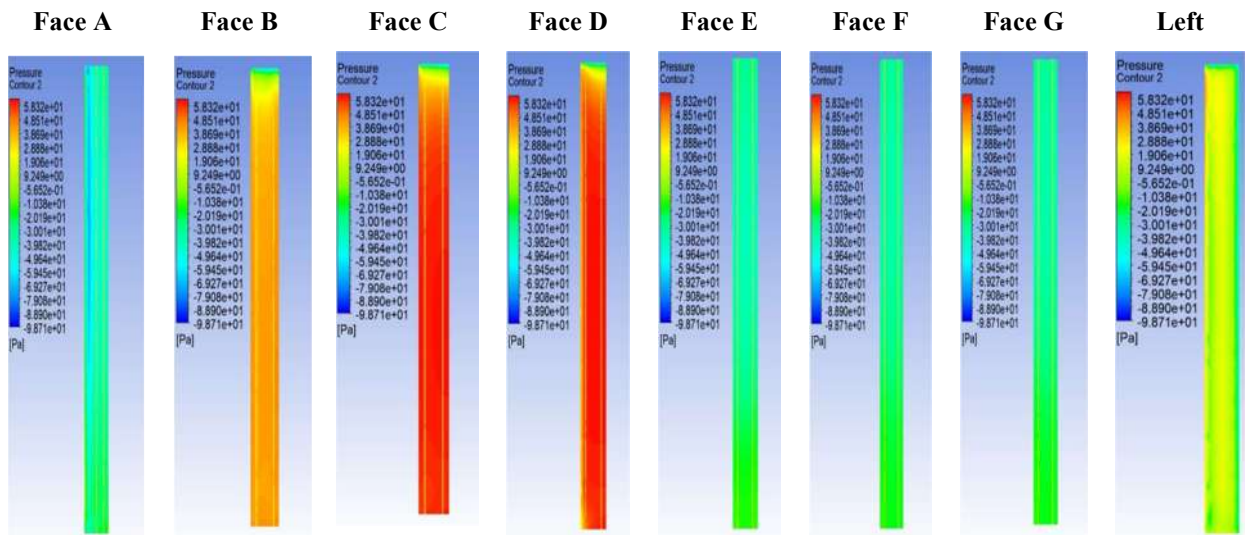




- Case 5 – The incident wind angle is 60°

The range of average pressure values for the wind inclination angle of 60° (Table 4.9) is between [-59.35, 58.14]. The maximum positive and negative pressure values of 58.14 and -59.35, respectively, occur on **Wall 3** and **Face A**. This suggests that Wall 3 and Face A experience the highest pressure and suction forces, respectively, from the fluid in this orientation. The range of pressure coefficient C_p lies in the range ϵ [-0.97, 0.95]. The maximum positive and negative values of 0.95 and -0.97 occur on **Wall 3** and **Face A** (Table 4.10).

Table 4.9: Pressure contour of faces at 60-degree wind inclination



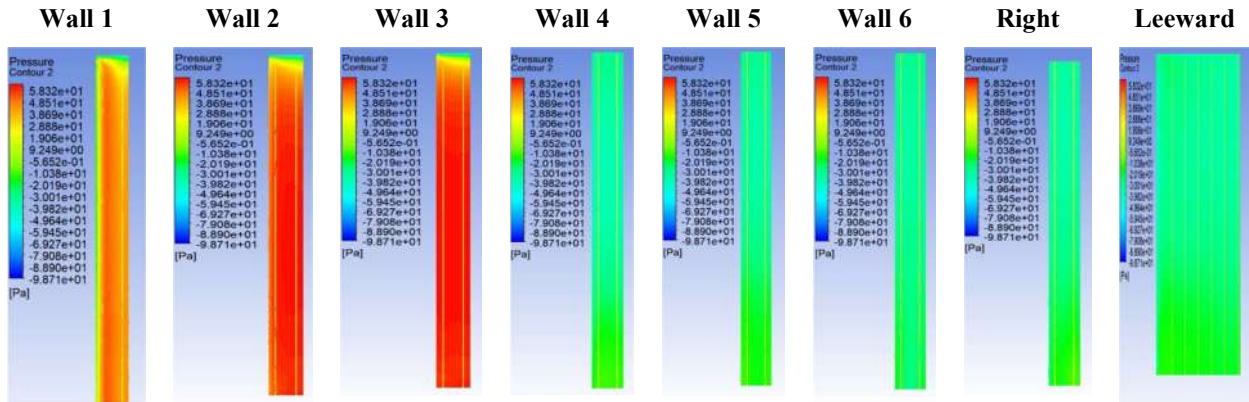


Table 4.10: Pressure and Cp values for each face of the Model at wind incidence of 60 degree

Wind Inclination Angle 60 deg						Force(N)		Moment(N-m)	
Faces/Wall	Line	Range of Pressure	Average value of Pressure	Range of Cp	Average Value of Cp	Fx	Fz	Mx	Mz
Face A	Line 0	(-22.33,-47.85)	-38.99	(-0.36,-0.78)	-0.64	-0.00106854	1.18131	0.391562	0.000313936
	Line 1	(-31.70,-71.71)	-59.35	(-0.52,-1.17)	-0.97				
Wall 1	Line 16	(-17.80,-44.06)	-36.46	(-0.29,-0.72)	-0.60	1.19552	0.00141352	0.00030508	-0.341342
	Line 2	(49.07,-49.23)	45.32	(0.80,-0.80)	0.74				
Face B	Line 3	(44.21,-54.59)	39.03	(0.72,-0.89)	0.64	-0.000941723	-1.17709	-0.323163	0.00025531
	Line 4	(44.70,-57.25)	39.86	(0.73,-0.93)	0.65				
Wall 2	Line 5	(43.12,-49.93)	36.20	(0.70,-0.82)	0.59	1.66213	0.000851663	0.000199159	-0.469147
	Line 6	(62.24,-57.54)	56.10	(1.02,-0.94)	0.92				
Face C	Line 7	(62.24,-57.54)	56.10	(1.02,-0.94)	0.92	0.000260762	-1.68708	-0.471963	-0.000179654
	Line 8	(62.08,-55.47)	55.86	(1.01,-0.91)	0.91				
Wall 3	Line 9	(61.05,-61.27)	54.81	(1.00,-1.00)	0.89	1.7446	6.81E-05	-7.53E-06	-0.495789
	Line 10	(63.19,-65.92)	58.14	(1.03,-1.08)	0.95				
Face D	Line 11	(62.95,-58.41)	57.22	(1.03,-0.95)	0.93	-0.00119508	-1.67905	-0.482852	0.000164266
	Line 12	(63.06,-46.95)	57.44	(1.03,-0.77)	0.94				
Left Building Wall	Line 13	(61.02,-41.45)	56.95	(1.00,-0.68)	0.93	0.177464	-0.00468213	-0.00137988	-0.0587663
	Line 14	(18.46,-50.25)	0.53	(0.30,-0.82)	0.01				
Wall 4	Line 15	(5.66,-30.44)	1.78	(0.09,-0.50)	0.03	0.882085	0.000709176	-0.000106018	-0.303568
	Line 17	(-12.41,-39.63)	-30.53	(-0.20,-0.65)	-0.50				
Face E	Line 18	(-12.46,-38.98)	-30.21	(-0.20,-0.64)	-0.49	-0.000195642	0.885898	0.304207	0.000251897
	Line 19	(-13.32,-39.34)	-30.61	(-0.22,-0.64)	-0.50				
Wall 5	Line 20	(-13.53,-41.99)	-31.78	(-0.22,-0.69)	-0.52	0.832707	-0.00034029	-8.69E-05	-0.283072
	Line 21	(-14.00,-35.94)	-27.22	(-0.23,-0.59)	-0.44				
Face F	Line 22	(-15.55,-36.10)	-28.33	(-0.25,-0.59)	-0.46	0.000565673	0.841497	0.000169806	0.000169806
	Line 23	(-15.14,-36.38)	-28.15	(-0.25,-0.59)	-0.46				
Wall 6	Line 24	(-17.16,-36.27)	-28.54	(-0.28,-0.59)	-0.47	0.912307	-0.000971664	-0.000103479	-0.290235
	Line 25	(-22.41,-34.87)	-29.58	(-0.37,-0.57)	-0.48				
Face G	Line 26	(-23.87,-34.86)	-30.22	(-0.39,-0.57)	-0.49	0.000894922	0.922983	0.291601	4.31E-05
	Line 27	(-22.09,-34.73)	-29.39	(-0.36,-0.57)	-0.48				
Right Building Wall	Line 28	(-25.79,-34.95)	-30.96	(-0.42,-0.57)	-0.51	0.856606	0.000953916	0.000267374	-0.289647
	Line 29	(-17.78,-35.57)	-29.17	(-0.29,-0.58)	-0.48				
Leeward Face	Line 30	(-10.65,-35.42)	-27.43	(-0.17,-0.58)	-0.45	-0.00698799	-5.85642	-1.94289	0.00141768
	Line 31	(-18.65,-41.74)	-34.73	(-0.30,-0.68)	-0.57				
	Line 32	(-14.94,-36.09)	-25.47	(-0.24,-0.59)	-0.42				
	Line 33	(-16.01,-37.08)	-27.03	(-0.26,-0.61)	-0.44				
	Line 34	(-16.82,-36.01)	-27.58	(-0.27,-0.59)	-0.45				
	Line 35	(-18.22,-34.22)	-28.15	(-0.30,-0.56)	-0.46				
	Line 36	(11.00,-34.57)	-28.87	(-0.32,-0.56)	-0.47				
Line 37	(-19.44,-35.30)	-29.15	(-0.32,-0.58)	-0.48					

- Case 6 – The incident wind angle is 75°

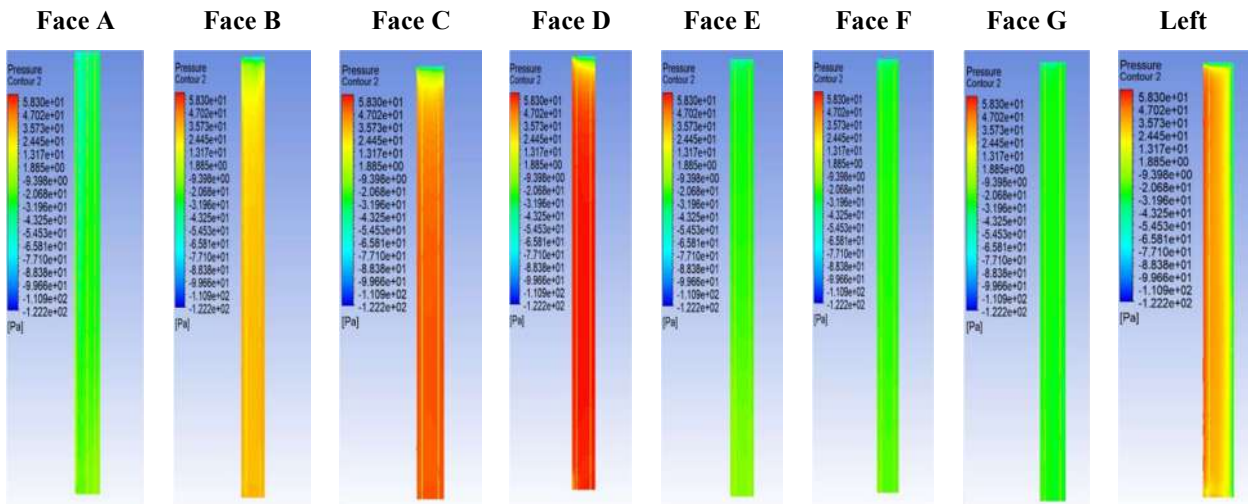
The range of average pressure values for the wind inclination angle of 75° (Table 4.11) is between [-68.97, 58.66]. The maximum positive and negative pressure values of 58.66 and -68.97, respectively, occur on **Face D** and **Leeward face**. The range of Cp lies in the range

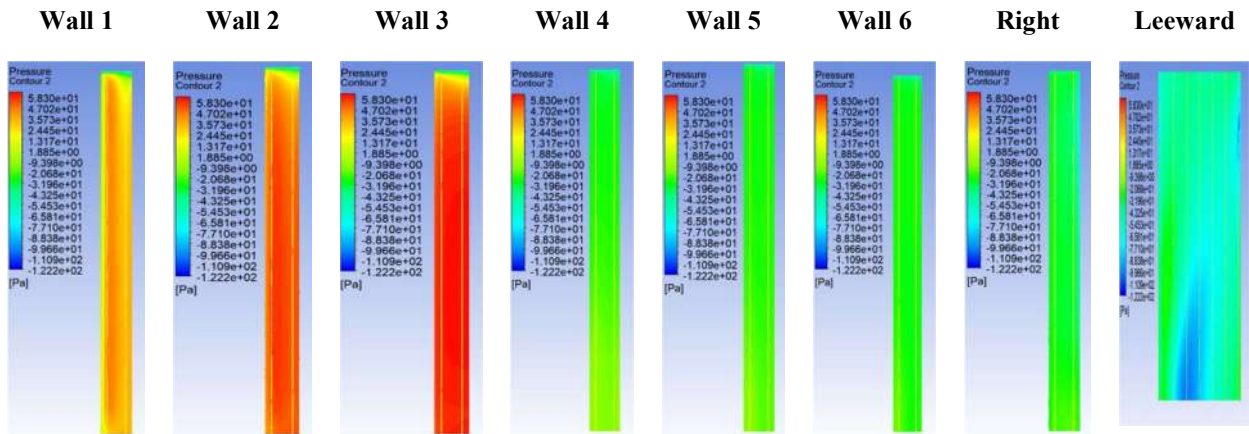
ϵ [-1.13, 0.96]. The maximum positive and negative values of 0.96 and -1.13 occur on **Face D** and **Leeward Face** (Table 4.12).

Table 4.11: Pressure and Cp values for each face of the Model at wind incidence of 75 degree

Wind Inclination Angle 75 deg						Force(N)		Moment(N-m)	
Faces/Wall	Line	Range of Pressure	Average value of Pressure	Range of Cp	Average Value of Cp	Fx	Fz	Mx	Mz
Face A	Line 0	(-15.83,-48.02)	-26.77	(-0.26,-0.78)	-0.44	-0.0013636	0.812054	0.273918	0.000339297
	Line 1	(-19.46,-72.14)	-39.88	(-0.32,-1.18)	-0.65				
	Line 16	(-12.31,-45.77)	-27.30	(-0.20,-0.75)	-0.45				
Wall 1	Line 2	(45.24,-59.76)	40.82	(0.74,-0.98)	0.67	0.984522	0.000770884	9.72E-05	-0.277463
	Line 3	(34.89,-65.87)	28.55	(0.57,-1.08)	0.47				
Face B	Line 4	(35.97,-67.04)	30.11	(0.59,-1.09)	0.49	-0.00131003	-0.872089	-0.228755	0.000377646
	Line 5	(34.34,-65.49)	25.12	(0.56,-1.07)	0.41				
Wall 2	Line 6	(53.55,-59.87)	46.98	(0.87,-0.98)	0.77	1.48244	0.000198568	-2.40E-05	-0.415357
	Line 7	(53.55,-59.87)	46.98	(0.87,-0.98)	0.77				
Face C	Line 8	(54.10,-67.53)	47.47	(0.88,-1.10)	0.77	-0.000707508	-1.42375	-0.386146	0.000132138
	Line 9	(53.10,-62.10)	45.36	(0.87,-1.01)	0.74				
Wall 3	Line 10	(61.80,-60.11)	56.70	(1.01,-0.98)	0.93	1.72184	0.000662372	0.000212496	-0.485981
	Line 11	(63.27,-65.40)	57.23	(1.03,-1.07)	0.93				
Face D	Line 12	(63.14,-70.12)	56.98	(1.03,-1.14)	0.93	-0.000097318	-1.74609	-0.495125	-0.00017202
	Line 13	(63.91,-41.25)	58.66	(1.04,-0.67)	0.96				
Left Building Wall	Line 14	(47.84,-58.81)	39.20	(0.78,-0.96)	0.64	0.817472	-0.00488936	-0.00136086	-0.244416
	Line 15	(17.22,-59.35)	13.58	(0.28,-0.97)	0.22				
Wall 4	Line 17	(-10.24,-48.33)	-21.20	(-0.17,-0.79)	-0.35	0.661748	-0.000440025	-0.000279231	-0.225045
	Line 18	(-13.80,-55.92)	-23.32	(-0.23,-0.91)	-0.38				
Face E	Line 19	(-12.04,-55.66)	-22.33	(-0.20,-0.91)	-0.36	0.000617594	0.686333	0.226919	-2.41E-05
	Line 20	(-14.29,-46.15)	-22.99	(-0.23,-0.75)	-0.38				
Wall 5	Line 21	(-13.57,-45.39)	-23.06	(-0.22,-0.74)	-0.38	0.733327	-0.000710056	-0.000224415	-0.236281
	Line 22	(-19.45,-0.32)	-25.33	(-0.50,-0.82)	-0.41				
Face F	Line 23	(-17.66,-0.29)	-24.12	(-0.50,-0.83)	-0.39	0.000622423	0.762486	0.238788	5.22447E-05
	Line 24	(-19.03,-46.72)	-24.77	(-0.31,-0.76)	-0.40				
Wall 6	Line 25	(-17.97,-43.08)	-25.82	(-0.29,-0.70)	-0.42	0.826801	-0.000940745	-0.000154549	-0.254069
	Line 26	(-27.09,-46.52)	-28.64	(-0.44,-0.76)	-0.47				
Face G	Line 27	(-24.77,-47.76)	-26.94	(-0.40,-0.78)	-0.44	0.000973748	0.872422	0.257318	0.000134369
	Line 28	(-26.42,-39.77)	-28.41	(-0.43,-0.65)	-0.46				
Right Building Wall	Line 29	(-21.84,-0.36)	-30.40	(-0.42,-0.70)	-0.50	0.924083	-0.00129752	-0.000518599	-0.302556
	Line 30	(-20.37,-40.39)	-33.02	(-0.33,-0.66)	-0.54				
Leeward Face	Line 31	(-28.52,-68.34)	-48.98	(-0.47,-1.12)	-0.80	-0.0372391	-11.8961	-3.36087	0.0101812
	Line 32	(-33.74,-69.55)	-46.05	(-0.55,-1.14)	-0.75				
	Line 33	(-42.16,-102.20)	-64.99	(-0.69,-1.67)	-1.06				
	Line 34	(-46.28,-88.89)	-68.97	(-0.76,-1.45)	-1.13				
	Line 35	(-45.49,-73.28)	-62.66	(-0.74,-1.20)	-1.02				
	Line 36	(-41.09,-63.06)	-54.71	(-0.67,-1.03)	-0.89				
	Line 37	(-34.08,-86.32)	-55.68	(-0.56,-1.41)	-0.91				

Table 4.12: Pressure contour of faces at 75-degree wind inclination





- Case 7 – The incident wind angle is 90°

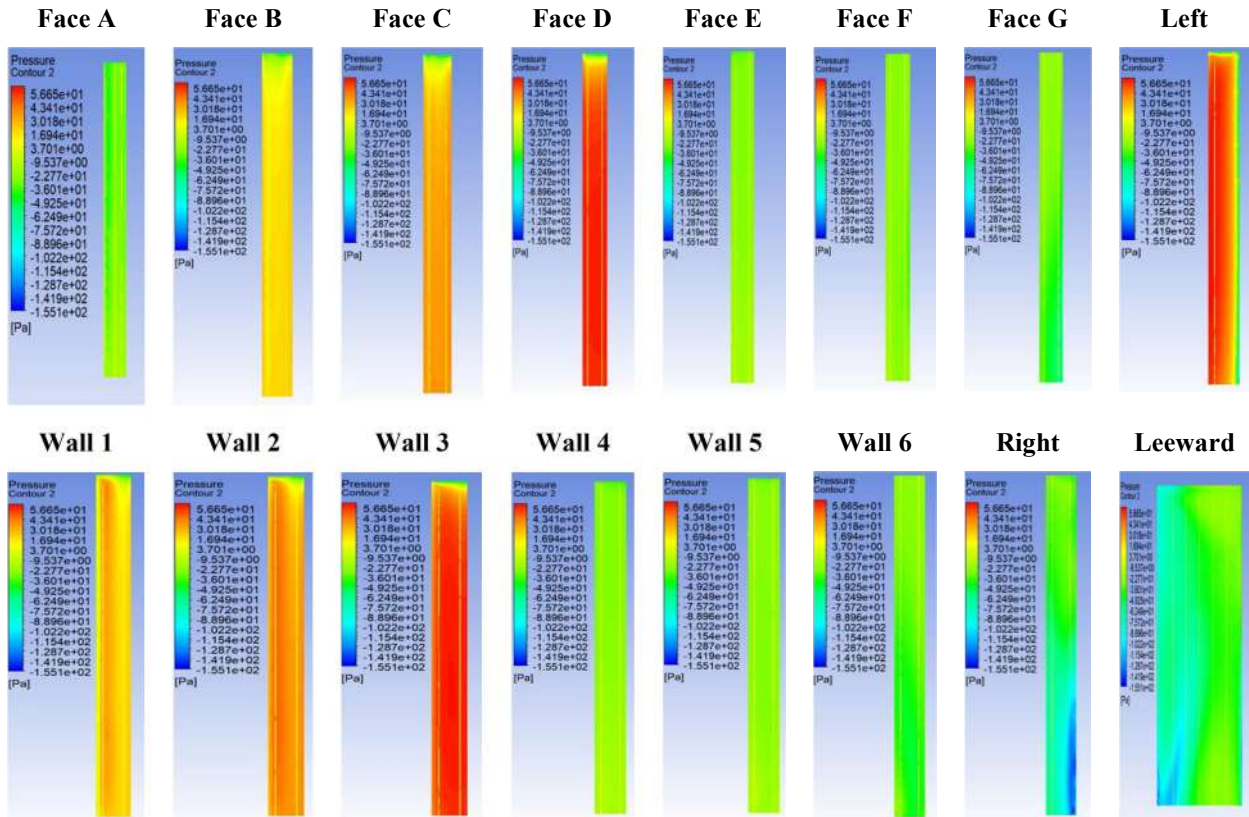
Table 4.13: Pressure and Cp values for each face of the Model at wind incidence of 90 degree

Wind Inclination Angle 90 deg						Force(N)		Moment(N-m)	
Faces/Wall	Line	Range of Pressure	Average value of Pressure	Range of Cp	Average Value of Cp	Fx	Fz	Mx	Mz
Face A	Line 0	(-19.3,-36.47)	-28.39	(-0.32,-0.6)	-0.46	-0.00110144	0.892786	0.286836	0.000344049
	Line 1	(-23.70,-49.58)	-40.91	(-0.39,-0.81)	-0.67				
	Line 16	(21.00,-37.71)	-30.25	(-0.34,-0.62)	-0.49				
Wall 1	Line 2	(39.87,-37.07)	32.56	(0.65,-0.61)	0.53	0.65043	0.000359911	-3.49E-05	-0.185296
	Line 3	(21.64,-50.13)	15.66	(0.35,-0.82)	0.26				
Face B	Line 4	(22.27,-54.89)	18.06	(0.6,-0.90)	0.29	-0.00144172	-0.488035	-0.120245	0.000432496
	Line 5	(20.19,-38.63)	11.74	(0.33,-0.63)	0.19				
Wall 2	Line 6	(38.01,-46.49)	30.66	(0.62,-0.76)	0.50	1.0853	-0.000481018	-0.000240869	-0.303877
	Line 7	(38.01,-46.49)	30.66	(0.62,-0.76)	0.50				
Face C	Line 8	(38.39,-61.02)	32.58	(0.63,-1.00)	0.53	-0.00143662	-0.923549	-0.23895	0.000380596
	Line 9	(36.92,-52.70)	28.01	(0.60,-0.86)	0.46				
Wall 3	Line 10	(56.97,-59.55)	52.88	(0.93,-0.97)	0.86	1.6058	0.000870698	0.00023076	-0.453918
	Line 11	(60.71,-63.66)	54.47	(0.99,-1.04)	0.89				
Face D	Line 12	(60.61,-70.61)	54.21	(0.99,-1.15)	0.89	-6.66E-05	-1.624	-0.447355	-8.21E-05
	Line 13	(59.68,-57.35)	52.83	(0.97,-0.94)	0.86				
Left Building Wall	Line 14	(62.35,-57.07)	58.54	(1.02,-0.93)	0.96	1.17301	-0.00366493	-0.000933282	-0.355847
	Line 15	(30.76,-27.09)	24.85	(0.50,-0.44)	0.41				
Wall 4	Line 17	(-14.60,-38.75)	-23.51	(-0.24,-0.63)	-0.38	0.722323	-5.20E-05	-0.000227397	-0.236834
	Line 18	(-17.43,-43.13)	-25.23	(-0.28,-0.70)	-0.41				
Face E	Line 19	(-17.52,-41.65)	-24.89	(-0.29,-0.68)	-0.41	0.000409233	0.741353	0.238221	-5.12E-05
	Line 20	(-17.69,-35.80)	24.72	(-0.29,-0.58)	-0.40				
Wall 5	Line 21	(-14.12,-34.72)	-24.64	(-0.23,-0.57)	-0.40	0.775275	-0.00107119	-0.000293089	-0.243667
	Line 22	(-20.36,-36.88)	-26.36	(-0.33,-0.60)	-0.43				
Face F	Line 23	(-18.94,-31.76)	-24.56	(-0.31,-0.52)	-0.40	0.00157545	0.80691	0.243575	-8.81E-05
	Line 24	(-23.41,-30.10)	-27.09	(-0.38,-0.49)	-0.44				
Wall 6	Line 25	(-25.92,-49.04)	-37.69	(-0.42,-0.80)	-0.62	1.05737	-0.00223886	-0.000394168	-0.294175
	Line 26	(-24.01,-48.76)	-35.33	(-0.39,-0.80)	-0.58				
Face G	Line 27	(-23.93,-39.33)	-31.10	(-0.39,-0.64)	-0.51	0.00288743	1.11741	0.292762	-0.000347812
	Line 28	(-24.60,-56.80)	-39.03	(-0.40,-0.93)	-0.64				
Right Building Wall	Line 29	(-30.50,-76.24)	-58.47	(-0.50,-1.24)	-0.47	1.88713	-0.0031287	-0.00073935	-0.465629
	Line 30	(-29.26,-134.51)	-73.77	(-0.48,-2.20)	-1.20				
Leeward Face	Line 31	(-78.06,-123.77)	-91.96	(-1.27,-2.02)	-1.50	-0.00239689	-10.7214	-3.09803	-0.00102201
	Line 32	(-60.65,-113.04)	-75.93	(-0.99,-1.85)	-1.24				
	Line 33	(-40.01,-90.07)	-67.17	(-0.65,-1.47)	-1.10				
	Line 34	(-29.45,-62.31)	-47.60	(-0.48,-1.02)	-0.78				
	Line 35	(-24.25,-46.19)	-36.07	(-0.40,-0.75)	-0.59				
	Line 36	(-22.81,-39.57)	-32.13	(-0.37,-0.65)	-0.52				
	Line 37	(-26.75,-54.56)	-41.77	(-0.44,-0.89)	-0.68				

The range of average pressure values for the wind inclination angle of 90° (Table 4.13) is between [-91.96, 58.54]. The maximum positive and negative pressure values of 58.54 and -91.96, respectively, occur on the **Left building wall** and **Leeward face**. The range of pressure coefficient Cp lies in the range ε [-1.50, 0.96]. The maximum positive and

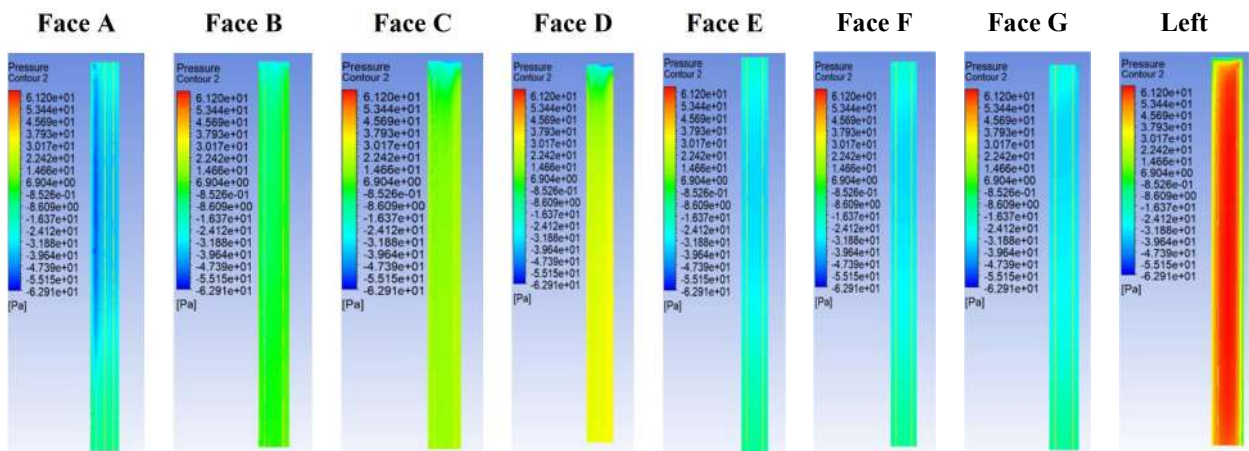
negative values of 0.96 and -1.50 occur on the Left building wall and Leeward Face (Table 4.14).

Table 4.14: Pressure contour of faces at 90-degree wind inclination



- Case 8 – The incident wind angle is 105°

Table 4.15: Pressure contour of faces at 105-degree wind inclination



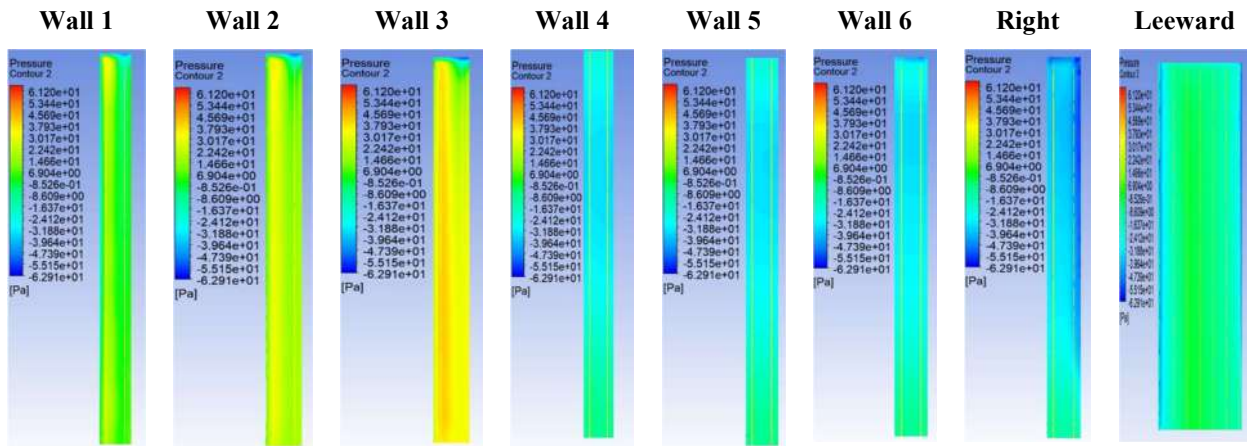


Table 4.16: Pressure and Cp values for each face of the Model at wind incidence of 105 degree

Wind Inclination Angle 105 deg						Force(N)		Moment(N-m)	
Faces/Wall	Line	Range of Pressure	Average value of Pressure	Range of Cp	Average Value of Cp	Fx	Fz	Mx	Mz
Face A	Line 0	(-10.28,-39.10)	-29.58	(-0.17,-0.64)	-0.48	-0.00105353	0.944364	0.318515	0.000336975
	Line 1	(-13.36,-53.87)	-41.44	(-0.22,-0.88)	-0.68				
	Line 16	(-11.78,-40.33)	-30.95	(-0.19,-0.66)	-0.51				
Wall 1	Line 2	(36.31,-24.26)	18.51	(0.59,-0.40)	0.30	0.157896	-0.00017348	-0.000183823	-0.0371026
	Line 3	(4.83,-45.60)	-2.36	(0.08,-0.74)	-0.04				
Face B	Line 4	(6.42,-32.80)	0.88	(0.10,-0.54)	0.01	-0.00154718	0.0439215	0.035471	0.000455937
	Line 5	(3.95,-26.43)	-6.75	(0.06,-0.43)	-0.11				
Wall 2	Line 6	(17.77,-51.06)	11.60	(0.29,-0.83)	0.19	0.563195	-0.000656774	-0.00028253	-0.156125
	Line 7	(17.77,-51.06)	1.60	(0.29,-0.83)	0.19				
Face C	Line 8	(19.01,-37.69)	14.52	(0.31,-0.62)	0.24	-0.00148632	-0.376467	-0.0860142	0.000385733
	Line 9	(16.36,-31.98)	8.11	(0.27,-0.52)	0.13				
Wall 3	Line 10	(41.99,-26.68)	39.96	(0.69,-0.44)	0.65	0.922618	-0.000511483	-0.000204013	-0.251951
	Line 11	(32.77,-54.81)	24.12	(0.54,-0.89)	0.39				
Face D	Line 12	(33.38,-44.84)	26.56	(0.54,-0.73)	0.43	-0.00151126	-0.727485	-0.177709	0.000338752
	Line 13	(30.67,-25.39)	19.72	(0.50,-0.41)	0.32				
Left Building Wall	Line 14	(57.46,-16.83)	54.30	(0.94,-0.27)	0.89	1.5383	-0.000365437	-2.20E-05	-0.453391
	Line 15	(59.22,-18.52)	56.30	(0.97,-0.30)	0.92				
Wall 4	Line 17	(-7.51,-33.84)	-25.07	(-0.12,-0.55)	-0.41	0.779111	8.83E-05	-0.00026825	-0.267811
	Line 18	(-9.85,-34.64)	-26.28	(-0.16,-0.57)	-0.43				
Face E	Line 19	(-9.73,-34.60)	-26.06	(-0.16,-0.56)	-0.43	0.000267057	0.801235	0.271259	0.000119122
	Line 20	(-10.87,-35.78)	-27.26	(-0.18,-0.58)	-0.45				
Wall 5	Line 21	(-8.23,-34.03)	-25.65	(-0.13,-0.56)	-0.42	0.785907	-1.56E-05	-6.37E-05	-0.267794
	Line 22	(-9.91,-34.68)	-26.40	(-0.16,-0.57)	-0.43				
Face F	Line 23	(-9.83,-34.69)	-26.26	(-0.16,-0.57)	-0.43	0.000214428	0.804858	0.272349	0.000266489
	Line 24	(-10.65,-35.67)	-27.25	(-0.17,-0.58)	-0.44				
Wall 6	Line 25	(-9.33,-0.15)	-26.99	(-39.00,-0.64)	-0.44	0.817607	-9.09E-05	-9.95E-05	-0.278478
	Line 26	(-10.64,-46.97)	-27.44	(-0.15,-0.77)	-0.45				
Face G	Line 27	(-10.56,-35.27)	-26.96	(-0.17,-0.58)	-0.44	0.000350303	0.822878	0.279621	0.000436761
	Line 28	(-10.96,-35.60)	-27.39	(-0.18,-0.58)	-0.45				
Right Building Wall	Line 29	(-12.30,-54.17)	-31.29	(-0.20,-0.88)	-0.51	1.02207	-0.00161662	-0.00025912	-0.346538
	Line 30	(-13.58,-52.34)	-38.45	(-0.22,-0.85)	-0.63				
Leeward Face	Line 31	(-32.17,-45.33)	-42.35	(-0.53,-0.74)	-0.69	0.033986	-2.69277	-0.852284	-0.0109946
	Line 32	(-10.46,-19.67)	-14.75	(-0.17,-0.32)	-0.24				
	Line 33	(-2.23,-20.58)	-4.37	(-0.04,-0.34)	-0.07				
	Line 34	(-2.45,-24.17)	-5.41	(-0.04,-0.39)	-0.09				
	Line 35	(-5.53,-25.85)	-9.17	(-0.09,-0.42)	-0.15				
	Line 36	(-9.55,-32.35)	-15.23	(-0.16,-0.53)	-0.23				
	Line 37	(-14.87,-34.60)	-28.43	(-0.24,-0.56)	-0.46				

The range of average pressure values for the wind inclination angle of 105° (Table 4.15) is between $[-42.35, 56.30]$. The maximum positive and negative pressure values of 56.30 and -42.35, respectively, occur on the **Left building wall** and **Leeward face**. The range of pressure coefficient Cp lies in the range $\epsilon [-0.69, 0.92]$. The maximum positive and

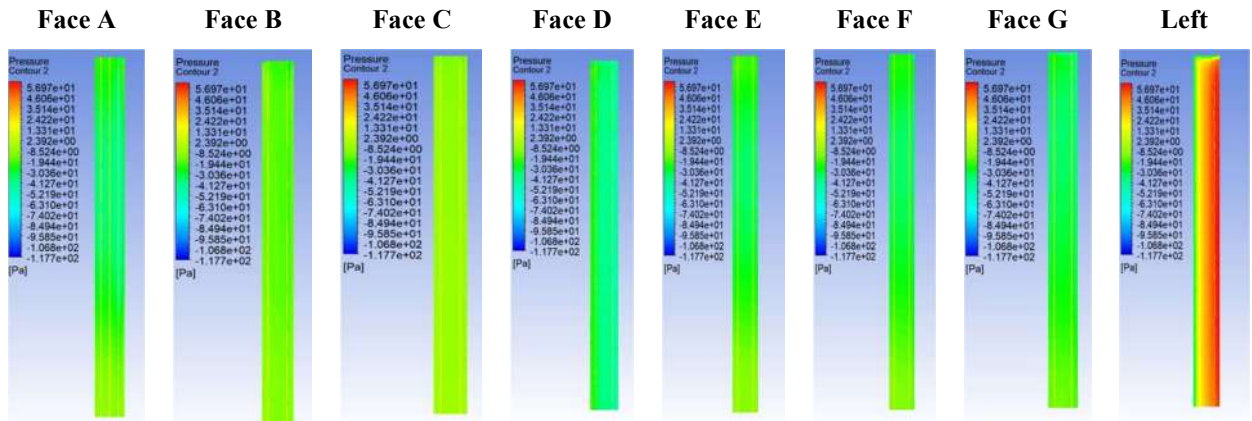
negative values of 0.92 and -0.69 occur on the **Left building wall** and **Leeward Face** (Table 4.16).

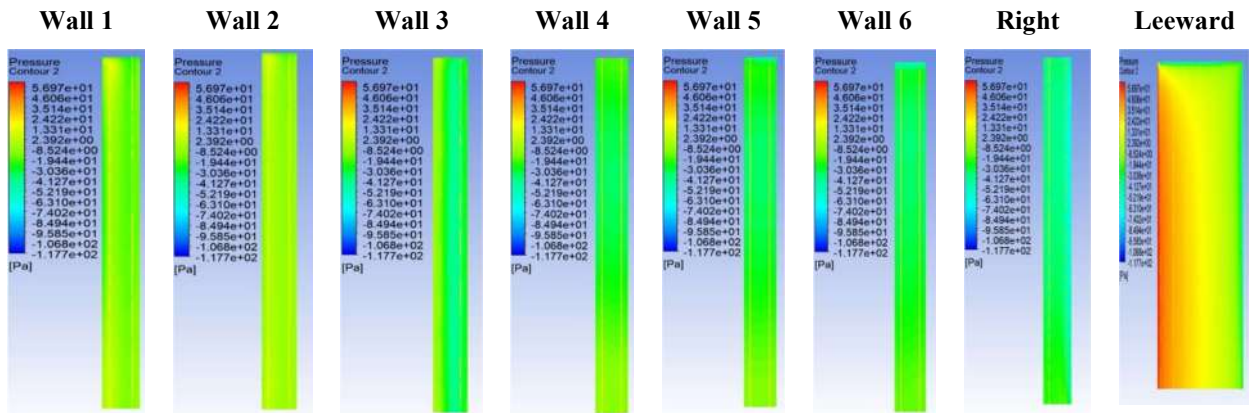
- Case 9 – The incident wind angle is 120°

Table 4.17: Pressure and Cp values for each face of the Model at wind incidence of 120 degree

Wind Inclination Angle 120 deg						Force(N)		Moment(N-m)	
Faces/Wall	Line	Range of Pressure	Average value of Pressure	Range of Cp	Average Value of Cp	Fx	Fz	Mx	Mz
Face A	Line 0	(-10.20,-36.81)	-27.44	(0.30,0.08)	0.22	-0.000676333	0.864719	0.293028	0.000216059
	Line 1	(-11.63,-46.08)	-34.97	(0.38,0.10)	0.29				
	Line 16	(-10.34,-38.00)	-28.26	(0.31,0.38)	0.23				
Wall 1	Line 2	(15.50,-18.73)	-3.37	(0.15,-0.13)	0.03	-0.364636	-0.000383536	-0.000167258	0.116337
	Line 3	(-11.82,-27.92)	-16.60	(0.23,0.10)	0.14				
Face B	Line 4	(-9.97,-22.26)	-14.61	(-0.18,0.08)	0.12	-0.000975659	0.480672	0.154844	0.000262263
	Line 5	(-12.25,-24.77)	-19.18	(0.20,0.10)	0.16				
Wall 2	Line 6	(-6.37,-21.62)	-8.95	(0.18,0.05)	0.07	-0.19132	-0.000377202	-0.000157266	0.0620502
	Line 7	(-6.37,-21.62)	-8.95	(0.18,0.05)	0.07				
Face C	Line 8	(-5.47,-15.60)	-7.76	(0.13,0.04)	0.06	-0.00045522	0.247438	0.0816289	8.98E-05
	Line 9	(-6.27,-16.15)	-9.14	(0.13,0.05)	0.07				
Wall 3	Line 10	(-6.58,-15.22)	-13.08	(0.12,0.05)	0.11	-0.819657	-0.00354145	-0.00101312	0.245179
	Line 11	(-31.35,-37.12)	-35.70	(0.30,0.26)	0.29				
Face D	Line 12	(-25.81,-35.45)	-30.63	(0.29,0.21)	0.25	-0.00322048	1.13072	0.337691	0.000895039
	Line 13	(-39.14,-49.01)	-44.91	(0.40,0.32)	0.37				
Left Building Wall	Line 14	(18.27,-37.94)	14.81	(0.31,-0.15)	-0.12	0.95164	0.00428834	0.00125295	-0.285428
	Line 15	(58.57,-35.23)	54.45	(0.29,-0.48)	-0.45				
Wall 4	Line 17	(-9.34,-33.90)	-24.51	(0.28,0.08)	0.20	0.753782	-3.05119E-06	-0.000239529	-0.256064
	Line 18	(-10.65,-34.53)	-25.21	(0.28,0.09)	-0.21				
Face E	Line 19	(-10.50,-34.51)	-25.03	(0.28,0.09)	0.21	0.000291687	0.765836	0.258543	7.94E-05
	Line 20	(-11.39,-35.17)	-25.69	(0.29,0.09)	0.21				
Wall 5	Line 21	(-13.22,-37.01)	-26.90	(0.30,0.11)	0.22	0.80669	-0.000353058	-0.0001375	-0.271152
	Line 22	(-12.72,-48.24)	-27.01	(0.40,0.10)	0.22				
Face F	Line 23	(-12.49,-34.88)	-26.30	(0.29,0.10)	0.22	0.000626066	0.808011	0.271033	0.000147233
	Line 24	(-13.90,-35.27)	-27.08	(0.29,0.11)	0.22				
Wall 6	Line 25	(-17.21,-54.48)	-30.48	(0.45,0.14)	0.25	0.885173	-0.000199424	1.97307E-05	-0.294422
	Line 26	(-16.12,-63.47)	-29.21	(0.52,0.13)	0.24				
Face G	Line 27	(-15.79,-35.83)	-28.47	(0.29,0.13)	0.23	0.000697018	0.870537	0.290549	0.000356353
	Line 28	(-16.62,-39.23)	-28.00	(0.32,0.14)	0.24				
Right Building Wall	Line 29	(-24.41,-40.69)	-36.12	(0.33,0.20)	0.30	1.16764	-0.00175174	-0.000334874	-0.376807
	Line 30	(-22.86,-53.31)	-44.33	(0.44,0.19)	0.36				
Leeward Face	Line 31	(54.90,-42.06)	41.68	(0.34,-0.45)	-0.34	0.0434259	3.19298	0.800796	-0.013101
	Line 32	(37.26,-62.07)	25.12	(0.51,-0.31)	-0.21				
	Line 33	(28.01,-53.15)	17.85	(0.44,-0.23)	-0.15				
	Line 34	(19.95,-59.34)	10.33	(0.49,-0.16)	-0.08				
	Line 35	(11.85,-49.53)	4.21	(0.41,-0.10)	-0.03				
	Line 36	(2.11,-40.56)	-4.09	(0.33,-0.02)	0.03				
	Line 37	(-17.68,-30.11)	-25.88	(0.25,0.14)	0.21				

Table 4.18: Pressure and Cp values for each face of the Model at wind incidence of 120 degree



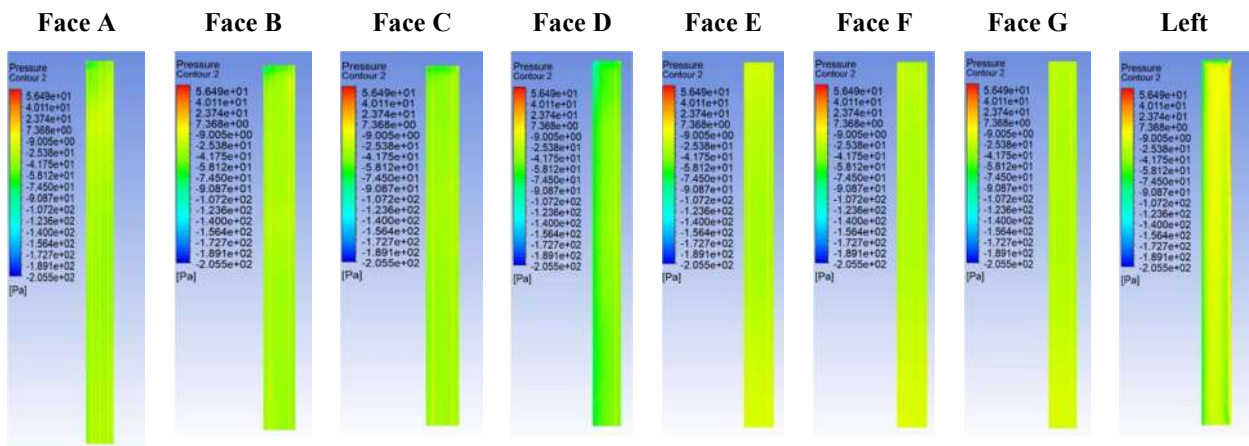


The range of average pressure values for the wind inclination angle of 120° (Table 4.17) is between [-44.91, 54.45]. The maximum positive and negative pressure values of 54.45 and -44.91, respectively, occur on the **Left building wall** and **face D**. The range of pressure coefficient C_p lies in the range ϵ [-0.45, 0.37]. The maximum positive and negative values of 0.37 and -0.45 occur on the Left building wall and face D (Table 4.18).

- Case 10 – The incident wind angle is 135°

The range of average pressure values for the wind inclination angle of 135° (Table 4.19) is between [-65.24, 62.83]. The maximum positive and negative pressure values of 62.83 and -65.24, respectively, occur on the **Leeward face** and **face D**. The range of pressure coefficient C_p lies in the range ϵ [-1.07, 1.03]. The maximum positive and negative values of 1.03 and -1.07 occur on Lee ward’s face and face D (Table 4.20).

Table 4.19: Pressure and C_p values for each face of the Model at wind incidence of 135 degree



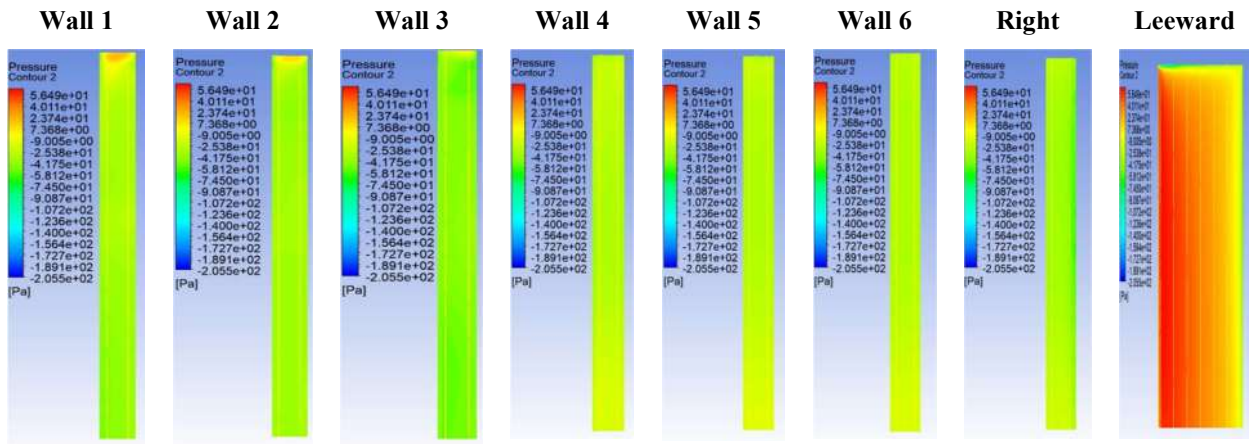


Table 4.20: Pressure and Cp values for each face of the Model at wind incidence of 135 degree

Wind Inclination Angle 135 deg						Force (N)		Moment (N-m)	
Faces/Wall	Line	Range of Pressure	Average value of Pressure	Range of Cp	Average Value of Cp	Fx	Fz	Mx	Mz
Face A	Line 0	(-23.68,-55.43)	-36.04	(-0.39,-0.90)	-0.59	-0.00222453	1.03863	0.321646	0.000468081
	Line 1	(-25.42,-72.07)	-37.27	(-0.42,-1.18)	-0.61				
	Line 16	(-23.48,-46.35)	-37.51	(-0.38,-0.76)	-0.61				
Wall 1	Line 2	(14.15,-48.43)	-36.25	(0.23,-0.79)	-0.59	-1.0663	0.000828753	0.00032875	0.286199
	Line 3	(15.27,-40.95)	-34.08	(0.25,-0.67)	-0.56				
Face B	Line 4	(-23.69,-54.05)	-35.95	(-0.39,-0.88)	-0.59	-0.000406917	1.08947	0.326571	0.000304096
	Line 5	(-31.00,-81.37)	-37.18	(-0.51,-1.33)	-0.61				
Wall 2	Line 6	(10.96,-42.26)	-36.29	(0.18,-0.69)	-0.59	-1.10211	0.000710363	0.000284749	0.322811
	Line 7	(10.96,-42.26)	-36.29	(0.18,-0.69)	-0.59				
Face C	Line 8	(-34.89,-59.09)	-38.01	(-0.57,-0.96)	-0.62	-0.000634276	1.16295	0.358849	0.000271462
	Line 9	(-34.61,-70.75)	-40.15	(-0.57,-1.16)	-0.66				
Wall 3	Line 10	(-19.48,-55.21)	-49.10	(-0.32,-0.90)	-0.80	-1.38978	-0.000951382	-8.27E-05	0.407767
	Line 11	(2.84,-55.42)	-46.35	(0.05,-0.90)	-0.76				
Face D	Line 12	(-40.69,-72.75)	-46.97	(-0.66,-1.19)	-0.77	-0.00196304	1.59342	0.483296	0.000514394
	Line 13	(-59.18,-88.34)	-65.24	(-0.97,-1.44)	-1.07				
Left Building Wall	Line 14	(-20.27,-80.63)	-24.96	(-0.33,-1.32)	-0.41	-0.654443	0.00565102	0.00173668	0.171716
	Line 15	(-9.07,-94.35)	-34.56	(-0.15,-1.54)	-0.56				
Wall 4	Line 17	(-14.33,-0.23)	-25.54	(-33.34,-0.54)	-0.42	0.779587	0.000512361	-0.000113156	-0.253177
	Line 18	(-15.27,-35.00)	-26.46	(-0.25,-0.57)	-0.43				
Face E	Line 19	(-15.79,-34.51)	-27.04	(-0.26,-0.56)	-0.44	2.08E-06	0.800015	0.257616	0.000126065
	Line 20	(-15.73,-35.19)	-27.56	(-0.26,-0.57)	-0.45				
Wall 5	Line 21	(-14.20,-35.14)	-26.20	(-0.23,-0.27)	-0.43	0.79745	-1.06E-05	-5.91E-05	-0.260057
	Line 22	(-14.17,-35.44)	-26.36	(-0.23,-0.58)	-0.43				
Face F	Line 23	(-14.30,-34.32)	-26.66	(-0.23,-0.56)	-0.44	0.000251514	0.808818	0.265969	0.000251448
	Line 24	(-14.45,-34.84)	-27.08	(-0.24,-0.57)	-0.44				
Wall 6	Line 25	(-15.88,-31.66)	-28.48	(-0.26,-0.54)	-0.47	0.848383	4.10E-05	9.03E-05	-0.275912
	Line 26	(-15.34,-32.57)	-27.45	(-0.25,-0.35)	-0.45				
Face G	Line 27	(-15.24,-32.78)	-27.61	(-0.25,-0.54)	-0.45	0.000367373	0.838631	0.274765	0.000447306
	Line 28	(-15.27,-32.31)	-27.43	(-0.25,-0.53)	-0.45				
Right Building Wall	Line 29	(-21.79,-38.01)	-33.39	(-0.36,-0.62)	-0.55	1.09097	-0.00146323	-0.000222807	-0.345949
	Line 30	(-21.62,-51.19)	-42.66	(-0.35,-0.84)	-0.70				
Leeward Face	Line 31	(62.33,-89.33)	62.83	(1.03,-1.46)	1.03	0.028541	6.63916	1.82298	-0.00874972
	Line 32	(57.56,-81.82)	41.27	(0.96,-1.34)	0.67				
	Line 33	(48.60,-66.02)	34.85	(0.79,-1.08)	0.57				
	Line 34	(39.73,-56.22)	28.23	(0.65,-0.92)	0.46				
	Line 35	(30.04,-42.83)	21.26	(0.49,-0.70)	0.35				
	Line 36	(17.44,-34.11)	10.89	(0.28,-0.56)	0.18				
	Line 37	(-10.24,-29.67)	-17.36	(-0.17,-0.48)	-0.28				

- Case 11 – The incident wind angle is 150°

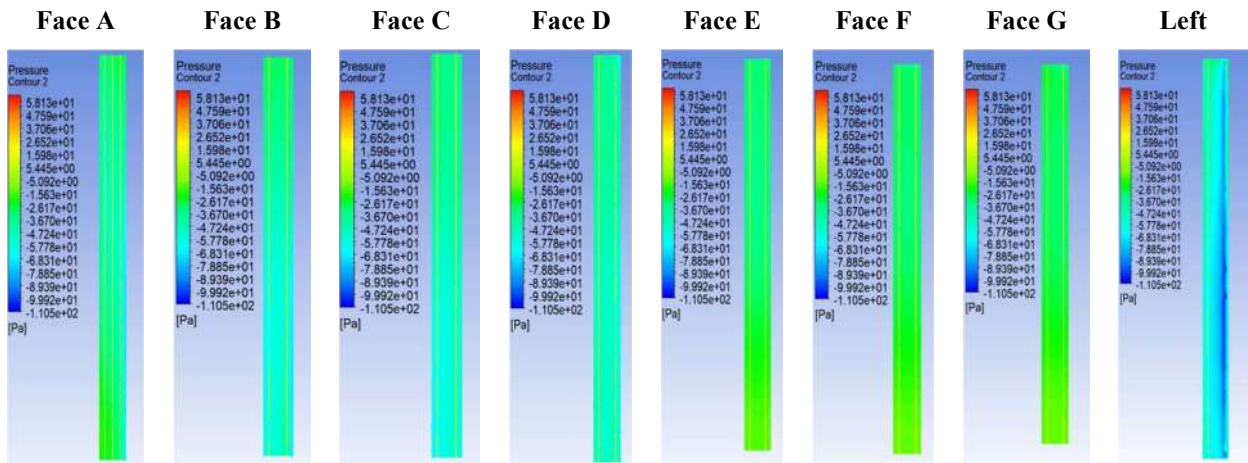
The range of average pressure values for the wind inclination angle of 150° (Table 4.21) is between [-89.17, 50.99]. The maximum positive and negative pressure values of 50.99 and -89.17, respectively, occur on the Leeward face and Left building wall. The range of

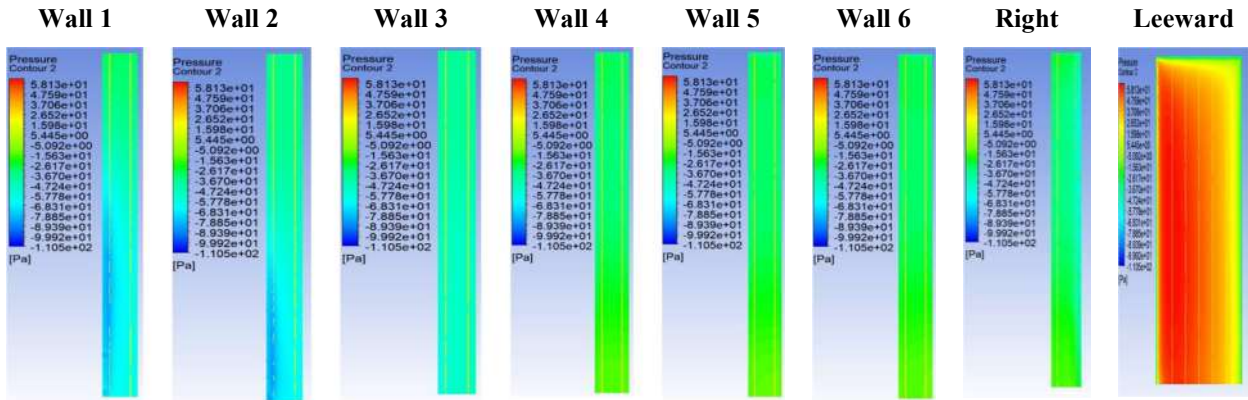
pressure coefficient C_p lies in the range ε [-1.46, 0.83]. The maximum positive and negative values of 0.83 and -1.46 occur on the **Leeward face** and **Left building wall** (Table 4.22).

Table 4.21: Pressure and C_p values for each face of the Model at wind incidence of 150 degree

Wind Inclination Angle 150 deg						Force (N)		Moment (N-m)	
Faces/Wall	Line	Range of Pressure	Average value of Pressure	Range of C_p	Average Value of C_p	Fx	Fz	Mx	Mz
Face A	Line 0	(-27.01,-49.42)	-39.75	(-0.44,-0.81)	-0.65	-0.0036429	1.09636	0.354605	0.000954599
	Line 1	(-29.24,-51.03)	-42.45	(-0.48,-0.83)	-0.69				
	Line 16	(-23.62,-50.14)	-39.49	(-0.39,-0.82)	-0.64				
Wall 1	Line 2	(-29.65,-82.46)	-63.64	(-0.48,-1.35)	-1.04	-1.52768	-4.94E-06	-0.000244971	0.42525
	Line 3	(-30.44,-61.48)	-50.86	(-0.50,-1.00)	-0.83				
Face B	Line 4	(-29.80,-61.25)	-50.99	(-0.49,-1.00)	-0.83	-0.000777762	1.36599	0.389174	1.91E-05
	Line 5	(-30.42,-55.35)	-45.96	(-0.50,-0.90)	-0.75				
Wall 2	Line 6	(-35.36,-63.42)	-49.16	(-0.58,-1.04)	-0.80	-1.58269	0.00080984	0.00012441	0.41385
	Line 7	(-35.36,-63.42)	-49.16	(-0.58,-1.04)	-0.80				
Face C	Line 8	(-33.55,-65.70)	-50.61	(-0.55,-1.07)	-0.83	0.000278097	1.41329	0.387504	-0.000202838
	Line 9	(35.38,-56.54)	-46.30	(-0.58,-0.92)	-0.76				
Wall 3	Line 10	(-36.75,-57.42)	-47.59	(-0.60,-0.94)	-0.78	-1.39709	0.000683915	5.98E-05	0.390423
	Line 11	(-38.68,-49.71)	-45.29	(-0.63,-0.81)	-0.74				
Face D	Line 12	(-37.65,-52.06)	-45.76	(-0.61,-0.85)	-0.75	-0.000573729	1.38927	0.397076	9.53E-05
	Line 13	(-40.12,-54.20)	-48.34	(-0.66,-0.88)	-0.79				
Left Building Wall	Line 14	(-33.65,-65.67)	-57.65	(-0.55,-1.07)	-0.94	-1.94312	-0.00231362	-0.000493223	0.567372
	Line 15	(-60.41,-99.73)	-89.17	(-0.99,-1.63)	-1.46				
Wall 4	Line 17	(-14.52,-35.54)	-26.97	(-0.24,-0.58)	-0.44	0.815257	0.000506794	-8.37E-05	-0.274536
	Line 18	(-14.56,-35.41)	-27.31	(-0.24,-0.58)	-0.45				
Face E	Line 19	(-14.82,-36.09)	-28.28	(-0.24,-0.59)	-0.46	-0.000246776	0.83026	0.281401	0.000255535
	Line 20	(-14.23,-37.28)	-28.58	(-0.23,-0.61)	-0.47				
Wall 5	Line 21	(-13.89,-37.33)	-26.26	(-0.23,-0.61)	-0.43	0.794548	0.000121364	-1.50E-05	-0.265484
	Line 22	(-13.49,-38.14)	-26.10	(-0.22,-0.62)	-0.43				
Face F	Line 23	(-13.57,-37.68)	-26.46	(-0.22,-0.62)	-0.43	-7.19E-05	0.788154	0.265148	0.00033945
	Line 24	(-13.05,-36.93)	-26.13	(-0.21,-0.60)	-0.43				
Wall 6	Line 25	(-13.95,-37.36)	-26.20	(-0.23,-0.61)	-0.43	0.785122	0.000165467	0.000111232	-0.260219
	Line 26	(-13.54,-37.84)	-25.59	(-0.22,-0.62)	-0.42				
Face G	Line 27	(-13.63,-37.44)	-25.82	(-0.22,-0.61)	-0.42	8.62E-05	0.769266	0.257162	0.000492339
	Line 28	(-12.47,-32.93)	-24.83	(-0.20,-0.54)	-0.41				
Right Building Wall	Line 29	(-16.78,-35.53)	-29.72	(-0.27,-0.58)	-0.49	0.983545	-0.00142693	-0.000202417	-0.317419
	Line 30	(-18.72,-48.94)	-39.37	(-0.31,-0.80)	-0.64				
Leeward Face	Line 31	(46.40,-38.80)	31.64	(0.76,-0.63)	0.52	0.0161553	8.63036	2.44182	-0.00501209
	Line 32	(63.39,-39.77)	50.99	(1.03,-0.65)	0.83				
	Line 33	(59.96,-41.18)	47.55	(0.98,-0.67)	0.78				
	Line 34	(53.79,-48.14)	41.40	(0.88,-0.79)	0.68				
	Line 35	(45.36,-37.22)	35.28	(0.74,-0.61)	0.58				
	Line 36	(32.72,-335.62)	24.48	(0.53,-0.58)	0.40				
	Line 37	(1.30,-33.91)	-7.03	(0.02,-0.55)	-0.11				

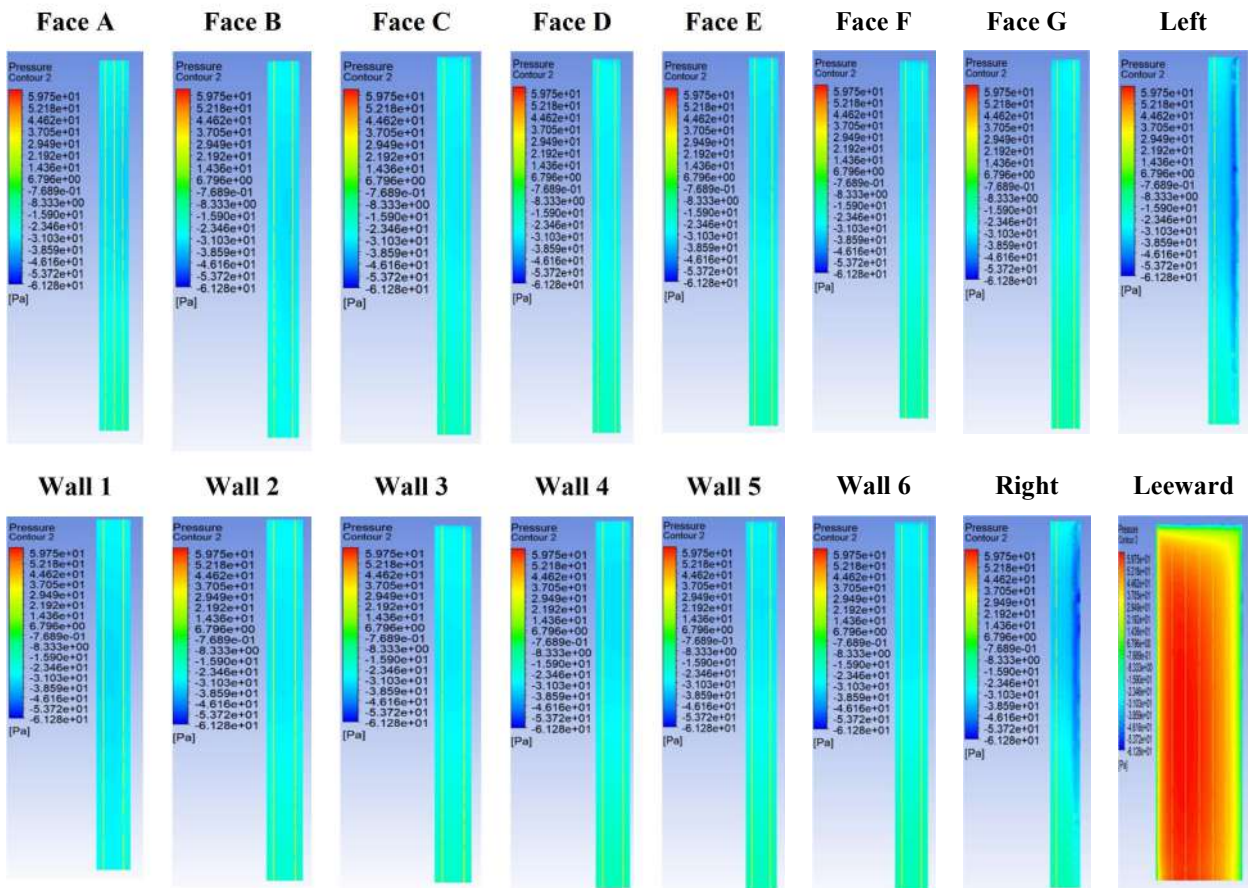
Table 4.22: Pressure and C_p values for each face of the Model at wind incidence of 150 degree





- Case 12 – The incident wind angle is 165°

Table 4.23: Pressure and Cp values for each face of the Model at wind incidence of 165 degree



The range of average pressure values for the wind inclination angle of 165° (Table 4.23) is between [-43.40, 50.22]. The maximum positive and negative pressure values of 50.22 and -43.40, respectively, occur on the Leeward face and Left building wall. The range of

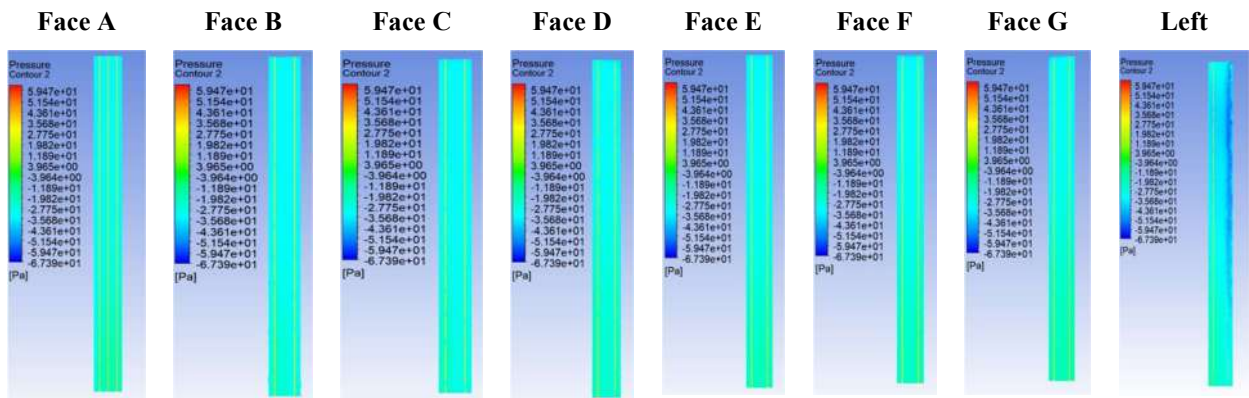
pressure coefficient C_p lies in the range ϵ [-0.71, 0.82]. The maximum positive and negative values of 0.82 and -0.71 occur on the **Leeward face** and **Left building wall** (Table 4.24).

Table 4.24: Pressure and C_p values for each face of the Model at wind incidence of 165 degree

Wind Inclination Angle 165 deg						Force (N)		Moment (N-m)	
Faces/Wall	Line	Range of Pressure	Average value of Pressure	Range of C_p	Average Value of C_p	Fx	Fz	Mx	Mz
Face A	Line 0	(-19.17,-34.25)	-29.18	(-0.31,-0.56)	-0.48	-0.000902573	0.888667	0.286694	0.000156383
	Line 1	(-21.34,-33.78)	-29.48	(-0.35,-0.55)	-0.48				
	Line 16	(-17.84,-36.10)	-30.06	(-0.29,-0.59)	-0.49				
Wall 1	Line 2	(-28.56,-34.05)	-31.74	(-0.47,-0.56)	-0.52	-0.93688	0.000799155	5.69E-05	0.285446
	Line 3	(-26.60,-33.10)	-30.32	(-0.43,-0.54)	-0.50				
Face B	Line 4	(-27.74,-33.69)	-31.12	(-0.45,-0.55)	-0.51	0.00083219	0.9052	0.280667	-0.00027244
	Line 5	(-21.94,-32.80)	-28.89	(-0.36,-0.54)	-0.47				
Wall 2	Line 6	(-20.54,-31.53)	-27.66	(-0.34,-0.51)	-0.45	-0.842589	0.000291331	2.94128e-05	0.26826
	Line 7	(-20.54,-31.53)	-27.66	(-0.34,-0.51)	-0.45				
Face C	Line 8	(-20.92,-32.45)	-28.04	(-0.34,-0.53)	-0.46	0.00029979	0.822625	0.264524	-0.0002933
	Line 9	(-18.30,-32.76)	-26.49	(-0.30,-0.53)	-0.43				
Wall 3	Line 10	(-19.49,-32.43)	-27.49	(-0.32,-0.53)	-0.45	-0.817806	0.00028133	0.000110945	0.262429
	Line 11	(-18.82,-34.21)	-26.79	(-0.31,-0.56)	-0.44				
Face D	Line 12	(-19.10,-34.39)	-27.14	(-0.31,-0.56)	-0.44	1.92E-05	0.797293	0.258885	-0.00039348
	Line 13	(-17.05,-31.67)	-25.40	(-0.28,-0.52)	-0.41				
Left Building Wall	Line 14	(-20.46,-37.65)	-31.76	(-0.33,-0.61)	-0.52	-0.999802	-0.00152583	-0.00026539	0.32101
	Line 15	(-24.18,-52.30)	-43.40	(-0.41,-0.85)	-0.71				
Wall 4	Line 17	(-16.10,-32.88)	-27.01	(-0.26,-0.54)	-0.44	0.816929	0.000209581	-0.00015336	-0.272478
	Line 18	(-16.30,-33.22)	-27.17	(-0.27,-0.54)	-0.44				
Face E	Line 19	(-16.32,-33.31)	-27.30	(-0.27,-0.54)	-0.45	-0.000159922	0.822547	0.275514	0.000166557
	Line 20	(-16.02,-34.24)	-27.78	(-0.26,-0.56)	-0.45				
Wall 5	Line 21	(-16.20,-33.36)	-26.28	(-0.26,-0.54)	-0.43	0.788563	0.000252773	1.09E-05	-0.264772
	Line 22	(-15.94,-33.22)	-26.10	(-0.26,-0.54)	-0.43				
Face F	Line 23	(-16.04,-34.58)	-26.31	(-0.26,-0.56)	-0.43	-0.000249764	0.784299	0.264687	0.000333935
	Line 24	(-15.59,-36.70)	-26.09	(-0.25,-0.60)	-0.43				
Wall 6	Line 25	(-15.67,-37.28)	-25.68	(-0.26,-0.61)	-0.42	0.766093	0.000172928	0.000101943	-0.259047
	Line 26	(-15.29,-34.85)	-25.32	(-0.25,-0.57)	-0.41				
Face G	Line 27	(-15.41,-35.82)	-25.52	(-0.25,-0.58)	-0.42	-6.73E-05	0.752129	0.255607	0.000498572
	Line 28	(-14.30,-32.09)	-24.25	(-0.23,-0.52)	-0.40				
Right Building Wall	Line 29	(-15.80,-37.33)	-28.86	(-0.26,-0.61)	-0.47	0.957686	-0.00169995	-0.00030298	-0.320079
	Line 30	(-19.84,-51.50)	-40.27	(-0.32,-0.84)	-0.66				
Leeward Face	Line 31	(35.89,-16.97)	27.66	(0.59,-0.28)	0.45	0.00860883	9.72395	2.75838	-0.00266892
	Line 32	(61.69,-39.38)	49.69	(1.01,-0.64)	0.81				
	Line 33	(63.35,-44.77)	50.22	(1.03,-0.73)	0.82				
	Line 34	(60.73,-41.06)	48.23	(0.99,-0.67)	0.79				
	Line 35	(55.08,-36.79)	43.89	(0.90,-0.60)	0.72				
	Line 36	(44.42,-33.87)	35.07	(0.73,-0.55)	0.57				
	Line 37	(10.40,-27.67)	3.08	(0.17,-0.45)	0.05				

- Case 13 – The incident wind angle is 180°

Table 4.25: Pressure and C_p values for each face of the Model at wind incidence of 180 degree



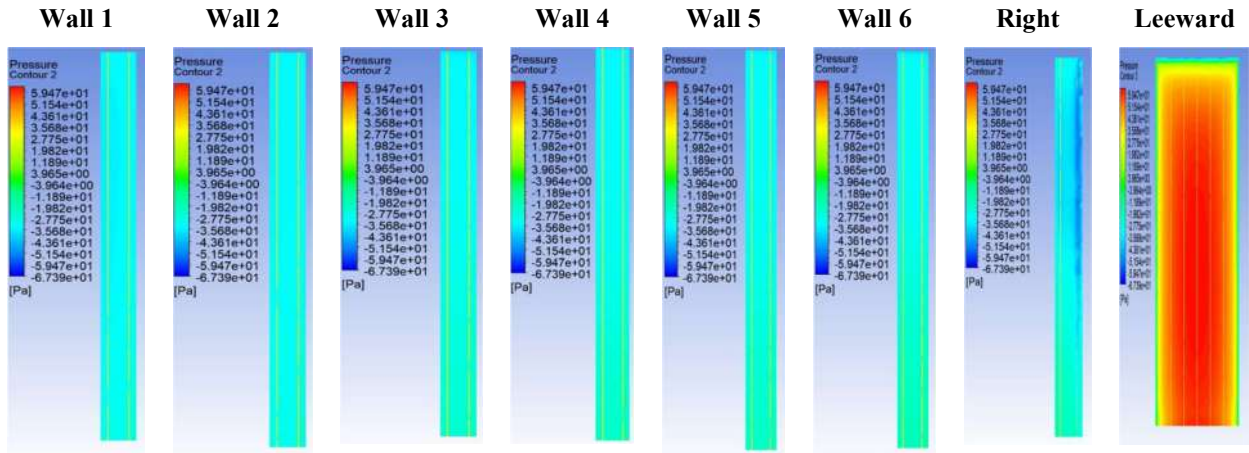


Table 4.26: Pressure and Cp values for each face of the Model at wind incidence of 180 degree

Wind Inclination Angle 180 deg						Force (N)		Moment (N-m)	
Faces/Wall	Line	Range of Pressure	Average value of Pressure	Range of Cp	Average Value of Cp	Fx	Fz	Mx	Mz
Face A	Line 0	(-18.92,-33.41)	-28.45	(-0.31,-0.55)	-0.46	-0.000607276	0.87408	0.283996	0.000148547
	Line 1	(-20.90,-33.41)	-29.00	(-0.34,-0.55)	-0.47				
	Line 16	(-18.83,-33.57)	-28.21	(-0.31,-0.55)	-0.46				
Wall 1	Line 2	(-30.75,-35.41)	-34.41	(-0.50,-0.58)	-0.56	-0.985167	0.000284187	-9.36E-05	0.303969
	Line 3	(-28.53,-34.09)	-32.22	(-0.47,-0.56)	-0.53				
Face B	Line 4	(-29.04,-34.11)	-32.53	(-0.47,-0.56)	-0.53	0.00014929	0.937702	0.294853	-0.000136475
	Line 5	(-23.87,-34.95)	-30.23	(-0.39,-0.57)	-0.49				
Wall 2	Line 6	(-27.96,-35.34)	-31.42	(-0.46,-0.58)	-0.51	-0.96202	0.000489906	6.98E-05	0.295505
	Line 7	(-27.96,-35.34)	-31.42	(-0.46,-0.58)	-0.51				
Face C	Line 8	(-28.86,-36.09)	-32.09	(-0.47,-0.59)	-0.52	0.000566201	0.923189	0.28927	-0.000310852
	Line 9	(-24.61,-36.91)	-29.93	(-0.40,-0.60)	-0.49				
Wall 3	Line 10	(-24.65,-37.32)	-29.89	(-0.40,-0.61)	-0.49	-0.882807	0.000524417	0.000156715	0.280088
	Line 11	(-22.99,-38.38)	-29.22	(-0.38,-0.63)	-0.48				
Face D	Line 12	(-23.79,-39.16)	-29.82	(-0.39,-0.64)	-0.49	0.000499809	0.862484	0.275682	-0.000422619
	Line 13	(-22.92,-35.65)	-27.80	(-0.37,-0.58)	-0.45				
Left Building Wall	Line 14	(-22.28,-39.80)	-32.22	(-0.36,-0.65)	-0.53	-1.02879	-0.00177634	-0.000358351	0.334014
	Line 15	(-28.33,-53.53)	-42.71	(-0.46,-0.87)	-0.70				
Wall 4	Line 17	(-22.77,-34.31)	-29.71	(-0.37,-0.56)	-0.49	0.892546	0.000319274	-8.72E-05	-0.2856
	Line 18	(-22.21,-35.18)	-29.10	(-0.36,-0.57)	-0.48				
Face E	Line 19	(-22.53,-36.20)	-29.38	(-0.37,-0.59)	-0.48	-0.00024395	0.873048	0.282611	0.000164674
	Line 20	(-19.80,-36.73)	-28.21	(-0.32,-0.60)	-0.46				
Wall 5	Line 21	(-23.01,-36.65)	-29.40	(-0.38,-0.60)	-0.48	0.875345	0.000423587	5.32E-05	-0.280003
	Line 22	(-22.20,-0.36)	-28.69	(-0.37,-0.61)	-0.47				
Face F	Line 23	(-22.68,-37.87)	-29.12	(-0.37,-0.62)	-0.48	-0.000468062	0.855259	0.276917	0.000316919
	Line 24	(-20.20,-38.25)	-27.78	(-0.33,-0.62)	-0.45				
Wall 6	Line 25	(-20.43,-38.54)	-27.93	(-0.33,-0.63)	-0.46	0.830319	0.000366298	0.000126006	-0.271552
	Line 26	(-19.61,-40.02)	-27.57	(-0.32,-0.65)	-0.45				
Face G	Line 27	(-19.93,-40.12)	-27.90	(-0.33,-0.66)	-0.46	-0.000211083	0.813743	0.267716	0.000420661
	Line 28	(-18.79,-34.99)	-26.07	(-0.31,-0.57)	-0.43				
Right Building Wall	Line 29	(-20.22,-40.26)	-32.27	(-0.33,-0.66)	-0.53	1.01425	-0.00174328	-0.00032734	-0.333513
	Line 30	(-24.45,-52.60)	-42.12	(-0.40,-0.60)	-0.69				
Leeward Face	Line 31	(19.88,-27.83)	12.87	(0.32,-0.45)	0.21	-7.10E-05	10.016	2.84145	1.64E-05
	Line 32	(54.70,-46.47)	42.79	(0.89,-0.76)	0.70				
	Line 33	(61.67,-45.85)	48.63	(1.01,-0.75)	0.79				
	Line 34	(63.40,-48.35)	49.78	(1.04,-0.79)	0.81				
	Line 35	(61.73,-37.53)	49.50	(1.01,-0.61)	0.81				
	Line 36	(54.79,-45.11)	43.00	(0.89,-0.74)	0.70				
	Line 37	(20.96,-28.41)	13.43	(0.34,-0.46)	0.22				

The range of average pressure values for the wind inclination angle of 180° (Table 4.25) is between [-42.71, 49.78]. The maximum positive and negative pressure values of 49.78 and -42.71, respectively, occur on the **Leeward face** and **Left building wall**. The range of pressure coefficient Cp lies in the range ε [-0.70, 0.81]. The maximum positive and

negative values of 0.81 and -0.70 occur on the Leeward face and Left building wall (Table 4.26). These results suggest that the model experiences a significant pressure difference between the Leeward face and the Left building wall when subjected to a wind inclination angle of 180 degrees.

4.5 VALIDATION OF CFD RESULTS WITH INTERNATIONAL CODES

To ensure accuracy, a separate **reference model** was created and subjected to thorough analysis. The design of the model involved utilizing a consistent square cross-section (as depicted in Figure 4.3), measuring 200mm x 200mm, spanning a total height of 600mm. It is compared with the acceptable values as given in International standards such as [3], [4], [5], [6] and [7], and the graphical representation of the same is plotted below in Table 4.28.

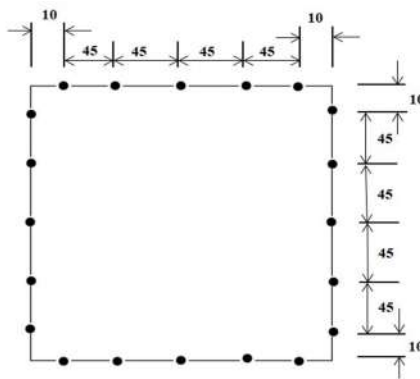
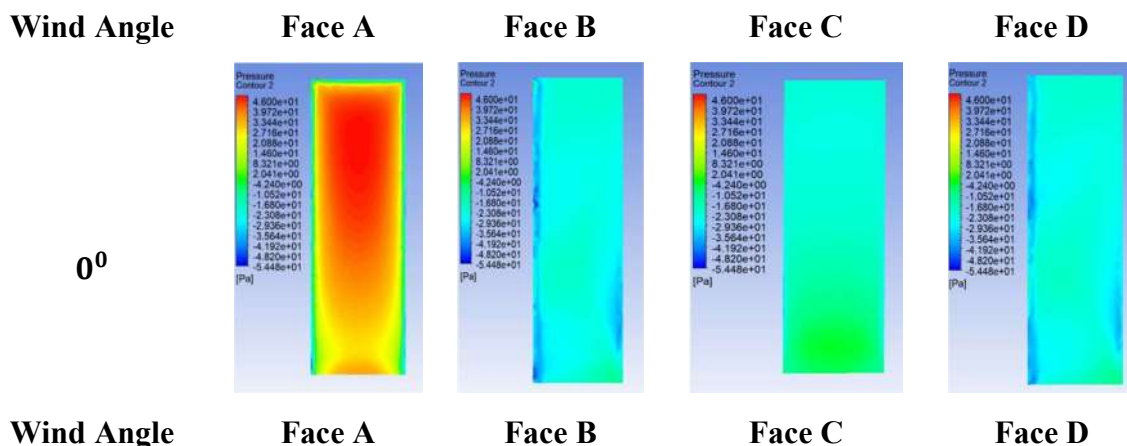


Figure 4.3: Square Model Shape for Validation

Table 4.27: Pressure contours for Square model



90°

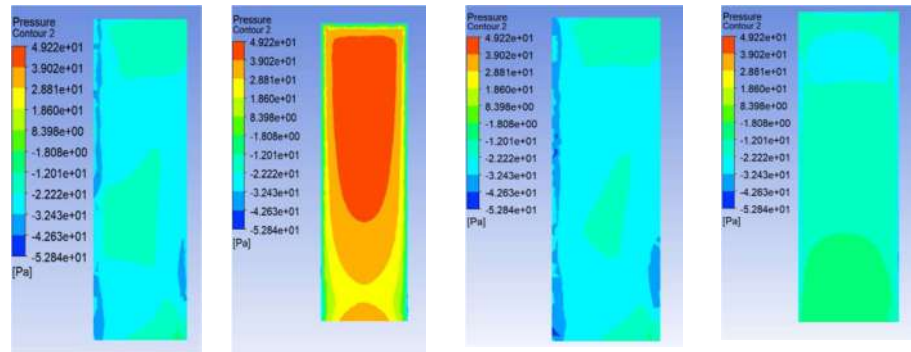


Table 4.28: Comparison of face pressure coefficient (C_p) on the Square plan shape tall building

International code	Wind Angle	Wind-ward Side	Lee-ward Side	Side walls
Simulation results	0°	0.63	-0.48	-0.53
	90°	0.67	-0.43	-0.53
CFD Sanyal and Dalui (2020)	0°	0.8	-0.5	-0.7
	90°	0.8	-0.5	-0.7
Experimental Raj (2015)	0°	0.71	-0.67	-0.41
	90°	0.73	-0.66	-0.42
IS 875 (PART 3): 2015	0°	0.8	-0.25	-0.8
	90°	0.8	-0.25	-0.8
ASCE-7:2010	0°	0.8	-0.5	-0.7
	90°	0.8	-0.5	-0.7
AS/NZS:11700.2:2002	0°	0.8	-0.5	-0.65
	90°	0.8	-0.5	-0.65
EN1991-1-4:2005	0°	0.8	-0.55	-0.8
	90°	0.8	-0.55	-0.8
BS6399-2:1997	0°	0.76	-0.5	-0.8
	90°	0.76	-0.5	-0.8
GB 50009-2001	0°	0.8	-0.5	-0.7
	90°	0.8	-0.5	-0.7
NSCP2015	0°	0.8	-0.5	-0.7
	90°	0.8	-0.5	-0.7
ES/ISO4354:2012	0°	0.8	-0.65	-0.7
	90°	0.8	-0.65	-0.7

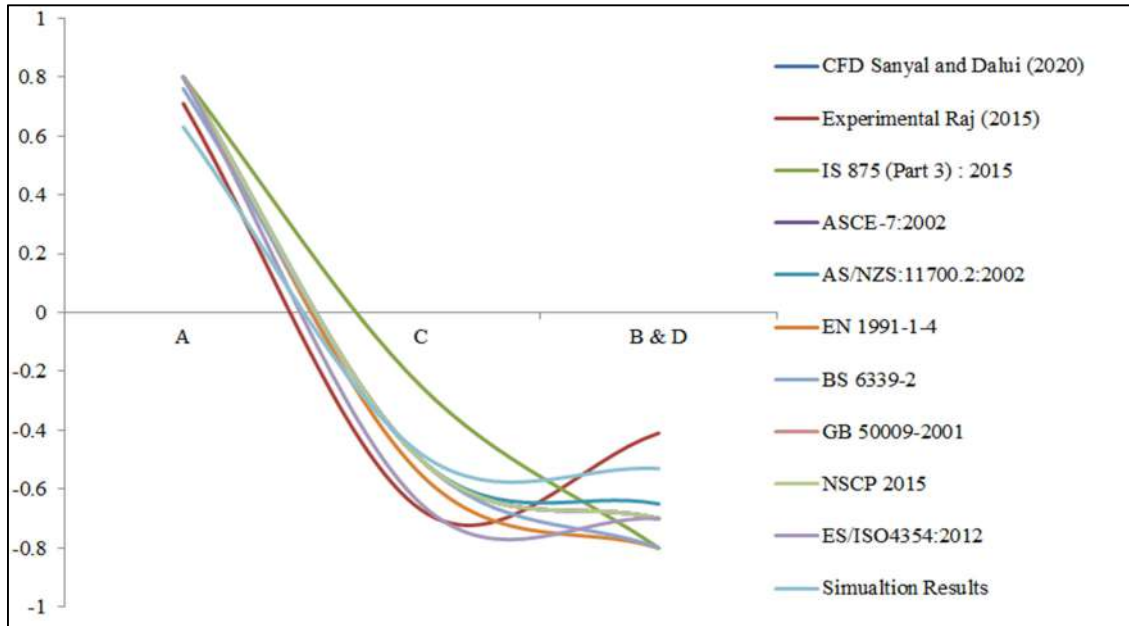


Figure 4.4: Results validation with experimental and different international standards when wind angle is 0 degree

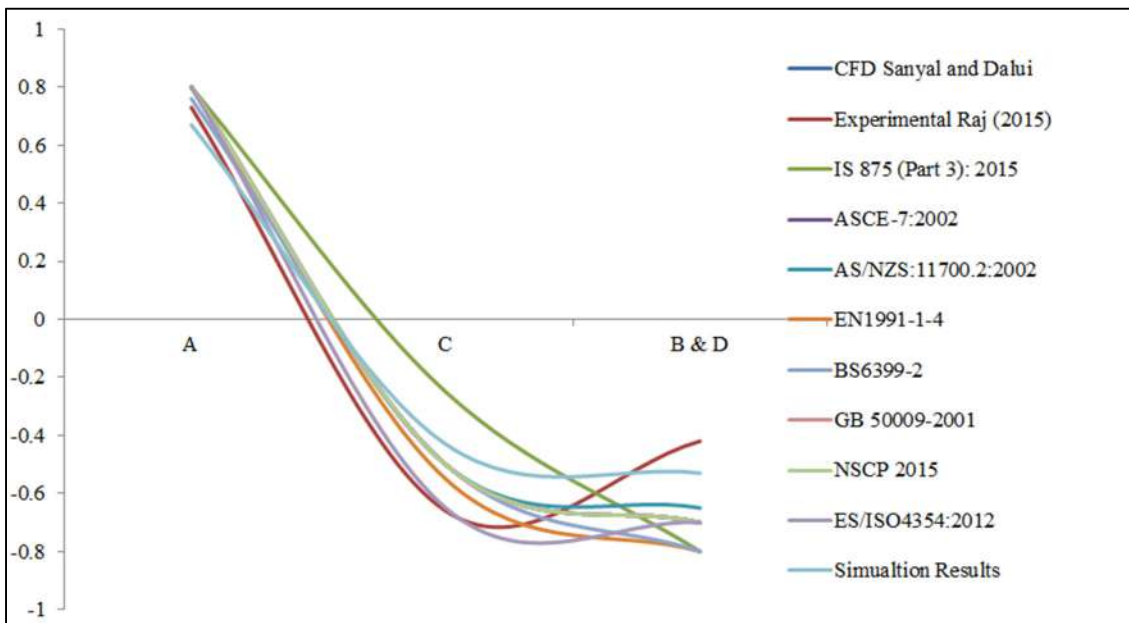


Figure 4.5: Results validation with experimental and different international standards when wind angle is 90 degree

From Table 4.27 and Table 4.29, it may be observed that the Pressure and C_p values for faces A, B, C and D respectively are varying, and the errors are within the allowable limit. C_p values are used to describe the distribution of pressure over a surface, and they are

calculated as the ratio of the pressure difference between the surface and the free stream velocity to the dynamic pressure of the free stream.

Table 4.29: Comparing C_p values of the Square model with acceptable C_p values in accordance with IS: 875 (Part III) – 2015

Coefficient of Pressure, C_p	Faces of Square Model			
	A	B	C	D
According to IS: 875 (Part III) – 2015	0.8	-0.25	-0.8	-0.8
Square Model	0.63	-0.66	-0.48	-0.40

The C_p values for each face of the Square model (A, B, C, and D) and the percentage variation of C_p values for each face have been recorded. This suggests that the performance of the Square model is satisfactory with respect to its response to wind loading, and the C_p values can be used to design and optimize the structure further. The graphical representation of the validation, in which the simulation results are compared with the international codes, is shown in **Figure 4.4** and **Figure 4.5**.

4.6 VELOCITY STREAMLINES

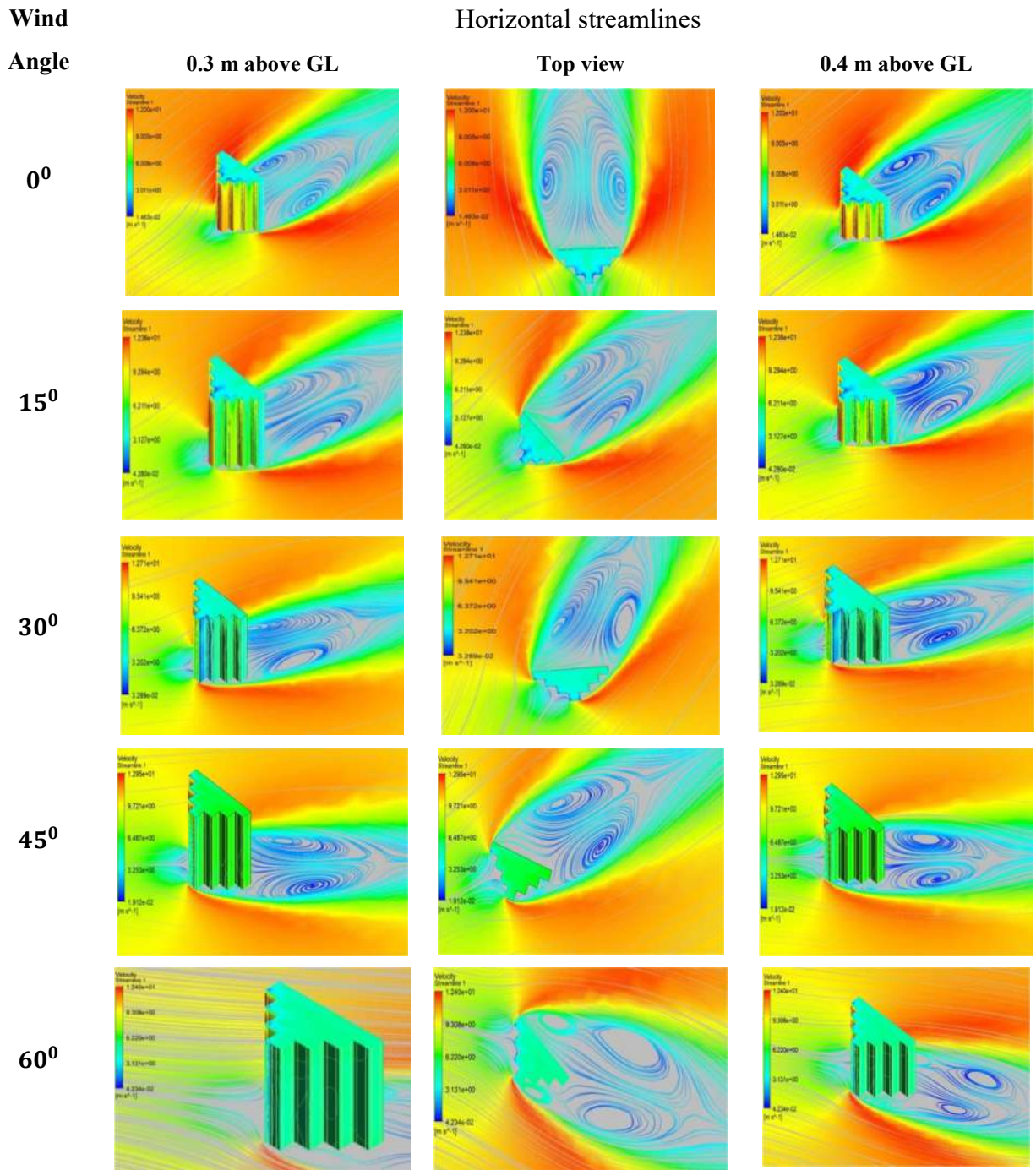
In computational fluid dynamics (CFD), velocity streamlines depict the trajectory a fluid particle would follow within a flow field. By examining the velocity streamlines in CFD, we can obtain valuable information about the characteristics of the fluid flow, such as its speed, direction, and any occurrences of turbulence or instability. These streamlines enable us to identify areas with varying fluid velocities, flow separation, swirling patterns, and other flow phenomena that impact the performance of a fluid system or device. Ultimately, velocity streamlines serve as a valuable visual and analytical tool in CFD simulations, offering essential insights for engineering design and optimization.

4.6.1 Horizontal streamlines

Horizontal streamlines are used to represent the flow of air along a horizontal plane, and they can be used to identify areas of high and low pressure on the surface of an object. This information can be used to optimize the design of the models by altering their shape, size, or surface texture to reduce areas of high pressure and increase areas of low pressure.

Vertical and horizontal streamlines are listed below figures for incident angles 0° to 180° at an interval for 15° . The following conclusions are drawn from the horizontal streamlines obtained in **Table 4.30**.

Table 4.30: Horizontal velocity streamlines for Wind incidence angle 0 to 180



Wind
Angle

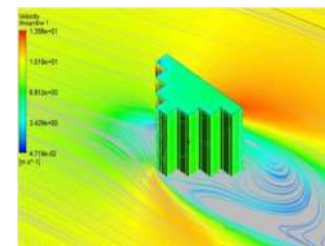
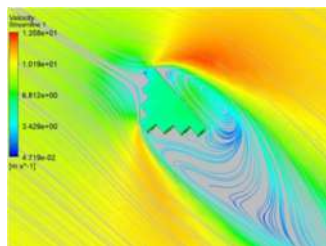
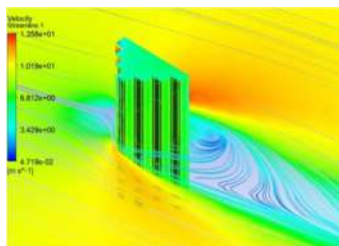
Horizontal streamlines

0.3 m above GL

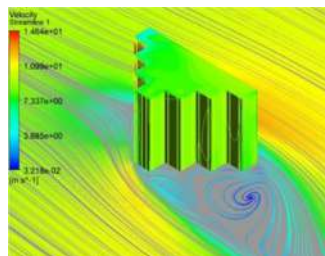
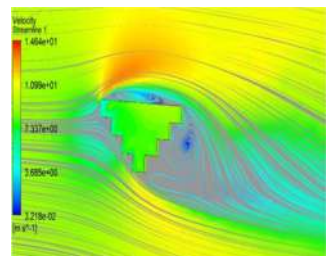
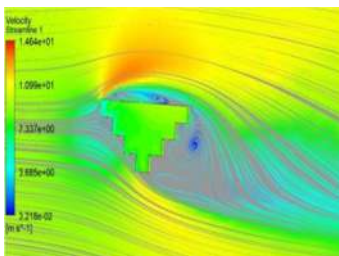
Top view

0.4 m above GL

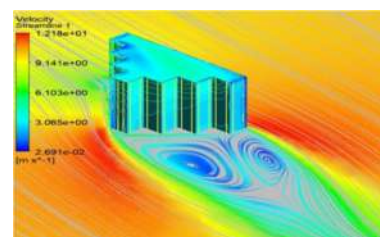
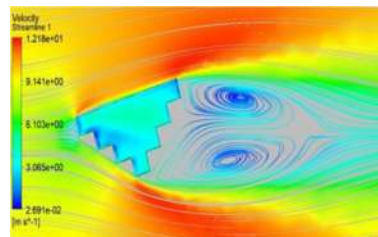
75°



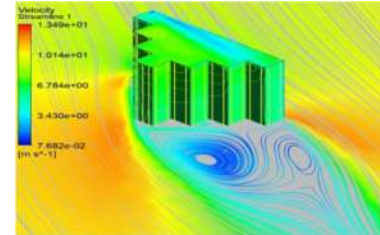
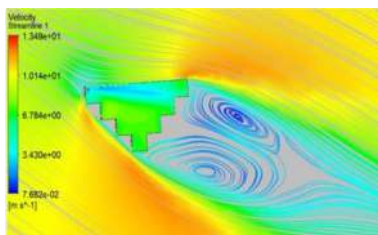
90°



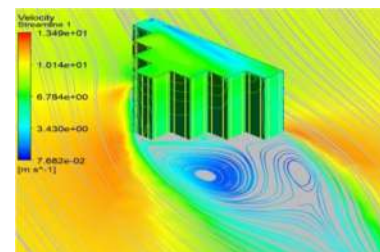
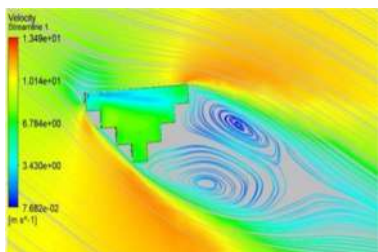
105°



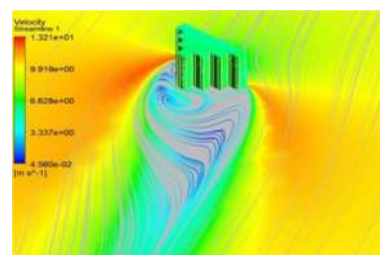
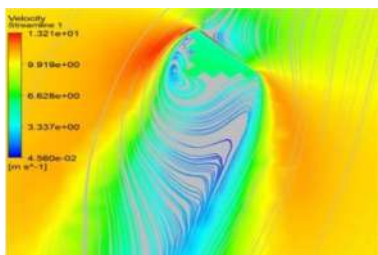
120°

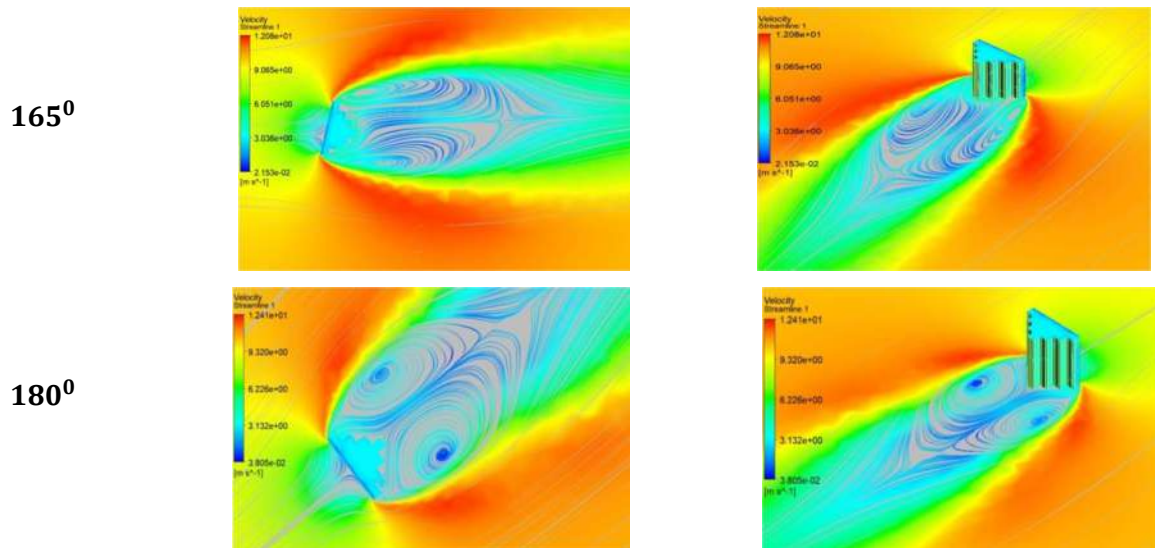


135°



150°





- It is observed that for wind incidence angle 0° , two vortices are formed at some distance away from the windward faces on the face at the leeward side where cross-section changes. Where flow lines are symmetrical, this indicates that the airflow around the model is characterized by areas of swirling motion and low velocity. This suggests that the airflow around the model is complex and has areas of high and low pressure. As the height of the building increases, the recirculation zones tend to shift away from the sides of the building and become more centralized above the building. This is because the wind is slowed down and deflected by the building, creating areas of low pressure and turbulence on the leeward side (the side sheltered from the wind).
- When the wind angle is 15° , it can be noticed that two vortices form at a certain distance from the leeward side of the surface where the shape changes. At other elevations, such as 400mm, symmetric flow separation is observed, although the number of flow lines becomes denser as the height increases. The heightened density of flow lines with increasing height might suggest an increase in wind speed or a transition to a more turbulent and intricate airflow.
- At an angle of 30° to the wind direction, two vortices are observed to develop on the leeward side of the structure, specifically where there is a change in the cross-sectional shape, at a certain distance from the face. The flow re-attachment occurs where there is a change in cross-sectional area. This means that the flow separates

from the surface of the object or structure and then re-attaches downstream where the cross-sectional area changes. This can lead to regions of recirculation, which can be seen at higher heights. The wind hits faces B, C, and D first, which means that these areas are likely to experience the most pressure from the wind. As the wind moves around the building, it creates a vortex or whirlwind effect, which can be more intense at the corners of the building where the wind is turning.

- For the wind incidence angle of 45° , it is observed that two vortexes are formed at some distance away from the face at the leeward side, where the cross-section changes. The wind hits faces B, C, and D first, which means that these areas are likely to experience the most pressure from the wind. As the wind moves around the building, it creates a vortex or whirlwind effect, which can be more intense at the corners of the building where the wind is turning. This vortex can create a suction effect, pulling air and debris towards the building. This effect can be particularly strong at the corners of the building, where the wind is turning and creating a more concentrated area of low pressure. Flow lines are, moreover, symmetrical, but as height increases, symmetry also increases.
- For the wind incidence angle of 60° , it is observed that four vortexes are formed at the windward and leeward faces. It appears that the wind is hitting faces C and D first, which creates two areas of low pressure or vortexes at some distance from face A and near the leeward face. Additionally, it appears that two more vortexes are formed at some distance from the windward faces on the leeward side of the building. This is because the wind is hitting the windward faces of the building at an angle, which can create areas of low pressure on the opposite side of the building. Flow separation is observed at other heights, i.e. 400mm, which is symmetrical, although the density of flow lines increases with height which may indicate that wind speed is increasing or that the flow of air is becoming more turbulent or complex.
- For a wind incidence angle of 75° , a solitary vortex forms on the downwind side of the building. It seems that the wind initially impacts the left wall of the building, resulting in a low-pressure area or vortex at a certain distance from the downwind face, close to the right wall. At other heights, such as 400mm, symmetrical flow

separation is observed, although the density of flow lines increases with elevation. The escalating density of flow lines with height might indicate a higher wind speed or a more turbulent and intricate airflow.

- After wind reaches a **90°** angle, it can be observed that two vortexes develop at a certain distance from the windward sides. It seems that the left wall of the building encounters the wind first, leading to the formation of low-pressure areas or vortexes near the leeward side and the right wall. The denser concentration of flow lines at higher elevations could indicate an increase in wind speed or a rise in turbulence and complexity within the airflow.
- When the wind hits the building at a **105°** angle, an intriguing phenomenon occurs on the leeward sides. The initial impact of the wind on the left wall results in the formation of two vortexes near the leeward side and at some distance from the right wall. This occurrence is attributed to the wind striking the windward surfaces of the building obliquely. At a height of 400mm, symmetrical flow separation is observed, although the density of flow lines increases with elevation. The heightened flow line density may indicate a higher wind speed or a transition to a more turbulent and complex airflow.
- "When the wind direction is at **120°**, two vortices can be seen forming on the downwind sides of the buildings. The wind first impacts the left wall of the building, leading to the creation of two low-pressure regions or vortices near the downwind surface, positioned some distance away from the right wall of the building. At a height of 400mm, the flow separation appears symmetric, although the density of flow lines increases as the height rises. The heightened density of flow lines might suggest an amplified wind speed or a transition towards a more turbulent and intricate airflow.
- At an incidence angle of **135°**, it is evident that the Left building wall encounters the wind first, resulting in the formation of two vortexes on the leeward faces. Near the leeward face and at some distance from the Right building wall, areas of low pressure or vortexes are observed. Flow separation is symmetrically observed at other heights, such as 400mm, albeit with an increasing concentration of flow lines.

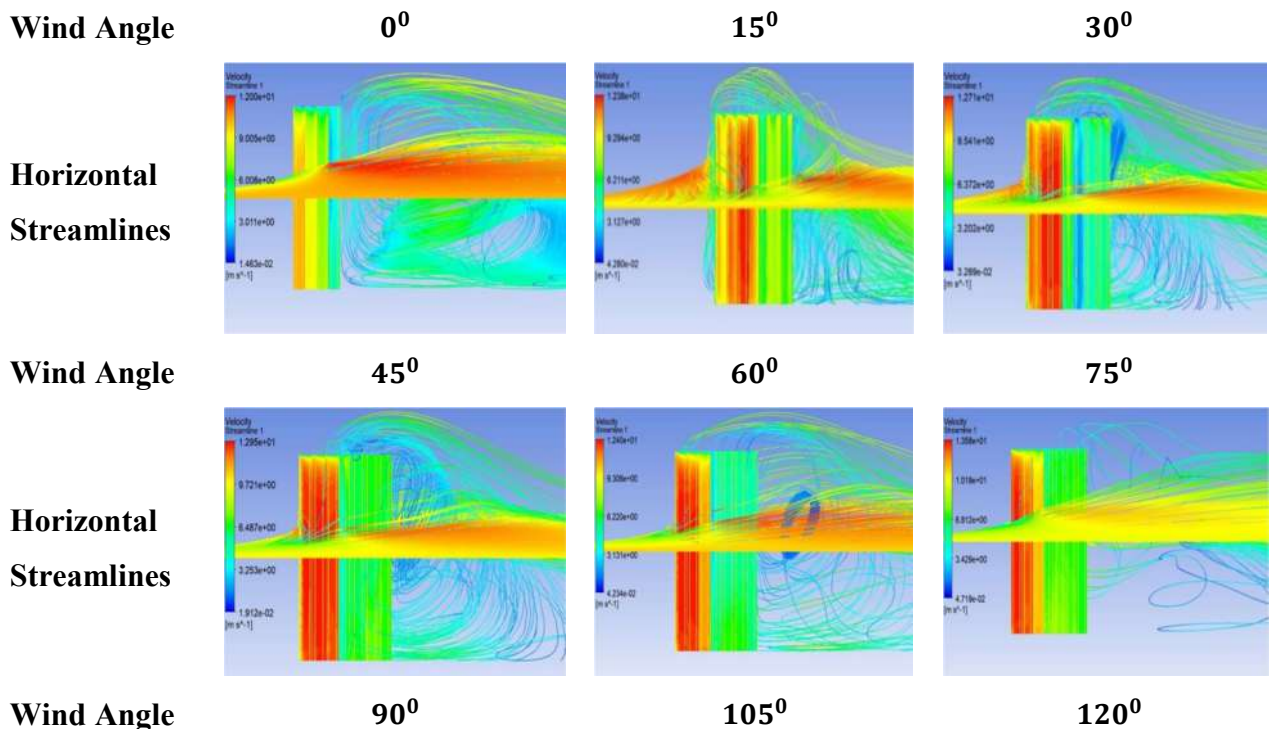
The heightened density of flow lines may indicate an augmentation in wind speed or a transition to a more turbulent or intricate airflow.

- For the wind incidence angle of **150°**, one major vortex is formed on leeward faces. It appears that the wind is hitting the backside face of the building, which causes vortices to form. These vortices can be major or minor, depending on the strength and direction of the wind, as well as the shape and orientation of the building. One another minor vortex is also formed near the Left building wall. This phenomenon is termed Vortex shedding when wind flows around an object such as a building. **Vortex shedding** can have both positive and negative effects on buildings.
- On the one hand, it can help to reduce wind loads on the building, which can help to improve its stability and structural integrity. On the other hand, it can also cause vibration and noise, which can be uncomfortable for building occupants and cause damage over time. Flow separation is observed at other heights, i.e. 400mm, which is symmetrical, although the density of flow lines increases with height.
- Upon observing a wind angle of **165°**, it becomes apparent that two vortices materialize on the leeward sides of the structure. This indicates that the wind initially strikes the backside of the building, generating areas of low pressure or vortices at specific distances from the wind-facing side. Furthermore, at different elevations, particularly at 400mm, a symmetrical division of airflow is noticed, although the concentration of flow lines intensifies as the height increases. Flow division transpires when the airflow can no longer conform to the building's surface contours and instead separates from it, leading to a turbulent and low-energy flow region.
- At a wind incidence angle of **180°**, two vortexes are observed forming on the leeward surfaces. It appears that the wind initially impacts the building's backside, leading to the creation of low-pressure areas or vortexes at a distance from the windward face. Flow separation is noticed at different heights, such as 400mm, exhibiting symmetry, albeit with an increasing density of flow lines as height increases.

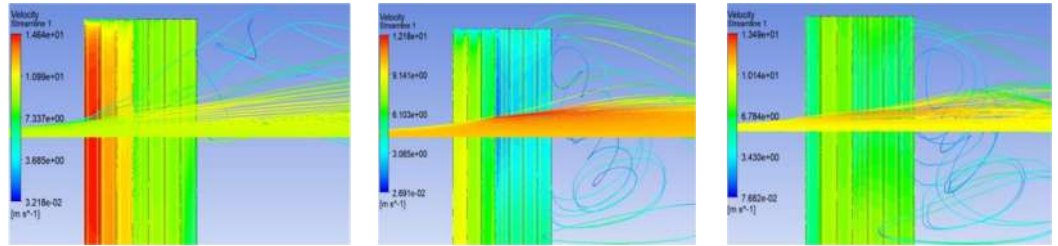
4.6.2 Vertical Streamline

A vertical streamline is a hypothetical line representing the path a fluid particle takes as it moves vertically through a fluid medium. It is a line that is perpendicular to the surface of the Earth, and the velocity and direction of the fluid flow determine its direction. By tracing the path of a vertical streamline from the ground up to the height of the building, one can observe how the air is affected by the presence of the structure and how it interacts with the surrounding flow. Vertical streamlines are a useful tool in fluid dynamics, as they can help to visualize and understand complex flows in three dimensions. They are often used in the design of buildings, bridges, and other structures that are exposed to extreme wind flows in order to optimize their performance and minimize potential damage from wind. Vertical streamline represents the **downward deflection** of the airflow over the top of the building that can create additional pressure on the leeward side of the building, which can lead to increased wind loads on the structure. This is an essential consideration for building design, as the structure must be able to withstand these wind loads without experiencing damage or failure. **Table 4.31** and **Table 4.32** show the vertical streamline for angle 0 to 180 degree.

Table 4.31: Vertical velocity streamlines for Wind incidence angle 0 to 120



Horizontal Streamlines



- When the wind blows parallel to the face of the building (at 0° incidence), the air flow near the top is less congested compared to the mid-section, indicating smoother and less turbulent airflow around the building's upper section. The wind passes over the building's top surface, creating a sort of "**wind shadow**" on the leeward face. This can cause the airflow to be slower and less turbulent near the top, as the wind is being diverted away from that area. At the mid-section, however, the wind hits the building more directly, which can create more turbulence and kinetic energy in the airflow. Turbulent flow induces intricate pressure distribution on the building's surface, amplifying pressure fluctuations that consequently generate increased lift and drag forces.
- At a wind incidence angle of 15° , the airflow over the top of the building is deflected downwards and creates vertical streamlines on both the windward and leeward sides of the building. However, the airflow over the top of the building still has some kinetic energy, albeit less than the flow over the mid-section of the building.
- At a wind incidence angle of 30° and 45° , the airflow around a building is similar to that at 0° wind incidence, with the flow of air being less congested near the top of the building compared to the mid-section. However, the flow of air near the top of the building is not significantly less than that at 0° wind incidence. The flow of air around the building is still relatively turbulent, with a large amount of kinetic energy present in the flow.
- At a wind angle of 60° , the airflow around a building exhibits similarities to that observed at a 45° wind angle, potentially making the distinction in air movement between the upper and middle sections of the building less noticeable
- In addition, a notable feature of the airflow at a 60° wind incidence angle is the formation of a **vertical vortex** on the leeward face of the building. This vortex can

be seen as a blue-coloured region in computational fluid dynamics (CFD) simulations. This low-pressure region draws in air from the surrounding areas, creating a swirling flow pattern or vortex.

- At a wind incidence angle of 75° , the airflow around a building is highly deflected and is primarily directed over the windward face of the building. The airflow over the top of the building is **significantly reduced** compared to the flow over the mid-section of the building. This is because the incoming air is deflected more horizontally than vertically, resulting in a reduced amount of air flowing over the top of the building.
- At a wind incidence angle of 90° , the airflow around a building is significantly reduced compared to other wind incidence angles. This is because most of the wind is blocked by the building surface, resulting in very little air being deflected downward the building. As a result, the airflow over the top of the building is also very low.
- At a wind incidence angle of $105^\circ, 120^\circ$ & 135° , the airflow around the building and over the top of the building is significantly reduced compared to other wind incidence angles.

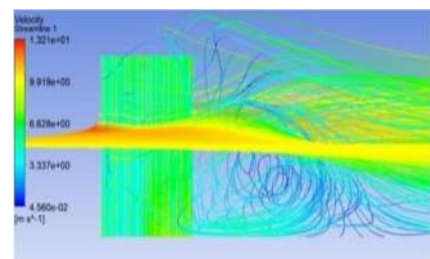
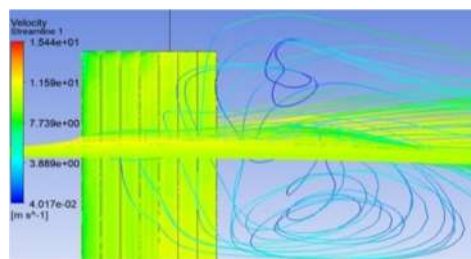
Table 4.32: Vertical velocity streamlines for Wind incidence angle 135 to 180

Wind Angle

135⁰

150⁰

**Horizontal
Streamlines**

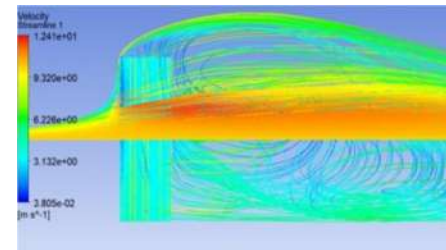
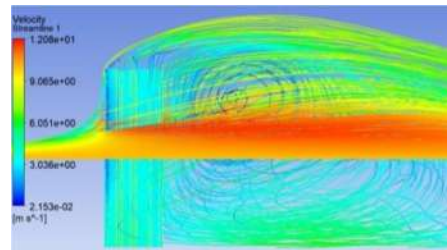


Wind Angle

165⁰

180⁰

**Horizontal
Streamlines**



- At a wind incidence angle of **150°**, there is a significant increment in the airflow around and top of the building. The flow of air around the building is still relatively turbulent, with a large amount of kinetic energy present in the flow.
- At a wind incidence angle of **165°**, the difference in the flow of air between the top and mid-section of the building is clearly noticeable at this angle as there is a significant increment in the amount of airflow. A vertical vortex formation is also seen at some distance from the leeward face.
- At a wind incidence angle of **180°**, which means it is blowing directly parallel to the face of the building, the flow of air is less congested near the top of the building compared to the mid-section. The airflow is significantly increased, and the streamlines are very symmetrical.

4.7 LIFT/ DRAG AND MOMENT FORCES

The equations (C_{fx} , C_{fy} , C_{mx} , and C_{my}) can be used to analyse the response of a building subjected to wind loading. In this case, the lift and moment coefficients are used to analyse and calculate the wind loads on the building. The building is considered as a solid body with a reference or projected area (A_p) and a reference length (H) that are used to calculate the dynamic pressure force of the wind flow. The wind loads acting on the building are resolved into lift and moment forces in the x, y, and z directions.

The lift force coefficients (C_{fx} and C_{fz}) represent the forces acting perpendicular to the wind flow direction, while the moment force coefficients (C_{mx} and C_{mz}) represent the moments acting about the x and z axes. These coefficients are normalized with respect to the dynamic pressure of the wind flow, reference area, and reference length, as described by below shown Equations.

The lift force coefficients (C_{fx} and C_{fz}) are given by:

$$C_{fx} = \frac{F_x}{0.5 * \rho * u_{h2}^2 * A_p} \quad Eq. (6)$$

$$C_{fz} = \frac{F_z}{0.5 * \rho * u_{h^2} * A_p} \quad Eq. (7)$$

Where F_x and F_z are the lift forces in the x and z directions respectively, ρ is the density of the fluid, V is the velocity of the fluid flow, and A_p is the reference area of the body perpendicular to the fluid flow.

The moment force coefficients (C_{mx} and C_{mz}) are given by:

$$C_{mx} = \frac{M_x}{0.5 * \rho * u_{h^2} * A_p * H} \quad Eq. (8)$$

$$C_{mz} = \frac{M_z}{0.5 * \rho * u_{h^2} * A_p * H} \quad Eq. (9)$$

Where M_x and M_z are the moment forces about the x and z axes respectively, and H is the reference length of the body perpendicular to the fluid flow.

The following set of equations calculates the resultant forces of lift (C_{fr}) and moment (C_{Mr}) by taking the square root of the sum of the squares of the individual coefficients of forces. The resultant forces provide an overall measure of the forces acting on the body placed in the fluid flow.

$$\text{Resultant Lift Force, } C_{fr} = \sqrt{C_{fx}^2 + C_{fz}^2} \quad Eq. (10)$$

$$\text{Resultant Moment Force, } C_{Mr} = \sqrt{C_{mx}^2 + C_{mz}^2} \quad Eq. (11)$$

Engineers utilize lift and moment coefficients to assess wind forces on buildings at various wind angles, enabling them to optimize the building's design for safety and wind load resistance. In regions susceptible to strong winds, it is crucial to ensure the building can withstand these forces. Wind tunnel tests and numerical simulations are employed to compute the lift and moment coefficients, allowing for the optimization of the building's design.

By varying the wind incidence angles, engineers can determine the worst-case scenario and design the building accordingly. The Lift/ Drag and Moment forces for each angle of wind inclination are calculated in **Table 4.33**. The simulation involved subjecting a model to wind at different angles of incidence, varying from 0 to 180 degrees in increments of 15 degrees.

Table 4.33: Lift/ Drag and Moment Force calculation

Lift and Drag Calculation													
Wind Incination	Aggregate force of all faces		Aggregate Moment of all faces		Projected Length		Lift Forces		Resultant Force	Moment Force		Resultant Moment	
Angle (deg)	Fx	Fz	Mx	Mz	Lx	Lz	CFx	CFz	CFr	CMx	CMz	CMr	
0	-0.474349005	-6.41390502	-2.689991282	-0.003862812	200	350	-0.01127781	-0.15249282	0.15290928	-0.10659246	-0.00015307	0.106592569	
15	2.454886863	-9.792075708	-3.170799124	-1.604704659	244.95	351.01	0.047518142	-0.18954081	0.195406479	-0.10229289	-0.05176924	0.114646805	
30	5.830396443	-5.328255387	-2.16009501	-0.490158666	273.21	328.11	0.108244771	-0.09892222	0.146637434	-0.06683908	-0.01516681	0.06853827	
45	6.916574429	-5.49050935	-1.681156335	-1.07814517	282.84	282.84	0.143891221	-0.11422361	0.183716402	-0.05829081	-0.03738258	0.069247929	
60	3.846587873	-0.713267175	-2.302732503	-2.225875909	273.21	218.3	0.107337192	-0.01990338	0.109166924	-0.10709441	-0.10352	0.148948327	
75	1.713255048	1.491104666	-2.751651755	-1.8846869	196.65	138.88	0.104403068	0.090865573	0.1384072	-0.27946888	-0.19141643	0.338737516	
90	5.640713343	-11.94504747	-2.968398792	-1.288681355	175	200	0.268219831	-0.56799529	0.628140532	-0.23524904	-0.10212949	0.256461577	
105	3.29142768	0.642758351	0.588595167	-0.846847677	154.36	42.29	0.839144518	0.163870271	0.854995314	0.250102415	-0.35983756	0.438217171	
120	1.689697053	6.061112347	1.63389642	0.035200692	98.21	131.7	0.21741638	0.779894302	0.809632636	0.350394019	0.007548895	0.350475326	
135	0.252840361	3.041780597	3.364174148	0.29930989	35.36	282.84	0.042074428	0.506173844	0.5079195	0.933037359	0.083012144	0.936722867	
150	-3.060359019	14.66244973	4.4919754	0.249973819	29.9	328.11	-0.51916645	2.487372225	2.540975087	1.270048668	0.070676904	1.272013696	
165	-0.259421611	4.867507165	1.365842984	0.02063129	99.6	351.01	-0.01234958	0.231714212	0.232043074	0.108366637	0.001636896	0.108379	
180	1.751517165	14.41991876	1.404755577	0.376354769	200	350	0.041642928	0.342838569	0.34535839	0.055664252	0.014913275	0.057627378	
							Average	0.11	0.27	0.53	0.15	-0.05	0.33
							Maximum	0.84	2.49	2.54	1.27	0.08	1.27
							Minimum	-0.52	-0.57	0.11	-0.28	-0.36	0.06

Graphs were plotted to show the values of Cfx, Cfz, Cfr, Cmx, Cmz, and Cmr for the model at each angle of incidence. The Graph provides the following conclusions drawn from these graphs: The average values of Cfx, Cfz, and Cfr are 0.11, 0.27, and 0.53, respectively. These values give us an idea of the overall force exerted on the model in the x, z, and roll directions, respectively. The average values of Cmx, Cmz, and Cmr are 0.15, -0.05, and 0.33, respectively.

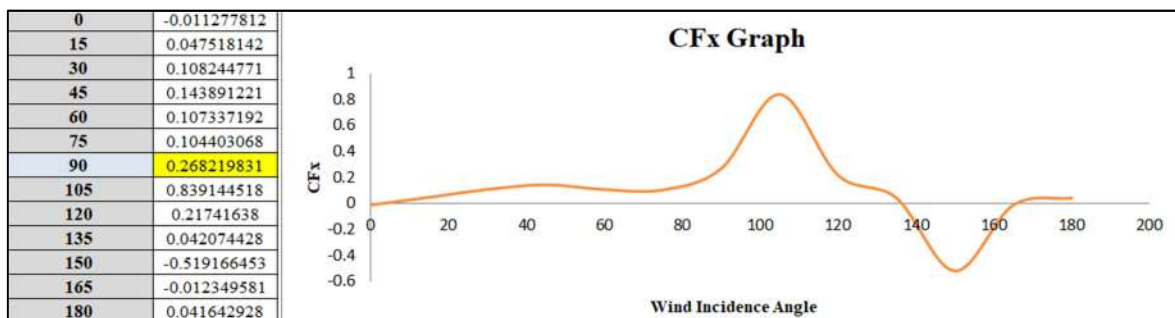


Figure 4.6: Comparative Cfx graph for Fish model at various wind incidence angle

Cfx: The maximum value of Cfx is 0.84, which occurs at a wind angle of 105 degrees. This indicates that there is significant force acting on the model in the x-direction at this wind angle. The minimum value of Cfx is -0.52, which occurs at a wind angle of 150 degrees. This suggests that at this angle, the force acting on the model in the x-direction is weak and may even be acting in the opposite direction. (See **Figure 4.6**)

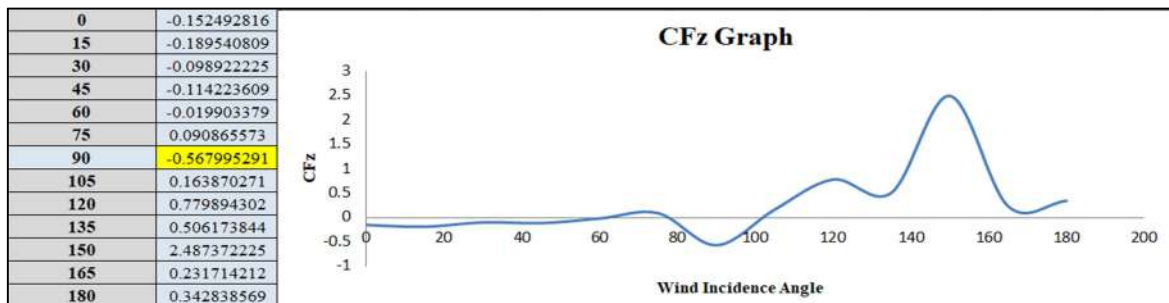


Figure 4.7: Comparative CFz graph for Fish model at various wind incidence angle

Cfz: The maximum value of Cfz is **2.49**, which occurs at a wind angle of **150** degrees. This indicates that there is strong force acting on the model in the z-direction at this wind angle. The minimum value of Cfz is **-0.57**, which occurs at a wind angle of **90** degrees. This suggests that at this angle, the force acting on the model in the z-direction is relatively weak. (See **Figure 4.7**)

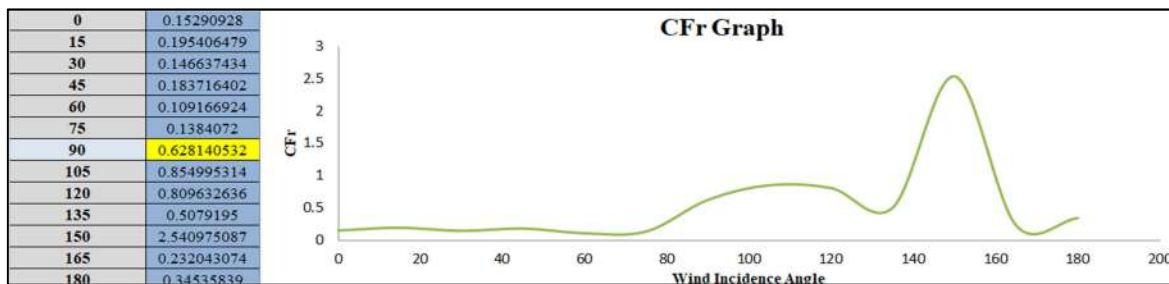


Figure 4.8: Comparative CFr graph for Fish model at various wind incidence angle

Cfr: The maximum value of Cfr is **2.54**, which occurs at a wind angle of **150** degrees. This indicates that there is strong force acting on the model in the roll direction at this wind angle. The minimum value of Cfr is **0.11**, which occurs at a wind angle of **60** degrees. This suggests that at this angle, the force acting on the model in the roll direction is relatively weak. (See **Figure 4.8**)

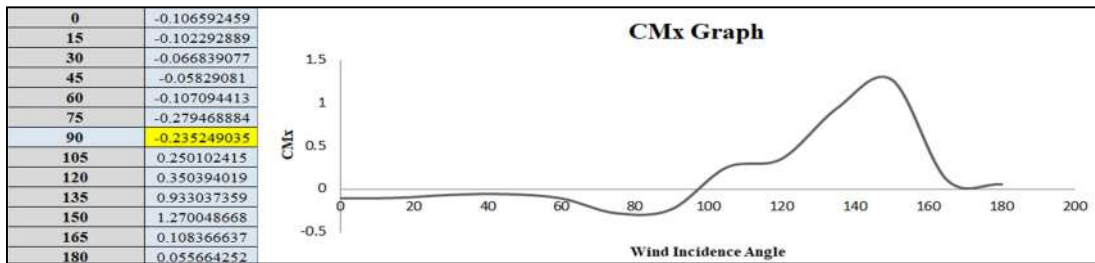


Figure 4.9: Comparative CMx graph for Fish model at various wind incidence angle

Cmx: The maximum value of Cmx is **1.27**, which occurs at a wind angle of **150** degrees. This indicates that there is significant moment acting on the model in the pitch direction at this wind angle. The minimum value of Cmx is **-0.28**, which occurs at a wind angle of **75** degrees. This suggests that at this angle, the moment acting on the model in the pitch direction is relatively weak. (See **Figure 4.9**)

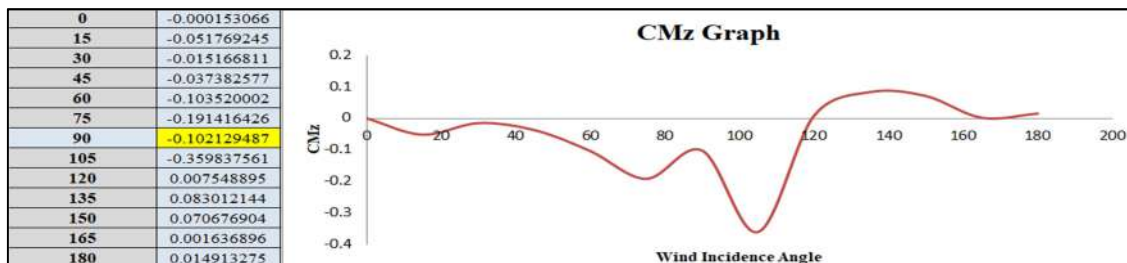


Figure 4.10: Comparative CMz graph for Fish model at various wind incidence angle

Cmz: The maximum value of Cmz is **0.08**, which occurs at a wind angle of **135** degrees. This indicates that there is small moment acting on the model in the yaw direction at this wind angle. The minimum value of Cmz is **-0.36**, which occurs at a wind angle of **105** degrees. This suggests that at this angle, there is significant moment acting on the model in the yaw direction, potentially causing the model to turn. (See **Figure 4.10**)

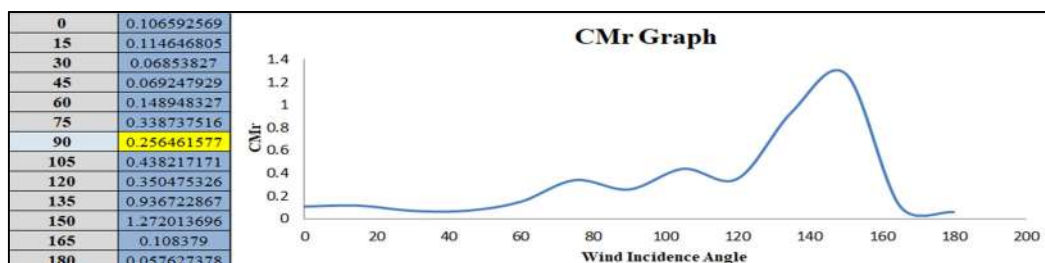


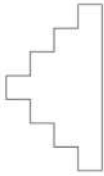
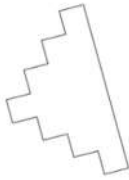
Figure 4.11: Comparative CMr graph for Fish model at various wind incidence angle

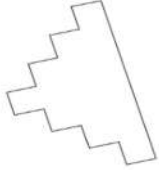

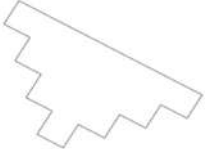
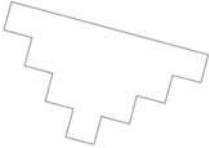
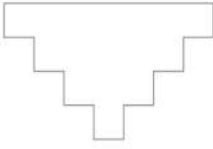
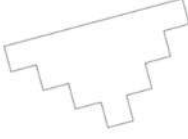
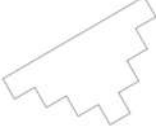
Cmr: The maximum value of Cmr is **1.27**, which occurs at a wind angle of **150** degrees. This indicates that there is significant moment acting on the model in the roll direction at this wind angle. The minimum value of Cmr is **0.06**, which occurs at a wind angle of **180** degrees. This suggests that at this angle, the moment acting on the model in the roll direction is relatively weak. These values can help inform design decisions for similar models or systems and can also be used to assess the stability of the model under various wind conditions. (See **Figure 4.11**)

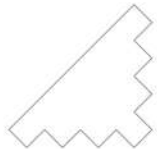
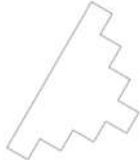
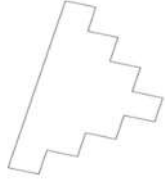
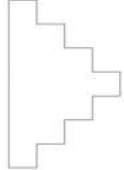
4.7.1 Reference Area calculation:

The reference area is a critical parameter used to quantify the effect of fluid flow on an object. The choice of reference area depends on the type of object and the flow regime it is experiencing. For buildings, the reference area (**Table 4.34**) is typically defined as the area of the building's face that is perpendicular to the wind direction, and for irregularly shaped buildings, an equivalent square or rectangular area is often used as an approximation. Accurate determination of the reference area is crucial for predicting the aerodynamic behaviour of buildings and optimizing their design for wind loads.

Table 4.34: Projected/Reference area at each wind incidence angle

Wind Angle	Wind Inclination on Model	Projected Length		Area
		Lx (mm)	Lz (mm)	10 ³ Sq. mm
0°		350	200	70.000
15°		351.01	244.95	86.979

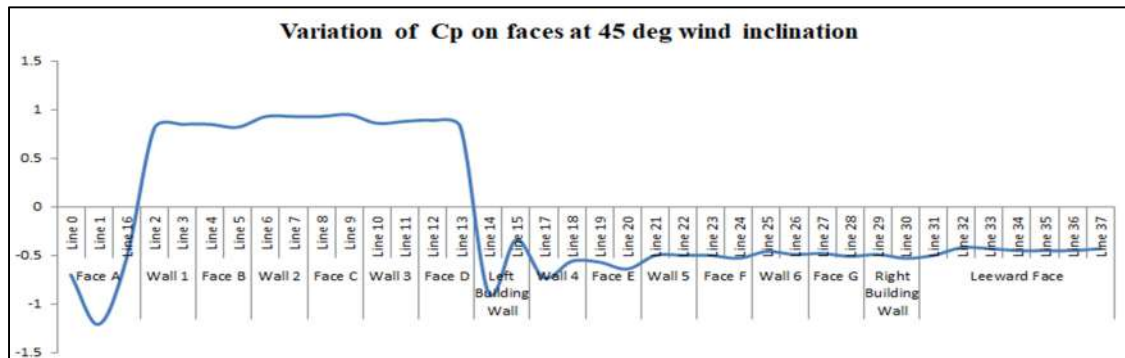
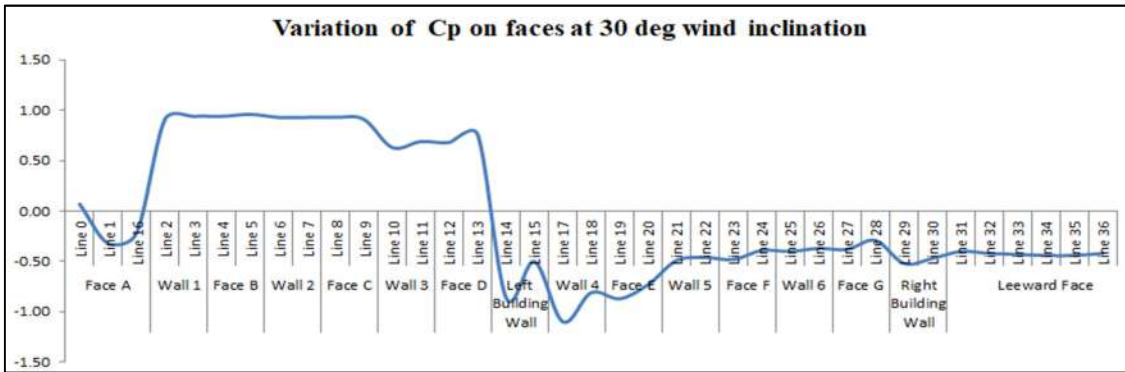
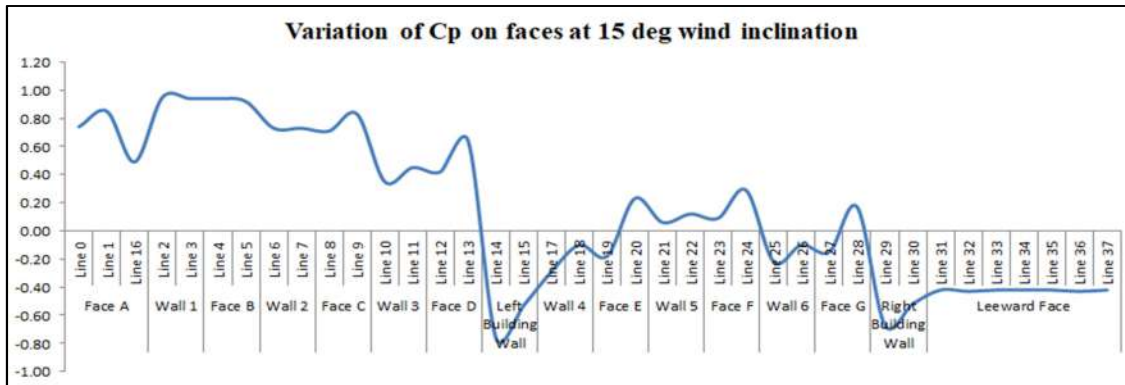
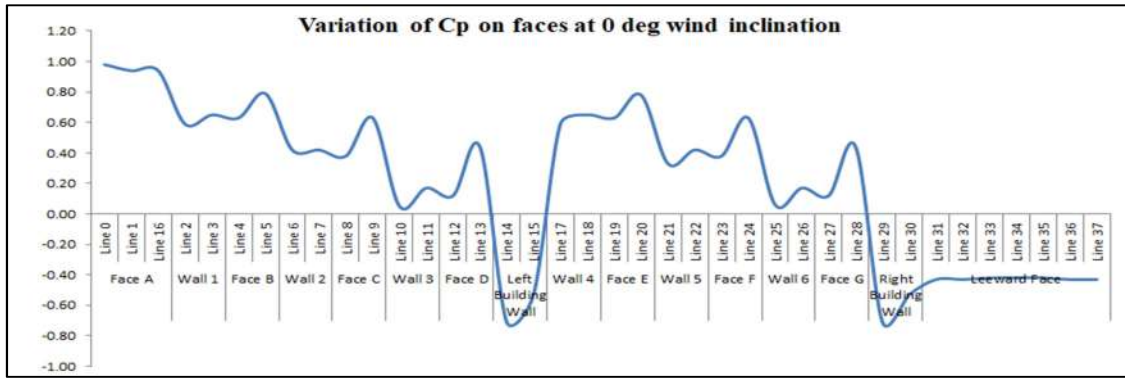
30°		328.11	273.21	89.642
45°		282.84	282.84	79.998
60°		218.30	273.21	59.641
75°		138.88	196.65	27.310
90°		175	200	35.000
105°		42.29	154.36	6.527
120°		131.7	98.21	12.93

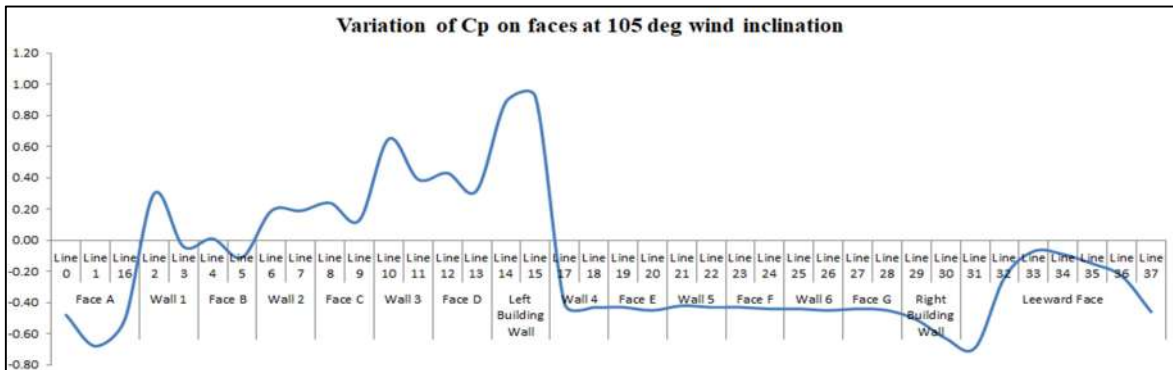
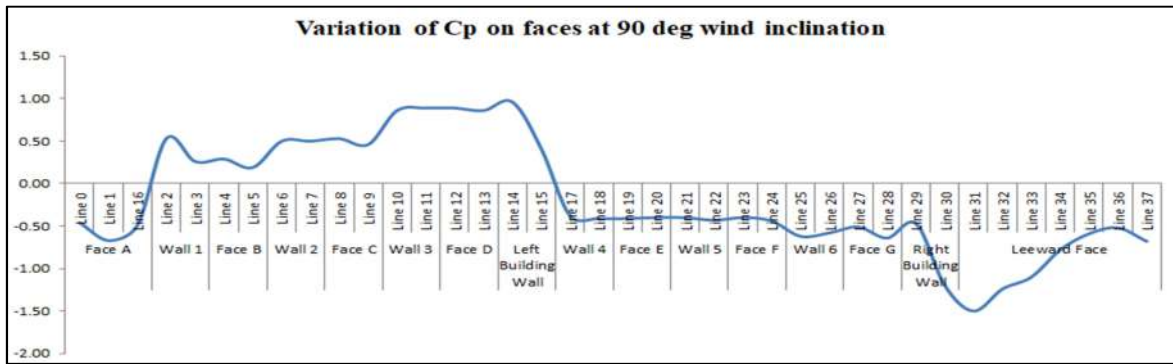
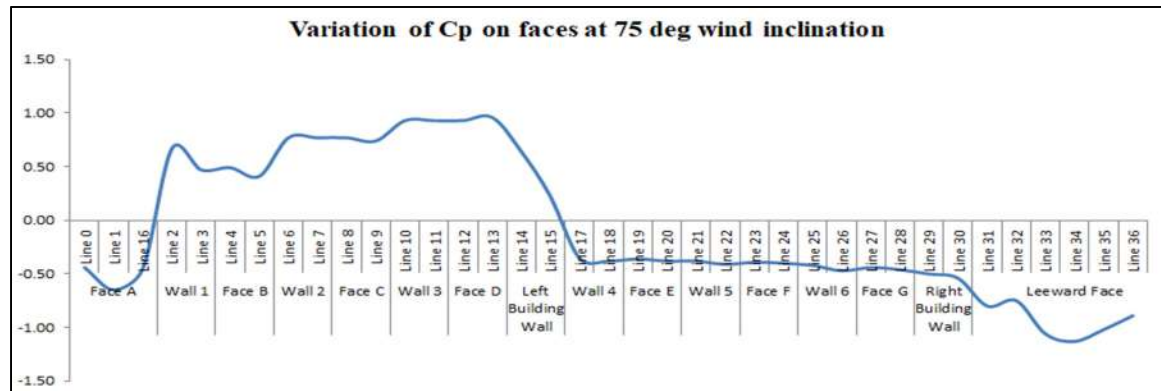
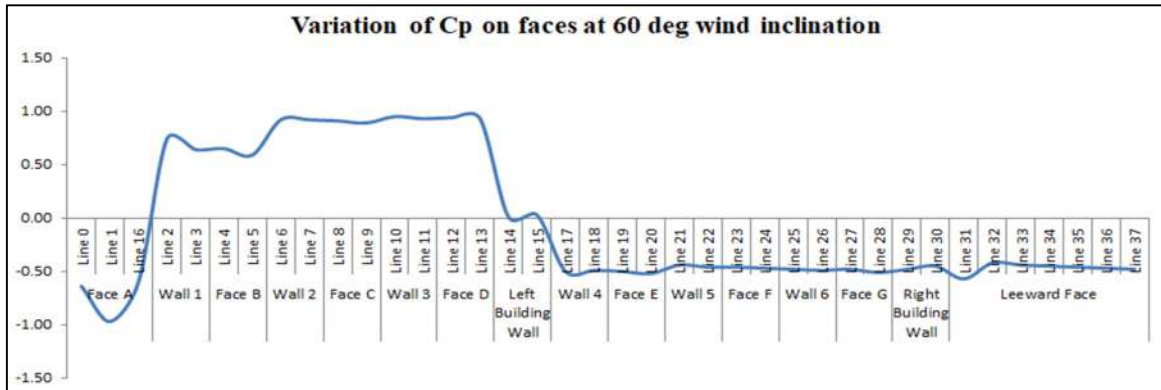
135⁰		282.84	35.36	10.001
150⁰		328.11	29.90	9.810
165⁰		351.01	99.60	34.960
180⁰		350	200	70.000

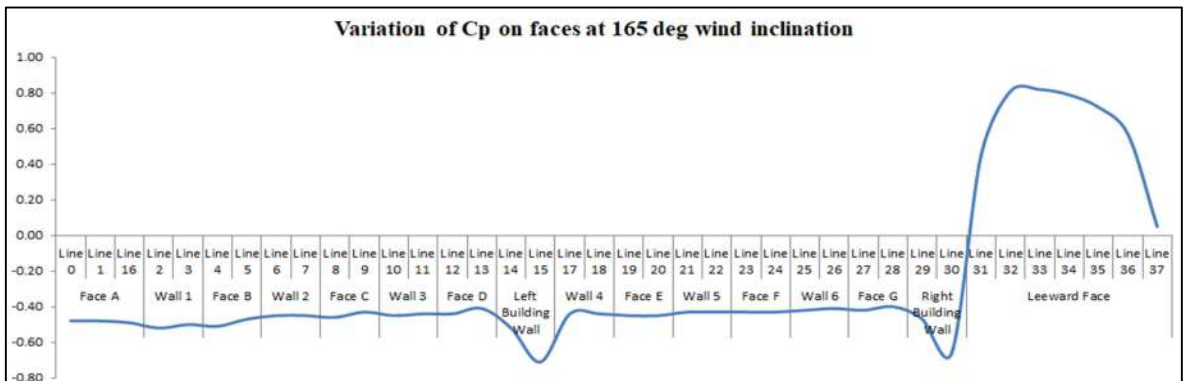
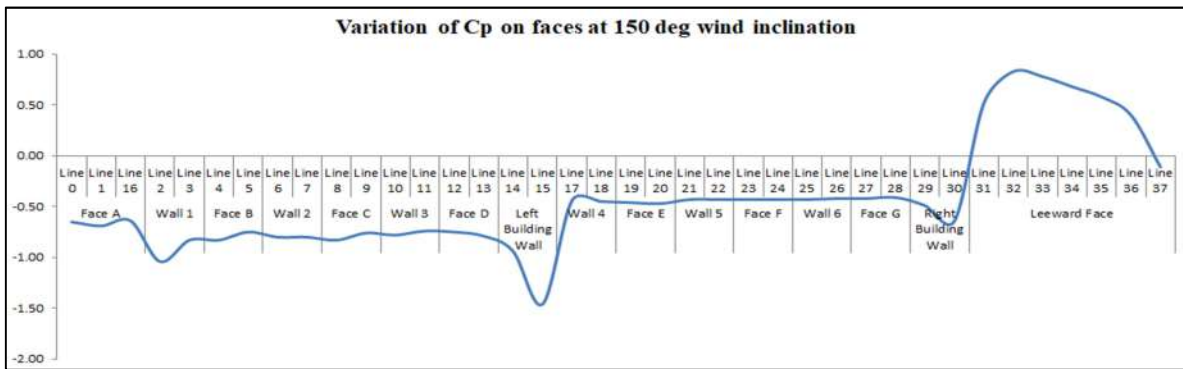
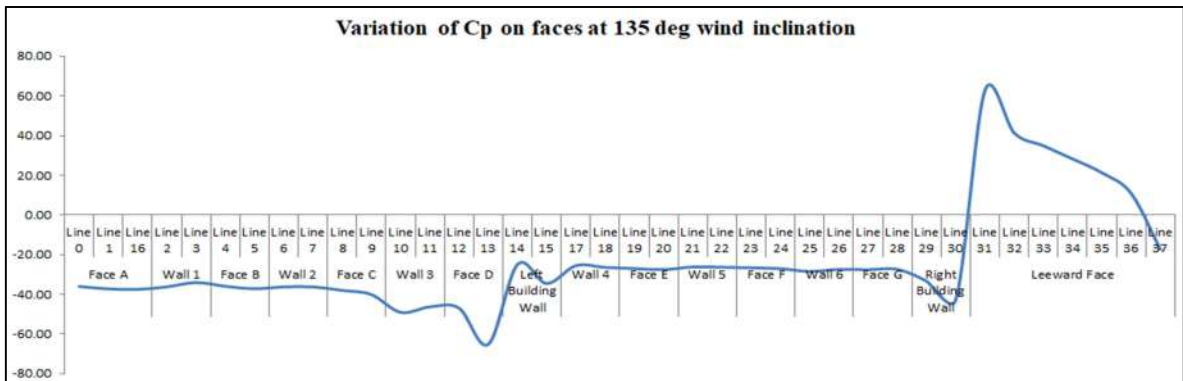
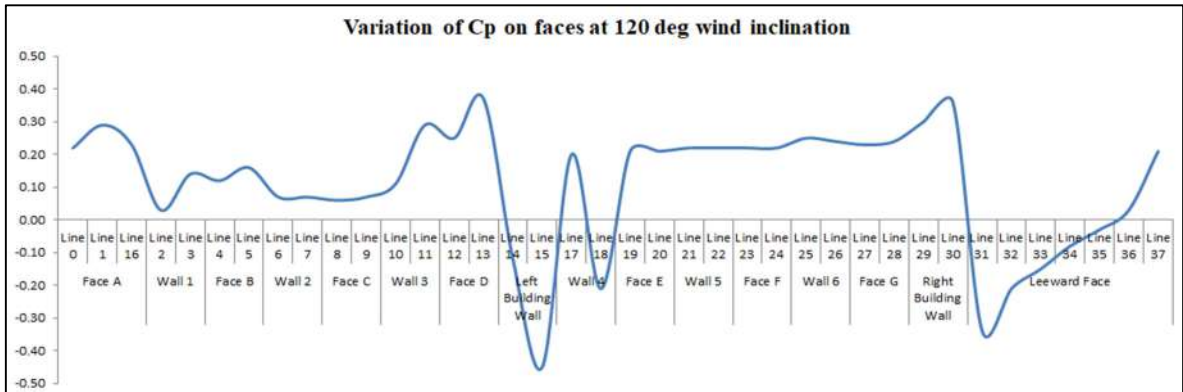
4.8 AVERAGE PRESSURE COEFFICIENT (C_p)

The C_p values serve as indicators of pressure distribution on a body placed in a fluid flow. These values are obtained by comparing the pressure at a specific point on the surface with the pressure of the surrounding flow. A C_p value of 1 signifies **stagnation pressure**, while a C_p value of 0 represents the pressure of the free stream. Negative C_p values indicate regions of reduced pressure, while positive C_p values indicate regions of increased pressure.

The analysis of wind loading on a building and the improvement of its design for enhanced performance and safety rely on examining the variation of C_p values for each face of the structure at different wind angles. **Figure 4.12** presents graphical representations illustrating the C_p values for every face of the building, ranging from 0° to 180° at 15° intervals. C_p values for all wind angles are shown on **Table 4.35**.







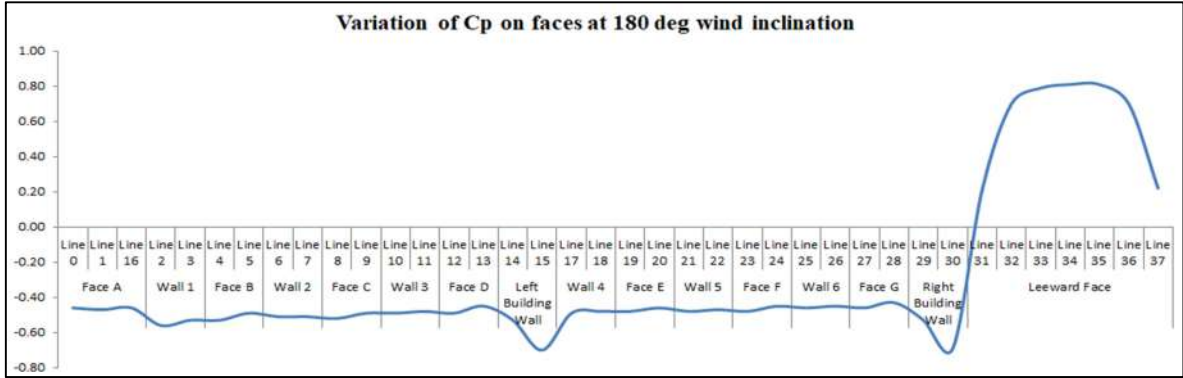


Figure 4.12: Variation of Cp on faces at 0 to 180 degree

Table 4.35: Average Cp for wind angle 0 to 180

Faces/Wall	Line	Average Value of Cp													
		0 Degree	15 Degree	30 Degree	45 Degree	60 Degree	75 Degree	90 Degree	105 Degree	120 Degree	135 Degree	150 Degree	165 Degree	180 Degree	
Face A	Line 0	0.98	0.74	0.07	-0.7	-0.64	-0.44	-0.46	-0.48	0.22	-0.59	-0.65	-0.48	-0.46	
	Line 1	0.94	0.85	-0.32	-1.21	-0.97	-0.65	-0.67	-0.68	0.29	-0.61	-0.69	-0.48	-0.47	
	Line 16	0.94	0.49	-0.22	-0.53	-0.60	-0.45	-0.49	-0.51	0.23	-0.61	-0.64	-0.49	-0.46	
Wall 1	Line 2	0.59	0.95	0.91	0.81	0.74	0.67	0.53	0.30	0.03	-0.59	-1.04	-0.52	-0.56	
	Line 3	0.65	0.94	0.94	0.85	0.64	0.47	0.26	-0.04	0.14	-0.56	-0.83	-0.50	-0.53	
Face B	Line 4	0.63	0.94	0.94	0.85	0.65	0.49	0.29	0.01	0.12	-0.59	-0.83	-0.51	-0.53	
	Line 5	0.79	0.92	0.96	0.82	0.59	0.41	0.19	-0.11	0.16	-0.61	-0.75	-0.47	-0.49	
Wall 2	Line 6	0.42	0.73	0.93	0.93	0.92	0.77	0.50	0.19	0.07	-0.59	-0.80	-0.45	-0.51	
	Line 7	0.42	0.73	0.93	0.93	0.92	0.77	0.50	0.19	0.07	-0.59	-0.80	-0.45	-0.51	
Face C	Line 8	0.38	0.71	0.93	0.93	0.91	0.77	0.53	0.24	0.06	-0.62	-0.83	-0.46	-0.52	
	Line 9	0.63	0.83	0.91	0.95	0.89	0.74	0.46	0.13	0.07	-0.66	-0.76	-0.43	-0.49	
Wall 3	Line 10	0.05	0.35	0.63	0.86	0.95	0.93	0.86	0.65	0.11	-0.80	-0.78	-0.45	-0.49	
	Line 11	0.17	0.45	0.69	0.88	0.93	0.93	0.89	0.39	0.29	-0.76	-0.74	-0.44	-0.48	
Face D	Line 12	0.12	0.42	0.68	0.89	0.94	0.93	0.89	0.43	0.25	-0.77	-0.75	-0.44	-0.49	
	Line 13	0.44	0.64	0.76	0.82	0.93	0.96	0.86	0.32	0.37	-1.07	-0.79	-0.41	-0.45	
Left Building Wall	Line 14	-0.71	-0.76	-0.86	-0.88	0.01	0.64	0.96	0.89	-0.12	-0.41	-0.94	-0.52	-0.53	
	Line 15	-0.53	-0.53	-0.50	-0.34	0.03	0.22	0.41	0.92	-0.45	-0.56	-1.46	-0.71	-0.70	
Wall 4	Line 17	0.59	-0.29	-1.10	-0.73	-0.50	-0.35	-0.38	-0.41	0.20	-0.42	-0.44	-0.44	-0.49	
	Line 18	0.65	-0.10	-0.81	-0.56	-0.49	-0.38	-0.41	-0.43	-0.21	-0.43	-0.45	-0.44	-0.48	
Face E	Line 19	0.63	-0.18	-0.87	-0.57	-0.50	-0.36	-0.41	-0.43	0.21	-0.44	-0.46	-0.45	-0.48	
	Line 20	0.78	0.23	-0.73	-0.64	-0.52	-0.38	-0.40	-0.45	0.21	-0.45	-0.47	-0.45	-0.46	
Wall 5	Line 21	0.33	0.06	-0.49	-0.50	-0.44	-0.38	-0.40	-0.42	0.22	-0.43	-0.43	-0.43	-0.48	
	Line 22	0.42	0.12	-0.46	-0.50	-0.46	-0.41	-0.43	-0.43	0.22	-0.43	-0.43	-0.43	-0.47	
Face F	Line 23	0.38	0.09	-0.48	-0.50	-0.46	-0.39	-0.40	-0.43	0.22	-0.44	-0.43	-0.43	-0.48	
	Line 24	0.63	0.29	-0.39	-0.53	-0.47	-0.40	-0.44	-0.44	0.22	-0.44	-0.43	-0.43	-0.45	
Wall 6	Line 25	0.06	-0.22	-0.40	-0.46	-0.48	-0.42	-0.62	-0.44	0.25	-0.47	-0.43	-0.42	-0.46	
	Line 26	0.17	-0.10	-0.37	-0.49	-0.49	-0.47	-0.58	-0.45	0.24	-0.45	-0.42	-0.41	-0.45	
Face G	Line 27	0.12	-0.15	-0.38	-0.48	-0.48	-0.44	-0.51	-0.44	0.23	-0.45	-0.42	-0.42	-0.46	
	Line 28	0.44	0.17	-0.29	-0.51	-0.51	-0.46	-0.64	-0.45	0.24	-0.45	-0.41	-0.40	-0.43	
Right Building Wall	Line 29	-0.71	-0.67	-0.52	-0.49	-0.48	-0.50	-0.47	-0.51	0.30	-0.55	-0.49	-0.47	-0.53	
	Line 30	-0.53	-0.52	-0.47	-0.53	-0.45	-0.54	-1.20	-0.63	0.36	-0.70	-0.64	-0.66	-0.69	
Leeward Face	Line 31	-0.43	-0.42	-0.40	-0.50	-0.57	-0.80	-1.50	-0.69	-0.34	1.03	0.52	0.45	0.21	
	Line 32	-0.43	-0.43	-0.42	-0.42	-0.42	-0.75	-1.24	-0.24	-0.21	0.67	0.83	0.81	0.70	
	Line 33	-0.42	-0.42	-0.43	-0.43	-0.44	-1.06	-1.10	-0.07	-0.15	0.57	0.78	0.82	0.79	
	Line 34	-0.42	-0.42	-0.44	-0.45	-0.45	-1.13	-0.78	-0.09	-0.08	0.46	0.68	0.79	0.81	
	Line 35	-0.42	-0.42	-0.44	-0.45	-0.46	-1.02	-0.59	-0.15	-0.03	0.35	0.58	0.72	0.81	
	Line 36	-0.43	-0.43	-0.42	-0.45	-0.47	-0.89	-0.52	-0.23	0.03	0.18	0.40	0.57	0.70	
	Line 37	-0.43	-0.42	-0.42	-0.43	-0.48	-0.91	-0.68	-0.46	0.21	-0.28	-0.11	0.05	0.22	

CHAPTER 5 - INTERFERENCE STUDY SIMULATION

Determining wind loads on tall buildings is a challenging task due to numerous factors involved, including wind speed, direction, turbulence, and the building's shape, size, and orientation. Moreover, the presence of neighboring buildings can complicate matters due to interference effects. Despite some research efforts, like wind tunnel tests and computational fluid dynamics simulations, the prediction of wind loads on intricate building shapes and in interference situations lacks comprehensive data in international standards.

In this study, we analyse the along-wind effects on Interference of asymmetrical buildings with varying dimensions but the same height and width of 600mm, using CFD simulations in ANSYS CFX, 2022 R2 and AutoCAD. The obstruction in the current investigation is determined by positioning twin architectural replicas at different angles, with a separation equivalent to 10% of the model's height, specifically 60 mm. We compute the wind effects for wind incidence angles between 0 to 180 degrees, with a 30-degree interval, using a mesh size of 0.005mm and 100 iterations. The Power Law equation is used to determine the wind speed profile within the atmospheric boundary layer. By comparing graphs of drag force, drag moment, lift force, and lift moment, we identify critical faces for different wind incidence angles.

5.1 WIND EFFECTS ON INTERFERENCE OF HIGH-RISE BUILDINGS

The research paper by (Sun, 2018) [27] describes a study on the interference effects of wind pressures on building groups. The results of the study showed that the wind pressure distribution on the buildings was affected by the shape and orientation of the buildings in the group. The paper "Evaluation of Wind Induced Interference Effects on Shape Remodelled Tall Buildings" by (Pal S. D., 2021) [28] investigates the effects of wind loads induced on duplicate building models of different shapes (Square, Fish-plan shape-1, and Fish-plan shape-2) at various orientations under 100% blockage conditions. (Anbukumar, 2019) [29] studied the bilateral interference of wind loads induced on duplicate building models of various shapes and investigated the effect of interference on wind pressure distribution and flow characteristics for different building shapes. (Gaur, 2021) [30]

examined the interference effect on corner-configured structures with variable geometry and blockage configurations under wind loads using CFD. The study analysed the interference effects on wind pressure distribution and flow characteristics for different blockage configurations. **(Nagar, 2019)** [31] investigated the effect of interference between tall twin buildings with recessed corners on wind-induced pressure. The study analysed the interference effects on pressure distribution and flow characteristics for tall twin buildings with different recessed corner configurations. **(Goyal, 2021)** [32] studied the wind interference on a hexagonal-shaped high-rise building with different openings. The study examined the wind pressure distribution and flow characteristics for a hexagonal-shaped high-rise building with different opening configurations.

(Bairagi, 2015) [33] optimized the interference effects on high-rise buildings for different wind angles. The study focused on the evaluation of pressure distribution and flow characteristics for different building shapes and wind angles. **(Kumar, 2021)** [34] conducted a CFD study of flow characteristics and pressure distribution on re-entrant wing faces of L-shaped buildings. The study analysed the interference effects on wind pressure distribution and flow characteristics for L-shaped buildings. **(Sun, 2017)** [35] used CFD simulation to study the interference effects of wind pressures in building groups. The study focused on the evaluation of pressure distribution and flow characteristics for different building shapes and wind directions.

The study **(Nagar, 2022)** [36] investigates the effects of wind on tall twin buildings with large recessed corners using wind tunnel model testing. The researchers conducted experiments for isolated and interference conditions with full blockage, half blockage, and no blockage orientation. They placed a building model of identical shape and size at different locations as per research requirement on the windward side of the principal building to create three interference conditions. Similarly **(Amin, 2012)** [37] This experimental study examines wind-induced pressure coefficients on low-rise buildings with different roof configurations. **(Kar, 2016)** [38] This CFD study investigates the interference effects on wind-induced responses of tall buildings, focusing on the impact of neighbouring structures.

The research investigates the impact of wind on tall buildings characterized by an unconventional Fish-plan shape. The study aims to analyse the influence of various forms of complete blockage interference from neighbouring buildings on the pressure distribution, base force, and overturning moment of the Fish-plan-shaped structure. Findings reveal that the effects of interference vary depending on the position of the interfering building, with oblique configurations leading to more severe consequences on windward surfaces, while re-entrant corners disrupt pressure distribution due to flow stagnation. The phrase "**full blockage**" pertains to shielding, where an obstructing model entirely prevents the incoming wind from reaching the main or instrumented model. This is important because current standards and methods for analysing wind effects on buildings do not account for the unique challenges posed by complex, non-standard shapes like the Fish plan (**Figure 5.1**). By identifying the interference factors specific to the Fish-plan shape, this research could contribute to the development of more insightful methods for analysing wind effects on unconventional tall buildings.

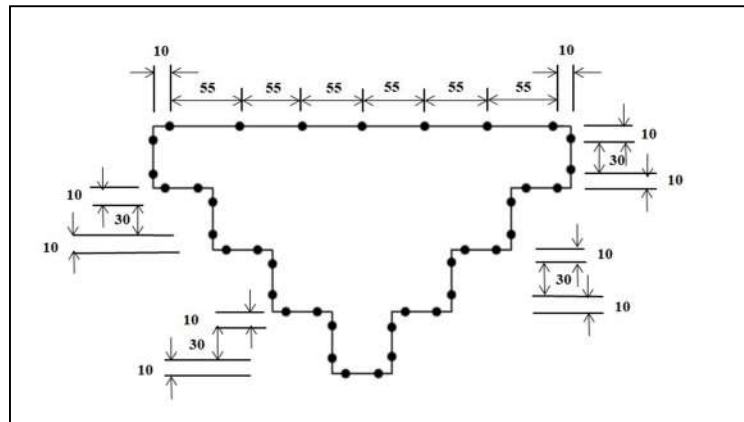


Figure 5.1: Isolated Fish Plan Shape Model

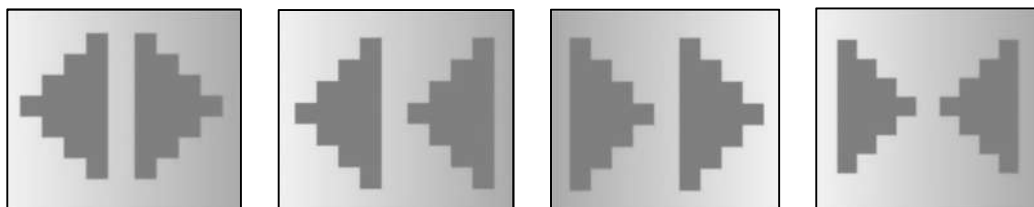


Figure 5.2: Back to Back, Back to Front, Front to Back and Front to Front

The present study also provides insights into the effect of the Interference of Fish-plan shape on pressure and moment coefficients, which were not investigated in detail in previous studies. The use of ANSYS 2022 R1 for CFD simulations also allows for a more accurate and precise evaluation of these coefficients compared to experimental studies. The blockage in the present study is established by placing twin-building models in various orientations at a distance of 10% of the height of the model, i.e., 60 mm, as suggested by (Cook, 1985) [39], (Houghton, 1979) [40]. (See Figure 5.3) The relative position of Fish shape buildings under different interference conditions, namely Back to Back, Back to Front, Front to Back and Front to Front (Figure 5.2).

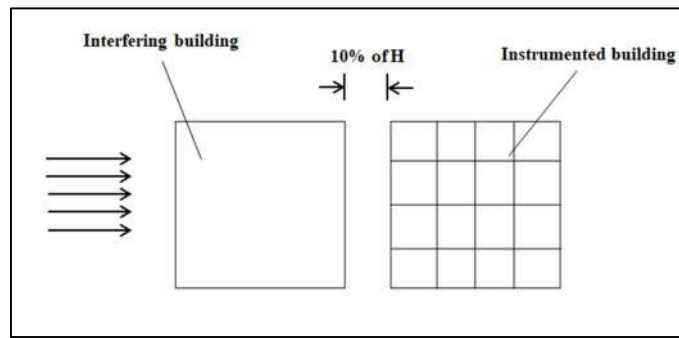


Figure 5.3: Full Blockage interference condition of Square-Plan shape building model

Furthermore, the study takes into account the limitations of using vortex generators and obstructions in wind tunnel experiments and addresses them by using CFD simulations. The variation of wind incidence from 0 to 180 degrees at an interval of 30 degrees and the use of different blockage conditions in the study also provides a comprehensive analysis of the wind effects on the Fish-plan shape. Overall, this project fills the gaps in previous research and provides a more detailed understanding of the wind effects on the Interference of asymmetric building shape, i.e. Fish-plan shape.

5.2 NUMERICAL MODEL DEVELOPMENT

To investigate how wind affects the interference of fish shapes, we conducted a study using two fish-shaped models of the same volume and height of 600mm that were placed together in different positions. The orientations of the twin models used in the interference study have been clearly illustrated in the accompanying figures.

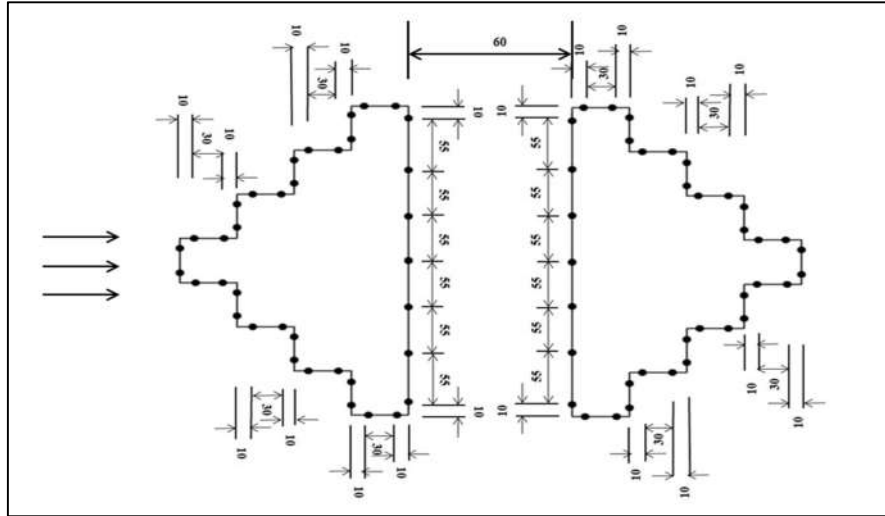


Figure 5.4: Back to Back interference condition

The model depicts a complete blockage interference condition of a fish-shaped model with two buildings, Model A and Model B. The orientation of the models is back to back (**Figure 5.4**), with the windward side indicated by arrows that show the direction of wind flow. The model covers an area of 40,000 square meters. This configuration is used to study the impact of an entirely obstructing building on the performance of an instrumented building when subjected to wind loads. Nomenclature of the faces of the model is shown in **Figure 5.5**.

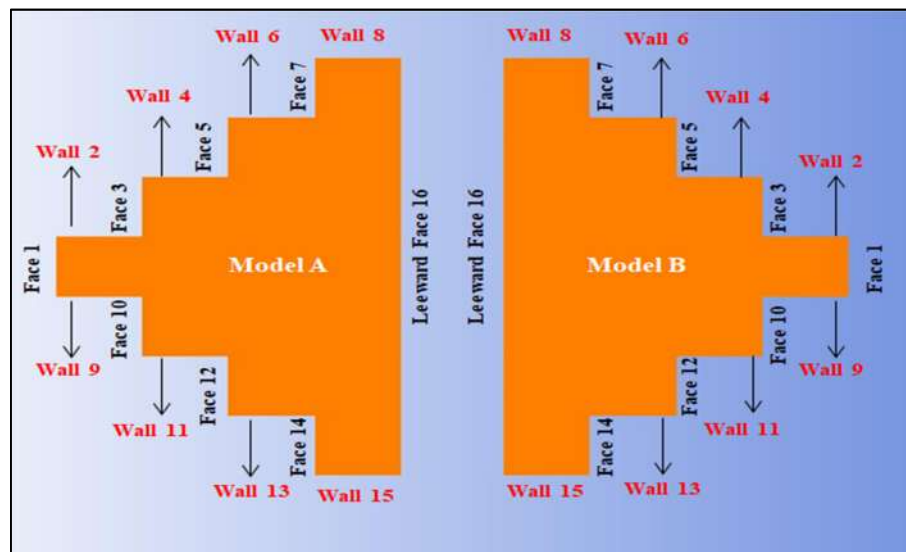


Figure 5.5: Nomenclature of the Model Windward and Leeward faces

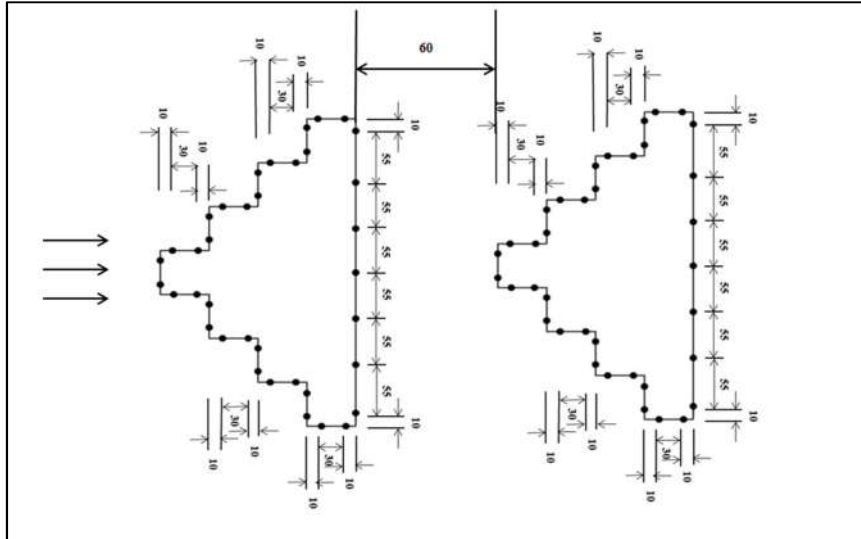


Figure 5.6: Back to Front interference condition

The second interference condition describes the same model but with the orientation of the models changed from back to front (**Figure 5.6**). In this configuration, the obstructing building (Model A) is placed in front of the instrumented building (Model B), and the windward side is shown by arrows indicating the direction of wind flow (**Figure 5.7**). The model covers an area of 40,000 square meters. This configuration can be used to evaluate and optimize the design of buildings for wind loads in complex wind conditions.

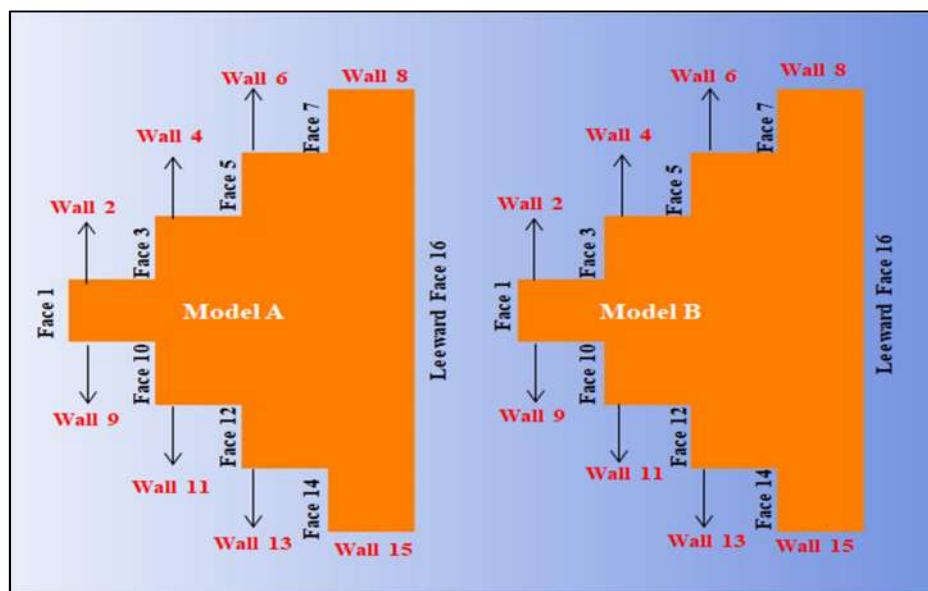


Figure 5.7: Nomenclature of the Model Windward and Leeward faces

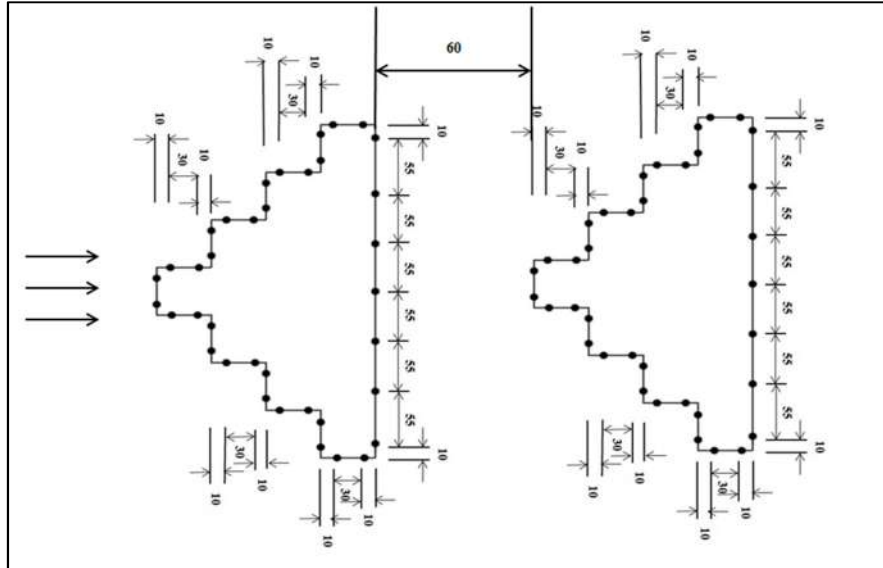


Figure 5.8: Front-to-back interference condition

The third interference condition also describes the same model but with the orientation of the models changed from front to back (**Figure 5.8**). In this configuration, the obstructing building (Model A) is placed behind the instrumented building (Model B), and the windward side is again shown by arrows indicating the direction of wind flow. The model covers an area of 40,000 square meters. Nomenclature of the faces of the model is shown in **Figure 5.9**.

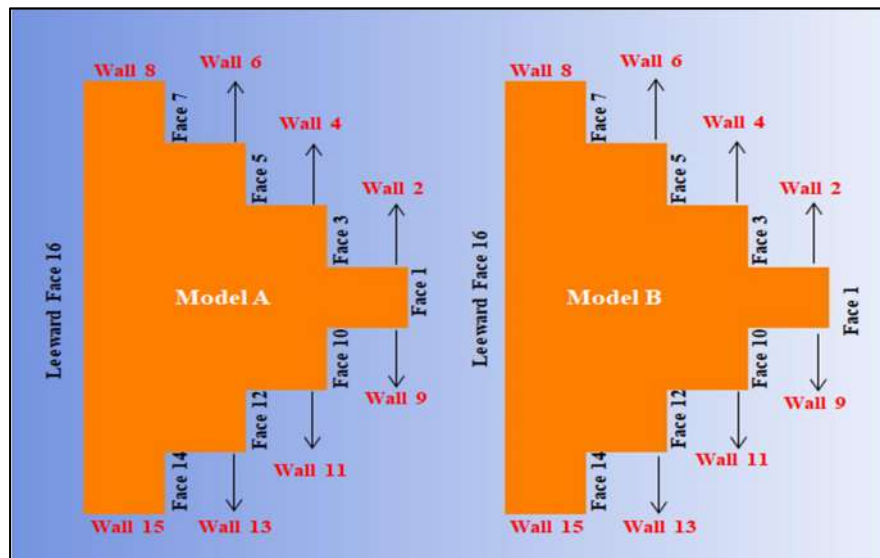


Figure 5.9: Nomenclature of the Model Windward and Leeward faces

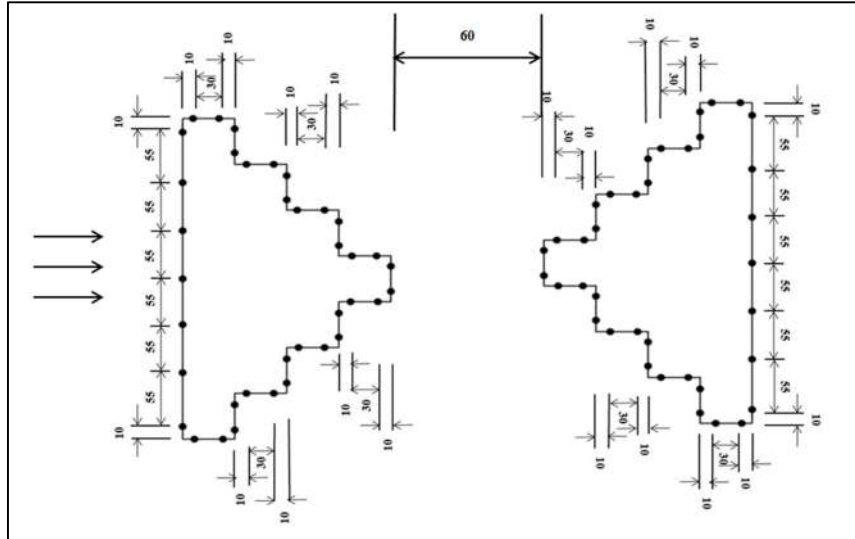


Figure 5.10: Front-to-front interference condition

Finally, the fourth interference condition describes the same model with the orientation of the models changed from front to front (**Figure 5.10**). In this configuration, both buildings are oriented in a back-to-back interference condition, and the windward side is again shown by arrows indicating the direction of wind flow. The model covers an area of 40,000 square meters. This configuration (**Figure 5.11**) can also be used to evaluate and optimize the design of buildings for wind loads in complex wind conditions, providing a comprehensive analysis of the performance of buildings under various wind directions.

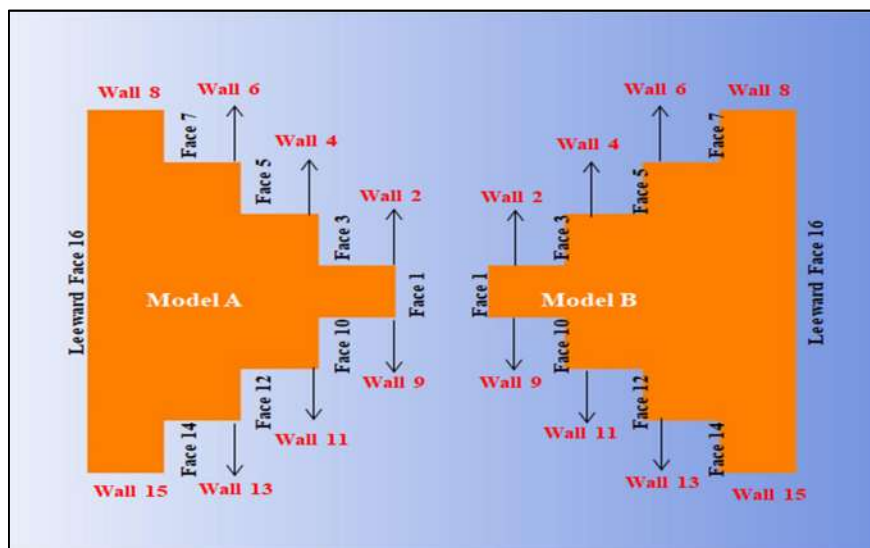


Figure 5.11: Nomenclature of the Model Windward and Leeward faces

The meshing (**Figure 5.13**), setup (**Figure 5.14**) and solution procedure (**Figure 5.15**) were similar to as they were for isolated model conditions. The wind angle was varied at 30 degrees, and simulations were studied up to 180-degree wind inclination angle. Geometry of the Back to back interference model at wind angle 0 degree is shown in **Figure 5.12**

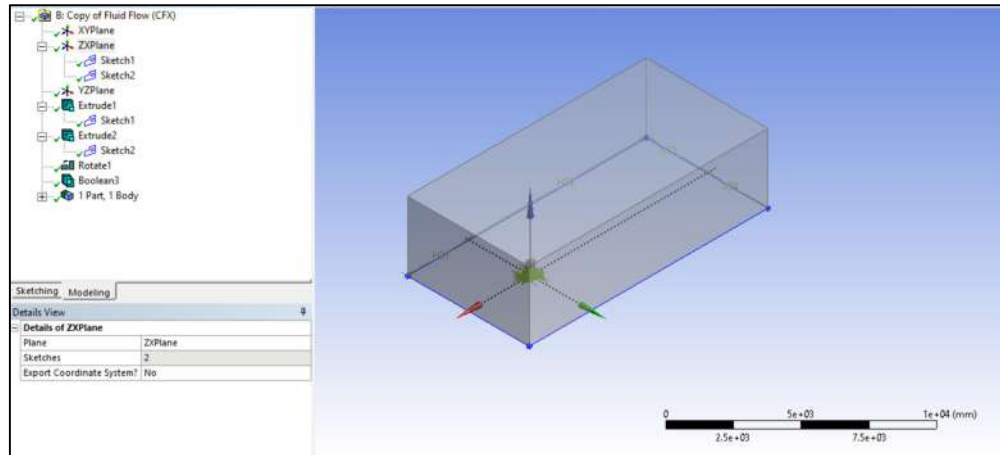


Figure 5.12: Geometry for back-to-back interference condition

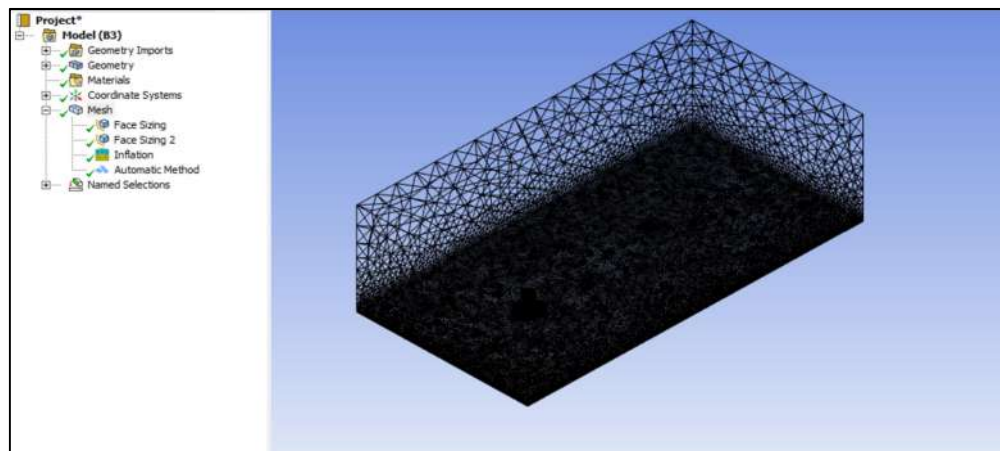


Figure 5.13: Meshing

Meshing plays a crucial role in achieving accurate and reliable simulation results. For our study on interference CFD of a fish-shaped building, we have employed a tetrahedral element shape with an element size of 0.2 m for meshing. In addition, to enhance the interpretation of simulation results, we have provided 15 layers of inflation around the building models. It should be noted that a poor mesh can always lead to a bad solution, while a good mesh does not guarantee an optimal solution.

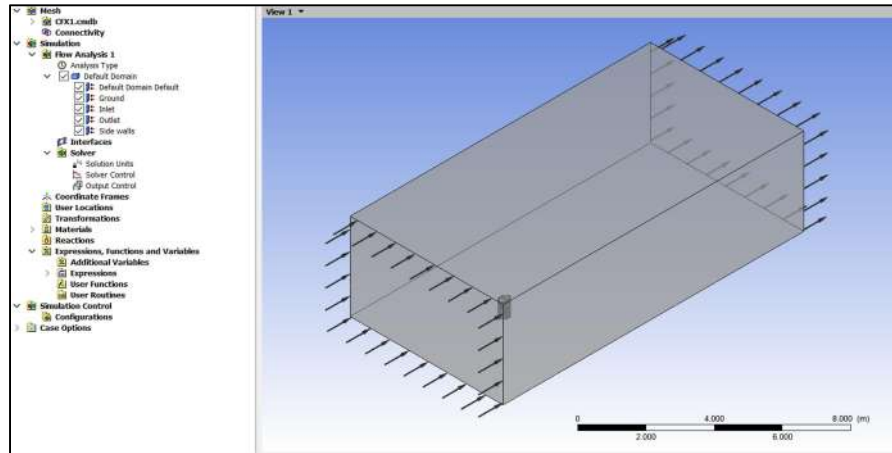


Figure 5.14: Setup in ANSYS 2022 R1

Details of Solver Control in How Analysis 1

Basic Settings Equation Class Settings Advanced Op

Advection Scheme
Option: High Resolution

Turbulence Numerics
Option: First Order

Convergence Control
Min. Iterations: 1
Max. Iterations: 100
Fluid Timescale Control
Timescale Control: Local Timescale Factor
Timescale Factor: []

Convergence Criteria
Residual Type: RMS
Residual Target: 0.000001
 Conservation Target
 Elapsed Wall Clock Time Control
Interrupt Control
Option: Any Interrupt
Convergence Conditions
Option: Default Conditions
User Interrupt Conditions

Details of Air at 25 C

Basic Settings Material Properties

Option: General Material

Thermodynamic Properties
Equation of State
Option: Value
Molar Mass: 28.96 [kg kmol⁻¹]
Density: 1.225 [kg m⁻³]
 Specific Heat Capacity
Option: Value
Specific Heat Capacity: 1.0044E+03 [J kg⁻¹ K⁻¹]
Specific Heat Type: Constant Pressure
 Reference State
Option: Specified Point
Ref. Temperature: 25 [C]
Reference Pressure: 1 [atm]
 Reference Specific Enthalpy
Ref. Spec. Enthalpy: 0. [J/kg]
 Reference Specific Entropy
Ref. Spec. Entropy: 0. [J/kg/K]

Transport Properties
Radiation Properties
 Buoyancy Properties
Option: Value
Thermal Expansivity: 0.003356 [K⁻¹]
Electromagnetic Properties

Expressions

- alpha 0.145
- power law $vRef^{alpha} (y/yRef)^{-alpha}$
- vRef 10[m/s]
- yRef 1[m]

Figure 5.15: Solver control, Material properties and Expressions as per Power Law

CHAPTER 6 - RESULTS & DISCUSSION FOR INTERFERENCE STUDY

The pressure coefficient is calculated in the same manner it was calculated for the isolated model. The values are then validated against international codes. Velocity streamlines are also calculated to get an idea of flow lines and vortex formation.

6.1 PRESSURE CONTOURS

Pressure contours obtained from ANSYS CFX analysis depict the distribution of pressure values on a surface. These contours can be used to observe and compare the impact of pressure at different points on the surface. In this particular analysis, pressure contours were obtained for wind inclinations varying from 0° to 180° at 30° intervals.

Upon analysing the pressure contours, it can be observed that the pressure values on the surface increase as the wind inclination angle increases. At a wind inclination of 0° , the pressure values are relatively low, while at 180° , the pressure values are the highest. This suggests that the direction of wind flow plays a significant role in determining the pressure distribution on a surface. Furthermore, the pressure contours also show that there are variations in pressure values along different sections of the surface.

6.1.1 Back to Back Interference Condition

- Case 1 – The incident wind angle is 0°

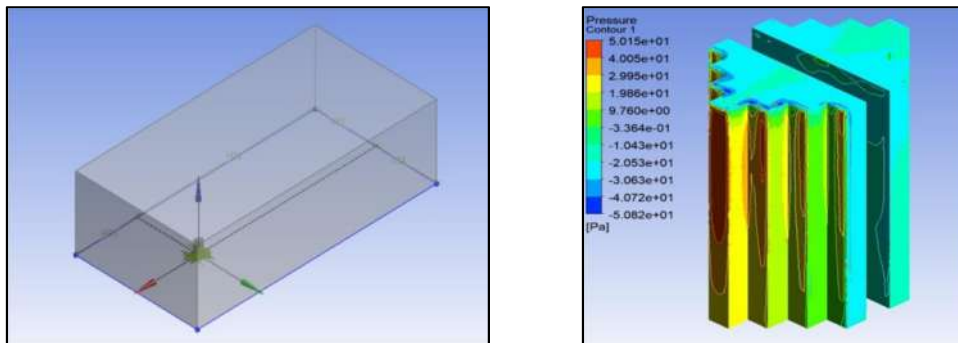
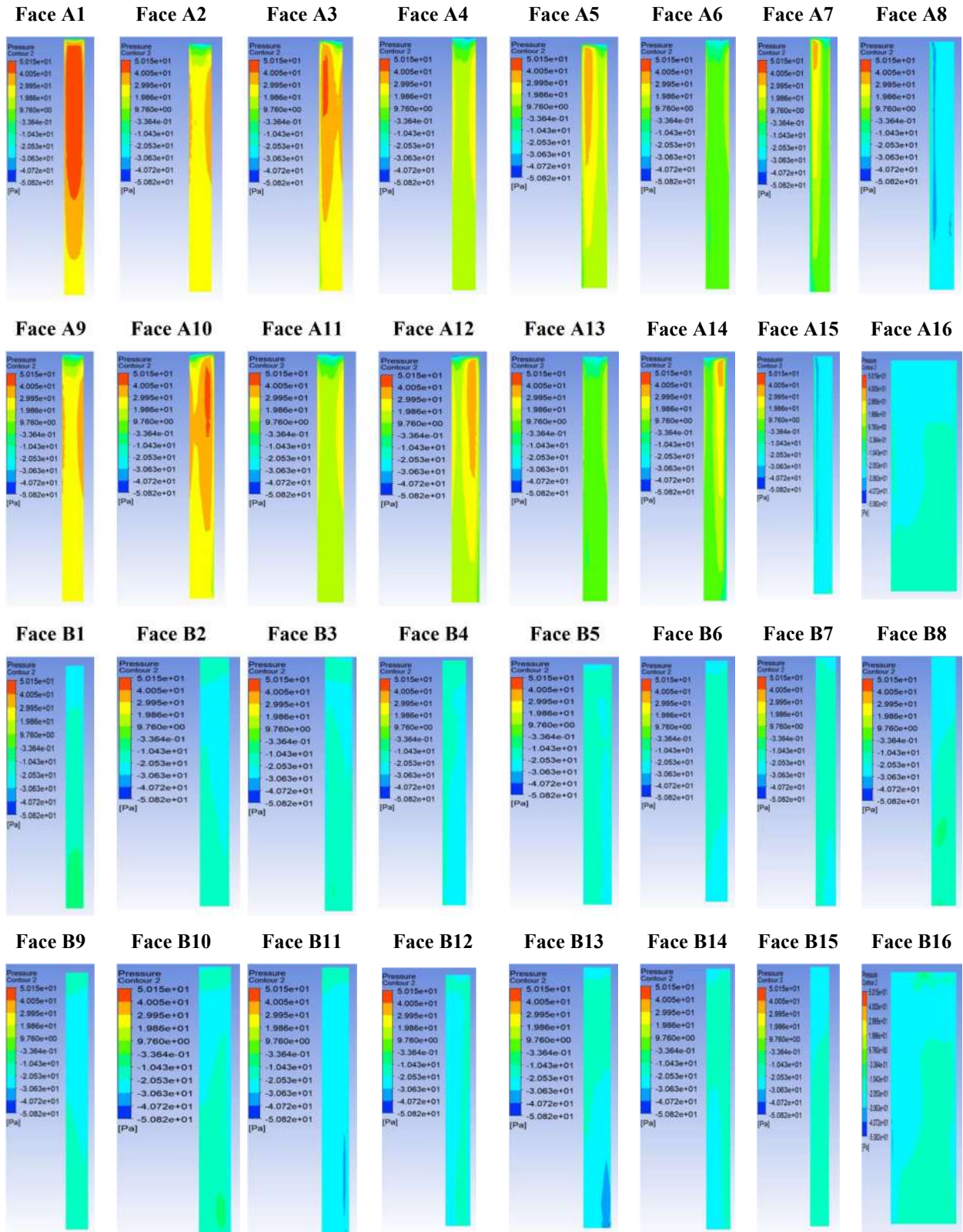


Figure 6.1: Geometry and Pressure contour of the model when the inclination is 0 degree

Table 6.1: Pressure contour of faces at 0-degree wind inclination for Model A and B



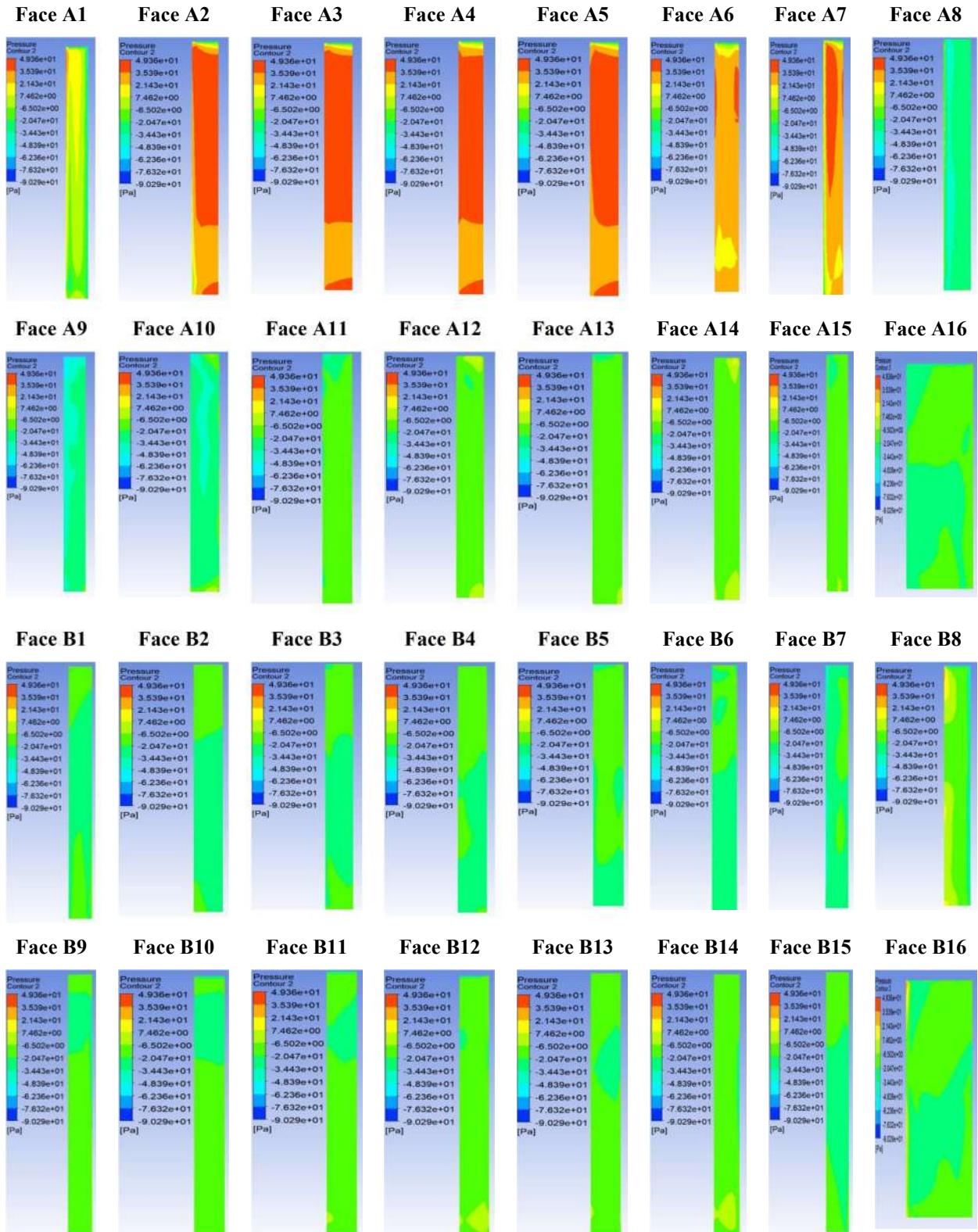
The range of average pressure values for the wind inclination angle of 0° (Figure 6.1) is between $[-23.84, 35.82]$ (Table 6.1). The maximum positive and negative pressure values of 35.82 and -23.84, respectively, occur on Face A1 and A8. The range of pressure coefficient C_p lies in the range $\varepsilon [-0.39, 0.58]$ (Table 6.2). The maximum positive and negative values of 0.58 and -0.39 occur on Faces A1 and A8.

Table 6.2: Average C_p value for wind inclination 0 degree

Wind Inclination Angle 0				
Faces/Wall	Range of Pressure	Average value of Pressure	Range of C_p	Average Value of C_p
A1	(-15.69,50.15)	35.82	(-0.26,0.82)	0.58
A2	(-42.68,34.80)	25.06	(-0.70,0.57)	0.41
A3	(-46.85,41.80)	27.50	(-0.76,0.68)	0.45
A4	(-40.48,25.46)	16.00	(-0.66,0.42)	0.26
A5	(-34.60,36.95)	19.17	(-0.56,0.60)	0.31
A6	(-34.1,15.45)	5.08	(-0.56,0.25)	0.08
A7	(-35.7,37.40)	7.94	(-0.58,0.61)	0.13
A8	(-43.34,-4.0)	-23.84	(-0.71,-0.07)	-0.39
A9	(-44.37,35.67)	25.09	(-0.72,0.63)	0.41
A10	(-44.37,41.95)	27.74	(-0.72,0.68)	0.45
A11	(-41.78,25.39)	15.89	(-0.68,0.41)	0.21
A12	(-39.30,37.10)	19.38	(-0.64,0.61)	0.32
A13	(-34.71,16.51)	5.19	(-0.57,0.27)	0.08
A14	(-35.81,36.73)	8.19	(-0.58,0.60)	0.13
A15	(-41.19,-0.25)	-22.57	(-0.67,0.00)	-0.37
A16	(-28.74,-15.26)	-20.35	(-0.47,-0.25)	-0.33
B1	(-26.89,-5.54)	-16.48	(-0.44,-0.09)	-0.27
B2	(-22.80,-14.35)	-19.75	(-0.37,-0.23)	-0.32
B3	(-24.45,-10.32)	-18.65	(-0.40,-0.17)	-0.30
B4	(-29.14,-19.81)	-21.57	(-0.48,-0.32)	-0.35
B5	(-25.78,-14.32)	-19.81	(-0.42,-0.23)	-0.32
B6	(-29.21,-15.57)	-20.23	(-0.48,-0.25)	-0.33
B7	(-27.91,-12.78)	-18.79	(-0.46,-0.21)	-0.31
B8	(-28.29,-9.28)	-18.24	(-0.46,-0.15)	-0.30
B9	(-24.13,-11.94)	-19.69	(-0.39,-0.19)	-0.32
B10	(-26.98,-9.40)	-18.77	(-0.44,-0.15)	-0.31
B11	(-32.98,-19.95)	-23.60	(-0.54,-0.33)	-0.39
B12	(-33.67,-15.05)	-21.31	(-0.55,-0.25)	-0.35
B13	(-35.64,-18.98)	-22.91	(-0.58,-0.31)	-0.37
B14	(-30.27,-16.41)	-20.82	(-0.49,-0.27)	-0.34
B15	(-27.65,-13.13)	-18.86	(-0.45,-0.21)	-0.31
B16	(-34.14,-3.34)	-20.59	(-0.56,-0.05)	-0.34

- Case 2 – The incident wind angle is 30°

Table 6.3: Pressure contour of faces at 30-degree wind inclination for Model A and B



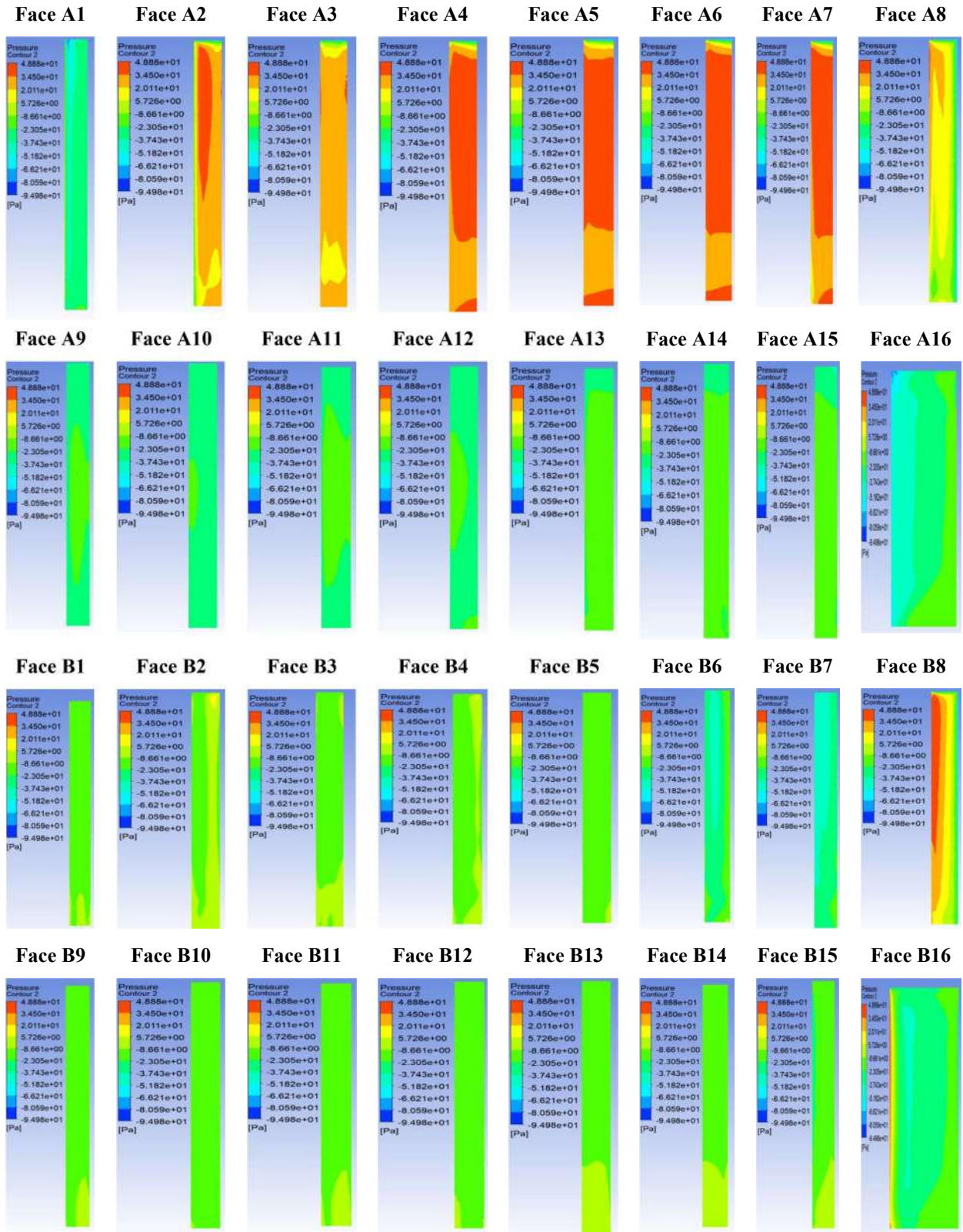
The range of average pressure values for the wind inclination angle of 30° is between [-33.79, 39.09] (Table 6.3). The maximum positive and negative pressure values of 39.09 and -33.79, respectively, occur on Face A3 and A9. The range of pressure coefficient C_p lies in the range ϵ [-0.55, 0.64] (Table 6.4). The maximum positive and negative values of 0.64 and -0.55 occur on Faces A3 and A9.

Table 6.4: Average C_p value for wind inclination 30 degree

Wind Inclination Angle 30				
Faces/Wall	Range of Pressure	Average value of Pressure	Range of C_p	Average Value of C_p
A1	(-63.77,36.81)	-4.13	(-1.04,0.60)	-0.07
A2	(-50.31,49.36)	36.00	(-0.82,0.81)	0.59
A3	(-39.52,48.74)	39.09	(-0.65,0.80)	0.64
A4	(-52.61,47.86)	38.19	(-0.86,0.78)	0.62
A5	(-43.70,48.16)	37.28	(-0.71,0.79)	0.61
A6	(-40.07,37.52)	27.06	(-0.65,0.61)	0.44
A7	(-39.54,45.86)	23.60	(-0.65,0.75)	0.39
A8	(-55.82,4.81)	-28.68	(-0.91,0.08)	-0.47
A9	(-63.77,-17.73)	-33.79	(-1.04,-0.29)	-0.55
A10	(-51.85,-0.78)	-27.59	(-0.85,-0.01)	-0.45
A11	(-41.56,-5.81)	-18.09	(-0.68,-0.09)	-0.30
A12	(-24.51,10.6)	-15.55	(-0.40,0.18)	-0.25
A13	(-32.84,-2.90)	-13.52	(-0.54,-0.05)	-0.22
A14	(-19.90,14.74)	-11.82	(-0.32,0.24)	-0.19
A15	(-28.66,-4.01)	-13.92	(-0.47,-0.07)	-0.23
A16	(-30.44,8.62)	-20.45	(-0.50,-0.14)	-0.33
B1	(-25.78,-14.34)	-20.84	(-0.42,-0.23)	-0.34
B2	(-27.50,-14.87)	-21.81	(-0.45,-0.24)	-0.36
B3	(-24.83,-14.87)	-20.70	(-0.41,-0.24)	-0.34
B4	(-25.81,-13.98)	-20.14	(-0.42,-0.23)	-0.33
B5	(-30.19,-16.85)	-19.94	(0.49,-0.28)	-0.33
B6	(-26.63,-12.60)	-21.50	(-0.43,-0.21)	-0.35
B7	(-47.58,-19.41)	-24.83	(-0.78,-0.32)	-0.41
B8	(-50.94,27.34)	-12.79	(-0.83,0.45)	-0.21
B9	(-24.58,-7.23)	-16.59	(-0.35,-0.12)	-0.27
B10	(-21.86,-7.05)	-16.24	(-0.36,-0.12)	-0.26
B11	(-22.78,-6.46)	-15.69	(-0.37,-0.11)	-0.26
B12	(-22.36,-5.69)	-15.35	(-0.37,-0.09)	-0.25
B13	(-22.06,-6.35)	-15.50	(-0.36,-0.10)	-0.25
B14	(-24.96,-4.86)	-14.93	(-0.41,-0.08)	-0.24
B15	(-32.74,-10.30)	-20.45	(-0.53,-0.17)	-0.33
B16	(-43.88,27.34)	-19.45	(-0.72,0.45)	-0.32

- Case 3 – The incident wind angle is 60°

Table 6.5: Pressure contour of faces at 60-degree wind inclination for Model A and B



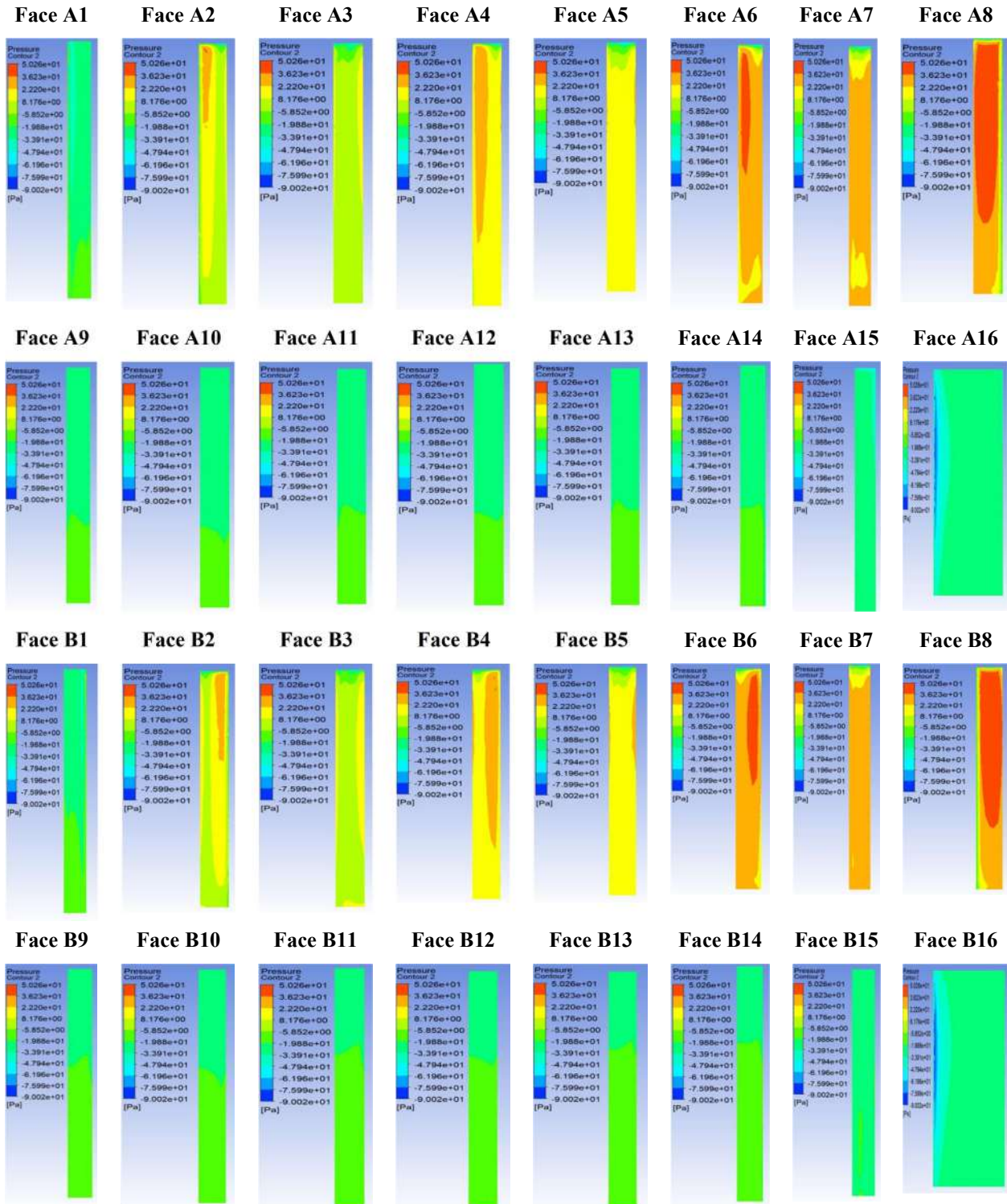
The range of average pressure values for the wind inclination angle of 60° is between [-35.36, 38.18] (Table 6.5). The maximum positive and negative pressure values of 38.18 and -35.36, respectively, occur on Face A6 and B7. The range of pressure coefficient C_p lies in the range ϵ [-0.58, 0.62] (Table 6.6). The maximum positive and negative values of 0.62 and -0.58 occur on Faces A6 and B7.

Table 6.6: Average C_p value for wind inclination 60 degree

Wind Inclination Angle 60				
Faces/Wall	Range of Pressure	Average value of Pressure	Range of C_p	Average Value of C_p
A1	(-79.5,-2.29)	-30.95	(-1.30,-0.04)	-0.51
A2	(-59.72,44.88)	22.49	(-0.98,0.73)	0.37
A3	(-54.10,35.79)	25.03	(-0.88,0.58)	0.41
A4	(-53.52,47.58)	36.03	(-0.87,0.78)	0.59
A5	(-60.20,46.63)	36.50	(-0.98,0.76)	0.60
A6	(-63.14,48.25)	38.18	(-1.03,0.79)	0.62
A7	(-66.83,48.88)	36.06	(-1.09,0.80)	0.59
A8	(-65.94,39.42)	1.68	(-1.08,0.64)	0.03
A9	(-44.13,-21.83)	-24.42	(-0.72,-0.36)	-0.40
A10	(-43.69,-22.77)	-24.62	(-0.71,-0.37)	-0.40
A11	(-35.85,-20.75)	-23.32	(-0.59,-0.34)	-0.38
A12	(-34.87,-21.10)	-24.07	(-0.57,-0.34)	-0.39
A13	(-27.47,-16.78)	-20.49	(-0.45,-0.27)	-0.33
A14	(-27.68,-16.47)	-20.63	(-0.45,-0.27)	-0.34
A15	(-44.78,-14.11)	-20.50	(-0.73,-0.23)	-0.33
A16	(-75.80,-14.46)	-31.89	(-1.24,-0.24)	-0.52
B1	(-22.18,-3.66)	-12.50	(-0.36,-0.06)	-0.20
B2	(-16.85,13.94)	-8.02	(-0.28,0.23)	-0.13
B3	(-19.84,-4.50)	-9.67	(-0.32,-0.07)	-0.16
B4	(-18.17,9.83)	-9.95	(-0.30,0.16)	-0.16
B5	(-20.20,-6.40)	-11.60	(-0.33,-0.10)	-0.19
B6	(-43.08,-7.02)	-27.54	(-0.70,-0.11)	-0.45
B7	(-53.29,-15.69)	-35.36	(-0.87,-0.26)	-0.58
B8	(-53.00,47.95)	11.29	(-0.87,0.78)	0.18
B9	(-14.52,-7.39)	-11.87	(-0.24,-0.12)	-0.19
B10	(-14.90,-8.50)	-12.37	(-0.24,-0.14)	-0.20
B11	(-14.89,-6.65)	-11.82	(-0.24,-0.11)	-0.19
B12	(-15.52,-8.05)	-12.37	(-0.25,-0.13)	-0.20
B13	(-14.93,-5.30)	-10.91	(-0.24,-0.09)	-0.18
B14	(-14.80,-5.84)	-11.04	(-0.24,-0.10)	-0.18
B15	(-35.64,-4.31)	-14.94	(-0.58,-0.07)	-0.24
B16	(-76.74,43.92)	-24.02	(-1.25,0.72)	-0.39

- Case 4 – The incident wind angle is 90°

Table 6.7: Pressure contour of faces at 90-degree wind inclination for Model A and B



The range of average pressure values for the wind inclination angle of 90° is between $[-29.58, 28.36]$ (Table 6.7). The maximum positive and negative pressure values of 28.36

and -29.58, respectively, occur on Face B6 and A16. The range of pressure coefficient C_p lies in the range ϵ [-0.48, 0.46] (Table 6.8). The maximum positive and negative values of 0.46 and -0.48 occur on Faces B6 and A16.

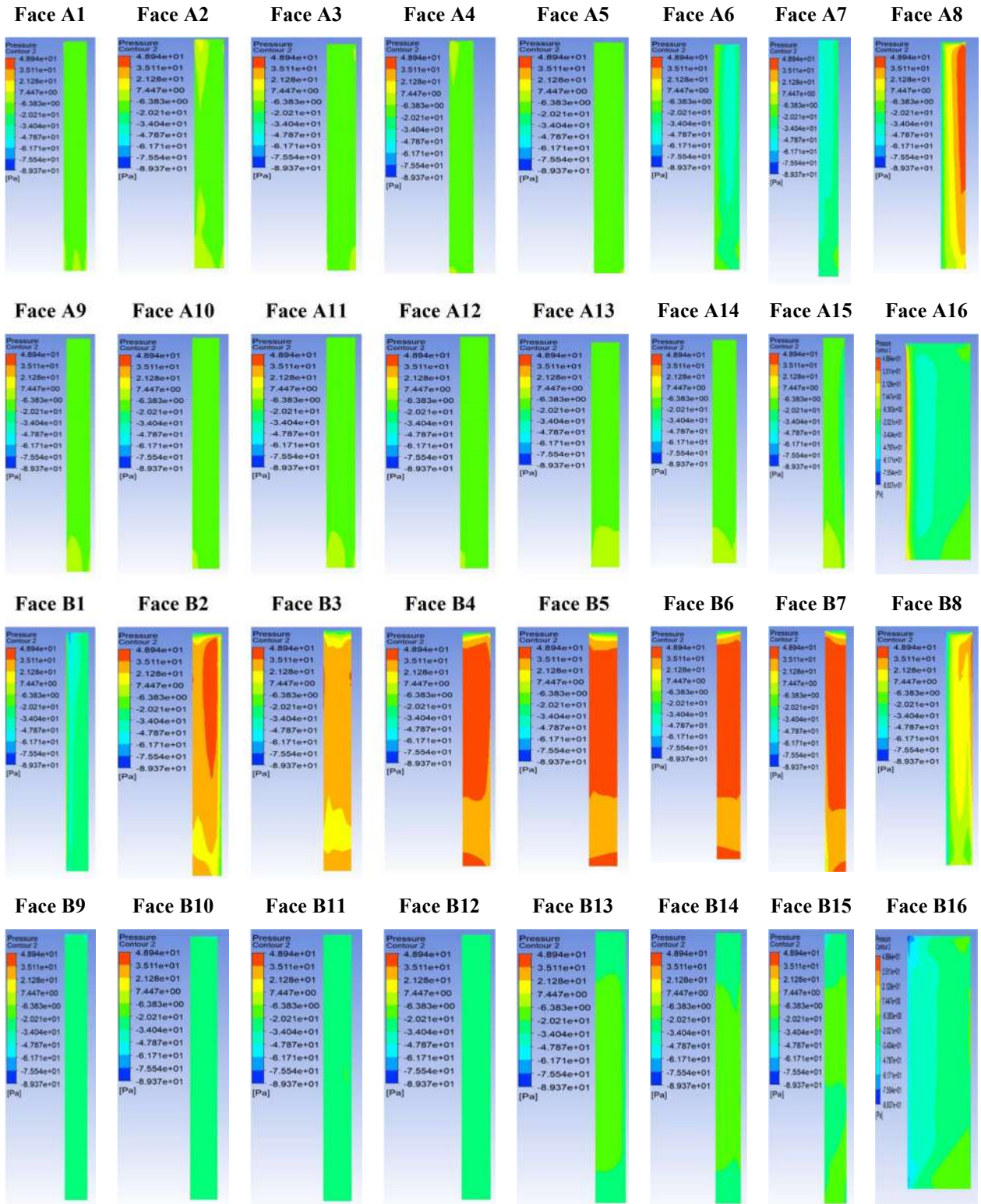
Table 6.8: Average C_p value for wind inclination 90 degree

Wind Inclination Angle 90				
Faces/Wall	Range of Pressure	Average value of Pressure	Range of C_p	Average Value of C_p
A1	(-46.26,-3.80)	-25.47	(-0.76,-0.06)	-0.42
A2	(-40.50,37.49)	6.65	(-0.66,0.61)	0.11
A3	(-49.12,14.12)	3.50	(-0.80,0.23)	0.06
A4	(-52.45,36.02)	17.39	(-0.86,0.59)	0.28
A5	(-52.52,24.00)	13.65	(-0.86,0.39)	0.22
A6	(-50.88,41.14)	26.79	(-0.83,0.67)	0.44
A7	(-59.98,34.27)	24.10	(-0.98,0.56)	0.39
A8	(-39.19,50.26)	27.79	(-0.64,0.82)	0.45
A9	(-31.30,-14.53)	-22.34	(-0.51,-0.24)	-0.36
A10	(-29.66,-15.62)	-22.78	(-0.49,-0.25)	-0.37
A11	(-27.92,-14.58)	-24.72	(-0.46,-0.24)	-0.35
A12	(-28.36,-15.33)	-22.05	(-0.46,-0.25)	-0.36
A13	(-28.54,-15.71)	-21.76	(-0.47,-0.26)	-0.36
A14	(-32.14,-16.22)	-21.97	(-0.52,-0.26)	-0.36
A15	(-49.56,-20.74)	-27.06	(-0.81,-0.34)	-0.44
A16	(-87.83,-10.31)	-29.58	(-1.43,-0.17)	-0.48
B1	(-41.45,0.26)	-20.93	(-0.68,0.00)	-0.34
B2	(-37.02,35.92)	8.61	(-0.60,0.59)	0.14
B3	(-40.54,14.98)	5.75	(-0.66,0.24)	0.09
B4	(-38.24,36.76)	18.91	(-0.62,0.60)	0.31
B5	(-45.08,26.49)	15.41	(-0.74,0.43)	0.25
B6	(-41.56,42.43)	28.36	(-0.68,0.69)	0.46
B7	(-49.56,35.56)	25.98	(-0.81,0.58)	0.42
B8	(-35.83,49.91)	27.73	(-0.59,0.81)	0.45
B9	(-29.82,-11.05)	-17.80	(-0.49,-0.18)	-0.29
B10	(-29.49,-11.91)	-18.31	(-0.48,-0.19)	-0.30
B11	(-26.93,-10.68)	-17.21	(-0.44,-0.17)	-0.28
B12	(-25.11,-11.35)	-17.39	(-0.41,-0.19)	-0.28
B13	(-23.65,-12.18)	-17.70	(-0.39,-0.20)	-0.29
B14	(-23.45,-12.47)	-18.12	(-0.38,-0.20)	-0.30
B15	(-33.27,-19.30)	-22.94	(-0.54,-0.32)	-0.37
B16	(-90.02,-15.77)	-29.42	(-1.47,-0.26)	-0.48

- Case 5 – The incident wind angle is 120°

The range of average pressure values for the wind inclination angle of 120° is between [-33.24, 38.67] (Table 6.9). The maximum positive and negative pressure values of 38.67 and -33.24, respectively, occur on Face B6 and A7.

Table 6.9: Pressure contour of faces at 120-degree wind inclination for Model A and B



The range of pressure coefficient C_p lies in the range ε [-0.54, 0.66] (Table 6.10). The maximum positive and negative values of 0.66 and -0.54 occur on Faces B6 and A7.

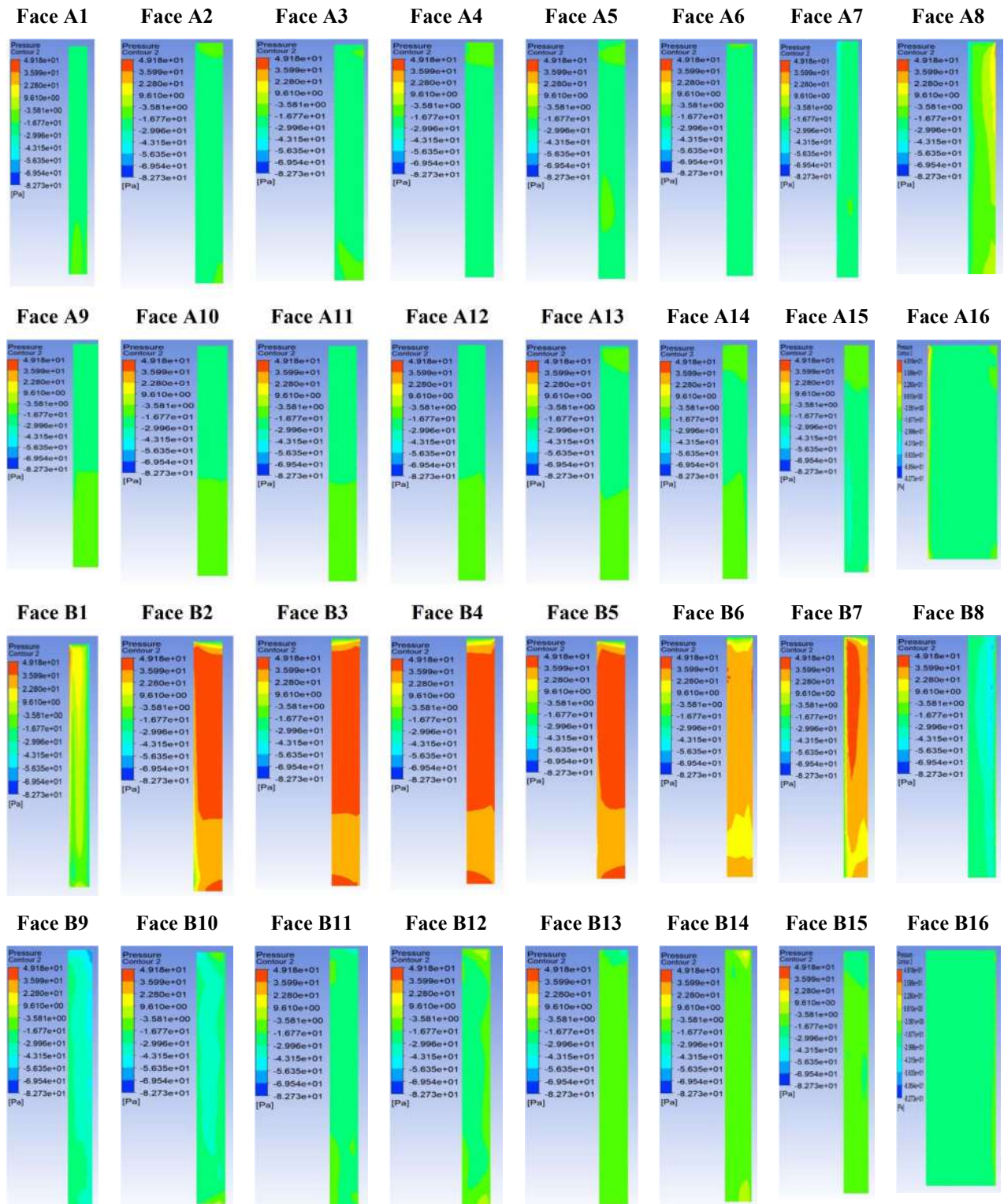
Table 6.10: Average C_p value for wind inclination 120 degree

Wind Inclination Angle 120				
Faces/Wall	Range of Pressure	Average value of Pressure	Range of C_p	Average Value of C_p
A1	(-20.08,-2.80)	-12.15	(-0.33,-0.05)	-0.20
A2	(-16.24,14.02)	-7.56	(-0.26,0.23)	-0.12
A3	(-17.15,-3.21)	-9.35	(-0.26,-0.04)	-0.14
A4	(-16.60,8.77)	-11.15	(-0.27,0.15)	-0.17
A5	(-17.77,-5.36)	-11.17	(-0.31,-0.09)	-0.18
A6	(-43.23,-6.21)	-27.03	(-0.71,-0.10)	-0.44
A7	(-51.39,-15.57)	-33.24	(-0.83,-0.25)	-0.54
A8	(-50.14,48.06)	11.85	(-0.82,0.78)	0.20
A9	(-15.03,-5.45)	-11.37	(-0.25,-0.09)	-0.18
A10	(-15.37,-6.04)	-11.66	(-0.25,-0.10)	-0.20
A11	(-15.48,-5.09)	-11.33	(-0.25,-0.08)	-0.18
A12	(-15.97,-6.00)	-11.75	(-0.26,-0.10)	-0.19
A13	(-15.64,-4.38)	-11.12	(-0.26,-0.07)	-0.18
A14	(-16.07,-5.02)	-11.53	(-0.26,-0.08)	-0.19
A15	(-37.45,-3.46)	-15.54	(-0.61,-0.06)	-0.24
A16	(-63.86,44.50)	-24.12	(-1.04,0.73)	0.40
B1	(-75.50,-4.77)	-30.22	(-1.23,-0.08)	-0.50
B2	(-59.24,4.93)	23.12	(-0.97,0.73)	0.37
B3	(-54.04,35.85)	25.25	(-0.88,0.59)	0.40
B4	(-55.82,47.66)	36.23	(-0.91,0.78)	0.60
B5	(-62.00,46.78)	36.45	(-1.01,0.76)	0.60
B6	(-58.70,48.37)	38.67	(-0.96,0.79)	0.66
B7	(-70.75,48.94)	36.33	(-1.16,0.80)	0.59
B8	(-80.93,39.29)	1.52	(-1.32,0.64)	0.04
B9	(-43.64,-21.39)	-24.15	(-0.71,-0.35)	-0.40
B10	(-43.32,22.34)	-24.32	(-0.71,-0.36)	-0.40
B11	(-36.55,-20.15)	-23.20	(-0.60,-0.33)	-0.38
B12	(-34.16,-21.28)	-23.76	(-0.56,-0.35)	-0.39
B13	(-27.20,-16.32)	-20.25	(-0.44,-0.27)	-0.32
B14	(-28.00,-16.74)	-20.35	(-0.46,-0.27)	-0.33
B15	(-47.35,-14.83)	-20.60	(-0.77,-0.24)	-0.34
B16	(-84.13,13.70)	-32.28	(-1.37,-0.22)	-0.54

- Case 6 – The incident wind angle is 150°

At 150 degrees of wind inclination, the wind has a similar effect to the previous degree of angle, Here faces B2, B3, B4, B5, B5, B6 and B7 face the most considerable impact of the wind pressure, which can be seen by re and yellowish coloured area.

Table 6.11: Pressure contour of faces at 150-degree wind inclination for Model A and B



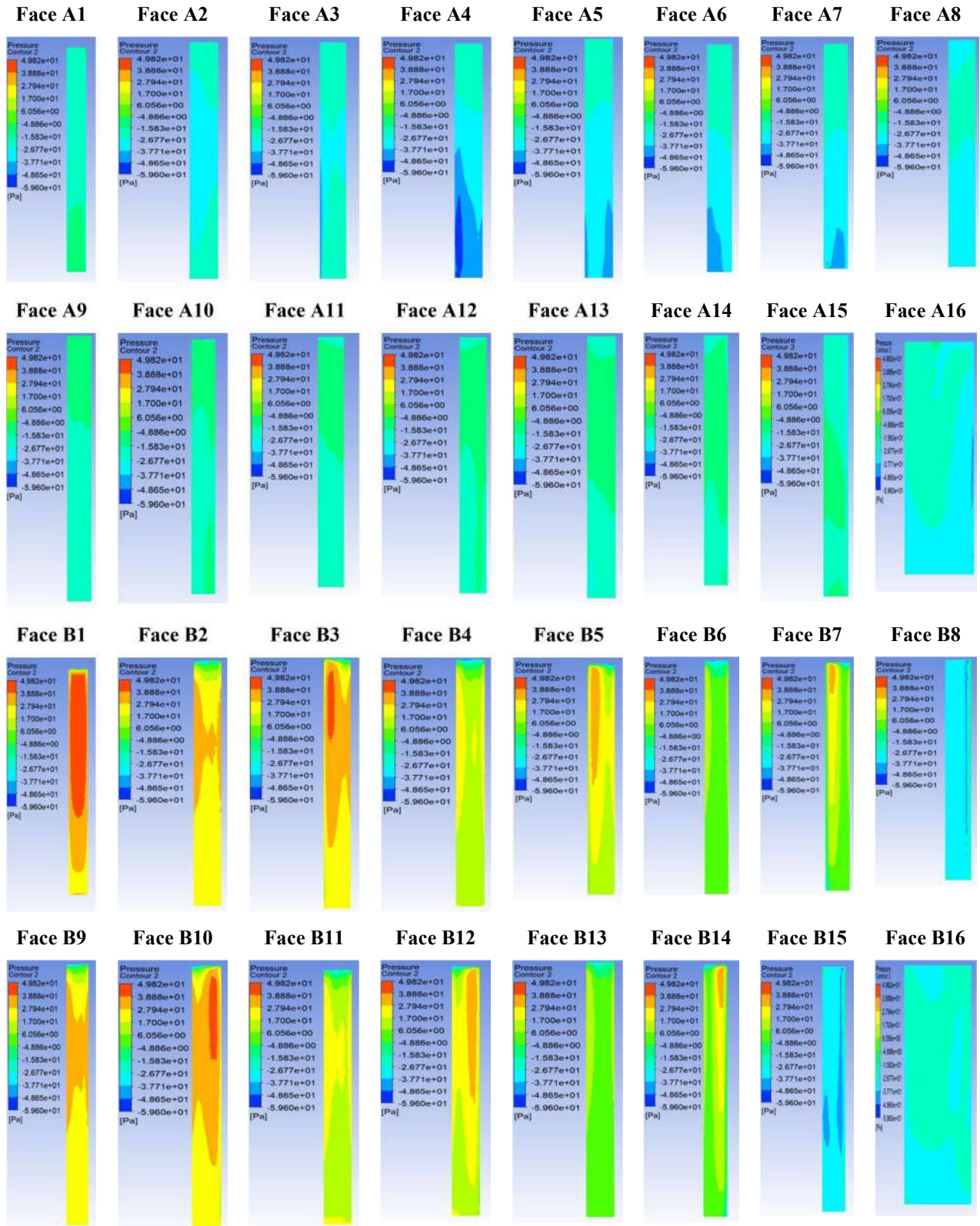
The range of average pressure values for the wind inclination angle of 150° is between [-34.74, 38.44] (Table 6.11). The maximum positive and negative pressure values of 38.44 and -34.74, respectively, occur on Faces B6 and A7. The range of pressure coefficient C_p lies in the range ε [-0.57, 0.63] (Table 6.12). The maximum positive and negative values of 0.63 and -0.57 occur on Faces B6 and A7.

Table 6.12: Table 38: Average C_p value for wind inclination 150 degree

Wind Inclination Angle 150				
Faces/Wall	Range of Pressure	Average value of Pressure	Range of C_p	Average Value of C_p
A1	(-20.08,-2.80)	-12.19	(-0.33,-0.05)	-0.20
A2	(-15.26,14.02)	-7.85	(-0.25,0.23)	-0.13
A3	(-17.15,-3.21)	-9.45	(-0.28,-0.05)	-0.15
A4	(-16.50,8.97)	-9.63	(-0.27,0.15)	-0.16
A5	(-18.77,-5.56)	-11.17	(-0.31,-0.09)	-0.18
A6	(-43.23,-6.21)	-27.03	(-0.71,-0.10)	-0.44
A7	(-51.89,-15.37)	-34.74	(-0.85,-0.25)	-0.57
A8	(-50.14,48.06)	11.85	(-0.82,0.78)	0.19
A9	(-15.03,-5.45)	-11.27	(-0.25,-0.09)	-0.18
A10	(-15.37,-6.04)	-11.66	(-0.25,-0.10)	-0.19
A11	(-15.48,-5.09)	-11.33	(-0.25,-0.08)	-0.18
A12	(-15.97,-6.00)	-11.80	(-0.26,-0.10)	-0.19
A13	(-15.64,-4.38)	-11.09	(-0.26,-0.07)	-0.18
A14	(-16.07,-5.02)	-11.52	(-0.26,-0.08)	-0.19
A15	(-37.45,-3.46)	-15.58	(-0.61,-0.06)	-0.25
A16	(-63.86,44.50)	-24.14	(-1.04,0.73)	-0.39
B1	(-75.50,-4.77)	-30.44	(-1.23,-0.08)	-0.50
B2	(-59.24,44.93)	23.02	(-0.97,0.73)	0.38
B3	(-54.04,35.85)	25.11	(-0.88,0.59)	0.41
B4	(-55.82,47.66)	36.01	(-0.91,0.78)	0.59
B5	(-62.00,46.78)	36.54	(-1.01,0.76)	0.60
B6	(-58.70,48.37)	38.44	(-0.96,0.79)	0.63
B7	(-70.75,48.94)	36.32	(-1.16,0.80)	0.59
B8	(-80.93,39.29)	1.59	(-1.32,0.64)	0.03
B9	(-43.64,-21.39)	-24.12	(-0.71,-0.35)	-0.39
B10	(-43.32,-22.34)	-24.31	(-0.71,-0.36)	-0.40
B11	(-36.55,-20.15)	-23.10	(-0.60,-0.33)	-0.38
B12	(-34.16,-21.28)	-23.76	(-0.56,-0.35)	-0.39
B13	(-27.20,-16.32)	-20.42	(-0.44,-0.27)	-0.33
B14	(-28.00,-16.74)	-20.45	(-0.46,-0.27)	-0.33
B15	(-47.35,-14.83)	-20.90	(-0.77,-0.24)	-0.34
B16	(-84.13,-13.70)	-32.19	(-1.37,-0.22)	-0.53

- Case 7 – The incident wind angle is 180°

Table 6.13: Pressure contour of faces at 180-degree wind inclination for Model A and B



The range of average pressure values for the wind inclination angle of 180^0 is between [-34.75, 35.54] (Table 6.13). The maximum positive and negative pressure values of 35.54 and -34.75, respectively, occur on Face B1 and A4. The range of pressure coefficient C_p lies in the range ε [-0.45, 0.37] (Table 6.14). The maximum positive and negative values of 0.37 and -0.45 occur on Faces B1 and A4

Table 6.14: Table 38: Average C_p value for wind inclination 180 degree

Wind Inclination Angle 180				
Faces/Wall	Range of Pressure	Average value of Pressure	Range of C_p	Average Value of C_p
A1	(-33.28,-10.04)	-18.61	(-0.54,-0.16)	-0.30
A2	(-38.13,-17.17)	-26.96	(-0.62,-0.28)	-0.44
A3	(-48.77,-17.47)	-26.16	(-0.80,-0.29)	-0.43
A4	(-59.60,-23.08)	-34.75	(-0.97,-0.38)	-0.57
A5	(-47.49,-23.53)	-31.12	(-0.78,-0.38)	-0.51
A6	(-47.49,-23.55)	-30.09	(-0.78,-0.38)	-0.49
A7	(-40.87,-20.94)	-29.35	(-0.67,-0.34)	-0.48
A8	(-36.65,-24.03)	-28.26	(-0.60,-0.39)	-0.46
A9	(-22.75,-14.67)	-17.91	(-0.37,-0.24)	-0.29
A10	(-22.42,-12.36)	-16.90	(-0.37,-0.20)	-0.28
A11	(-26.30,-14.60)	-17.72	(-0.43,-0.24)	-0.29
A12	(-25.48,-14.01)	-16.62	(-0.42,-0.23)	-0.27
A13	(-29.60,-12.80)	-17.40	(-0.48,-0.21)	-0.28
A14	(-31.07,-1152)	-16.23	(-0.51,-0.19)	-0.27
A15	(-39.05,-10.05)	-19.86	(-0.64,-0.16)	-0.32
A16	(-51.62,-6.13)	-27.24	(-0.84,-0.10)	-0.44
B1	(-16.99,49.82)	35.54	(-0.28,0.81)	0.58
B2	(-53.23,34.95)	23.98	(-0.87,0.57)	0.39
B3	(-53.23,41.17)	26.66	(-0.87,0.67)	0.44
B4	(-49.06,24.11)	14.33	(-0.80,0.39)	0.23
B5	(-50.01,36.13)	17.79	(-0.82,0.59)	0.29
B6	(-46.12,14.21)	2.47	(-0.75,0.23)	0.04
B7	(-44.99,35.87)	5.46	(-0.73,0.59)	0.09
B8	(-48.66,-9.07)	-29.24	(-0.79,-0.15)	-0.48
B9	(-45.80,35.05)	24.87	(-0.75,0.57)	0.41
B10	(-47.67,41.86)	27.22	(-0.78,0.68)	0.44
B11	(-42.45,24.57)	15.06	(-0.69,0.40)	0.25
B12	(-33.32,37.07)	18.39	(-0.63,0.61)	0.30
B13	(-35.11,13.82)	3.07	(-0.57,0.23)	0.05
B14	(-39.04,36.99)	5.71	(-0.64,0.60)	0.09
B15	(-49.34,-5.91)	-31.58	(-0.81,-0.10)	-0.52
B16	(-38.53,-18.04)	-26.56	(-0.63,-0.29)	-0.43

Summary of the results: The results of the study show that the range of average pressure values varies significantly with wind inclination angle. The highest range of average pressure values is observed at an inclination angle of 30 degrees, with a range between -33.79 and 39.09, while the lowest range of average pressure values is observed at an

inclination angle of 90 degrees, with a range between -29.58 and 28.36. Similarly, the range of pressure coefficient C_p also varies significantly with wind inclination angle. The maximum positive and negative values of C_p are observed at an inclination angle of 30 degrees, with values of 0.64 and -0.55, respectively, while the minimum values of C_p are observed at an inclination angle of 0 degrees, with values of 0.58 and -0.39, respectively (See **Figure 6.2**).

Overall, it is observed that the maximum positive and negative pressure values occur on different faces at different inclination angles, with Face B1 and A4 having the maximum values at 180 degrees, while Faces B6 and A7 have the maximum values at 150 and 120 degrees. Similarly, the faces with the maximum positive and negative values of pressure coefficient C_p also vary with wind inclination angle. The results of the CFD simulation results for wind inclination angles from 0 to 180 degrees are presented graphically in the figures below **Table 6.15**.

Table 6.15: Average C_p value for wind inclination 0 to 180 degrees

Faces/Wall	Average value of C_p at wind inclination angle						
	0 Degree	30 Degree	60 Degree	90 Degree	120 Degree	150 Degree	180 Degree
A1	0.58	-0.07	-0.51	-0.42	-0.20	-0.20	-0.30
A2	0.41	0.59	0.37	0.11	-0.12	-0.13	-0.44
A3	0.45	0.64	0.41	0.06	-0.14	-0.15	-0.43
A4	0.26	0.62	0.59	0.28	-0.17	-0.16	-0.57
A5	0.31	0.61	0.60	0.22	-0.18	-0.18	-0.51
A6	0.08	0.44	0.62	0.44	-0.44	-0.44	-0.49
A7	0.13	0.39	0.59	0.39	-0.54	-0.57	-0.48
A8	-0.39	-0.47	0.03	0.45	0.20	0.19	-0.46
A9	0.41	-0.55	-0.40	-0.36	-0.18	-0.18	-0.29
A10	0.45	-0.45	-0.40	-0.37	-0.20	-0.19	-0.28
A11	0.21	-0.30	-0.38	-0.35	-0.18	-0.18	-0.29
A12	0.32	-0.25	-0.39	-0.36	-0.19	-0.19	-0.27
A13	0.08	-0.22	-0.33	-0.36	-0.18	-0.18	-0.28
A14	0.13	-0.19	-0.34	-0.36	-0.19	-0.19	-0.27
A15	-0.37	-0.23	-0.33	-0.44	-0.24	-0.25	-0.32
A16	-0.33	-0.33	-0.52	-0.48	0.40	-0.39	-0.44
B1	-0.27	-0.34	-0.20	-0.34	-0.50	-0.50	0.58
B2	-0.32	-0.36	-0.13	0.14	0.37	0.38	0.39
B3	-0.30	-0.34	-0.16	0.09	0.40	0.41	0.44
B4	-0.35	-0.33	-0.16	0.31	0.60	0.59	0.23
B5	-0.32	-0.33	-0.19	0.25	0.60	0.60	0.29
B6	-0.33	-0.35	-0.45	0.46	0.66	0.63	0.04
B7	-0.31	-0.41	-0.58	0.42	0.59	0.59	0.09
B8	-0.30	-0.21	0.18	0.45	0.04	0.03	-0.48
B9	-0.32	-0.27	-0.19	-0.29	-0.40	-0.39	0.41
B10	-0.31	-0.26	-0.20	-0.30	-0.40	-0.40	0.44
B11	-0.39	-0.26	-0.19	-0.28	-0.38	-0.38	0.25
B12	-0.35	-0.25	-0.20	-0.28	-0.39	-0.39	0.30
B13	-0.37	-0.25	-0.18	-0.29	-0.32	-0.33	0.05
B14	-0.34	-0.24	-0.18	-0.30	-0.33	-0.33	0.09
B15	-0.31	-0.33	-0.24	-0.37	-0.34	-0.34	-0.52
B16	-0.34	-0.32	-0.39	-0.48	-0.54	-0.53	-0.43

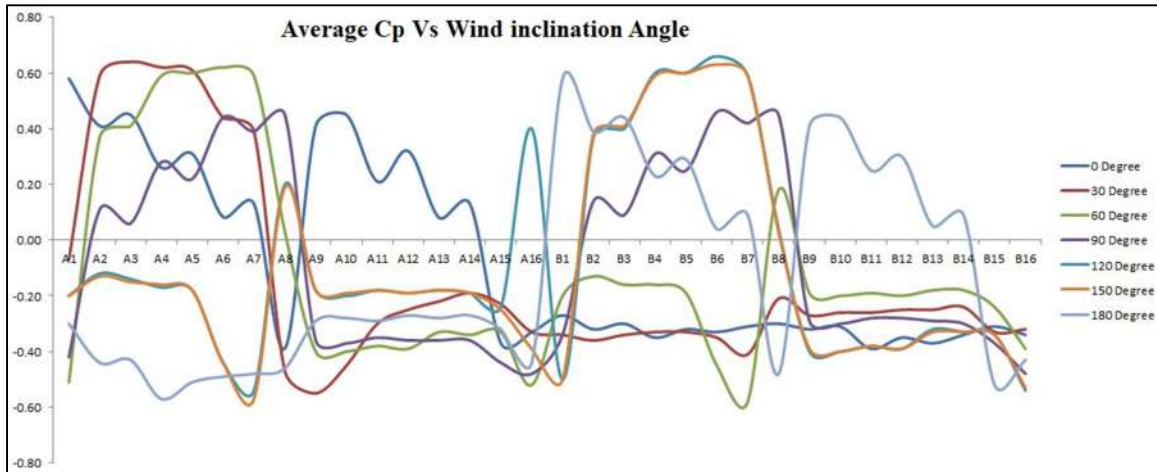
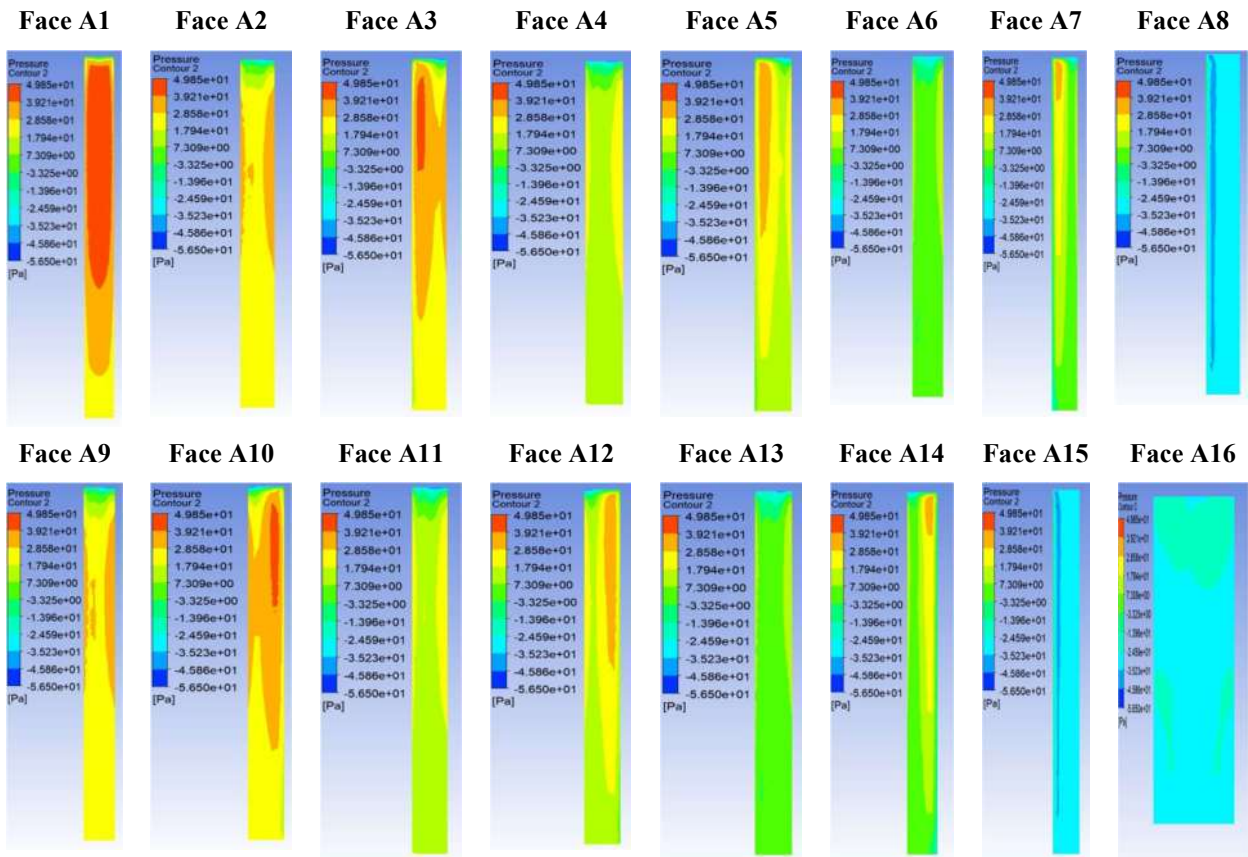


Figure 6.2: Graphical representation of Average Cp value

6.1.2 Back to Front Interference Condition

Case 1 – The incident wind angle is 0°

Table 6.16: Pressure contour of faces at 0-degree wind inclination for Model A and B



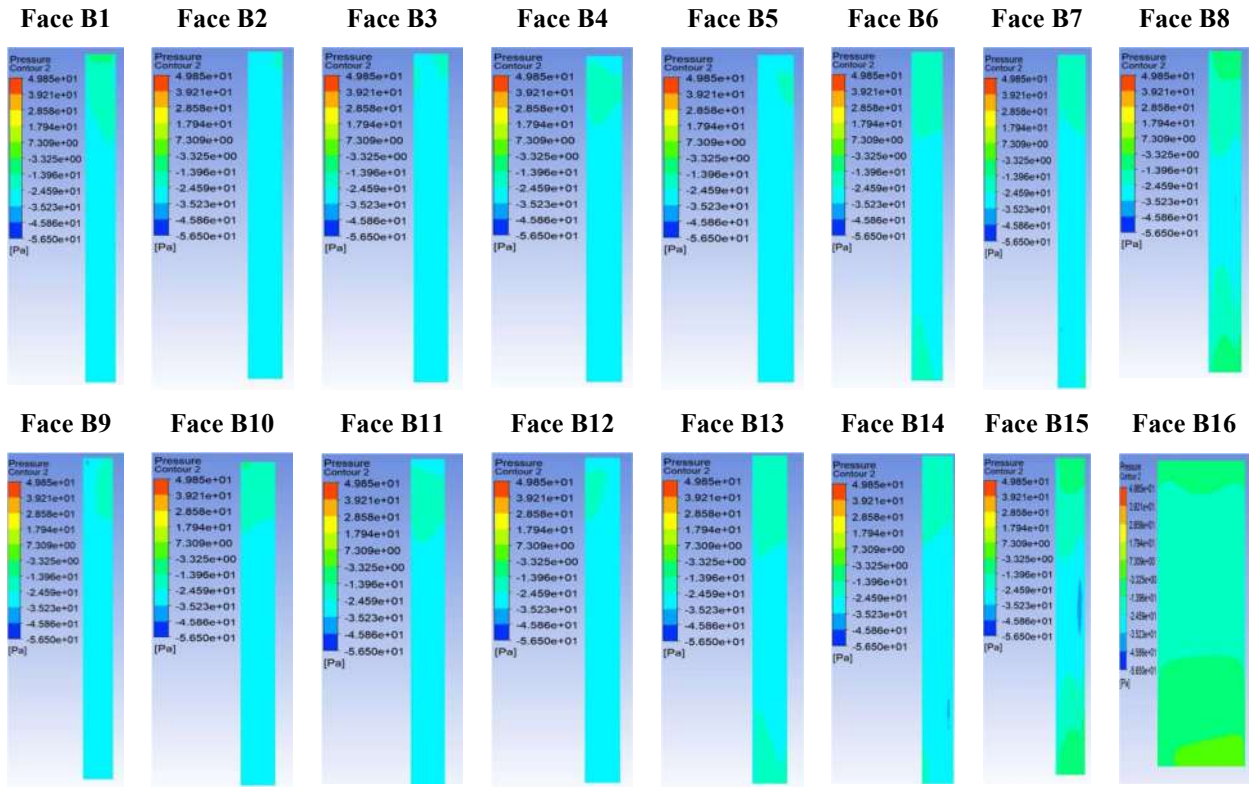


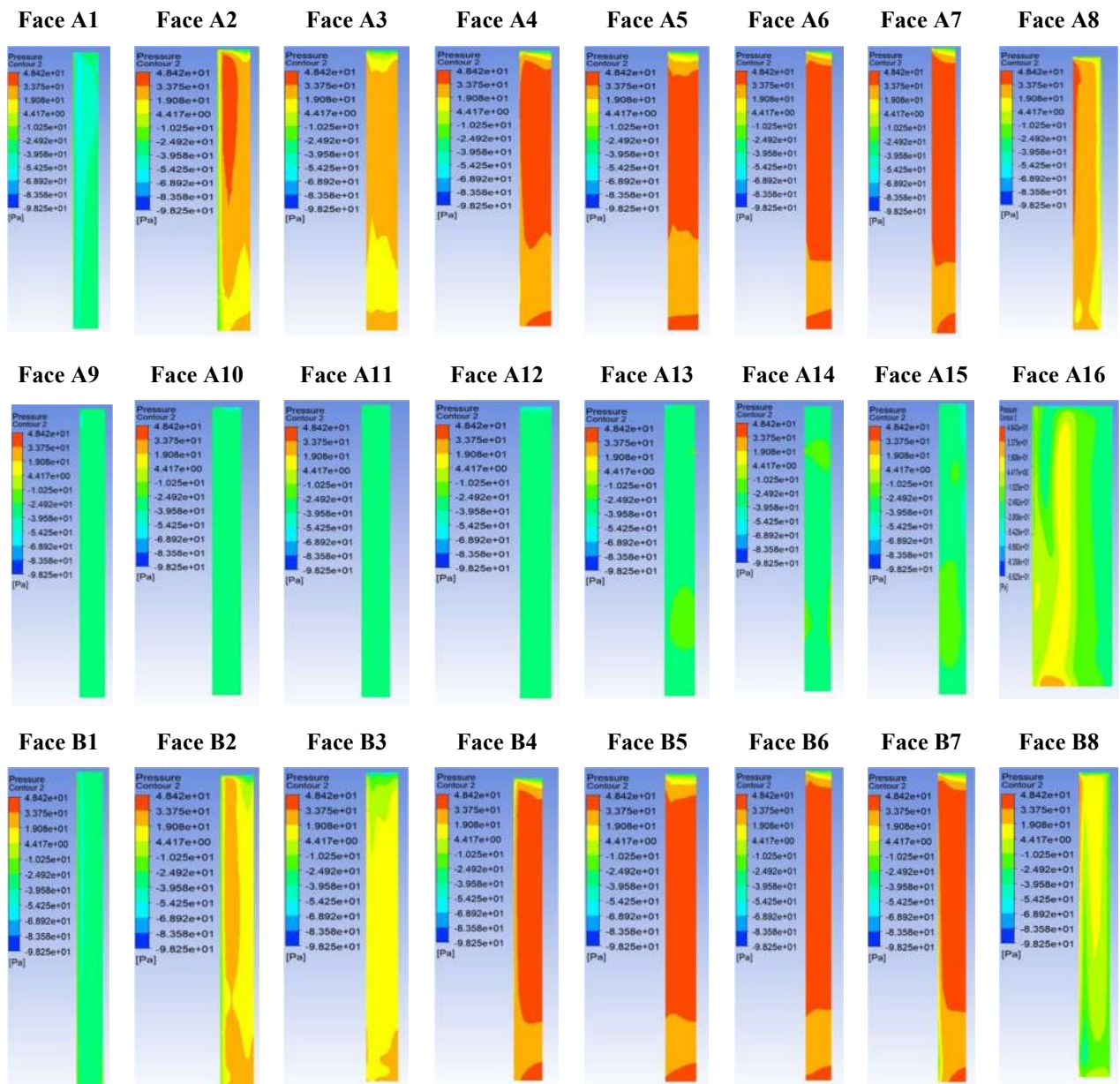
Table 6.17: Average Cp value for wind inclination 0 degree

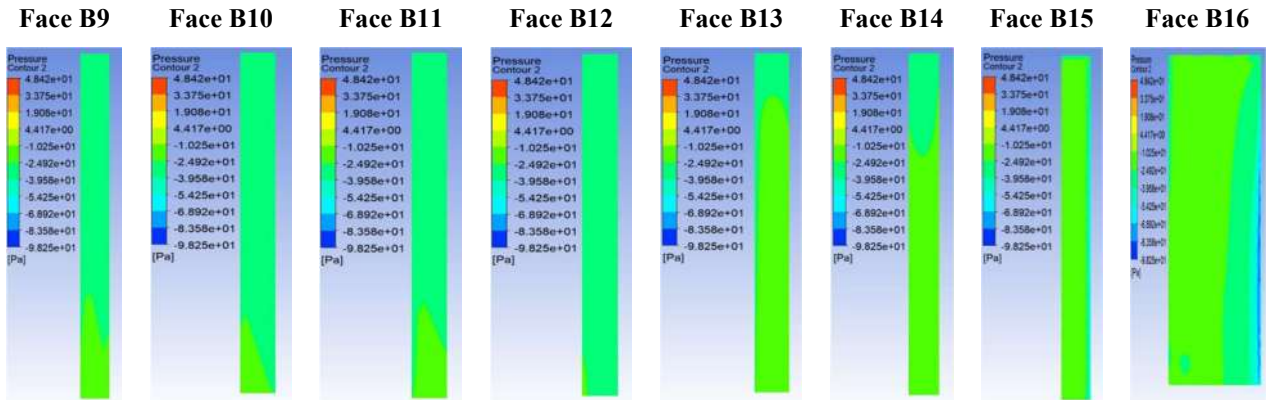
Wind Inclination Angle 0				
Faces/Wall	Range of Pressure	Average value of Pressure	Range of Cp	Average Value of Cp
A1	(-18.03,49.85)	35.48	(-0.29,0.81)	0.58
A2	(-47.07,35.12)	24.18	(-0.77,0.57)	0.39
A3	(-51.51,41.15)	26.83	(-0.84,0.67)	0.43
A4	(-43.70,24.16)	14.66	(-0.71,0.39)	0.24
A5	(-41.18,36.26)	17.91	(-0.67,0.59)	0.29
A6	(-36.36,13.25)	2.72	(-0.59,0.22)	0.04
A7	(-38.28,37.06)	5.50	(-0.63,0.61)	0.09
A8	(-49.18,-9.13)	-29.61	(-0.80,-0.15)	-0.48
A9	(-49.89,34.69)	24.30	(-0.81,0.57)	0.40
A10	(-49.89,41.37)	26.97	(-0.81,0.68)	0.44
A11	(-47.22,24.17)	14.51	(-0.77,0.39)	0.24
A12	(-45.19,36.24)	18.07	(-0.74,0.59)	0.30
A13	(-41.72,14.59)	2.87	(-0.68,0.24)	0.05
A14	(-41.01,36.82)	5.83	(-0.67,0.60)	0.10
A15	(-49.08,-3.59)	-28.90	(-0.80,-0.06)	-0.47
A16	(-30.29,-19.07)	-25.27	(-0.49,-0.31)	-0.41
B1	(-28.66,-5.12)	-24.95	(-0.47,-0.08)	-0.41
B2	(-34.68,-19.35)	-26.25	(-0.57,-0.32)	-0.43
B3	(-28.18,-17.05)	-26.02	(-0.46,-0.28)	-0.42
B4	(-29.70,-22.44)	-26.42	(-0.48,-0.37)	-0.43
B5	(-32.24,-23.03)	-27.02	(-0.53,-0.38)	-0.44
B6	(-31.95,-17.11)	-25.33	(-0.52,-0.28)	-0.41
B7	(-36.21,-16.41)	-26.80	(-0.59,-0.27)	-0.44
B8	(-35.91,-7.80)	-22.24	(-0.59,-0.13)	-0.36
B9	(-39.09,-15.18)	-25.59	(-0.64,-0.25)	-0.42
B10	(-27.43,-10.03)	-25.11	(-0.45,-0.16)	-0.41
B11	(-30.80,-20.55)	-26.03	(-0.50,-0.34)	-0.43
B12	(-3.1.98,-20.55)	-26.70	(-0.52,-0.34)	-0.44
B13	(-32.48,-15.12)	-24.36	(-0.53,-0.25)	-0.40
B14	(-36.02,-14.61)	-26.15	(-0.59,-0.24)	-0.43
B15	(-37.98,-4.78)	-21.78	(-0.62,-0.08)	-0.36
B16	(-32.42,-2.35)	-14.00	(-0.53,-0.04)	-0.23

The range of average pressure values for the wind inclination angle of 0° is between [-29.61, 35.48] (Table 6.16). The maximum positive and negative pressure values of 35.48 and -29.61, respectively, occur on Face A1 and A8. The range of pressure coefficient C_p lies in the range ε [-0.48, 0.58] (Table 6.17). The maximum positive and negative values of 0.58 and -0.48 occur on Faces A1 and A8.

- Case 2 – The incident wind angle is 60°

Table 6.18: Pressure contour of faces at 60-degree wind inclination for Model A and B





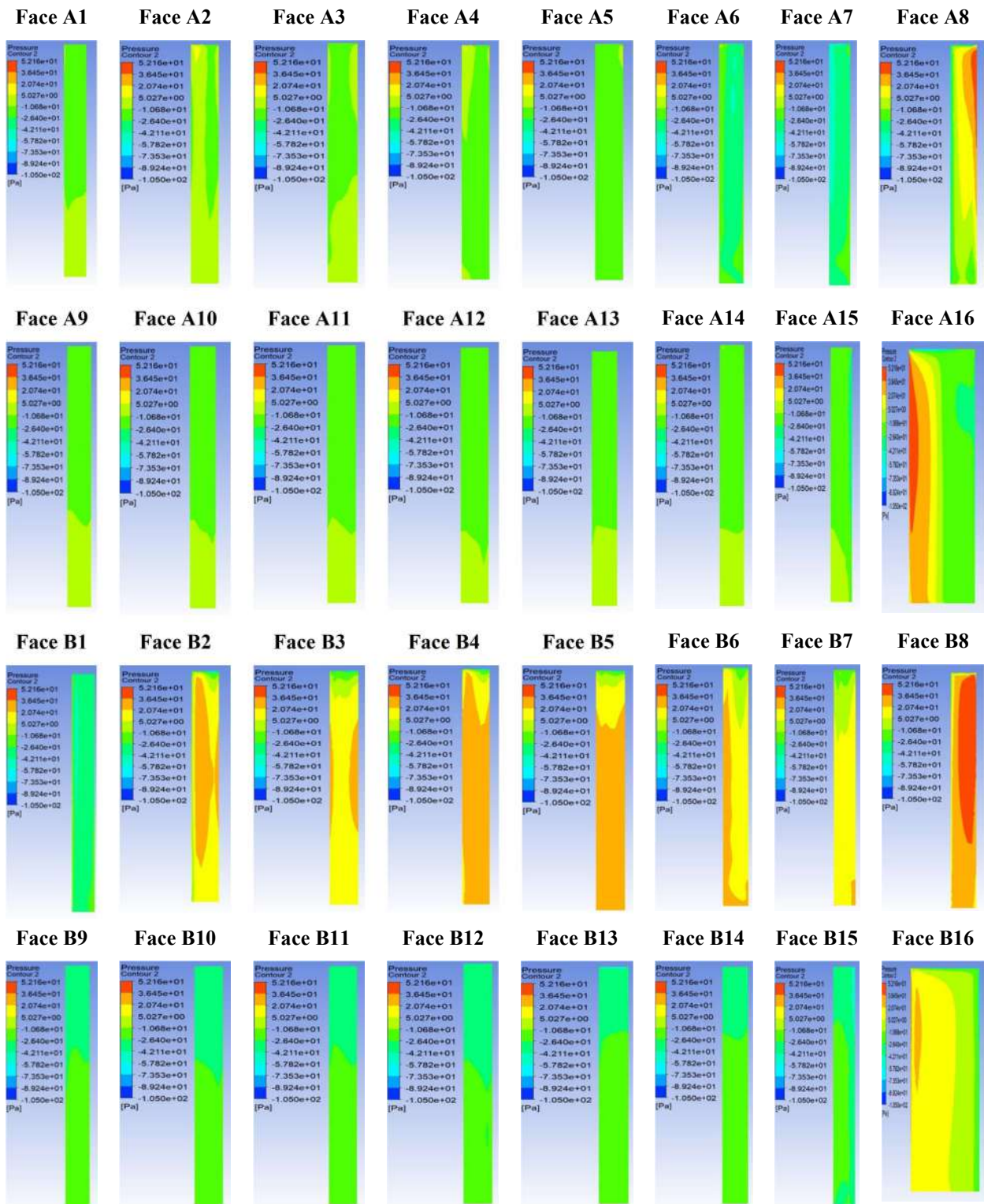
The range of average pressure values for the wind inclination angle of 60° is between $[-38.35, 37.95]$ (Table 6.18). The maximum positive and negative pressure values of 37.95 and -38.35, respectively, occur on Faces A6 and A1. The range of pressure coefficient C_p lies in the range $\varepsilon [-0.63, 0.62]$ (Table 6.19). The maximum positive and negative values of 0.62 and -0.63 occur on Faces A6 and A1.

Table 6.19: Average C_p value for wind inclination 60 degree

Wind Inclination Angle 60				
Faces/Wall	Range of Pressure	Average value of Pressure	Range of C_p	Average Value of C_p
A1	(-67.88,0.61)	-38.35	(-1.11,0.01)	-0.63
A2	(-66.54,43.81)	19.15	(-1.09,0.72)	0.31
A3	(-53.12,33.29)	21.23	(-0.87,0.54)	0.35
A4	(-59.42,46.98)	34.07	(-0.97,0.77)	0.56
A5	(-59.42,44.71)	34.07	(-0.97,0.73)	0.56
A6	(-62.17,47.85)	37.95	(-1.02,0.78)	0.62
A7	(-45.49,48.42)	37.69	(-0.74,0.79)	0.62
A8	(-43.12,43.79)	21.51	(-0.70,0.71)	0.35
A9	(-43.53,-29.45)	-32.98	(-0.71,-0.48)	-0.54
A10	(-42.06,-28.47)	-32.97	(-0.69,-0.46)	-0.54
A11	(-40.36,-27.55)	-31.20	(-0.66,-0.45)	-0.51
A12	(-42.22,-26.51)	-31.12	(-0.69,-0.43)	-0.51
A13	(-42.08,-23.46)	-27.96	(-0.69,-0.38)	-0.46
A14	(-36.41,-19.88)	-26.99	(-0.59,-0.32)	-0.44
A15	(-60.39,-19.53)	-30.32	(-0.99,-0.32)	-0.50
A16	(-60.39,28.47)	-12.53	(-0.99,0.46)	-0.20
B1	(-51.60,-5.48)	-30.49	(-0.84,-0.09)	-0.50
B2	(-61.32,29.99)	12.63	(-1.00,0.49)	0.21
B3	(-72.95,23.65)	10.63	(-1.19,0.39)	0.17
B4	(-54.51,46.22)	37.75	(-0.89,0.75)	0.55
B5	(-53.65,45.40)	36.31	(-0.88,0.74)	0.59
B6	(-55.57,47.92)	37.94	(-0.91,0.78)	0.62
B7	(-65.67,48.27)	34.12	(-1.07,0.79)	0.56
B8	(-64.42,34.55)	-3.59	(-1.05,0.56)	-0.06
B9	(-41.30,-23.34)	-26.35	(-0.67,-0.38)	-0.43
B10	(-40.98,-23.82)	-27.20	(-0.67,-0.39)	-0.44
B11	(-35.46,-23.34)	-26.72	(-0.58,-0.38)	-0.44
B12	(-34.59,-24.69)	-28.88	(-0.56,-0.40)	-0.47
B13	(-35.99,-17.49)	-22.65	(-0.59,-0.29)	-0.37
B14	(-38.02,-17.48)	-22.53	(-0.62,-0.29)	-0.37
B15	(-63.69,-16.32)	-24.71	(-1.04,-0.27)	-0.40
B16	(-95.64,-7.35)	-25.78	(-1.56,-0.12)	-0.42

- Case 3 – The incident wind angle is 120°

Table 6.20: Pressure contour of faces at 120-degree wind inclination for Model A and B



The range of average pressure values for the wind inclination angle of 120° is between [-35.57, 31.54] (Table 6.20). The maximum positive and negative pressure values of 31.54 and -35.57, respectively, occur on Face B8 and A7. The range of pressure coefficient C_p lies in the range ε [-0.58, 0.52] (Table 6.21). The maximum positive and negative values of 0.52 and -0.58 occur on Faces B8 and A7.

Table 6.21: Average C_p value for wind inclination 120 degree

Wind Inclination Angle 120				
Faces/Wall	Range of Pressure	Average value of Pressure	Range of C_p	Average Value of C_p
A1	(-22.79,-4.19)	-12.72	(-0.37,-0.07)	-0.21
A2	(-15.92,13.21)	-9.24	(-0.26,0.22)	-0.15
A3	(-17.37,-5.16)	-10.70	(-0.28,-0.08)	-0.17
A4	(-16.45,9.30)	-13.12	(-0.27,0.15)	-0.21
A5	(-24.25,-8.22)	-14.84	(-0.40,-0.13)	-0.24
A6	(-43.31,-7.33)	-29.37	(-0.71,-0.12)	-0.48
A7	(-52.24,-20.96)	-35.57	(-0.85,-0.34)	-0.58
A8	(-57.91,46.50)	2.23	(-0.95,0.76)	0.04
A9	(-16.52,-6.91)	-12.00	(-0.27,-0.11)	-0.20
A10	(-15.96,-7.23)	-12.32	(-0.26,-0.12)	-0.20
A11	(-21.08,-7.22)	-12.39	(-0.34,-0.12)	-0.20
A12	(-19.51,-8.17)	-12.81	(-0.32,-0.13)	-0.21
A13	(-28.86,-6.60)	-12.74	(-0.47,-0.11)	-0.21
A14	(-20.13,-6.72)	-12.87	(-0.33,-0.11)	-0.21
A15	(-41.97,-6.32)	-17.86	(-0.69,-0.10)	-0.29
A16	(-75.25,48.21)	-1.53	(-1.23,0.79)	-0.03
B1	(-53.43,-9.23)	-30.71	(-0.87,-0.15)	-0.50
B2	(-55.61,33.42)	15.25	(-0.91,0.55)	0.25
B3	(-4040,24.83)	15.78	(-0.66,0.41)	0.26
B4	(-56.03,32.92)	21.55	(-0.91,0.54)	0.35
B5	(-46.70,26.74)	19.91	(-0.76,0.44)	0.33
B6	(-35.17,27.36)	15.60	(-0.57,0.45)	0.25
B7	(-30.19,21.92)	11.26	(-0.49,0.36)	0.18
B8	(-15.16,52.16)	31.54	(-0.25,0.85)	0.52
B9	(-31.60,-22.10)	-25.74	(-0.52,-0.36)	-0.42
B10	(-32.82,-23.22)	-25.98	(-0.54,-0.38)	-0.42
B11	(-36.19,-21.64)	-25.84	(-0.59,-0.35)	-0.42
B12	(-38.75,-23.55)	-26.77	(-0.63,-0.38)	-0.44
B13	(-53.13,-17.49)	-24.00	(-0.87,-0.29)	-0.39
B14	(-40.25,-17.77)	-23.25	(-0.66,-0.29)	-0.38
B15	(-55.45,-18.32)	-29.04	(-0.91,-0.30)	-0.47
B16	(-55.45,40.76)	4.98	(-0.91,0.67)	0.08

- Case 4 – The incident wind angle is 180°

The range of average pressure values for the wind inclination angle of 180° is between [-27.21, 30.45] (Table 6.22). The maximum positive and negative pressure values of 30.45 and -27.21, respectively, occur on Face B16 and B8. The range of pressure coefficient C_p lies in the range ε [-0.44, 0.50] (Table 6.23). The maximum positive and negative values of 0.50 and -0.44 occur on Faces B16 and B8.

Table 6.22: Pressure contour of faces at 180-degree wind inclination for Model A and B

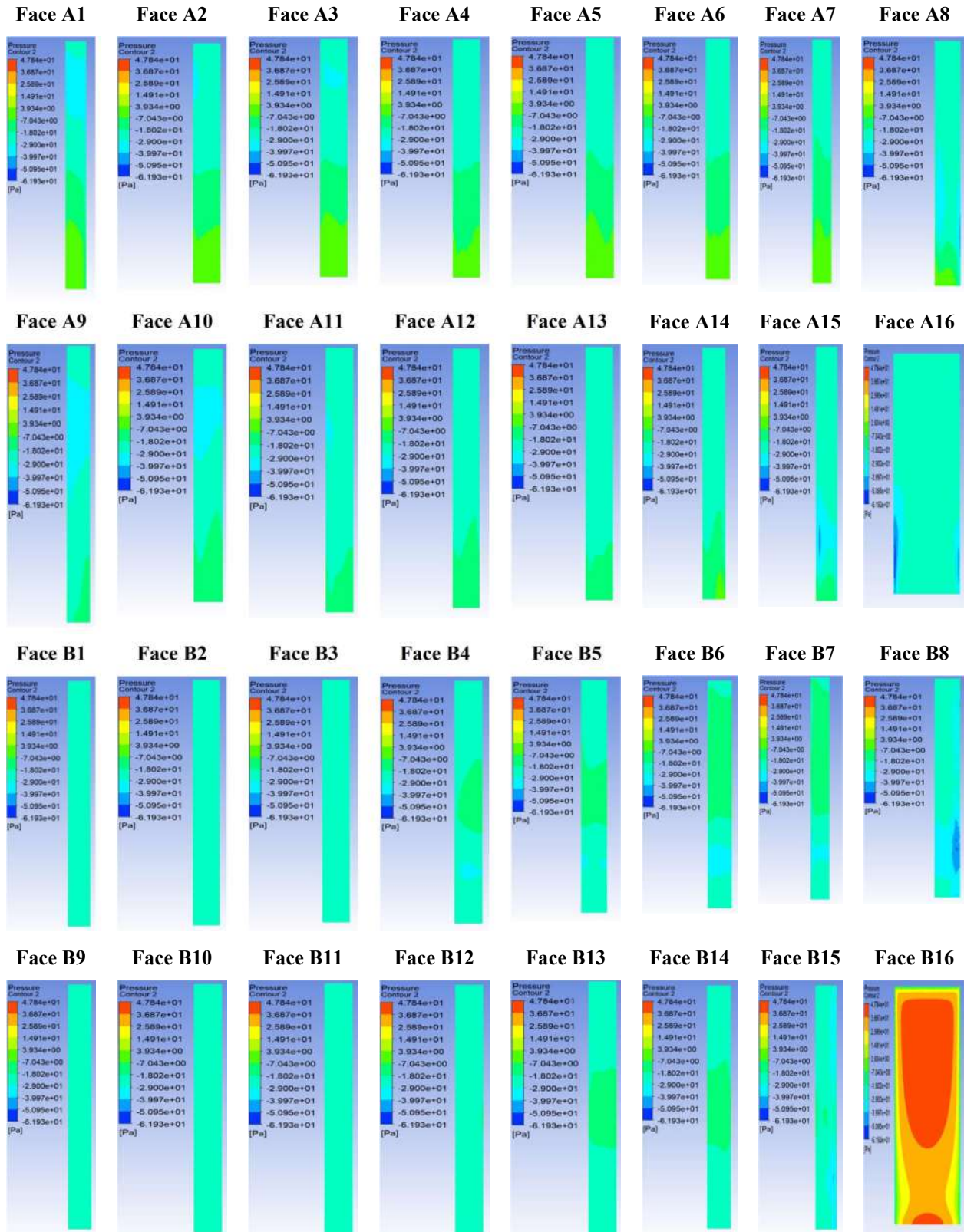


Table 6.23: Average Cp value for wind inclination 180 degree

Wind Inclination Angle 180				
Faces/Wall	Range of Pressure	Average value of Pressure	Range of Cp	Average Value of Cp
A1	(-32.16,2.08)	-19.03	(-0.53,0.03)	-0.31
A2	(-30.53,-1.34)	-17.68	(-0.5,-0.02)	-0.29
A3	(-29.35,0.47)	-17.11	(-0.48,0.01)	-0.28
A4	(-29.5,-1.75)	-17.34	(-0.48,-0.03)	-0.28
A5	(-26.47,0.91)	-16.51	(-0.43,0.01)	-0.27
A6	(-29.44,1.79)	-15.62	(-0.48,0.03)	-0.26
A7	(-26.62,3.93)	-15.15	(-0.43,0.06)	-0.25
A8	(-48.54,2.64)	-23.32	(-0.79,0.04)	-0.38
A9	(-32.81,-13.51)	-25.25	(-0.54,-0.22)	-0.41
A10	(-31.35,-7.25)	-23.07	(-0.51,-0.12)	-0.38
A11	(-29.27,-12.58)	-23.42	(-0.48,-0.21)	-0.38
A12	(-28.6,-7.25)	-21.85	(-0.47,-0.12)	-0.36
A13	(-26.51,-9.21)	-21.88	(-0.43,-0.15)	-0.36
A14	(-29.69,-2.55)	-20.59	(-0.48,-0.04)	-0.34
A15	(-44.96,-4.88)	-24.48	(-0.73,-0.08)	-0.4
A16	(-61.93,-20.04)	-24.3	(-1.01,-0.33)	-0.4
B1	(-27.05,-20.57)	-23.32	(-0.44,-0.34)	-0.38
B2	(-27.11,-20.49)	-23.45	(-0.44,-0.33)	-0.38
B3	(-28.43,-21.02)	-24.16	(-0.46,-0.34)	-0.39
B4	(-29.36,-13.12)	-21.77	(-0.48,-0.21)	-0.36
B5	(-29.71,-12.9)	-21.1	(-0.49,-0.21)	-0.34
B6	(-30.58,-12.9)	-20.78	(-0.5,-0.21)	-0.34
B7	(-31.68,-12.47)	-20.31	(-0.52,-0.2)	-0.33
B8	(-54.73,-8.3)	-27.21	(-0.89,-0.14)	-0.44
B9	(-25.04,-20.42)	-22.23	(-0.41,-0.41)	-0.36
B10	(-25.18,-20.42)	-22.34	(-0.41,-0.33)	-0.36
B11	(-26.31,-18.55)	-21.92	(-0.43,-0.3)	-0.36
B12	(-25.46,-17.02)	-21.82	(-0.42,-0.28)	-0.36
B13	(-26.00,-13.28)	-20.19	(-0.42,-0.23)	-0.33
B14	(-26.85,-11.17)	-19.83	(-0.44,-0.18)	-0.32
B15	(-41.75,-14.94)	-25.28	(-0.68,-0.24)	-0.41
B16	(-50.96,47.84)	30.45	(-0.83,0.78)	0.5

- Similarly for the wind inclination angle of 30° the average pressure is between $[-32.07, 38.82]$. The maximum positive and negative pressure values of 38.82 and -32.07, respectively, occur on Face A3 and A9. The range of pressure coefficient Cp lies in the range $\epsilon [-0.52, 0.63]$. The maximum positive and negative values of 0.63 and -0.52 occur on Faces A3 and A9.
- For the wind inclination angle of 90° the average pressure is between $[-37.55, 36.61]$. The maximum positive and negative pressure values of 36.61 and -37.55, respectively, occur on Face B6 and B1. The range of pressure coefficient Cp lies in the range $\epsilon [-0.61, 0.60]$. The maximum positive and negative values of 0.66 and -0.61 occur on Faces B1 and B6.

- For the wind inclination angle of 150° the average pressure is between [-39.29, 26.26]. The maximum positive and negative pressure values of 26.26 and -39.29, respectively, occur on Face B16 and B8. The range of pressure coefficient Cp lies in the range ε [-0.64, 0.43]. The maximum positive and negative values of 0.43 and -0.64 occur on Faces B16 and B8 (See Table 6.24).

Table 6.24: Average Cp value for wind inclination 30, 90 and 150 degrees

Wind Inclination Angle 30					Wind Inclination Angle 90				
Faces/Wall	Range of Pressure	Average value of Pressure	Range of Cp	Average Value of Cp	Faces/Wall	Range of Pressure	Average value of Pressure	Range of Cp	Average Value of Cp
A1	(-61.90,36.40)	-4.60	(-1.01,0.59)	-0.08	A1	(-33.67,3.88)	-13.75	(-0.55,0.06)	-0.22
A2	(-44.37,49.11)	35.65	(-0.72,0.80)	0.58	A2	(-27.89,37.89)	11.26	(-0.46,0.62)	0.18
A3	(-60.71,48.69)	38.82	(-0.99,0.79)	0.63	A3	(-30.20,17.66)	8.39	(-0.49,0.29)	0.14
A4	(-47.32,48.05)	38.36	(-0.77,0.78)	0.63	A4	(-40.61,37.16)	20.46	(-0.66,0.61)	0.33
A5	(-50.41,48.19)	37.45	(-0.82,0.79)	0.61	A5	(-30.52,26.41)	17.34	(-0.50,0.43)	0.28
A6	(-47.54,38.54)	28.55	(-0.78,0.63)	0.47	A6	(-43.29,41.69)	27.15	(-0.71,0.68)	0.44
A7	(-43.30,46.23)	25.68	(-0.71,0.75)	0.42	A7	(-42.47,34.11)	24.17	(-0.69,0.56)	0.39
A8	(-53.59,5.53)	-20.26	(-0.87,0.09)	-0.33	A8	(-18.95,49.23)	33.61	(-0.31,0.80)	0.55
A9	(-61.90,-16.68)	-32.07	(-1.01,-0.27)	-0.52	A9	(-18.53,-4.38)	-11.52	(-0.30,-0.07)	-0.19
A10	(-48.26,-1.07)	-26.77	(-0.79,-0.02)	-0.44	A10	(-17.81,-6.11)	-12.01	(-0.29,-0.10)	-0.20
A11	(-33.39,-6.98)	-17.29	(-0.55,-0.11)	-0.28	A11	(-17.43,-4.48)	-11.80	(-0.28,-0.07)	-0.19
A12	(-22.73,5.80)	-15.18	(-0.37,0.09)	-0.25	A12	(-18.05,-6.02)	-12.49	(-0.29,-0.10)	-0.20
A13	(-32.80,-3.38)	-12.81	(-0.54,-0.06)	-0.21	A13	(-18.23,-4.11)	-11.87	(-0.30,-0.07)	-0.19
A14	(-17.48,12.35)	-10.92	(-0.29,0.20)	-0.18	A14	(-19.92,-4.71)	-12.16	(-0.33,-0.08)	-0.20
A15	(-25.48,-3.23)	-12.29	(-0.42,-0.05)	-0.20	A15	(-43.94,-4.03)	-17.12	(-0.72,-0.07)	-0.28
A16	(-36.94,8.92)	-14.81	(-0.80,0.15)	-0.24	A16	(-43.94,32.34)	-7.87	(-0.72,0.53)	-0.13
B1	(-26.27,-13.04)	-18.37	(-0.43,-0.21)	-0.30	B1	(-61.67,-11.04)	-37.55	(-1.01,-0.18)	-0.61
B2	(-32.81,-6.39)	-23.72	(-0.54,-0.10)	-0.39	B2	(-54.69,37.43)	18.01	(-0.89,0.61)	0.29
B3	(-61.16,-11.15)	-30.33	(-1.00,-0.18)	-0.50	B3	(-58.96,29.34)	18.90	(-0.96,0.48)	0.31
B4	(-50.32,23.09)	2.60	(-0.82,0.38)	0.04	B4	(-62.40,42.71)	30.76	(-1.02,0.70)	0.50
B5	(-38.77,20.94)	4.47	(-0.63,0.34)	0.07	B5	(-56.40,37.52)	28.80	(-0.92,0.61)	0.47
B6	(-29.34,46.22)	30.60	(-0.48,0.75)	0.50	B6	(-54.43,47.20)	36.61	(-0.89,0.77)	0.60
B7	(-29.34,49.07)	31.03	(-0.48,0.80)	0.51	B7	(-57.36,47.50)	36.00	(-0.94,0.78)	0.59
B8	(-65.30,17.01)	-16.78	(-1.07,0.28)	-0.27	B8	(-60.75,48.49)	15.47	(-0.99,0.79)	0.25
B9	(-19.90,-11.69)	-16.35	(-0.32,-0.19)	-0.27	B9	(-43.13,-28.88)	-31.89	(-0.70,-0.47)	-0.52
B10	(-19.53,-12.03)	-16.38	(-0.32,-0.20)	-0.27	B10	(-43.13,-30.01)	-32.04	(-0.70,-0.49)	-0.52
B11	(-18.57,-12.21)	-15.95	(-0.30,-0.20)	-0.26	B11	(-39.47,-29.05)	-31.42	(-0.64,-0.47)	-0.51
B12	(-19.46,-12.61)	-16.45	(-0.32,-0.21)	-0.27	B12	(-39.47,-30.27)	-31.91	(-0.64,-0.49)	-0.52
B13	(-22.30,-16.34)	-17.62	(-0.36,-0.27)	-0.29	B13	(-36.63,-27.76)	-30.79	(-0.60,-0.45)	-0.50
B14	(-19.01,-16.30)	-17.49	(-0.31,-0.27)	-0.29	B14	(-35.04,-29.40)	-31.69	(-0.57,-0.48)	-0.52
B15	(-22.87,-13.58)	-17.91	(-0.37,-0.22)	-0.29	B15	(-46.12,-21.90)	-29.76	(-0.75,-0.36)	-0.49
B16	(-73.97,49.11)	-9.24	(-0.36,-0.24)	-0.22	B16	(-66.85,-23.67)	-34.27	(-1.09,-0.39)	-0.56

Wind Inclination Angle 150				
Faces/Wall	Range of Pressure	Average value of Pressure	Range of Cp	Average Value of Cp
A1	(-39.71,-15.24)	-22.34	(-0.65,-0.25)	-0.36
A2	(-29.33,2.27)	-21.29	(-0.48,0.04)	-0.35
A3	(-45.44,-12.39)	-20.94	(-0.74,-0.20)	-0.34
A4	(-33.03,1.83)	-18.93	(-0.57,0.03)	-0.31
A5	(-31.21,-12.61)	-18.94	(-0.51,-0.21)	-0.31
A6	(-26.69,-2.61)	-20.98	(-0.44,-0.04)	-0.34
A7	(-54.36,-17.08)	-25.80	(-0.89,-0.28)	-0.42
A8	(-92.54,29.28)	-12.00	(-1.51,0.48)	-0.20
A9	(-26.40,-8.38)	-16.96	(-0.43,-0.14)	-0.28
A10	(-25.00,-9.51)	-17.14	(-0.41,-0.16)	-0.28
A11	(-23.22,-6.96)	-15.10	(-0.38,-0.11)	-0.25
A12	(-24.12,-7.22)	-15.88	(-0.39,-0.12)	-0.26
A13	(-22.86,-5.46)	-14.51	(-0.37,-0.09)	-0.24
A14	(-25.49,-5.16)	-15.23	(-0.42,-0.08)	-0.25
A15	(-51.50,-4.20)	-21.04	(-0.84,-0.07)	-0.34
A16	(-69.20,53.96)	-9.45	(-1.13,0.88)	-0.15
B1	(-51.65,-9.78)	-23.19	(-0.84,-0.16)	-0.38
B2	(-39.27,5.10)	-15.09	(-0.64,0.08)	-0.25
B3	(-36.73,-1.28)	-19.92	(-0.60,-0.02)	-0.33
B4	(-40.85,-13.72)	-27.84	(-0.67,-0.22)	-0.45
B5	(-36.29,-20.32)	-26.74	(-0.59,-0.33)	-0.44
B6	(-37.84,-24.02)	-29.13	(-0.62,-0.39)	-0.48
B7	(-56.85,-25.14)	-29.74	(-0.93,-0.41)	-0.49
B8	(-77.24,10.26)	-39.39	(-1.26,0.17)	-0.64
B9	(-30.84,-17.79)	-21.24	(-0.50,-0.29)	-0.35
B10	(-29.78,-18.08)	-20.87	(-0.49,-0.30)	-0.34
B11	(-31.28,-16.53)	-20.29	(-0.51,-0.27)	-0.33
B12	(-30.92,-18.61)	-21.12	(-0.50,-0.30)	-0.34
B13	(-32.60,-9.07)	-17.93	(-0.53,-0.15)	-0.29
B14	(-33.15,-7.61)	-17.62	(-0.54,-0.12)	-0.29
B15	(-41.81,-7.61)	-24.13	(-0.68,-0.12)	-0.39
B16	(-45.57,48.88)	26.26	(-0.74,0.80)	0.43

Summary of the results: The results for wind CFD simulation testing at various wind inclination angles (0 to 180 degrees) are presented graphically in the figures provided. The average pressure values for each angle range from (-39.29 to 38.82), with the highest positive and negative pressure values occurring on different faces depending on the angle. The range of pressure coefficient C_p lies between -0.64 and 0.66, with the maximum positive and negative values occurring on different faces depending on the angle (See **Figure 6.3**).

The results indicate that as the wind inclination angle increases, the range of pressure coefficient and the maximum pressure values tend to decrease, with the exception of 90 degrees, where the maximum positive and negative pressure values are relatively high. Overall, the results demonstrate the complex nature of wind flow around the building and the importance of considering wind inclination angles when designing structures for wind loads (See **Table 6.25**).

Table 6.25: Average C_p value for wind inclination 0 to 180 degrees

Faces/Wall	Average value of C_p at wind inclination angle						
	0 Degree	30 Degree	60 Degree	90 Degree	120 Degree	150 Degree	180 Degree
A1	0.58	-0.08	-0.63	-0.22	-0.21	-0.36	-0.31
A2	0.39	0.58	0.31	0.18	-0.15	-0.35	-0.29
A3	0.43	0.63	0.35	0.14	-0.17	-0.34	-0.28
A4	0.24	0.63	0.56	0.33	-0.21	-0.31	-0.28
A5	0.29	0.61	0.56	0.28	-0.24	-0.31	-0.27
A6	0.04	0.47	0.62	0.44	-0.48	-0.34	-0.26
A7	0.09	0.42	0.62	0.39	-0.58	-0.42	-0.25
A8	-0.48	-0.33	0.35	0.55	0.04	-0.20	-0.38
A9	0.40	-0.52	-0.54	-0.19	-0.20	-0.28	-0.41
A10	0.44	-0.44	-0.54	-0.20	-0.20	-0.28	-0.38
A11	0.24	-0.28	-0.51	-0.19	-0.20	-0.25	-0.38
A12	0.30	-0.25	-0.51	-0.20	-0.21	-0.26	-0.36
A13	0.05	-0.21	-0.46	-0.19	-0.21	-0.24	-0.36
A14	0.10	-0.18	-0.44	-0.20	-0.21	-0.25	-0.34
A15	-0.47	-0.20	-0.50	-0.28	-0.29	-0.34	-0.4
A16	-0.41	-0.24	-0.20	-0.13	-0.03	-0.15	-0.4
B1	-0.41	-0.30	-0.50	-0.61	-0.50	-0.38	-0.38
B2	-0.43	-0.39	0.21	0.29	0.25	-0.25	-0.38
B3	-0.42	-0.50	0.17	0.31	0.26	-0.33	-0.39
B4	-0.43	0.04	0.55	0.50	0.35	-0.45	-0.36
B5	-0.44	0.07	0.59	0.47	0.33	-0.44	-0.34
B6	-0.41	0.50	0.62	0.60	0.25	-0.48	-0.34
B7	-0.44	0.51	0.56	0.59	0.18	-0.49	-0.33
B8	-0.36	-0.27	-0.06	0.25	0.52	-0.64	-0.44
B9	-0.42	-0.27	-0.43	-0.52	-0.42	-0.35	-0.36
B10	-0.41	-0.27	-0.44	-0.52	-0.42	-0.34	-0.36
B11	-0.43	-0.26	-0.44	-0.51	-0.42	-0.33	-0.36
B12	-0.44	-0.27	-0.47	-0.52	-0.44	-0.34	-0.36
B13	-0.40	-0.29	-0.37	-0.50	-0.39	-0.29	-0.33
B14	-0.43	-0.29	-0.37	-0.52	-0.38	-0.29	-0.32
B15	-0.36	-0.29	-0.40	-0.49	-0.47	-0.39	-0.41
B16	-0.23	-0.22	-0.42	-0.56	0.08	0.43	0.5

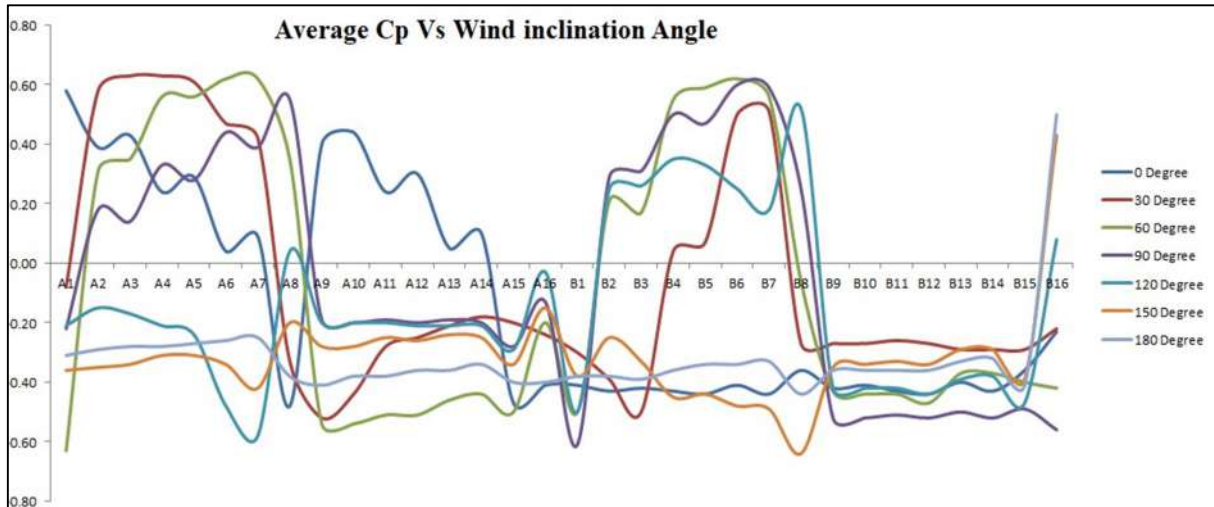
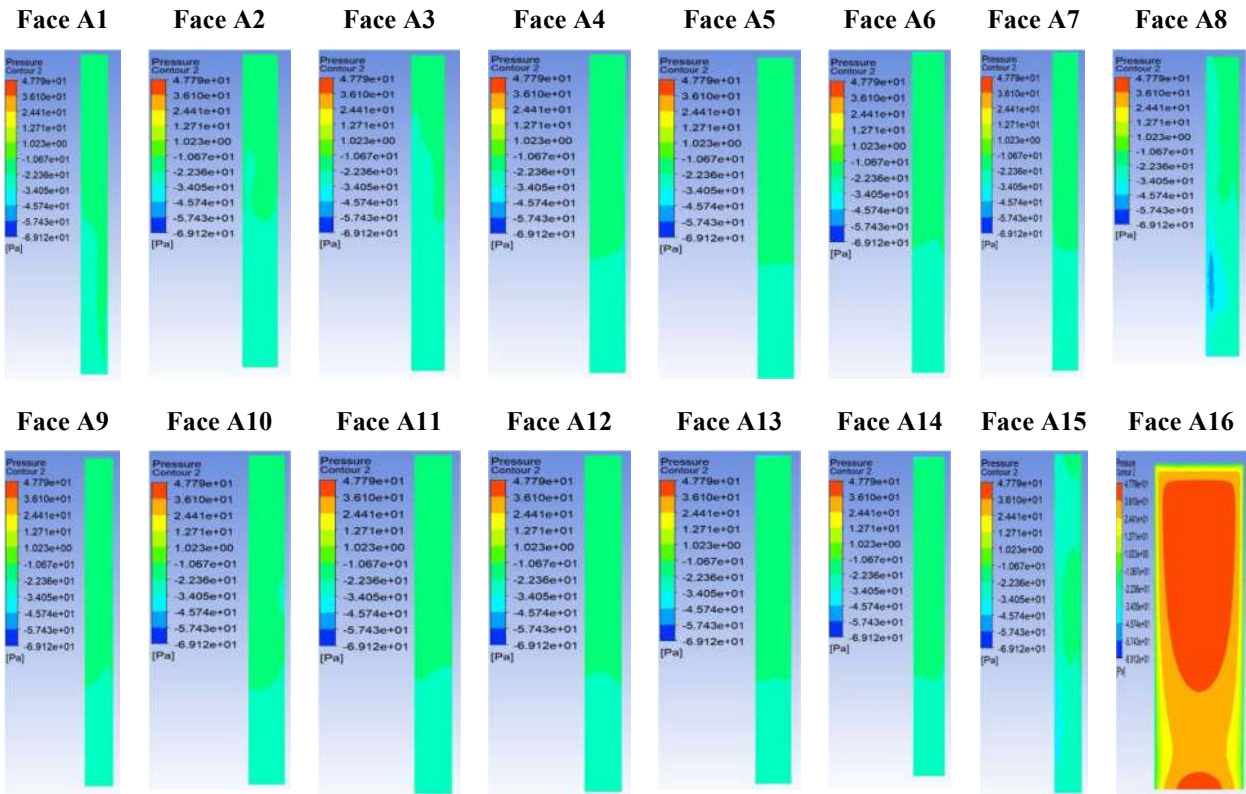


Figure 6.3: Graphical representation of Average Cp value

6.1.3 Front to Back Interference Condition

Case 1 – The incident wind angle is 0°

Table 6.26: Pressure contour of faces at 0-degree wind inclination for Model A and B



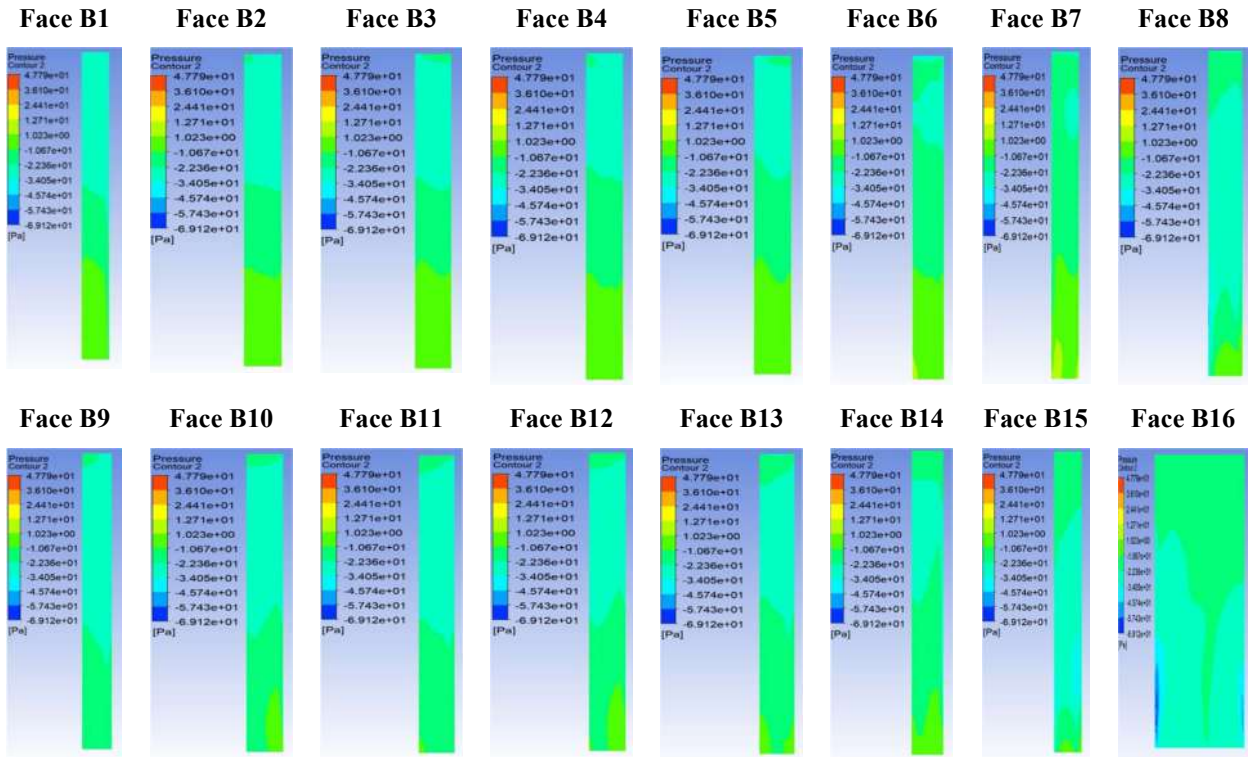


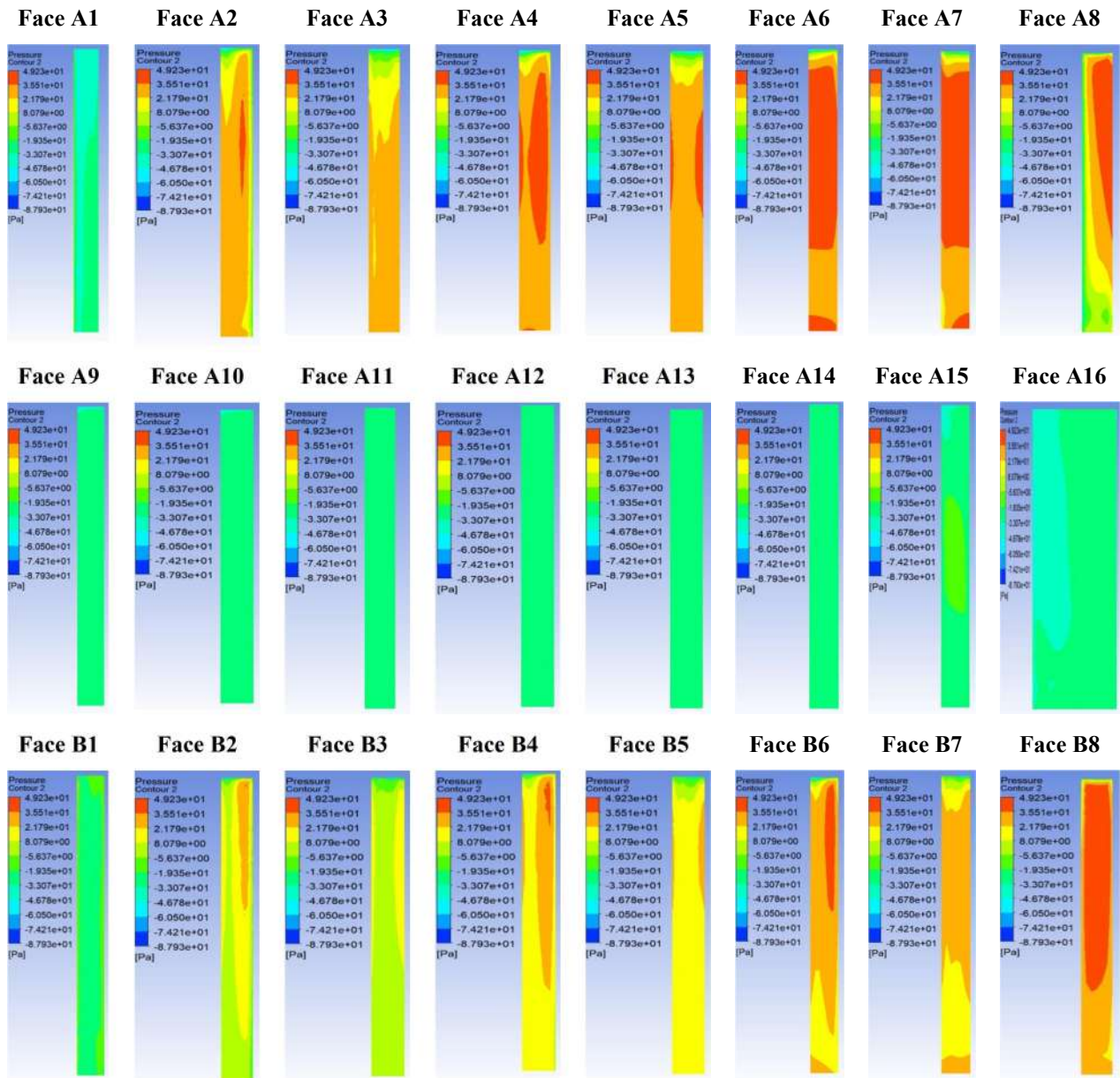
Table 6.27: Average Cp value for wind inclination 0 degree

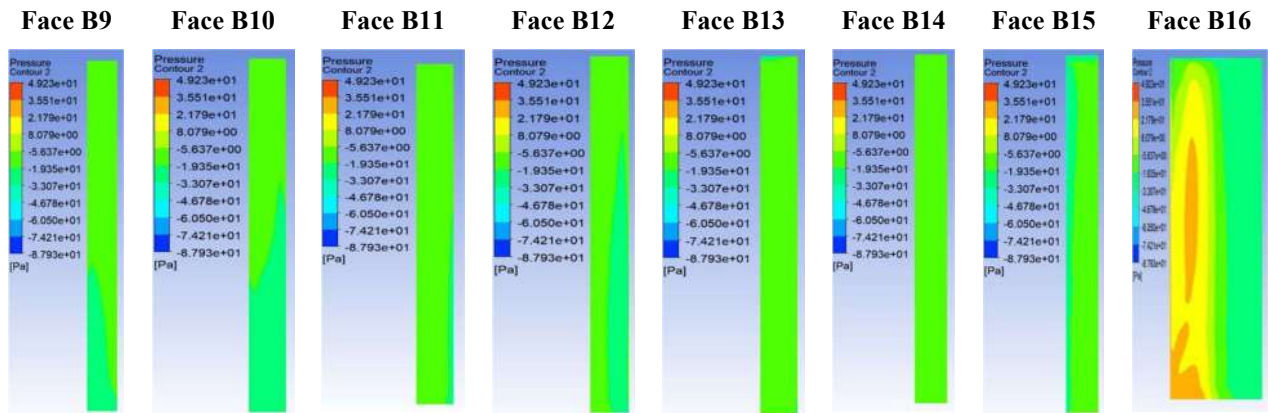
Wind Inclination Angle 0				
Faces/Wall	Range of Pressure	Average value of Pressure	Range of Cp	Average Value of Cp
A1	(-29.80,-19.79)	-22.42	(-0.49,-0.32)	-0.37
A2	(-29.80,-19.89)	-23.58	(-0.49,-0.32)	-0.38
A3	(-28.18,-20.31)	-23.73	(-0.46,-0.33)	-0.39
A4	(-29.24,-16.16)	-22.58	(-0.48,-0.26)	-0.37
A5	(-29.66,-14.95)	-21.95	(-0.48,-0.24)	-0.36
A6	(-30.90,-16.25)	-22.34	(-0.50,-0.27)	-0.36
A7	(-30.92,-16.08)	-21.86	(-0.50,-0.26)	-0.36
A8	(-57.24,-15.63)	-28.10	(-0.93,-0.26)	-0.46
A9	(-26.37,-19.66)	-22.23	(-0.43,-0.32)	-0.36
A10	(-27.02,-19.66)	-22.32	(-0.44,-0.32)	-0.36
A11	(-27.19,-17.38)	-21.93	(-0.44,-0.28)	-0.36
A12	(-26.69,-15.55)	-21.65	(-0.44,-0.25)	-0.35
A13	(-27.15,-14.09)	-20.29	(-0.44,-0.23)	-0.33
A14	(-28.09,-12.20)	-19.91	(-0.46,-0.20)	-0.33
A15	(-44.85,-16.37)	-25.84	(-0.73,-0.27)	-0.42
A16	(-42.02,47.79)	30.36	(-0.69,0.78)	0.50
B1	(-31.16,0.53)	-18.60	(-0.51,0.01)	-0.30
B2	(-29.30,-1.85)	-17.16	(-0.48,-0.03)	-0.28
B3	(-28.01,-0.13)	-16.52	(-0.46,0.00)	-0.27
B4	(-26.83,-0.47)	-16.09	(-0.44,-0.01)	-0.26
B5	(-25.36,0.88)	-15.32	(-0.41,0.01)	-0.25
B6	(-27.89,2.48)	-14.46	(-0.46,0.04)	-0.24
B7	(-24.84,3.29)	-14.34	(-0.41,0.05)	-0.23
B8	(-48.70,1.91)	-22.71	(-0.80,0.03)	-0.37
B9	(-31.51,-11.31)	-23.41	(-0.51,-0.18)	-0.38
B10	(-30.00,-6.30)	-21.50	(-0.49,-0.10)	-0.35
B11	(-27.94,-9.64)	-21.49	(-0.46,-0.16)	-0.35
B12	(-27.31,-5.45)	-20.09	(-0.45,-0.09)	-0.33
B13	(-25.28,-6.63)	-19.90	(-0.41,-0.11)	-0.32
B14	(-28.70,-1.94)	-18.91	(-0.47,-0.03)	-0.31
B15	(-43.53,-4.09)	-24.25	(-0.71,-0.07)	-0.40
B16	(-69.12,-19.63)	-24.30	(-1.13,-0.32)	-0.40

The range of average pressure values for the wind inclination angle of 0° is between [-28.10, 30.36] (Table 6.26). The maximum positive and negative pressure values of 30.36 and -28.10, respectively, occur on Face A16 and A8. The range of pressure coefficient C_p lies in the range ε [-0.46, 0.50] (Table 6.27). The maximum positive and negative values of 0.50 and -0.46 occur on Faces A16 and A8.

- Case 2 – The incident wind angle is 90°

Table 6.28: Pressure contour of faces at 60-degree wind inclination for Model A and B





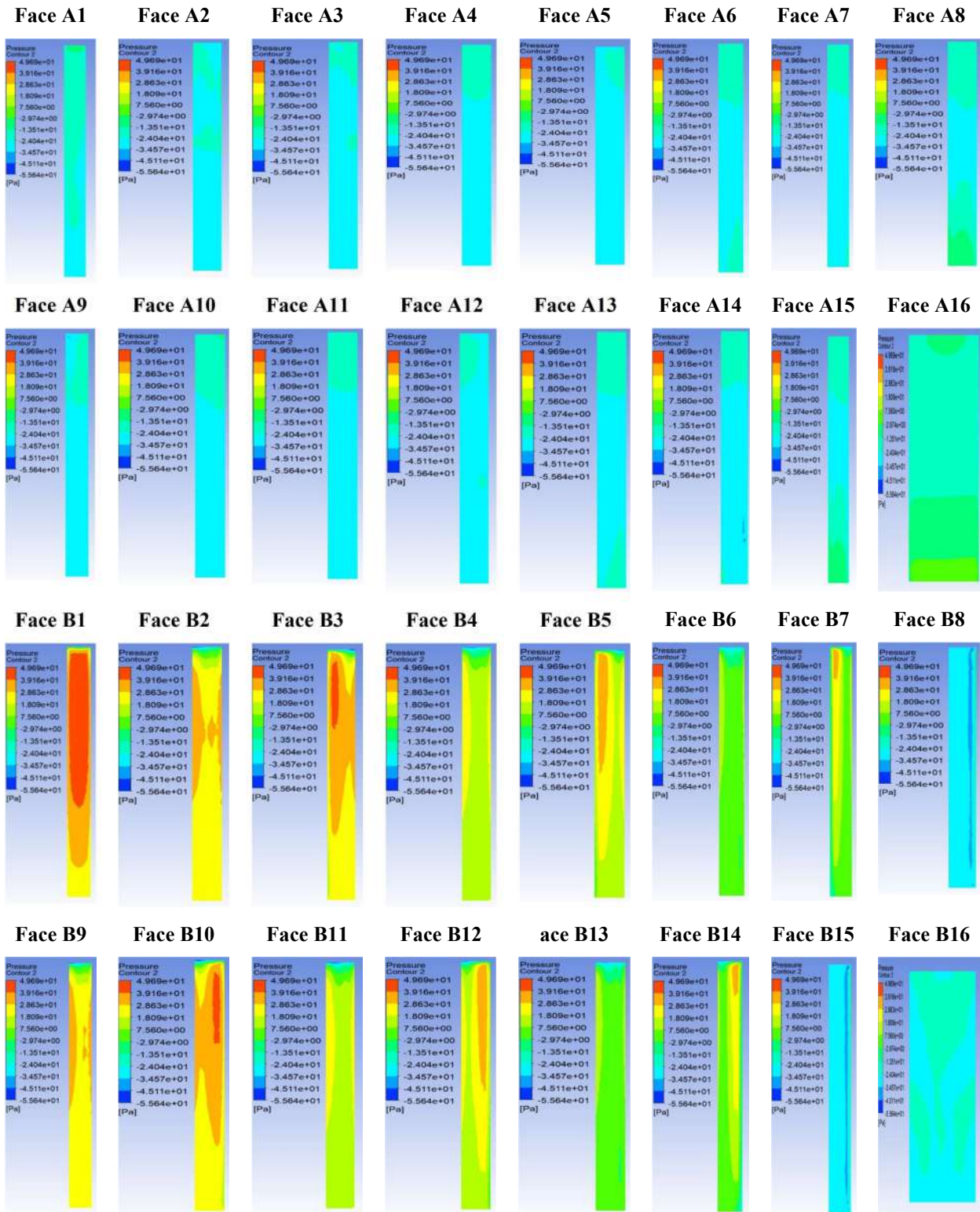
The range of average pressure values for the wind inclination angle of 90° is between $[-31.61, 37.19]$ (Table 6.28). The maximum positive and negative pressure values of 37.19 and -31.61, respectively, occur on Faces A7 and A1. The range of pressure coefficient C_p lies in the range $\varepsilon [-0.52, 0.61]$ (Table 6.29). The maximum positive and negative values of 0.61 and -0.52 occur on Faces A7 and A1.

Table 6.29: Average C_p value for wind inclination 90 degree

Wind Inclination Angle 90				
Faces/Wall	Range of Pressure	Average value of Pressure	Range of C_p	Average Value of C_p
A1	(-56.45,-8.41)	-31.61	(-0.92,-0.14)	-0.52
A2	(-51.93,37.95)	19.52	(-0.85,0.62)	0.32
A3	(-58.16,29.34)	20.18	(-0.95,0.48)	0.33
A4	(-63.78,42.99)	31.14	(-1.04,0.70)	0.51
A5	(-62.25,37.63)	29.00	(-1.02,0.61)	0.47
A6	(-61.49,46.91)	36.67	(-1.00,0.77)	0.60
A7	(-61.49,47.59)	37.19	(-1.00,0.78)	0.61
A8	(-40.54,48.47)	16.82	(-0.66,0.79)	0.27
A9	(-39.39,-22.95)	-26.48	(-0.64,-0.37)	-0.43
A10	(-39.03,-24.22)	-26.79	(-0.64,-0.40)	-0.44
A11	(-33.87,-22.66)	-26.12	(-0.55,-0.37)	-0.43
A12	(-31.88,-24.23)	-26.76	(-0.52,-0.40)	-0.44
A13	(-32.01,-20.87)	-25.60	(-0.52,-0.34)	-0.42
A14	(-32.01,-22.44)	-26.54	(-0.52,-0.37)	-0.43
A15	(-46.17,-16.74)	-24.34	(-0.75,-0.27)	-0.40
A16	(-62.78,-15.58)	-29.78	(-1.03,-0.25)	-0.49
B1	(-33.11,3.95)	-19.84	(-0.54,0.06)	-0.32
B2	(-33.32,36.06)	8.24	(-0.54,0.59)	0.13
B3	(-29.55,15.98)	5.36	(-0.48,0.26)	0.09
B4	(-41.63,37.23)	18.39	(-0.68,0.61)	0.30
B5	(-36.16,27.09)	15.15	(-0.59,0.44)	0.25
B6	(-48.93,41.19)	25.42	(-0.80,0.67)	0.41
B7	(-42.71,32.70)	22.20	(-0.70,0.53)	0.36
B8	(-21.28,49.23)	33.54	(-0.35,0.80)	0.55
B9	(-21.77,-15.72)	-18.15	(-0.36,-0.26)	-0.30
B10	(-29.53,-15.61)	-19.56	(-0.48,-0.25)	-0.32
B11	(-26.48,-15.04)	-17.20	(-0.43,-0.25)	-0.28
B12	(-26.10,-15.70)	-18.75	(-0.43,-0.26)	-0.31
B13	(-24.63,-9.73)	-14.37	(-0.40,-0.16)	-0.23
B14	(-21.04,-10.48)	-14.66	(-0.34,-0.17)	-0.24
B15	(-40.82,-12.57)	-19.30	(-0.67,-0.21)	-0.32
B16	(-41.49,33.18)	-5.32	(-0.68,0.54)	-0.09

- Case 3 – The incident wind angle is 180°

Table 6.30: Pressure contour of faces at 180-degree wind inclination for Model A and B



The range of average pressure values for the wind inclination angle of 180° is between [-28.19, 35.36] (Table 6.30). The maximum positive and negative pressure values of 35.36 and -28.19, respectively, occur on Face B1 and B15. The range of pressure coefficient C_p lies in the range ε [-0.46, 0.58] (Table 6.31). The maximum positive and negative values of 0.58 and -0.46 occur on Faces B1 and B15.

Table 6.31: Average C_p value for wind inclination 180 degree

Wind Inclination Angle 180				
Faces/Wall	Range of Pressure	Average value of Pressure	Range of C_p	Average Value of C_p
A1	(-28.38,-3.72)	-23.65	(-0.46,-0.06)	-0.39
A2	(-31.18,-18.13)	-24.80	(-0.51,-0.30)	-0.40
A3	(-26.30,-16.31)	-24.63	(-0.43,-0.27)	-0.40
A4	(-29.50,-20.52)	-25.19	(-0.48,-0.34)	-0.41
A5	(-35.00,-20.52)	-25.93	(-0.57,-0.34)	-0.42
A6	(-33.15,-14.78)	-23.90	(-0.54,-0.24)	-0.39
A7	(-32.42,-16.27)	-24.94	(-0.53,-0.27)	-0.41
A8	(-32.69,-5.32)	-20.51	(-0.53,-0.09)	-0.33
A9	(-37.50,-14.31)	-24.78	(-0.61,-0.23)	-0.40
A10	(-26.04,-10.03)	-24.27	(-0.43,-0.16)	-0.40
A11	(-30.39,-20.42)	-25.15	(-0.50,-0.33)	-0.41
A12	(-34.21,-20.42)	-25.82	(-0.56,-0.33)	-0.42
A13	(-32.37,-14.42)	-24.49	(-0.53,-0.24)	-0.40
A14	(-37.05,-16.33)	-26.16	(-0.60,-0.27)	-0.43
A15	(-32.92,-3.90)	-20.83	(-0.54,-0.06)	-0.34
A16	(-28.93,-2.07)	-14.47	(-0.47,-0.03)	-0.24
B1	(-17.03,49.69)	35.36	(-0.28,0.81)	0.58
B2	(-50.63,35.12)	24.35	(-0.83,0.57)	0.40
B3	(-50.63,41.49)	26.92	(-0.83,0.68)	0.44
B4	(-41.48,24.61)	14.86	(-0.68,0.40)	0.24
B5	(-41.39,36.27)	18.24	(-0.68,0.59)	0.30
B6	(-38.14,14.46)	3.23	(-0.62,0.24)	0.05
B7	(-38.23,36.02)	6.05	(-0.62,0.59)	0.10
B8	(-46.69,-8.41)	-28.16	(-0.76,-0.14)	-0.46
B9	(-47.69,34.50)	24.31	(-0.78,0.56)	0.40
B10	(-51.62,41.44)	26.71	(-0.84,0.68)	0.44
B11	(-46.45,24.14)	14.66	(-0.76,0.39)	0.24
B12	(-43.55,36.62)	18.08	(-0.71,0.60)	0.30
B13	(-37.86,13.50)	3.19	(-0.62,0.22)	0.05
B14	(-38.75,36.73)	6.09	(-0.63,0.60)	0.10
B15	(-48.79,-6.28)	-28.19	(-0.80,-0.10)	-0.46
B16	(-29.97,-20.10)	-24.28	(-0.49,-0.33)	-0.40

- Similarly, for the wind inclination angle of 30° the average pressure is between [-43.51, 25.75]. The maximum positive and negative pressure values of 25.75 and -43.51, respectively, occur on Face A16 and A8. The range of pressure coefficient C_p lies in the range ε [-0.71, 0.42]. The maximum positive and negative values of 0.42 and -0.71 occur on Faces A16 and A8.

- For the wind inclination angle of 60° the average pressure is between [-35.49, 31.93]. The maximum positive and negative pressure values of 31.93 and -35.49, respectively, occur on Face A8 and B7. The range of pressure coefficient Cp lies in the range ε [-0.58, 0.52]. The maximum positive and negative values of 0.52 and -0.58 occur on Faces A8 and B7 (See Table 6.32).

Table 6.32: Average Cp value for wind inclination 30, 60, 120 and 150 degrees

Wind Inclination Angle 30				
Faces/Wall	Range of Pressure	Average value of Pressure	Range of Cp	Average Value of Cp
A1	(-45.29,-8.49)	-25.17	(-0.74,-0.14)	-0.41
A2	(-31.84,9.35)	-15.04	(-0.52,0.15)	-0.25
A3	(-33.09,3.19)	-18.88	(-0.54,0.05)	-0.31
A4	(-38.46,-18.68)	-25.38	(-0.63,-0.31)	-0.41
A5	(-32.54,-17.60)	-24.20	(-0.53,-0.29)	-0.40
A6	(-35.71,-24.36)	-26.55	(-0.58,-0.40)	-0.43
A7	(-36.57,-24.40)	-26.57	(-0.60,-0.40)	-0.43
A8	(-84.57,-3.61)	-43.51	(-1.38,-0.06)	-0.71
A9	(-35.49,-19.33)	-23.42	(-0.58,-0.32)	-0.38
A10	(-29.04,-19.61)	-22.97	(-0.47,-0.32)	-0.37
A11	(-30.02,-18.01)	-22.20	(-0.49,-0.29)	-0.36
A12	(-29.59,-18.69)	-22.86	(-0.48,-0.31)	-0.37
A13	(-31.79,-11.02)	-19.44	(-0.52,-0.18)	-0.32
A14	(-32.56,-10.33)	-19.36	(-0.53,-0.17)	-0.32
A15	(-44.08,-15.48)	-28.27	(-0.72,-0.25)	-0.46
A16	(-62.06,49.04)	25.75	(-1.01,0.80)	0.42
B1	(-34.08,-12.39)	-19.16	(-0.56,-0.20)	-0.31
B2	(-25.30,3.22)	-17.33	(-0.42,0.05)	-0.28
B3	(-51.45,-12.80)	-18.27	(-0.84,-0.21)	-0.30
B4	(-38.31,2.05)	-18.22	(-0.63,0.03)	-0.30
B5	(-34.15,-12.70)	-18.93	(-0.56,-0.21)	-0.31
B6	(-28.79,-1.67)	-21.69	(-0.47,-0.08)	-0.35
B7	(-52.60,-16.14)	-26.31	(-0.86,-0.26)	-0.43
B8	(-72.80,29.14)	-13.44	(-1.19,0.48)	-0.22
B9	(-22.59,-9.97)	-15.63	(-0.37,-0.16)	-0.26
B10	(-22.67,-9.53)	-16.09	(-0.37,-0.16)	-0.26
B11	(-20.46,-8.57)	-14.28	(-0.33,-0.14)	-0.23
B12	(-21.66,-9.38)	-15.14	(-0.35,-0.15)	-0.25
B13	(-21.57,-6.33)	-14.27	(-0.35,-0.10)	-0.23
B14	(-29.60,-6.44)	-14.69	(-0.48,-0.11)	-0.24
B15	(-51.58,-6.81)	-24.52	(-0.84,-0.11)	-0.40
B16	(-80.49,55.67)	-9.78	(-1.31,0.91)	-0.15

Wind Inclination Angle 60				
Faces/Wall	Range of Pressure	Average value of Pressure	Range of Cp	Average Value of Cp
A1	(-53.48,-8.92)	-30.80	(-0.87,-0.15)	-0.50
A2	(-57.15,33.96)	15.24	(-0.93,0.55)	0.23
A3	(-41.48,24.74)	15.55	(-0.68,0.40)	0.25
A4	(-53.49,33.75)	21.85	(-0.87,0.55)	0.36
A5	(-47.89,27.43)	20.14	(-0.78,0.45)	0.33
A6	(-32.37,27.82)	15.64	(-0.53,0.45)	0.26
A7	(-24.23,21.90)	12.90	(-0.40,0.36)	0.21
A8	(-15.65,52.03)	31.93	(-0.26,0.85)	0.52
A9	(-31.90,-22.40)	-25.92	(-0.52,-0.37)	-0.42
A10	(-33.22,-23.56)	-26.21	(-0.54,-0.38)	-0.43
A11	(-39.48,-21.89)	-26.16	(-0.64,-0.36)	-0.43
A12	(-38.65,-23.93)	-27.02	(-0.63,-0.39)	-0.44
A13	(-56.59,-17.33)	-24.17	(-0.92,-0.28)	-0.39
A14	(-40.92,-17.60)	-23.35	(-0.67,-0.29)	-0.38
A15	(-54.21,-17.60)	-28.87	(-0.88,-0.29)	-0.47
A16	(-54.21,41.34)	5.07	(-0.88,0.67)	0.08
B1	(-22.57,-4.19)	-12.74	(-0.37,-0.07)	-0.21
B2	(-15.63,12.95)	-9.39	(-0.26,0.21)	-0.15
B3	(-19.60,-6.05)	-10.80	(-0.32,-0.10)	-0.18
B4	(-16.80,9.98)	-13.42	(-0.27,0.16)	-0.22
B5	(-24.41,-9.01)	-15.11	(-0.40,-0.15)	-0.25
B6	(-42.10,-7.46)	-29.24	(-0.69,-0.12)	-0.48
B7	(-55.20,-20.93)	-35.49	(-0.90,-0.34)	-0.58
B8	(63.31,46.32)	1.75	(-1.03,0.76)	0.03
B9	(-16.45,-6.79)	-12.12	(-0.27,-0.11)	-0.20
B10	(-16.09,-7.13)	-12.42	(-0.26,-0.12)	-0.20
B11	(-23.92,-7.09)	-12.55	(-0.39,-0.12)	-0.20
B12	(-20.63,-8.21)	-13.03	(-0.34,-0.13)	-0.21
B13	(-31.67,-6.28)	-12.69	(-0.52,-0.10)	-0.21
B14	(-20.86,-6.50)	-12.73	(-0.34,-0.11)	-0.21
B15	(-42.02,-5.91)	-17.19	(-0.69,-0.10)	-0.28
B16	(-99.24,48.18)	-1.42	(-1.62,0.79)	-0.02

Wind Inclination Angle 120				
Faces/Wall	Range of Pressure	Average value of Pressure	Range of Cp	Average Value of Cp
A1	(-49.17,-11.17)	-28.42	(-0.80,-0.18)	-0.46
A2	(-61.00,29.49)	12.18	(-1.00,0.48)	0.20
A3	(-76.94,23.28)	9.92	(-1.26,0.38)	0.16
A4	(-65.71,46.18)	33.66	(-1.07,0.75)	0.55
A5	(-57.65,45.67)	36.30	(-0.94,0.75)	0.59
A6	(-56.54,47.99)	37.99	(-0.92,0.78)	0.62
A7	(-37.10,47.71)	35.27	(-0.61,0.78)	0.58
A8	(-44.89,36.29)	-3.88	(-0.73,0.59)	-0.06
A9	(-41.54,-22.17)	-24.75	(-0.68,-0.36)	-0.40
A10	(-41.54,-22.67)	-26.11	(-0.68,-0.37)	-0.43
A11	(-37.65,-20.66)	-24.43	(-0.61,-0.34)	-0.40
A12	(-36.69,-18.96)	-25.32	(-0.60,-0.31)	-0.41
A13	(-40.43,-15.06)	-20.06	(-0.66,-0.25)	-0.33
A14	(-40.56,-15.97)	-20.57	(-0.66,-0.26)	-0.34
A15	(73.31,-18.33)	-27.96	(-1.20,-0.30)	-0.46
A16	(-117.53,-11.99)	-30.59	(-1.92,-0.20)	-0.50
B1	(-65.29,-3.59)	-34.98	(-1.07,-0.06)	-0.57
B2	(-62.45,44.03)	20.58	(-1.02,0.72)	0.34
B3	(-50.86,33.73)	22.26	(-0.83,0.55)	0.36
B4	(-61.28,47.16)	34.47	(-1.00,0.77)	0.56
B5	(-57.84,45.09)	34.57	(-0.94,0.74)	0.56
B6	(-57.65,47.91)	38.39	(-0.94,0.78)	0.63
B7	(-44.68,48.49)	38.07	(-0.73,0.79)	0.62
B8	(-41.32,43.65)	21.19	(-0.67,0.71)	0.35
B9	(-40.06,-26.11)	-29.98	(-0.65,-0.43)	-0.49
B10	(-40.23,-25.37)	-30.04	(-0.66,-0.41)	-0.49
B11	(-37.38,-24.60)	-28.34	(-0.61,-0.40)	-0.46
B12	(-38.41,-23.54)	-28.10	(-0.63,-0.38)	-0.46
B13	(-38.41,-20.30)	-25.25	(-0.63,-0.33)	-0.41
B14	(-35.31,-18.15)	-24.37	(-0.58,-0.30)	-0.40
B15	(-53.75,-17.66)	-27.93	(-0.88,-0.29)	-0.46
B16	(-54.11,79.64)	-11.74	(-0.89,0.48)	-0.19

Wind Inclination Angle 150				
Faces/Wall	Range of Pressure	Average value of Pressure	Range of Cp	Average Value of Cp
A1	(-27.91,-9.37)	-18.86	(-0.46,-0.15)	-0.31
A2	(-34.55,-3.55)	-23.53	(-0.56,-0.06)	-0.38
A3	(-61.49,-16.40)	-29.55	(-1.00,-0.27)	-0.48
A4	(-50.91,25.53)	3.55	(-0.83,0.42)	0.06
A5	(-40.60,26.27)	5.13	(-0.66,0.43)	0.08
A6	(-23.84,43.00)	30.71	(-0.39,0.70)	0.50
A7	(-23.79,45.45)	32.71	(-0.39,0.74)	0.53
A8	(-37.76,22.06)	-13.64	(-0.62,0.36)	-0.22
A9	(-20.74,-11.11)	-16.76	(-0.34,-0.18)	-0.27
A10	(-20.86,-11.37)	-16.75	(-0.34,-0.19)	-0.27
A11	(-18.96,-11.87)	-15.93	(-0.31,-0.19)	-0.26
A12	(-18.88,-12.91)	-16.34	(-0.31,-0.21)	-0.27
A13	(-20.22,-15.31)	-16.91	(-0.33,-0.25)	-0.28
A14	(-19.00,-15.31)	-17.13	(-0.31,-0.25)	-0.28
A15	(-21.92,-11.95)	-17.43	(-0.36,-0.20)	-0.28
A16	(-35.72,-9.15)	-18.32	(-0.58,-0.15)	-0.30
B1	(-58.79,36.75)	-4.42	(-0.96,0.60)	-0.07
B2	(-45.82,49.02)	35.75	(-0.75,0.80)	0.58
B3	(-47.70,48.60)	38.59	(-0.78,0.79)	0.63
B4	(-47.39,47.79)	38.24	(-0.77,0.78)	0.62
B5	(-55.75,48.07)	37.41	(-0.91,0.78)	0.61
B6	(-59.68,38.54)	28.43	(-0.97,0.65)	0.46
B7	(-46.75,45.73)	26.62	(-0.76,0.75)	0.43
B8	(-54.68,5.22)	-19.63	(-0.89,0.09)	-0.32
B9	(-58.79,-15.99)	-31.80	(-0.96,-0.26)	-0.52
B10	(-47.11,-0.67)	-26.53	(-0.77,-0.01)	-0.43
B11	(-32.44,-6.63)	-17.33	(-0.53,-0.11)	-0.28
B12	(-23.50,5.66)	-15.25	(-0.38,0.09)	-0.25
B13	(-34.34,-2.97)	-12.81	(-0.56,-0.03)	-0.21
B14	(-17.83,15.29)	-10.85	(-0.29,0.25)	-0.18
B15	(-26.68,-3.38)	-12.52	(-0.44,-0.06)	-0.20
B16	(-39.25,8.92)	-14.91	(-0.64,0.15)	-0.24

- The range of average pressure values for the wind inclination angle of 120° is between **[-34.98, 38.39]**. The maximum positive and negative pressure values of 35.82 and -23.84, respectively, occur on Face B6 and B1. The range of pressure coefficient C_p lies in the range ϵ **[-0.57, 0.63]**. The maximum positive and negative values of 0.58 and -0.39 occur on Faces B6 and B1.
- For the wind inclination angle of 150° the average pressure is between **[-31.80, 38.59]**. The maximum positive and negative pressure values of 38.59 and -31.80, respectively, occur on Face B3 and B9. The range of pressure coefficient C_p lies in the range ϵ **[-0.52, 0.63]**. The maximum positive and negative values of 0.63 and -0.52 occur on Faces B3 and B9.

Summary of the results: The results demonstrate that the average pressure and pressure coefficient values are significantly affected by changes in the wind inclination angle. The maximum positive and negative pressure values vary across different faces for different wind inclination angles. The range of average pressure values was found to be between -39.29 to 38.82, and the range of pressure coefficient lies in the range of -0.64 to 0.66 (**Figure 6.4**). It is worth noting that the maximum positive and negative pressure coefficient values occur on different faces for different wind inclination angles (**Table 6.33**).

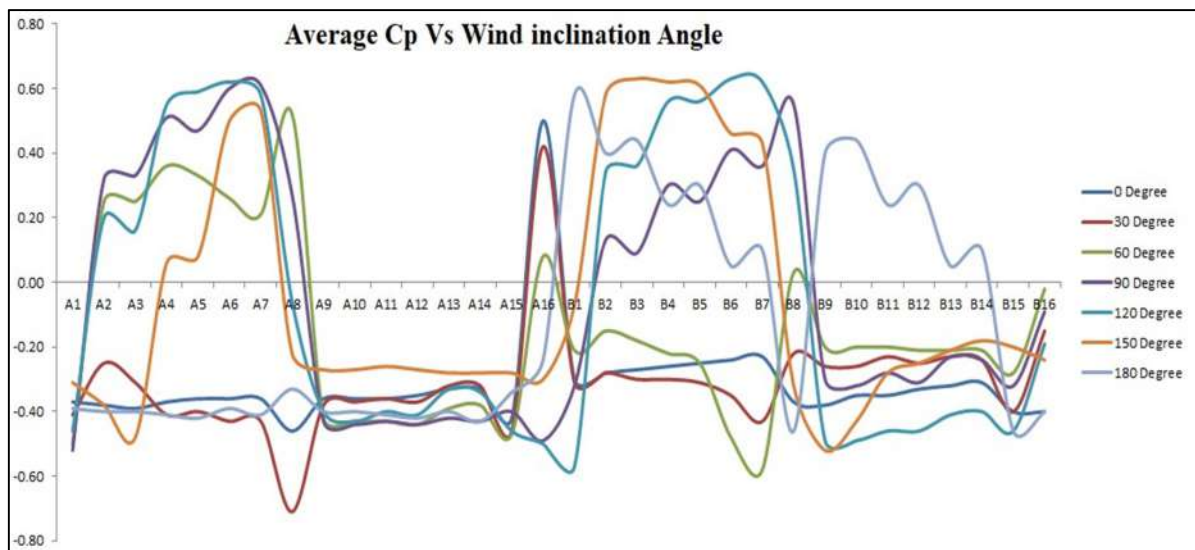


Figure 6.4: Graphical representation of Average C_p value

Table 6.33: Average Cp value for wind inclination 0 to 180 degrees

Faces/Wall	Average value of Cp at wind inclination angle						
	0 Degree	30 Degree	60 Degree	90 Degree	120 Degree	150 Degree	180 Degree
A1	-0.37	-0.41	-0.50	-0.52	-0.46	-0.31	-0.39
A2	-0.38	-0.25	0.25	0.32	0.20	-0.38	-0.40
A3	-0.39	-0.31	0.25	0.33	0.16	-0.48	-0.40
A4	-0.37	-0.41	0.36	0.51	0.55	0.06	-0.41
A5	-0.36	-0.40	0.33	0.47	0.59	0.08	-0.42
A6	-0.36	-0.43	0.26	0.60	0.62	0.50	-0.39
A7	-0.36	-0.43	0.21	0.61	0.58	0.53	-0.41
A8	-0.46	-0.71	0.52	0.27	-0.06	-0.22	-0.33
A9	-0.36	-0.38	-0.42	-0.43	-0.40	-0.27	-0.40
A10	-0.36	-0.37	-0.43	-0.44	-0.43	-0.27	-0.40
A11	-0.36	-0.36	-0.43	-0.43	-0.40	-0.26	-0.41
A12	-0.35	-0.37	-0.44	-0.44	-0.41	-0.27	-0.42
A13	-0.33	-0.32	-0.39	-0.42	-0.33	-0.28	-0.40
A14	-0.33	-0.32	-0.38	-0.43	-0.34	-0.28	-0.43
A15	-0.42	-0.46	-0.47	-0.40	-0.46	-0.28	-0.34
A16	0.50	0.42	0.08	-0.49	-0.50	-0.30	-0.24
B1	-0.30	-0.31	-0.21	-0.32	-0.57	-0.07	0.58
B2	-0.28	-0.28	-0.15	0.13	0.34	0.58	0.40
B3	-0.27	-0.30	-0.18	0.09	0.36	0.63	0.44
B4	-0.26	-0.30	-0.22	0.30	0.56	0.62	0.24
B5	-0.25	-0.31	-0.25	0.25	0.56	0.61	0.30
B6	-0.24	-0.35	-0.48	0.41	0.63	0.46	0.05
B7	-0.23	-0.43	-0.58	0.36	0.62	0.43	0.10
B8	-0.37	-0.22	0.03	0.55	0.35	-0.32	-0.46
B9	-0.38	-0.26	-0.20	-0.30	-0.49	-0.52	0.40
B10	-0.35	-0.26	-0.20	-0.32	-0.49	-0.43	0.44
B11	-0.35	-0.23	-0.20	-0.28	-0.46	-0.28	0.24
B12	-0.33	-0.25	-0.21	-0.31	-0.46	-0.25	0.30
B13	-0.32	-0.23	-0.21	-0.23	-0.41	-0.21	0.05
B14	-0.31	-0.24	-0.21	-0.24	-0.40	-0.18	0.10
B15	-0.40	-0.40	-0.28	-0.32	-0.46	-0.20	-0.46
B16	-0.40	-0.15	-0.02	-0.09	-0.19	-0.24	-0.40

6.1.4 Front to Front Interference Condition

Case 1 – The incident wind angle is 0°

The range of average pressure values for the wind inclination angle of 0° is between [-32.37, 29.67] (Table 6.34). The maximum positive and negative pressure values of 29.67 and -32.37, respectively, occur on Face A16 and A15. The range of pressure coefficient Cp lies in the range ϵ [-0.53, 0.48] (Table 6.35). The maximum positive and negative values of 0.48 and -0.53 occur on Faces A16 and A15.

Table 6.34: Pressure contour of faces at 0-degree wind inclination for Model A and B

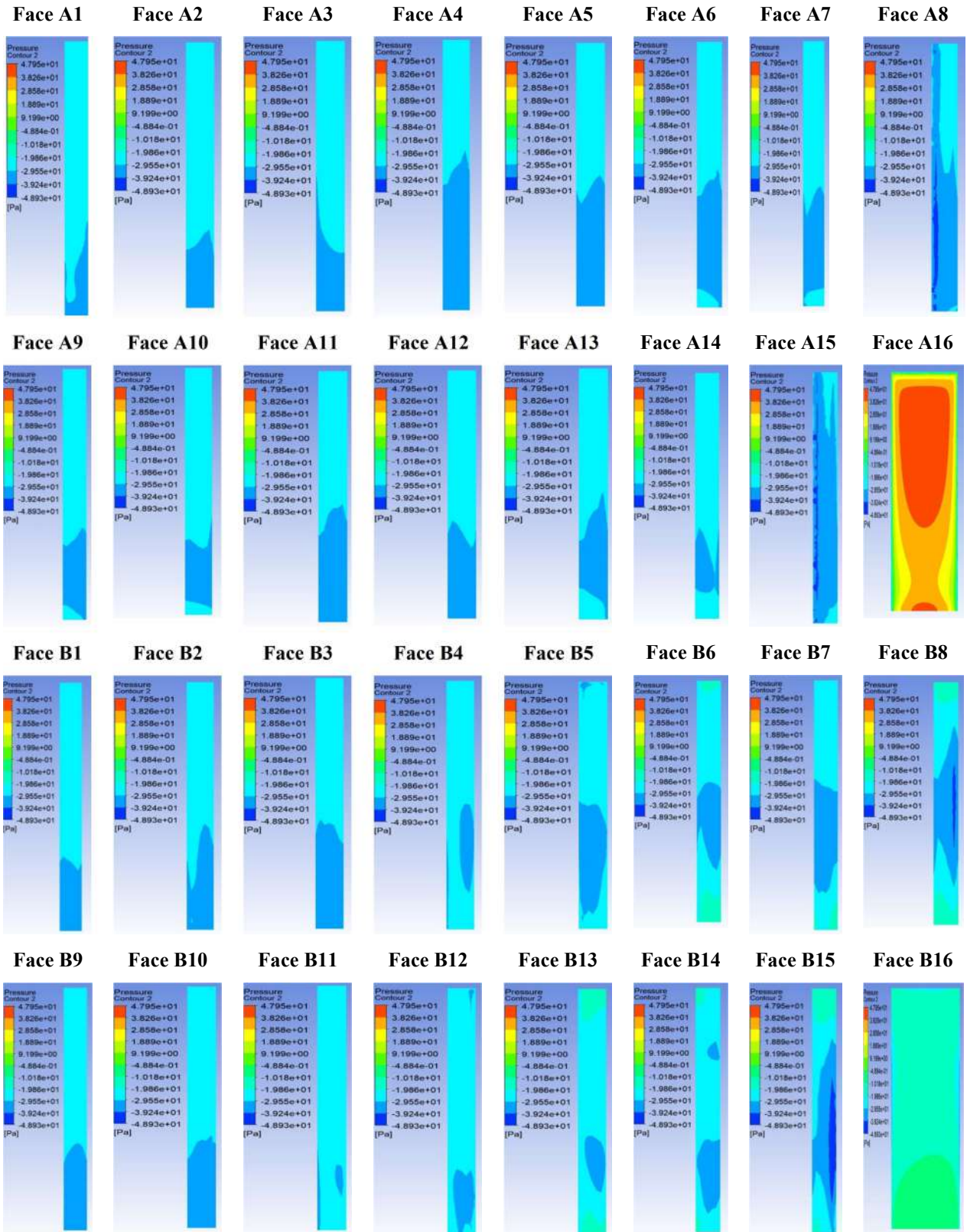
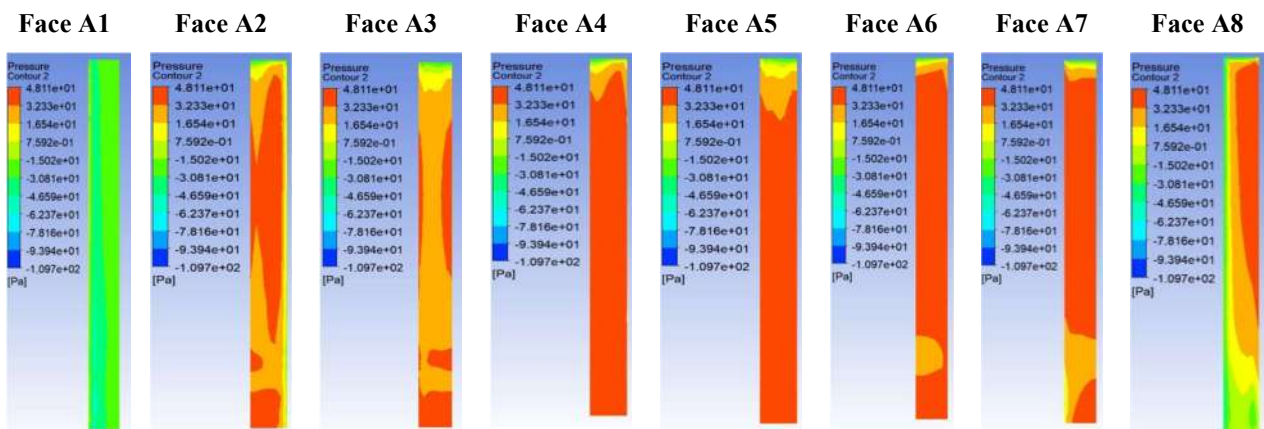


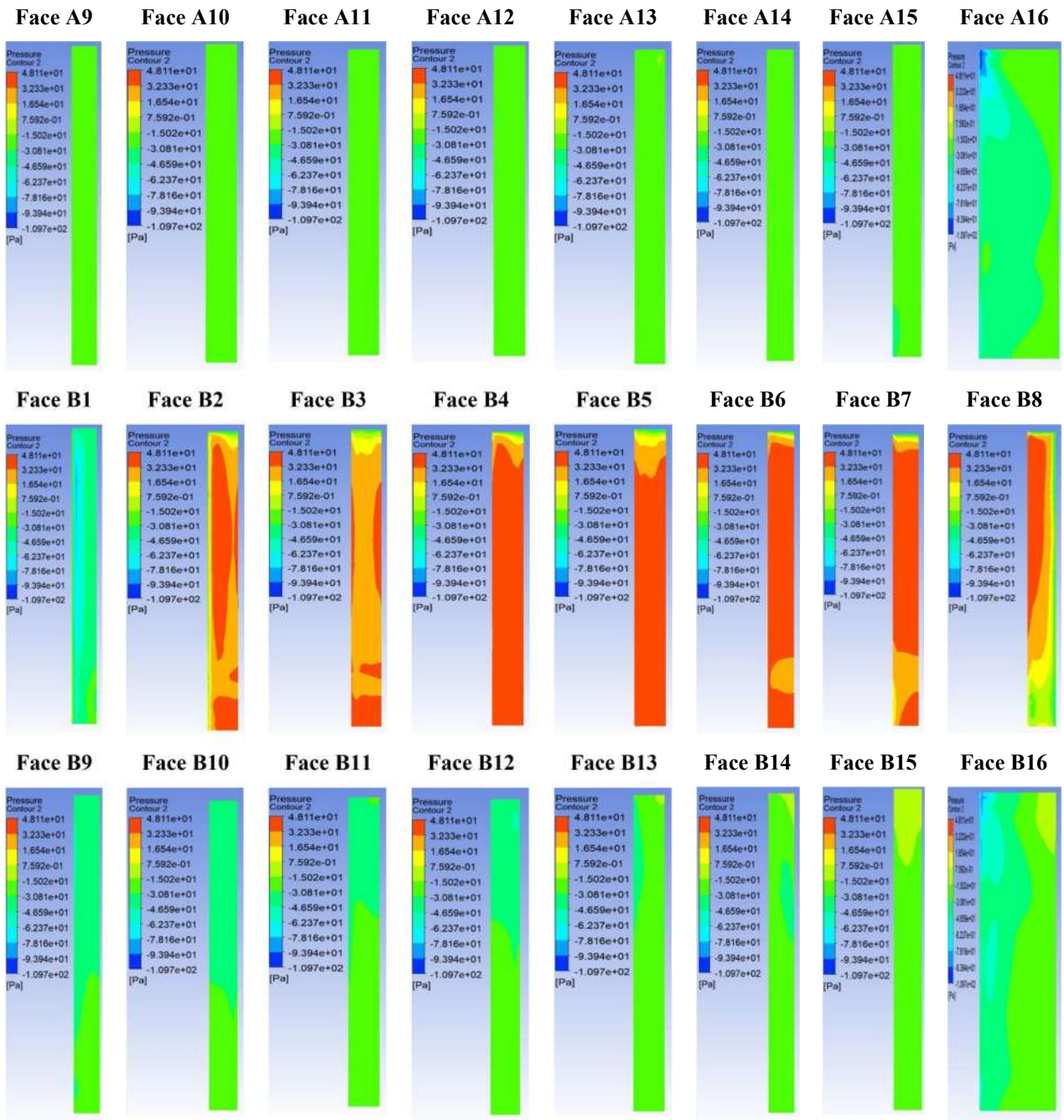
Table 6.35: Average Cp value for wind inclination 0 degree

Wind Inclination Angle 0				
Faces/Wall	Range of Pressure	Average value of Pressure	Range of Cp	Average Value of Cp
A1	(-32.39,-21.11)	-25.80	(-0.53,-0.34)	-0.42
A2	(-31.79,-20.65)	-25.31	(-0.52,-0.34)	-0.41
A3	(-32.57,-20.50)	-25.59	(-0.53,-0.33)	-0.42
A4	(-33.73,-23.45)	-28.44	(-0.55,-0.38)	-0.46
A5	(-32.73,-22.07)	-27.63	(-0.53,-0.36)	-0.45
A6	(-31.84,-24.34)	-28.21	(-0.52,-0.40)	-0.46
A7	(-32.03,-22.71)	-27.58	(-0.52,-0.37)	-0.45
A8	(-46.03,-21.53)	-32.01	(-0.75,-0.35)	-0.52
A9	(-32.90,-21.83)	-27.00	(-0.54,-0.36)	-0.44
A10	(-31.51,-20.89)	-26.50	(-0.51,-0.34)	-0.43
A11	(-33.31,-24.56)	-28.41	(-0.54,-0.40)	-0.46
A12	(-32.76,-21.83)	-27.65	(-0.53,-0.36)	-0.45
A13	(-31.25,-25.54)	-28.39	(-0.51,-0.42)	-0.46
A14	(-30.92,-23.39)	-27.74	(-0.50,-0.38)	-0.45
A15	(-44.69,-23.71)	-32.37	(-0.73,-0.39)	-0.53
A16	(-43.23,47.95)	29.67	(-0.71,0.78)	0.48
B1	(-31.65,-23.07)	-27.06	(-0.52,-0.38)	-0.44
B2	(-32.35,-23.52)	-27.27	(-0.53,-0.38)	-0.45
B3	(-34.69,-24.17)	-28.04	(-0.57,-0.39)	-0.46
B4	(-34.16,-22.38)	-26.70	(-0.56,-0.37)	-0.44
B5	(-33.89,-24.28)	-27.97	(-0.55,-0.40)	-0.46
B6	(-35.15,-13.33)	-25.97	(-0.57,-0.22)	-0.42
B7	(-35.97,-13.33)	-27.51	(-0.59,-0.22)	-0.45
B8	(-42.45,-10.31)	-27.31	(-0.69,-0.17)	-0.45
B9	(-31.63,-21.47)	-27.38	(-0.52,-0.35)	-0.45
B10	(-32.00,-23.72)	-27.92	(-0.52,-0.39)	-0.46
B11	(-32.00,-20.65)	-26.45	(-0.52,-0.34)	-0.43
B12	(-33.72,-22.27)	-27.41	(-0.55,-0.36)	-0.45
B13	(-33.86,-15.00)	-25.54	(-0.55,-0.24)	-0.42
B14	(-35.49,-16.27)	-27.07	(-0.58,-0.27)	-0.44
B15	(-48.93,-11.34)	-29.07	(-0.80,-0.19)	-0.47
B16	(-42.93,-4.51)	-14.73	(-0.70,-0.07)	-0.24

- Case 2 – The incident wind angle is 90°

Table 6.36: Pressure contour of faces at 60-degree wind inclination for Model A and B





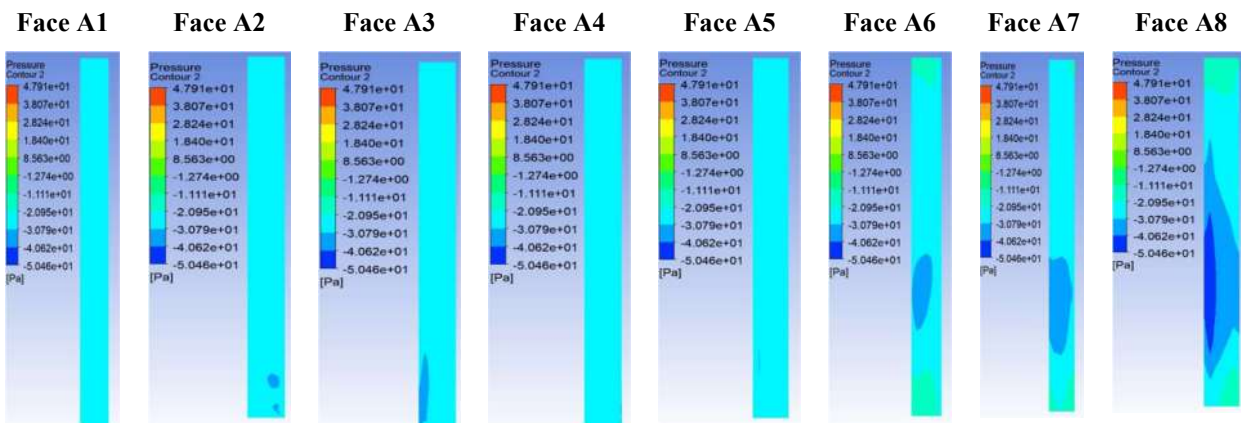
The range of average pressure values for the wind inclination angle of 90° is between $[-43.31, 38.18]$ (Table 6.36). The maximum positive and negative pressure values of 38.18 and -43.31, respectively, occur on Faces A6 and B1. The range of pressure coefficient C_p lies in the range $\varepsilon [-0.71, 0.62]$ (Table 6.37). The maximum positive and negative values of 0.62 and -0.71 occur on Faces A6 and B1.

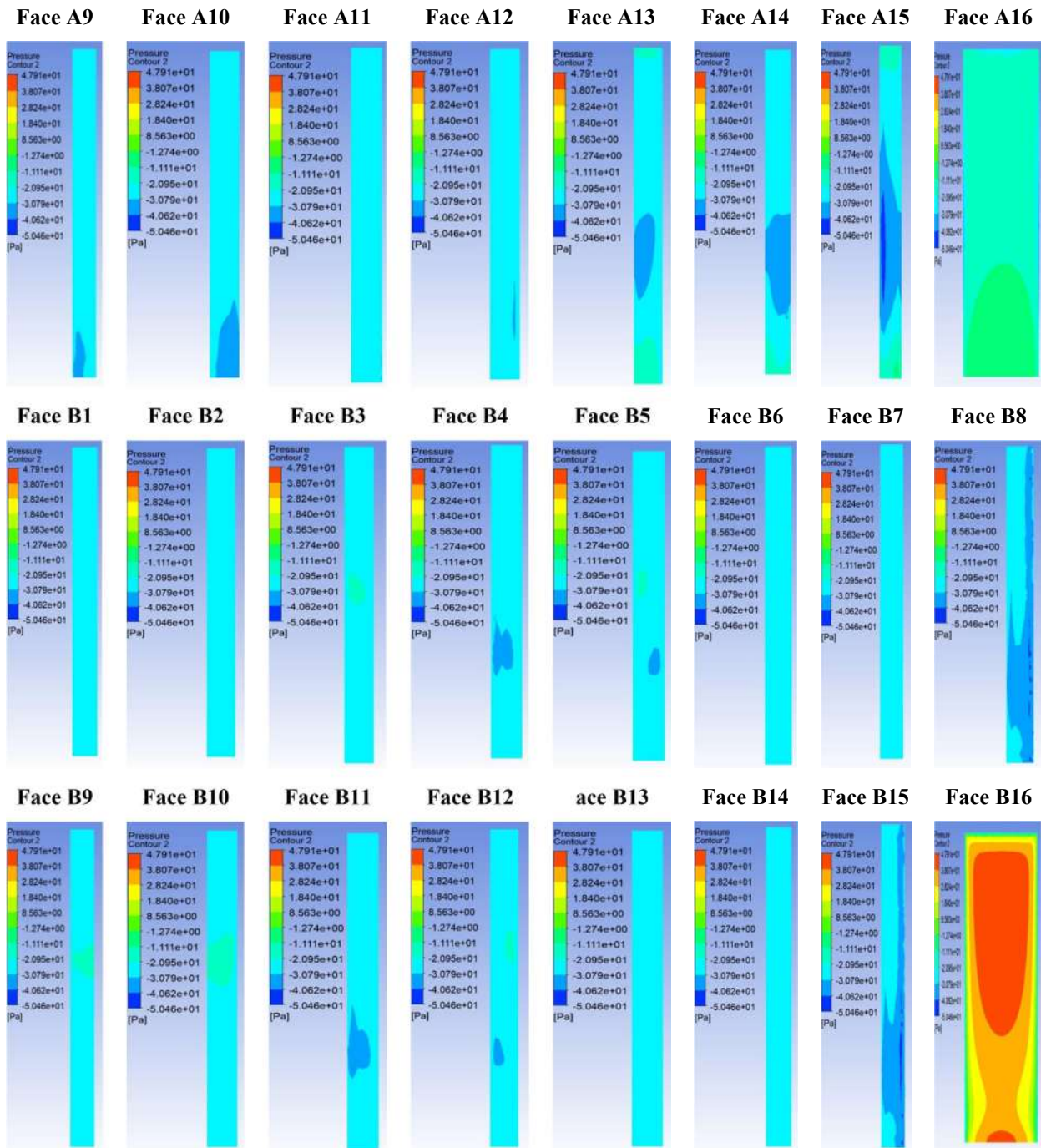
Table 6.37: Average Cp value for wind inclination 90 degree

Wind Inclination Angle 90				
Faces/Wall	Range of Pressure	Average value of Pressure	Range of Cp	Average Value of Cp
A1	(-59.63,0.23)	-28.59	(-0.97,0.00)	-0.47
A2	(-38.39,43.29)	26.55	(-0.63,0.71)	0.43
A3	(-4.56,36.96)	29.05	(-0.71,0.60)	0.47
A4	(-42.67,45.40)	35.65	(-0.70,0.74)	0.58
A5	(-44.90,41.84)	33.61	(-0.73,0.68)	0.55
A6	(-37.21,47.82)	38.18	(-0.61,0.78)	0.62
A7	(-40.89,48.09)	37.07	(-0.67,0.79)	0.61
A8	(-86.18,48.11)	13.30	(-1.41,0.79)	0.22
A9	(-31.30,-18.66)	-21.78	(-0.51,-0.30)	-0.36
A10	(-26.25,-19.78)	-22.12	(-0.43,-0.32)	-0.36
A11	(-25.98,-15.25)	-20.47	(-0.42,-0.25)	-0.33
A12	(-26.35,-16.01)	-21.04	(-0.43,-0.26)	-0.34
A13	(-27.38,-14.66)	-20.73	(-0.45,-0.24)	-0.34
A14	(-28.90,-15.21)	-21.21	(-0.47,-0.25)	-0.35
A15	(-35.68,-16.11)	-23.19	(-0.58,-0.26)	-0.38
A16	(-108.68,-18.15)	-35.40	(-1.77,-0.30)	-0.58
B1	(-84.11,-5.30)	-43.31	(-1.37,-0.09)	-0.71
B2	(-45.65,43.57)	25.00	(-0.75,0.71)	0.41
B3	(-39.48,37.05)	28.65	(-0.64,0.60)	0.47
B4	(-55.42,45.16)	35.31	(-0.90,0.74)	0.58
B5	(-60.07,41.52)	33.07	(-0.98,0.68)	0.54
B6	(-43.35,47.66)	37.88	(-0.71,0.78)	0.62
B7	(-50.46,47.94)	36.55	(-0.82,0.78)	0.60
B8	(-60.92,48.04)	13.01	(-0.99,0.78)	0.21
B9	(-50.24,-22.69)	-32.91	(-0.82,-0.37)	-0.54
B10	(-38.07,-23.57)	-31.08	(-0.62,-0.38)	-0.51
B11	(-38.07,-21.00)	-28.47	(-0.62,-0.34)	-0.46
B12	(-50.45,-21.51)	-29.70	(-0.82,-0.35)	-0.48
B13	(-45.82,-10.87)	-25.21	(-0.75,-0.18)	-0.41
B14	(-36.56,-6.96)	-24.56	(-0.60,-0.11)	-0.40
B15	(-32.69,-5.44)	-18.84	(-0.53,-0.09)	-0.31
B16	(-94.32,-4.33)	-32.18	(-1.54,-0.07)	-0.53

- Case 3 – The incident wind angle is 180°

Table 6.38: Pressure contour of faces at 180-degree wind inclination for Model A and B





The range of average pressure values for the wind inclination angle of 180^0 is between $[-31.58, 29.57]$ (Table 6.38). The maximum positive and negative pressure values of 29.57 and -31.58, respectively, occur on Faces B16 and B8. The range of pressure coefficient C_p lies in the range $\varepsilon [-0.52, 0.48]$ (Table 6.39). The maximum positive and negative values of 0.48 and -0.52 occur on B16 and B8.

Table 6.39: Average Cp value for wind inclination 180 degree

Wind Inclination Angle 180				
Faces/Wall	Range of Pressure	Average value of Pressure	Range of Cp	Average Value of Cp
A1	(-30.15,-23.06)	-25.75	(-0.49,-0.38)	-0.42
A2	(-30.91,-22.82)	-26.66	(-0.50,-0.37)	-0.44
A3	(-31.32,-23.66)	-27.02	(-0.51,-0.39)	-0.44
A4	(-31.18,-22.12)	-26.07	(-0.51,-0.36)	-0.43
A5	(-31.29,-23.71)	-26.99	(-0.51,-0.39)	-0.44
A6	(-33.85,-14.26)	-25.28	(-0.55,-0.23)	-0.41
A7	(-34.91,-14.26)	-26.63	(-0.57,-0.23)	-0.43
A8	(-50.46,-11.38)	-29.88	(-0.82,-0.19)	-0.49
A9	(-31.35,-23.15)	-26.50	(-0.51,-0.38)	-0.43
A10	(-32.67,-23.62)	-26.98	(-0.53,-0.39)	-0.44
A11	(-32.62,-22.76)	-26.20	(-0.53,-0.37)	-0.43
A12	(-31.15,-23.87)	-27.29	(-0.51,-0.39)	-0.45
A13	(-34.36,-14.63)	-25.77	(-0.56,-0.24)	-0.42
A14	(-34.78,-14.63)	-27.04	(-0.57,-0.24)	-0.44
A15	(-46.26,-9.83)	-28.51	(-0.76,-0.16)	-0.47
A16	(-46.06,-4.28)	-15.38	(-0.75,-0.07)	-0.25
B1	(-30.05,-21.32)	-25.08	(-0.49,-0.35)	-0.41
B2	(-30.37,-21.21)	-25.24	(-0.50,-0.35)	-0.41
B3	(-30.59,-20.18)	-25.10	(-0.50,-0.33)	-0.41
B4	(-31.59,-22.88)	-27.35	(-0.52,-0.37)	-0.45
B5	(-31.09,-20.11)	-26.64	(-0.51,-0.33)	-0.43
B6	(-30.66,-24.80)	-27.52	(-0.50,-0.40)	-0.45
B7	(-30.64,-22.48)	-26.83	(-0.50,-0.37)	-0.44
B8	(-44.85,-13.15)	-31.58	(-0.73,-0.21)	-0.52
B9	(-30.38,-20.49)	-24.79	(-0.50,-0.33)	-0.40
B10	(-30.74,-19.66)	-24.82	(-0.50,-0.32)	-0.41
B11	(-31.89,-22.72)	-27.27	(-0.52,-0.37)	-0.45
B12	(-31.00,-20.13)	-26.55	(-0.51,-0.33)	-0.43
B13	(-30.76,-24.75)	-27.40	(-0.50,-0.40)	-0.45
B14	(-30.82,-21.70)	-26.74	(-0.50,-0.35)	-0.44
B15	(-44.77,-23.85)	-31.23	(-0.73,-0.39)	-0.51
B16	(-41.53,47.91)	29.57	(-0.68,0.78)	0.48

- Similarly for the wind inclination angle of 30⁰ the average pressure is between [-33.43, 38.20]. The maximum positive and negative pressure values of 38.20 and -33.43, respectively, occur on Face B4 and B16. The range of pressure coefficient Cp lies in the range ϵ [-0.55, 0.62]. The maximum positive and negative values of 0.62 and -0.55 occur on Faces B4 and B16.
- For the wind inclination angle of 60⁰ the average pressure is between [-36.95, 37.58]. The maximum positive and negative pressure values of 37.58 and -36.95, respectively, occur on Face B5 and A1. The range of pressure coefficient Cp lies in the range ϵ [-0.60, 0.61]. The maximum positive and negative values of 0.61 and -0.60 occur on Faces B5 and A1.

Table 6.40: Average Cp value for wind inclination 30, 60, 120 and 150 degrees

Wind Inclination Angle 30				
Faces/Wall	Range of Pressure	Average value of Pressure	Range of Cp	Average Value of Cp
A1	(-46.35,24.99)	-8.03	(-0.76,0.41)	-0.13
A2	(-19.95,21.35)	2.70	(-0.33,0.35)	0.04
A3	(-16.07,22.63)	0.32	(-0.26,0.37)	0.01
A4	(-21.21,11.56)	-7.39	(-0.35,0.19)	-0.12
A5	(-18.95,11.56)	-6.23	(-0.31,0.19)	-0.10
A6	(-24.11,-4.99)	-7.88	(-0.39,-0.08)	-0.13
A7	(-24.11,-4.30)	-8.26	(-0.39,-0.07)	-0.13
A8	(-73.57,13.04)	-19.25	(-1.20,0.21)	-0.31
A9	(-47.30,-17.04)	-26.39	(-0.77,-0.28)	-0.43
A10	(-35.81,-12.93)	-22.76	(-0.58,-0.21)	-0.37
A11	(-42.01,-17.37)	-21.90	(-0.69,-0.28)	-0.36
A12	(-27.76,-16.99)	-21.15	(-0.45,-0.28)	-0.35
A13	(-23.40,-12.68)	-18.80	(-0.38,-0.21)	-0.31
A14	(-22.03,-12.70)	-17.65	(-0.36,-0.21)	-0.29
A15	(-40.05,-12.58)	-21.69	(-0.65,-0.21)	-0.35
A16	(-94.14,49.41)	26.61	(-1.54,0.81)	0.43
B1	(-54.62,-10.15)	-25.58	(-0.89,-0.17)	-0.42
B2	(-41.12,42.17)	24.28	(-0.67,0.69)	0.40
B3	(-55.65,41.39)	29.33	(-0.91,0.68)	0.48
B4	(-50.97,48.02)	38.20	(-0.83,0.78)	0.62
B5	(-47.76,48.19)	38.19	(-0.78,0.79)	0.62
B6	(-39.93,43.52)	31.82	(-0.65,0.71)	0.52
B7	(-39.93,45.59)	26.62	(-0.65,0.74)	0.43
B8	(-61.26,0.75)	-28.11	(-1.00,0.01)	-0.46
B9	(-28.96,-17.10)	-20.40	(-0.47,-0.28)	-0.33
B10	(-30.02,-17.91)	-21.03	(-0.49,-0.29)	-0.34
B11	(-30.15,-16.76)	-19.72	(-0.49,-0.27)	-0.32
B12	(-30.15,-16.91)	-19.87	(-0.49,-0.28)	-0.32
B13	(-27.91,-16.91)	-20.63	(-0.46,-0.28)	-0.34
B14	(-27.43,-18.63)	-21.14	(-0.45,-0.30)	-0.35
B15	(-24.27,-15.92)	-20.02	(-0.40,-0.26)	-0.33
B16	(-59.40,-14.99)	-33.43	(-0.97,-0.24)	-0.55

Wind Inclination Angle 60				
Faces/Wall	Range of Pressure	Average value of Pressure	Range of Cp	Average Value of Cp
A1	(-71.74,30.74)	-36.95	(-1.17,0.50)	-0.60
A2	(-57.98,36.26)	17.50	(-0.95,0.59)	0.29
A3	(-42.67,31.48)	19.44	(-0.70,0.51)	0.32
A4	(-52.04,36.10)	25.11	(-0.85,0.59)	0.41
A5	(-45.65,30.11)	23.37	(-0.75,0.49)	0.38
A6	(-42.08,33.35)	22.51	(-0.69,0.54)	0.37
A7	(-33.30,27.24)	18.68	(-0.54,0.44)	0.30
A8	(-12.16,52.52)	33.06	(-0.20,0.86)	0.54
A9	(-61.44,-26.84)	-31.93	(-1.00,-0.44)	-0.52
A10	(-39.75,-27.66)	-32.01	(-0.65,-0.45)	-0.52
A11	(-38.64,-21.78)	-28.01	(-0.63,-0.36)	-0.46
A12	(-32.97,-15.59)	-27.06	(-0.54,-0.25)	-0.44
A13	(-47.14,-16.12)	-23.71	(-0.77,-0.26)	-0.39
A14	(-33.57,-8.63)	-23.47	(-0.55,-0.14)	-0.38
A15	(-46.32,-0.70)	-20.10	(-0.76,-0.01)	-0.33
A16	(-46.32,34.71)	3.99	(-0.76,0.57)	0.07
B1	(-75.47,2.63)	-29.60	(-1.23,0.04)	-0.48
B2	(-42.25,45.06)	28.96	(-0.69,0.74)	0.47
B3	(-42.22,42.25)	33.71	(-0.69,0.69)	0.55
B4	(-45.01,46.46)	37.44	(-0.73,0.76)	0.61
B5	(-46.63,46.58)	37.58	(-0.76,0.76)	0.61
B6	(-47.13,46.51)	36.34	(-0.77,0.76)	0.59
B7	(-60.55,46.85)	32.21	(-0.99,0.76)	0.53
B8	(-60.63,30.21)	-8.16	(-0.99,0.49)	-0.13
B9	(-31.79,-9.98)	-17.03	(-0.52,-0.16)	-0.28
B10	(-25.66,-10.34)	-16.57	(-0.42,-0.17)	-0.27
B11	(-23.87,-11.63)	-17.71	(-0.39,-0.19)	-0.29
B12	(-23.43,-12.58)	-18.49	(-0.38,-0.21)	-0.30
B13	(-26.17,-13.67)	-20.48	(-0.43,-0.22)	-0.33
B14	(-32.91,-16.13)	-23.83	(-0.54,-0.26)	-0.39
B15	(-30.36,-3.60)	-16.80	(-0.50,-0.06)	-0.27
B16	(-34.49,-6.55)	-17.12	(-0.56,-0.11)	-0.28

Wind Inclination Angle 120				
Faces/Wall	Range of Pressure	Average value of Pressure	Range of Cp	Average Value of Cp
A1	(-81.10,-1.82)	-31.03	(-1.32,-0.03)	-0.51
A2	(-45.93,44.83)	28.68	(-0.75,0.73)	0.47
A3	(-54.10,42.19)	33.46	(-0.88,0.69)	0.55
A4	(-47.83,46.44)	37.23	(-0.78,0.76)	0.61
A5	(-50.23,46.60)	37.30	(-0.82,0.76)	0.61
A6	(-51.69,46.52)	36.10	(-0.84,0.76)	0.59
A7	(-71.00,46.93)	31.40	(-1.16,0.77)	0.51
A8	(-64.88,30.20)	-11.48	(-1.06,0.49)	-0.19
A9	(-42.55,-10.54)	-19.11	(-0.69,-0.17)	-0.31
A10	(-28.60,-10.67)	-18.18	(-0.47,-0.17)	-0.30
A11	(-27.03,-11.33)	-18.90	(-0.44,-0.19)	-0.31
A12	(-28.62,-12.36)	-20.15	(-0.47,-0.20)	-0.33
A13	(-28.91,-9.79)	-18.95	(-0.47,-0.16)	-0.31
A14	(-38.45,-10.56)	-21.65	(-0.63,-0.17)	-0.35
A15	(-34.61,-6.76)	-17.77	(-0.57,-0.11)	-0.29
A16	(-36.79,-14.51)	-22.55	(-0.60,-0.24)	-0.37
B1	(-75.84,29.59)	-38.92	(-1.24,0.48)	-0.64
B2	(-57.17,35.75)	16.96	(-0.93,0.58)	0.28
B3	(-40.69,30.61)	18.94	(-0.66,0.50)	0.31
B4	(-56.00,35.58)	24.62	(-0.91,0.58)	0.40
B5	(-44.02,29.49)	22.83	(-0.72,0.48)	0.37
B6	(-39.93,32.66)	21.87	(-0.65,0.53)	0.36
B7	(-32.44,26.88)	17.95	(-0.53,0.44)	0.29
B8	(-13.58,52.20)	32.68	(-0.22,0.85)	0.53
B9	(-63.10,-26.63)	-33.72	(-1.03,0.43)	-0.55
B10	(-37.55,-26.94)	-32.86	(-0.61,-0.44)	-0.54
B11	(-36.82,-23.50)	-28.78	(-0.60,-0.38)	-0.47
B12	(-40.70,-14.77)	-28.61	(-0.66,-0.24)	-0.47
B13	(-46.86,-7.93)	-24.55	(-0.77,-0.13)	-0.40
B14	(-36.78,5.28)	-21.79	(-0.60,0.09)	-0.36
B15	(-50.00,2.79)	-20.46	(-0.82,0.05)	-0.33
B16	(-50.00,36.54)	4.53	(-0.82,0.60)	0.07

Wind Inclination Angle 150				
Faces/Wall	Range of Pressure	Average value of Pressure	Range of Cp	Average Value of Cp
A1	(-45.98,-9.95)	-24.42	(-0.75,-0.16)	-0.40
A2	(-46.39,41.63)	24.73	(-0.76,0.68)	0.40
A3	(-46.45,39.91)	29.74	(-0.76,0.65)	0.49
A4	(-52.67,48.11)	38.29	(-0.86,0.79)	0.63
A5	(-50.55,48.33)	38.27	(-0.83,0.79)	0.62
A6	(-42.22,43.78)	32.12	(-0.69,0.71)	0.52
A7	(-41.71,45.84)	27.30	(-0.68,0.75)	0.45
A8	(-59.57,2.39)	-25.93	(-0.97,0.04)	-0.42
A9	(-30.10,-17.58)	-19.38	(-0.49,-0.29)	-0.32
A10	(-29.60,-18.28)	-19.87	(-0.48,-0.30)	-0.32
A11	(-30.47,-15.93)	-19.59	(-0.50,-0.26)	-0.32
A12	(-29.58,-16.82)	-20.18	(-0.48,-0.27)	-0.33
A13	(-28.63,-19.28)	-21.04	(-0.47,-0.31)	-0.34
A14	(-28.63,-20.02)	-21.37	(-0.47,-0.33)	-0.35
A15	(-24.62,-16.80)	-19.94	(-0.40,-0.27)	-0.33
A16	(-53.95,-15.26)	-32.02	(-0.88,-0.25)	-0.52
B1	(-41.59,24.63)	-7.28	(-0.68,0.40)	-0.12
B2	(-15.15,22.08)	3.35	(-0.25,0.36)	0.05
B3	(-18.02,24.06)	0.65	(-0.29,0.39)	0.01
B4	(-22.68,10.52)	-7.12	(-0.37,0.17)	-0.12
B5	(-17.48,10.52)	-5.71	(-0.29,0.17)	-0.09
B6	(-21.65,-4.63)	-7.30	(-0.35,-0.08)	-0.12
B7	(-22.43,-4.16)	-7.85	(-0.37,-0.07)	-0.13
B8	(-72.53,19.63)	-19.58	(-1.18,0.32)	-0.32
B9	(-46.18,-17.08)	-26.14	(-0.75,-0.28)	-0.43
B10	(-36.93,-13.09)	-22.63	(-0.60,-0.21)	-0.37
B11	(-42.56,-17.31)	-21.55	(-0.69,-0.28)	-0.35
B12	(-29.31,-17.83)	-20.87	(-0.48,-0.29)	-0.34
B13	(-23.52,-13.25)	-18.71	(-0.38,-0.22)	-0.31
B14	(-21.62,-13.36)	-17.58	(-0.35,-0.22)	-0.29
B15	(-37.82,-12.67)	-21.97	(-0.62,-0.21)	-0.36
B16	(-69.39,49.36)	26.65	(-1.12,0.81)	0.44

- The range of average pressure values for the wind inclination angle of 120° is between [-38.92, 37.30]. The maximum positive and negative pressure values of 37.30 and -38.92, respectively, occur on Face A5 and B1. The range of pressure

coefficient C_p lies in the range ε [-0.64, 0.61]. The maximum positive and negative values of 0.61 and -0.64 occur on Faces A5 and B1.

- For the wind inclination angle of 150° the average pressure is between [-32.02, 38.29]. The maximum positive and negative pressure values of 38.29 and -32.02, respectively, occur on Face A4 and A16. The range of pressure coefficient C_p lies in the range ε [-0.52, 0.63]. The maximum positive and negative values of 0.63 and -0.52 occur on Faces A4 and A16 (See **Table 6.40**).

Summary of the results: The results show that for a wind inclination angle of 120° , the average pressure ranges from -38.92 to 37.30, with maximum positive and negative pressure values occurring on Faces A5 and B1, respectively. The pressure coefficient (C_p) ranges from -0.64 to 0.61, with maximum positive and negative values occurring on Faces A5 and B1 (**Figure 6.5**). Similar trends are observed for other wind inclination angles, with varying ranges of average pressure and C_p .

For example, for a wind inclination angle of 90° , the average pressure ranges from -43.31 to 38.18, with maximum positive and negative pressure values occurring on Faces A6 and B1, respectively. The C_p ranges from -0.71 to 0.62, with maximum positive and negative values occurring on Faces A6 and B1 (See **Table 6.41**).

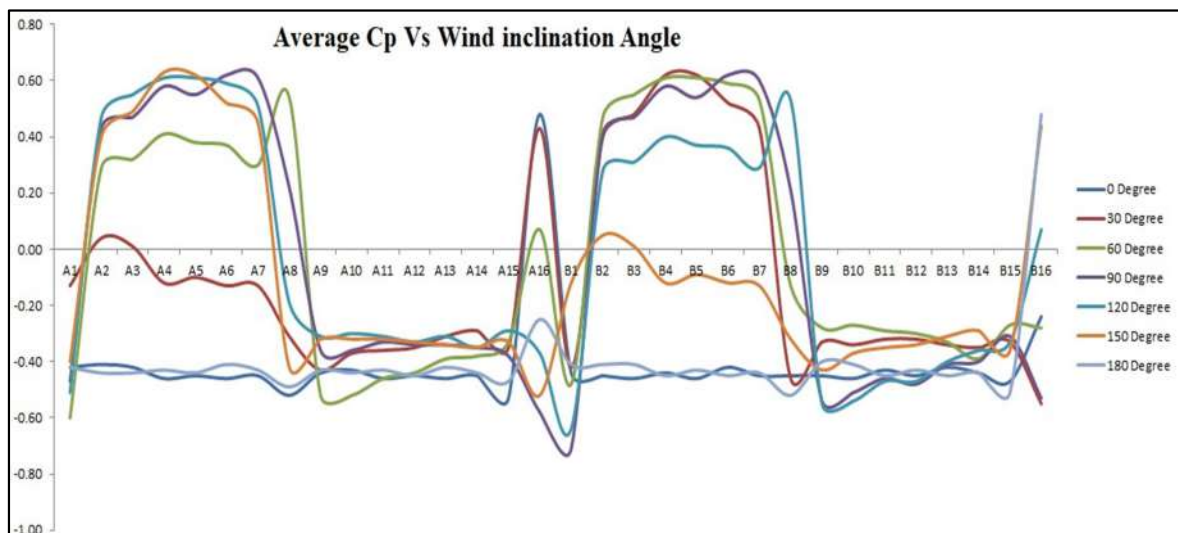


Figure 6.5: Graphical representation of Average C_p value

Table 6.41: Average Cp value for wind inclination 0 to 180 degrees

Faces/Wall	Average value of Cp at wind inclination angle						
	0 Degree	30 Degree	60 Degree	90 Degree	120 Degree	150 Degree	180 Degree
A1	-0.42	-0.13	-0.60	-0.47	-0.51	-0.40	-0.42
A2	-0.41	0.04	0.29	0.43	0.47	0.40	-0.44
A3	-0.42	0.01	0.32	0.47	0.55	0.49	-0.44
A4	-0.46	-0.12	0.41	0.58	0.61	0.63	-0.43
A5	-0.45	-0.10	0.38	0.55	0.61	0.62	-0.44
A6	-0.46	-0.13	0.37	0.62	0.59	0.52	-0.41
A7	-0.45	-0.13	0.30	0.61	0.51	0.45	-0.43
A8	-0.52	-0.31	0.54	0.22	-0.19	-0.42	-0.49
A9	-0.44	-0.43	-0.52	-0.36	-0.31	-0.32	-0.43
A10	-0.43	-0.37	-0.52	-0.36	-0.30	-0.32	-0.44
A11	-0.46	-0.36	-0.46	-0.33	-0.31	-0.32	-0.43
A12	-0.45	-0.35	-0.44	-0.34	-0.33	-0.33	-0.45
A13	-0.46	-0.31	-0.39	-0.34	-0.31	-0.34	-0.42
A14	-0.45	-0.29	-0.38	-0.35	-0.35	-0.35	-0.44
A15	-0.53	-0.35	-0.33	-0.38	-0.29	-0.33	-0.47
A16	0.48	0.43	0.07	-0.58	-0.37	-0.52	-0.25
B1	-0.44	-0.42	-0.48	-0.71	-0.64	-0.12	-0.41
B2	-0.45	0.40	0.47	0.41	0.28	0.05	-0.41
B3	-0.46	0.48	0.55	0.47	0.31	0.01	-0.41
B4	-0.44	0.62	0.61	0.58	0.40	-0.12	-0.45
B5	-0.46	0.62	0.61	0.54	0.37	-0.09	-0.43
B6	-0.42	0.52	0.59	0.62	0.36	-0.12	-0.45
B7	-0.45	0.43	0.53	0.60	0.29	-0.13	-0.44
B8	-0.45	-0.46	-0.13	0.21	0.53	-0.32	-0.52
B9	-0.45	-0.33	-0.28	-0.54	-0.55	-0.43	-0.40
B10	-0.46	-0.34	-0.27	-0.51	-0.54	-0.37	-0.41
B11	-0.43	-0.32	-0.29	-0.46	-0.47	-0.35	-0.45
B12	-0.45	-0.32	-0.30	-0.48	-0.47	-0.34	-0.43
B13	-0.42	-0.34	-0.33	-0.41	-0.40	-0.31	-0.45
B14	-0.44	-0.35	-0.39	-0.40	-0.36	-0.29	-0.44
B15	-0.47	-0.33	-0.27	-0.31	-0.33	-0.36	-0.51
B16	-0.24	-0.55	-0.28	-0.53	0.07	0.44	0.48

6.2 VALIDATION WITH INTERNATIONAL CODES

To validate the simulation results of a square plan shape isolated building model, a simulation study was carried out. The isolated building model had a height of 600 mm and a plan area of 40,000 mm² and was simulated under the current environmental conditions. The square models, A and B, for interference, are shown below in **Figure 6.6**. The simulation results were then compared with various international codes.

The graphical representation shows the variation of Cp for a square model when wind inclination is 0 and 90 degrees (**Figure 6.7**). For wind inclination 0 degree, the windward sides will be A1, and for 90 degrees, it will be Face A2 and B2. The leeward side will be Face A4 and B4 for 0 and 90 degree wind inclination, respectively. Pressure and Cp

variation on the faces of square model is shown in (Table 6.42), which is validated against international codes (Table 6.43).

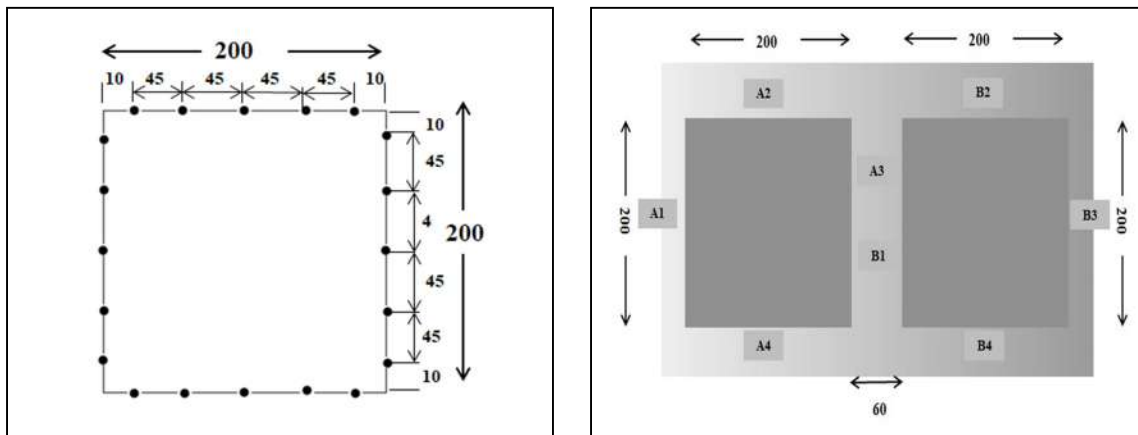


Figure 6.6: Square Plan Shape Model for validation and Nomenclature for the Interference model

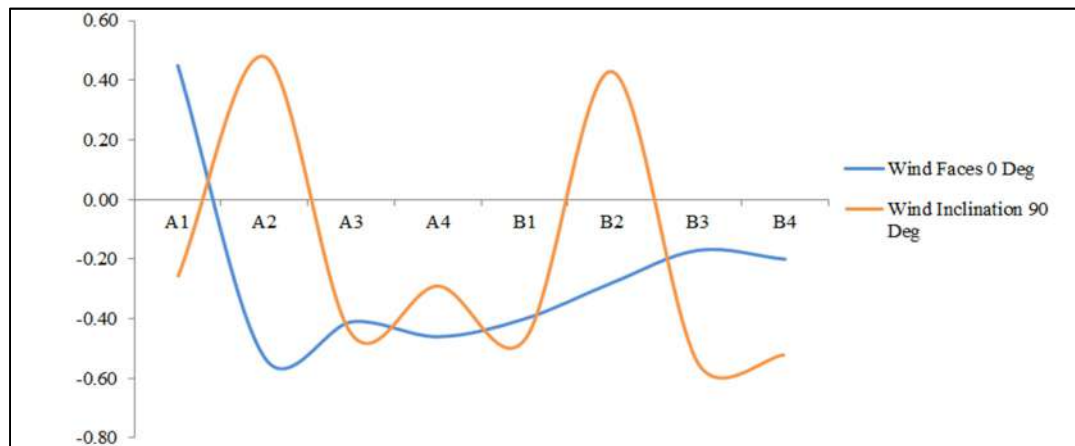


Figure 6.7: Graphical representation of the variation of Cp for Square Model Interference

Table 6.42: Pressure and Cp variation on the faces of Square Model

Faces	0 Degree wind inclination				90 Degree wind inclination			
	Range of Pressure	Avg. Pressure	Range of Cp	Avg. Cp	Range of Pressure	Avg. Pressure	Range of Cp	Avg. Cp
A1	(-49.44,48.74)	27.58	(-0.81,0.80)	0.45	(-44.89,-8.71)	-15.91	(-0.73,-0.14)	-0.26
A2	(-75.62,-15.96)	-32.26	(-1.23,-0.26)	-0.53	(-36.10,47.53)	29.56	(-0.59,0.78)	0.48
A3	(-40.76,-17.92)	-24.84	(-0.67,-0.29)	-0.41	(-76.50,-3.81)	-27.30	(-1.25,-0.06)	-0.45
A4	(-61.13,-17.15)	-28.30	(-1.00,-0.28)	-0.46	(-23.36,-8.71)	-17.69	(-0.38,-0.14)	-0.29
B1	(-34.09,-3.53)	-24.80	(-0.56,-0.06)	-0.40	(-82.56,-2.53)	-29.05	(-1.35,-0.04)	-0.47
B2	(-31.67,-3.96)	-17.30	(-0.52,-0.06)	-0.28	(-60.49,47.60)	26.28	(-0.99,0.78)	0.43
B3	(-35.16,-6.47)	-10.20	(-0.57,-0.11)	-0.17	(-63.08,-25.36)	-33.98	(-1.03,-0.41)	-0.55
B4	(-38.56,-3.73)	-16.89	(-0.55,-0.09)	-0.20	(-82.56,47.60)	-15.26	(-1.06,-0.32)	-0.52

Table 6.43: Comparison of pressure coefficient (C_p) on the Square plan shape tall building

International code	Wind Angle	Wind-ward Side	Lee-ward Side	Side walls
Simulation results	0°	0.45	-0.41	-0.50
	90°	0.48	-0.52	-0.47
CFD Sanyal and Dalui (2020)	0°	0.8	-0.5	-0.7
	90°	0.8	-0.5	-0.7
Experimental Raj (2015)	0°	0.71	-0.67	-0.41
	90°	0.73	-0.66	-0.42
IS 875 (PART 3): 2015	0°	0.8	-0.25	-0.8
	90°	0.8	-0.25	-0.8
AS/NZS:11700.2:2002	0°	0.8	-0.5	-0.65
	90°	0.8	-0.5	-0.65
EN1991-1-4:2005	0°	0.8	-0.55	-0.8
	90°	0.8	-0.55	-0.8
BS6399-2:1997	0°	0.76	-0.5	-0.8
	90°	0.76	-0.5	-0.8
GB 50009-2001	0°	0.8	-0.5	-0.7
	90°	0.8	-0.5	-0.7

6.3 INTERFERENCE FACTOR

An interference factor is a crucial tool used in this research paper to assess the impact of obstructing buildings on tall buildings' performance in CFD simulations. This factor indicates the severity of the obstruction and is calculated by comparing the pressure distribution or coefficient of pressure between the principal object and interfering objects. To evaluate the interference factor, the entire surface of the principal object is considered, taking into account both obstructed and unobstructed flow cases. The maximum and minimum coefficient of pressure on isolated and interference of the models are shown in **Table 6.44** for 0 and 90 degrees of wind inclination.

Table 6.44: Maximum and minimum C_p at face for different interference conditions

Model Description	Interference condition	Maximum C_p	Minimum C_p
Isolated Square plan	0°	0.63	-0.53
	90°	0.67	-0.53
Square Interference	0°	0.45	-0.53
	90°	0.48	-0.55
Isolated Fish plan	0°	0.98	-0.71
	180°	0.81	-0.70
Back to Back	0°	0.58	-0.39
	180°	0.58	-0.57
Back to Front	0°	0.58	-0.48
	180°	0.50	-0.44
Front to Back	0°	0.50	-0.46
	180°	0.58	-0.46
Front to Front	0°	0.48	-0.53
	180°	0.48	-0.52

The interference factor is then used to analyse the face pressure variation on the instrumented tall building, providing valuable insights into the building's safety and comfort for occupants. Overall, the interference factor is an essential tool for understanding the complex interactions between tall buildings and their surroundings in urban areas, enabling informed decisions regarding the design and placement of tall buildings in areas with high-rise buildings or complex geometries. Eq. (12) gives the interference factor for selected models at 0 and 180-degree wind incidence.

$$\text{Interference factor (IF}_p) = \frac{C_{pi} \text{ with interfering building}}{C_{pi} \text{ without interfering building}} \quad \text{Eq. (12)}$$

The interference factor is a dimensionless quantity that represents the severity of the impact of obstructing objects on the performance of a principal object, such as a tall building, in a fluid flow simulation. The value of the interference factor ranges from -1 to 1, with a value of zero indicating no interference. Positive values indicate that the obstruction is causing a pressure increase on the surface of the principal object, while negative values indicate a pressure decrease. It is important to note that the interference factor cannot be greater than one or less than -1, as such values are not physically meaningful. (See **Table 6.45**)

Table 6.45: Interference factor for Square and Fish Shape Model

Interference Factor			
Model Description	Wind Angle	For Max Cp	For Min. Cp
Square Model	0 degree	0.71	1
	90 degree	0.62	0.41
Back to Back Interference	0 degree	0.59	0.55
	180 degree	0.72	0.81
Back to Front Interference	0 degree	0.59	0.68
	180 degree	0.62	0.63
Front to Back Interference	0 degree	0.51	0.65
	180 degree	0.72	0.66
Front to Front Interference	0 degree	0.49	0.75
	180 degree	0.59	0.74

6.4 VELOCITY STREAMLINES

The analysis of airflow patterns around buildings is an essential aspect of designing energy-efficient, comfortable, and safe buildings, as well as evaluating the impact of wind loads on building structures. Velocity lines are a valuable tool in this regard, enabling the identification of areas of high or low velocity and recirculation zones within the flow field. Such information is critical for designing buildings that are optimized for occupant comfort and energy efficiency while also ensuring structural safety. The utilization of velocity lines can aid in the identification of potential issues with airflow patterns, such as turbulent flow, and assist in the development of effective solutions to address such problems. Therefore, the use of velocity lines in analysing airflow patterns around buildings is an important aspect of modern building design and engineering.

6.5 HORIZONTAL STREAMLINES

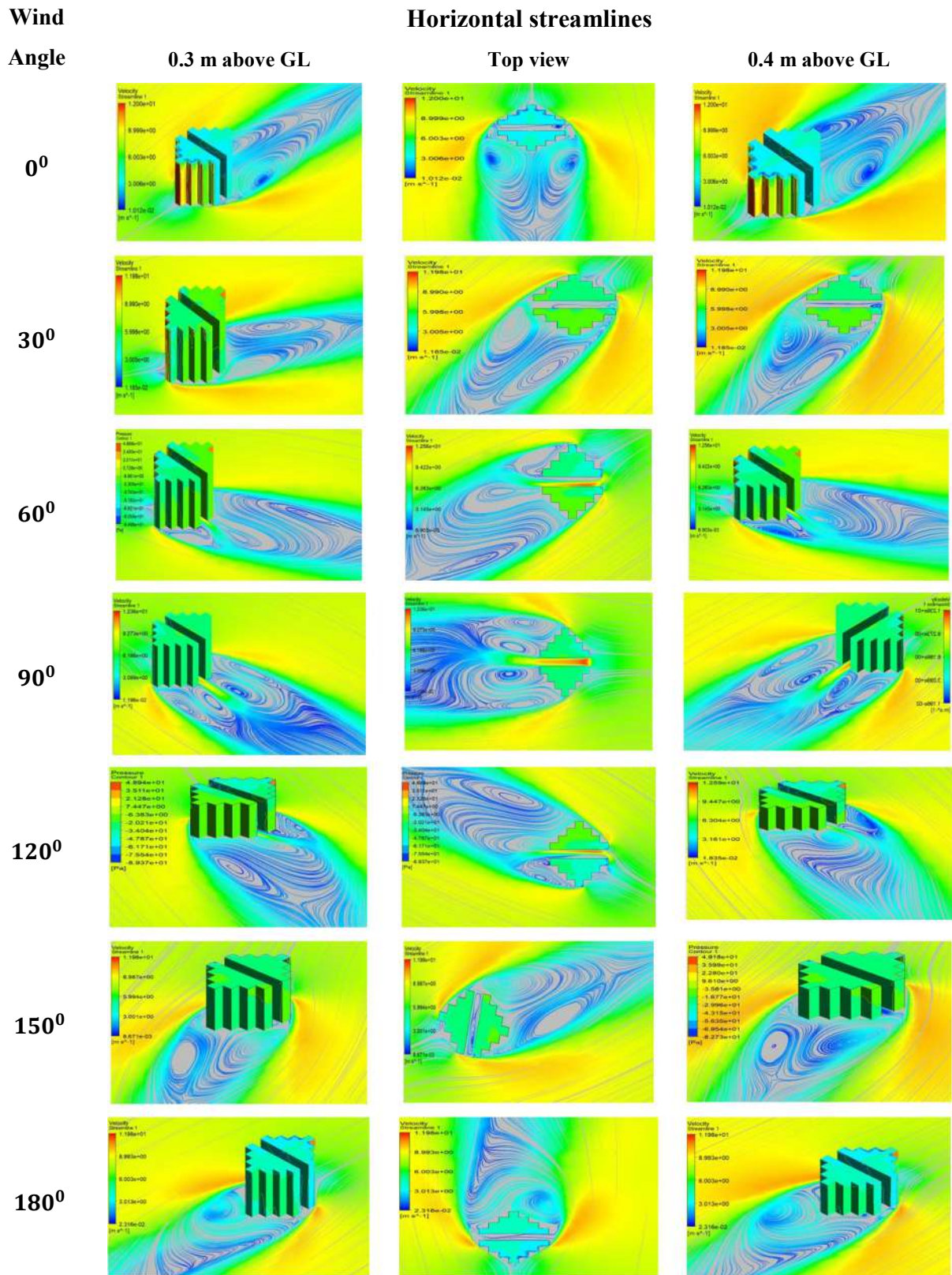
Horizontal streamlines are used to represent the flow of air along a horizontal plane, and they can be used to identify areas of high and low pressure on the surface of an object. This information can be used to optimize the design of the models by altering their shape, size, or surface texture to reduce areas of high pressure and increase areas of low pressure. Vertical and horizontal streamlines are listed below figures for incident angles 0° to 180° at an interval for 30° . The following conclusions are drawn from the horizontal streamlines obtained.

6.5.1 Back-to-Back Interference Condition

- Case 1: When wind Incidence angle is 0°

At an incidence angle of 0 degrees (**Table 6.46**), two major vortices have been observed to form on the face at the leeward side of Model B, some distance away from the windward faces. In addition, a minor vortex has been observed to form between Model A and Model B. At 0.4m above ground level, the recirculation zones tend to shift away from the sides of the building and become more centralized and dense on the leeward side. This can result in increased turbulence and wind loads.

Table 6.46: Horizontal velocity streamlines for Back to back interference, for wind angle 0 to 180



- Case 2: When the wind Incidence angle is 60°

At a 60 degree (**Table 6.46**), incidence angle, wind hitting the A3 and A8 faces of a model creates a flow field with areas of high and low pressure, characterized by the formation of a major vortex and two minor vortices. A high-pressure zone is seen near face B16. At 0.4m above ground level, the vortex becomes more symmetrical due to less interference from the model's geometry, resulting in a more organized flow pattern.

- Case 3: When wind Incidence angle is 120°

At 120 degree (**Table 6.46**), incidence, wind hitting B3 and B8 faces a complex flow field with one major vortex and three minor vortices due to interactions between wind and the model's geometry. A high-pressure zone is observed near face A16 due to compressed air caused by wind flow around the model's shape. Vortices near the leeward face near Model A and between the two models are due to flow around edges and corners. At 0.4m above ground level, the vortex becomes more pronounced and symmetrical, with denser and uniform streamlines, indicating less turbulence and lower energy loss, desirable for wind-sensitive structures.

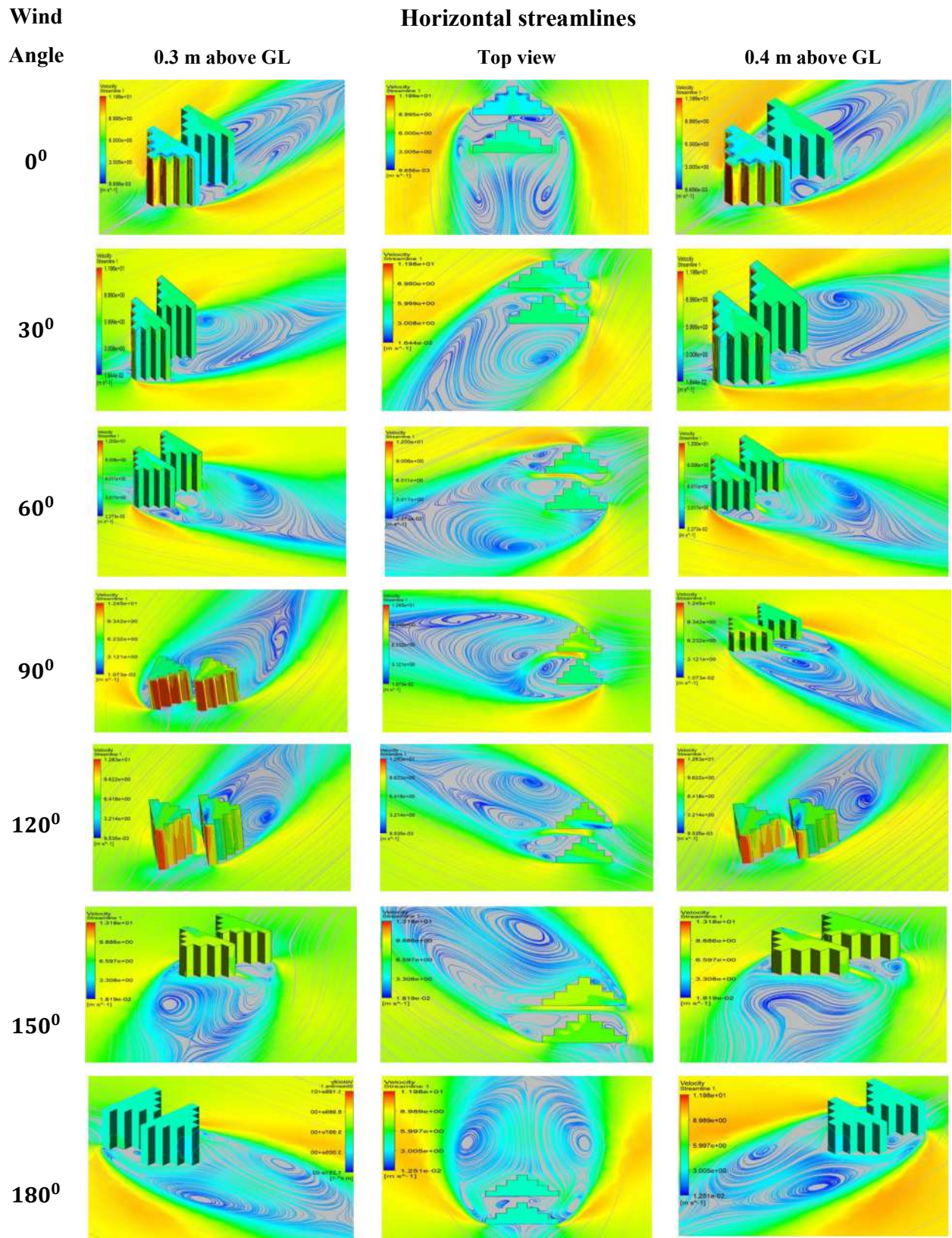
- Case 4: When the wind Incidence angle is 180°

At an incidence of 180 degrees, the results showed that wind striking the B1 face of Model B caused the air to deflect towards the edges of the model, while a small amount of air passed through the gap between the two models (see **Table 6.46**). The flow field was characterized by the formation of a major vortex on the leeward face of Model A, located near Model B. At the height of 0.4m above ground level, the vortex became more pronounced near the leeward face and weaker at the gap between the models. The streamlines throughout the flow field became denser and symmetrical, indicating a uniform flow pattern.

6.5.2 Back to Front Interference Condition

- Case 1: When wind Incidence angle is 60°

Table 6.47: Horizontal velocity streamlines for Back to front interference, for wind angle 0 to 180



At an incidence angle of 60 degrees (**Table 6.47**), wind flow impacted the A3 and A8 faces, causing air to deflect towards the leeward side of the model while creating a flow passage between the two models. The resulting flow field exhibited the formation of a primary vortex at a considerable distance from Model B, along with three minor vortices near Model A and the gap between the models.

At a height of 0.4m above the ground level, the vortex near the leeward face became more pronounced, while the density of the vortex at the gap between the models increased. This led to the formation of denser and symmetrical streamlines throughout the flow field, indicating a uniform flow pattern.

- Case 2: When the wind Incidence angle is 120°

At an incidence angle of 120 degrees (**Table 6.47**), one major vortex has been observed to form on the face at the leeward side of Model B. In addition, two minor vortices have been observed to form near the gap between Model A and Model B. At a height of 0.4m above the ground level, the vortex near the leeward face became more pronounced, while the density of the vortex at the gap between the models increased.

- Case 3: When wind Incidence angle is 180°

At an incidence angle of 180 degrees (See **Table 6.47**), two major vortices have been observed to form on the face at the leeward side of Model A. In addition, two minor vortices have been observed to form near the gap between Model A and Model B. As building height increases, recirculation zones tend to shift towards the leeward side and become more centralized and denser, potentially leading to increased turbulence and wind loads.

The study analysed the flow patterns and vortex formation at different incidence angles of wind on two building models (Model A and Model B) placed in proximity to each other. The study also noted that the recirculation zones tended to shift towards the leeward side and become more centralized and denser as the building height increased, potentially leading to increased turbulence and wind loads.

6.5.3 Front-to-Back Interference Condition

- Case 1: When wind Incidence angle is 60°

The study found that wind hitting a building at a 60 degree (**Table 6.48**) angle creates vortices and areas of high and low pressure, with two major vortices on the leeward side of Model B and two minor vortices near Model A. These findings are consistent with previous studies of complex geometries, where vortices are common due to corners and edges.

- Case 2: When the wind Incidence angle is 120°

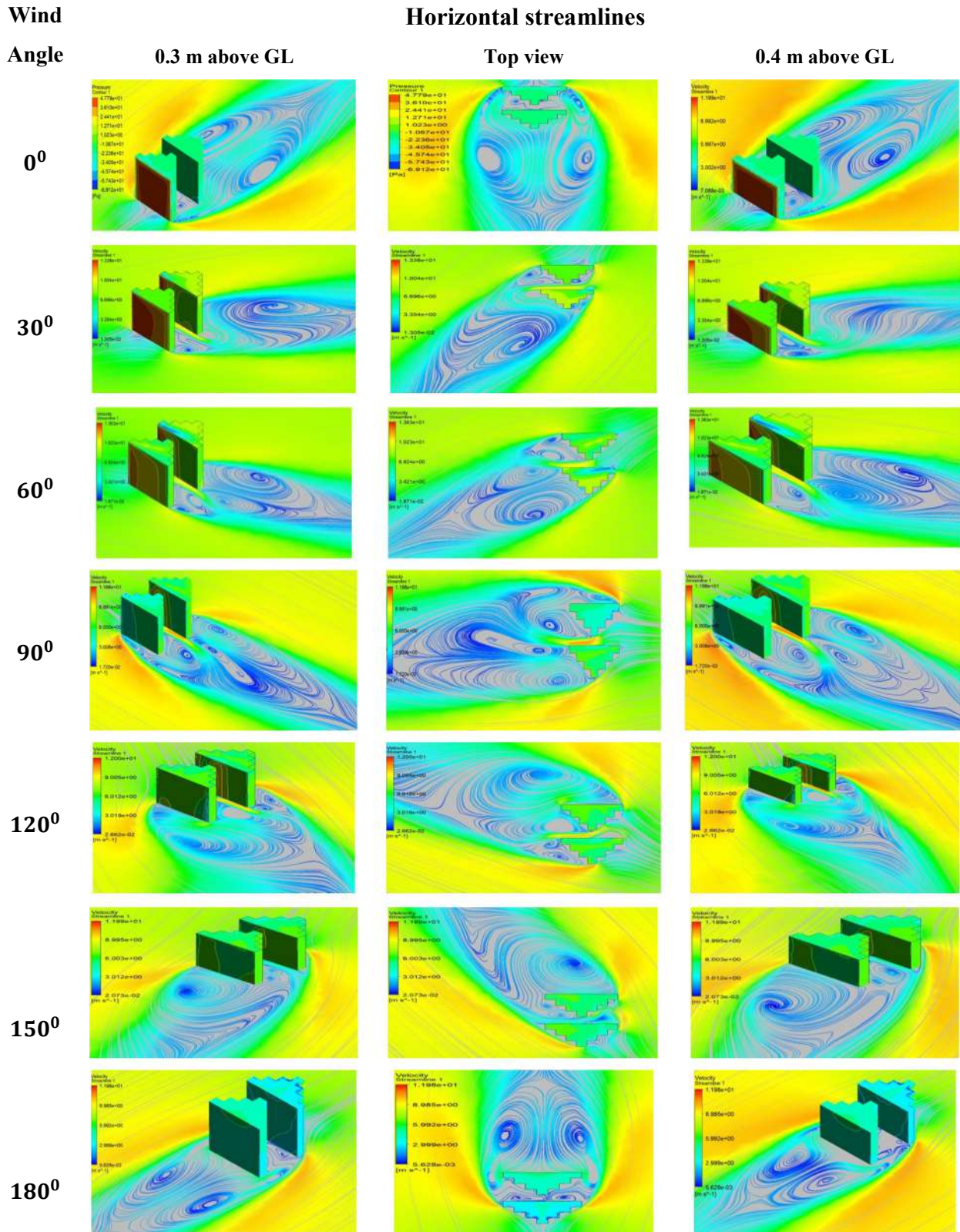
It appears that the formation of vortices and areas of high and low pressure is more complex than previously described. In addition to the two major vortices on the leeward side of Model A, there are also two minor vortices near the faces B9 and B15 of Model B. This suggests that the geometry of both the building and the surrounding structures can have a significant impact on the flow field. Furthermore, the increased density of the vortex at the gap between the models indicates that this area experienced higher levels of turbulence, which could have implications for the structural integrity of nearby buildings (See **Table 6.48**).

- Case 3: When wind Incidence angle is 180°

The virtual wind tunnel experiments revealed that when the wind strikes Face B1 of the Model, it deflects towards the corner of the building, and some air passes through the gaps between the building and surrounding structures (**Table 6.48**). As a result, two major vortices form on the leeward side of the building, while two minor vortices develop near the gap between model A and model B.

We also observed that the vortex near the leeward face becomes more pronounced at a height of 0.4m above the ground level, indicating that the flow field is more intense at this height. Additionally, the density of the vortex at the gap between the models increases, suggesting that this area experiences higher levels of turbulence.

Table 6.48: Horizontal velocity streamlines for Front to back interference, for wind angle 0 to 180



6.5.4 Front-to-Front Interference Condition

- Case 1: When wind Incidence angle is 60°

When wind strikes a building at a 60 degree (**Table 6.49**) angle, it creates a distinct flow field that includes vortices and areas of varying pressure. As the air is deflected by the building, it passes through the gaps between the structures and creates pockets of high pressure, visible in the figure as a densely coloured red area. On the leeward side of model A and model B, this leads to the formation of two significant vortices. The study also found that the vortex near the leeward face of the building is particularly pronounced at a height of 0.4m above the ground level, indicating that the flow field is more intense at this height. Furthermore, the vortex density at the gap between the models increases, and a minor vortex forms near this area, indicating that there is higher turbulence present in this region.

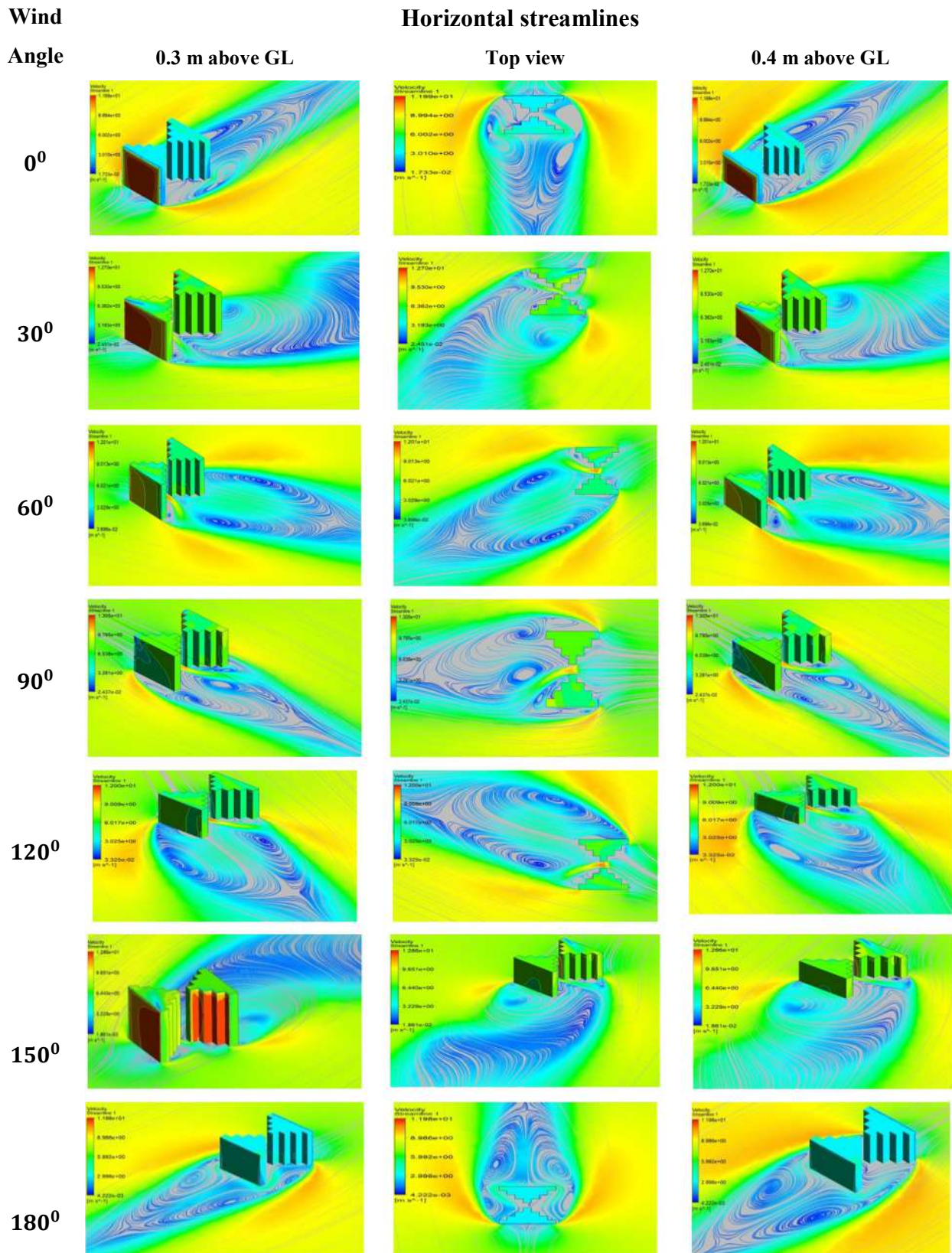
- Case 2: When the wind Incidence angle is 120°

When wind strikes a building at an angle of 120 degrees (**Table 6.49**) the resulting flow field is characterized by the formation of two significant vortices near the windward area of both models. As the wind is deflected by the buildings, the air passes through the gaps between the structures, resulting in the formation of high and low-pressure areas. At a height of 0.4 m above the ground level, the streamlines become denser, suggesting that the flow field is more intense at this height. In addition to the two major vortices, the study also found that an additional vortex is formed near the gap of both models.

- Case 3: When wind Incidence angle is 180° .

When wind strikes a building at an angle of 180 degrees (**Table 6.49**), it creates a complex flow field that is characterized by the formation of two major vortices in the leeward area of the model and two minor vortices near the gaps between the structures. The presence of buildings deflects the wind, causing it to pass through the edges rather than the gaps between the structures. This results in the formation of high and low-pressure areas near the edges of the structures, which can have significant effects on the overall flow field.

Table 6.49: Horizontal velocity streamlines for Front to front interference, for wind angle 0 to 180



6.6 VERTICAL STREAMLINE

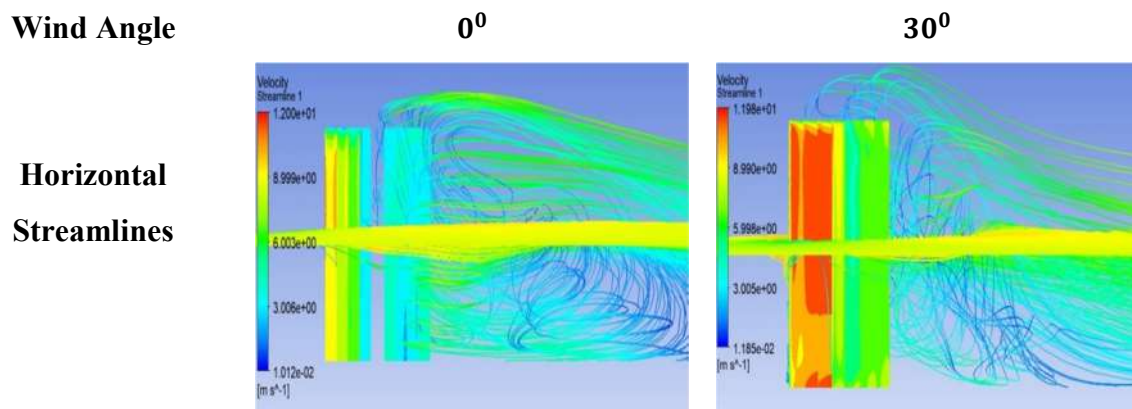
Vertical streamlines are an essential tool in fluid dynamics that helps visualize and understand complex flows in three dimensions. They represent the path that a fluid particle takes as it moves vertically through a fluid medium. By tracing the path of a vertical streamline from the ground up to the height of the building, we can observe how the air is affected by the presence of the structure and how it interacts with the surrounding flow. In this paper, we will use CFD simulations to study the interference between two fish-shaped structures and analyse the path of vertical streamlines around the structures.

6.6.1 Back-to-Back Interference Condition

The behaviour of wind around buildings is highly influenced by the angle at which it strikes the building. When the wind hits the building perpendicularly (0 degrees), the top of the building tends to experience smoother airflow, while the middle section may experience turbulence and pressure fluctuations due to the formation of large vortices.

However, when the wind strikes the building at other angles, such as 120, 30, 60, 90, 150, and 180 degrees **Table 6.50**, the airflow patterns can vary significantly, which can impact the building's design and performance. Therefore, understanding the impact of wind incidence angles on building aerodynamics is crucial for optimizing building design and ensuring occupant comfort and safety.

Table 6.50: Vertical velocity streamlines for Back to back interference for Wind incidence angle 0 to 180

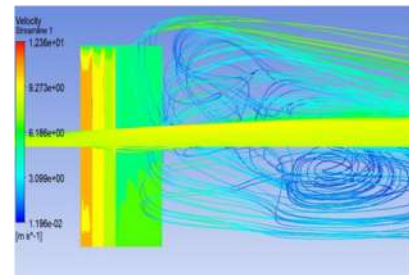
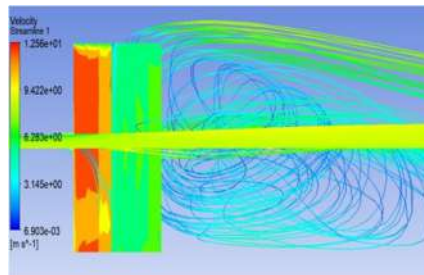


Wind Angle

60°

90°

**Horizontal
Streamlines**

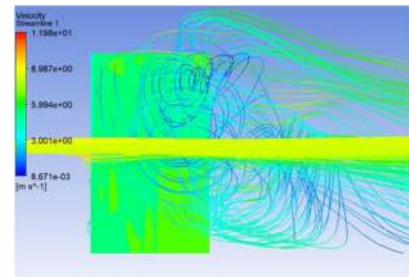
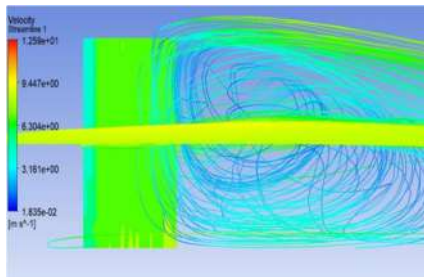


Wind Angle

120°

150°

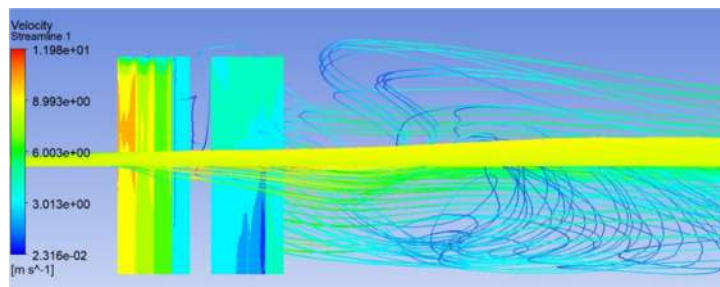
**Horizontal
Streamlines**



Wind Angle

180°

**Horizontal
Streamlines**



When the wind is blowing directly parallel to the face of a building, at 0° incidence, the flow of air can vary across different sections of the building. Research suggests that the airflow around the top of the building is smoother and less turbulent than at the midsection. This is because the wind is flowing over the top of the building, creating a "wind shadow" on the leeward face, which diverts the wind away from that area, leading to less congestion and turbulence.

However, at the mid-section, the wind is hitting the building more directly, and a large vortices formation can be seen at the bottom of the building. This can create more turbulence and kinetic energy in the airflow, leading to a more complex pressure distribution on the building's surface. The larger pressure fluctuations can result in larger

lift and drag forces on the building, which can have significant implications for the structural integrity and energy efficiency of the building.

Therefore, understanding the flow of wind around buildings is crucial for architects and engineers to design buildings that can withstand wind loads and maintain energy efficiency. By accounting for the effects of wind turbulence and pressure fluctuations, buildings can be designed to optimize airflow and reduce energy consumption, making them more sustainable and cost-effective also in the long run.

When wind hits the building at 120 degrees, a similar vertical streamline can be observed, but with some differences in the airflow patterns. Unlike the 0-degree incidence, there is less congestion near the top of the building, and a major vortex formation or swirling air can be seen near the building model. The swirling motion creates turbulence, leading to pressure fluctuations that can result in larger lift and drag forces on the building. Interestingly, the horizontal streamlines show that a significant amount of air passes through the gap between the building and the ground. However, in the vertical streamlines, there is not much significant air congestion or vortex formation observed. This could be due to the nature of the wind flow and the building's geometry, which can affect the airflow patterns in different ways.

Similarly, for the other wind angles, such as 30 degrees, the centre and bottom experience very little air influence with low air density velocity streamline. At 60 degrees, there is also very little air congestion at the top and bottom, but there is swirling air some distance away from the model. At 90 degrees, there is very little air congestion, but there is high-density air swirling some distance away from the model.

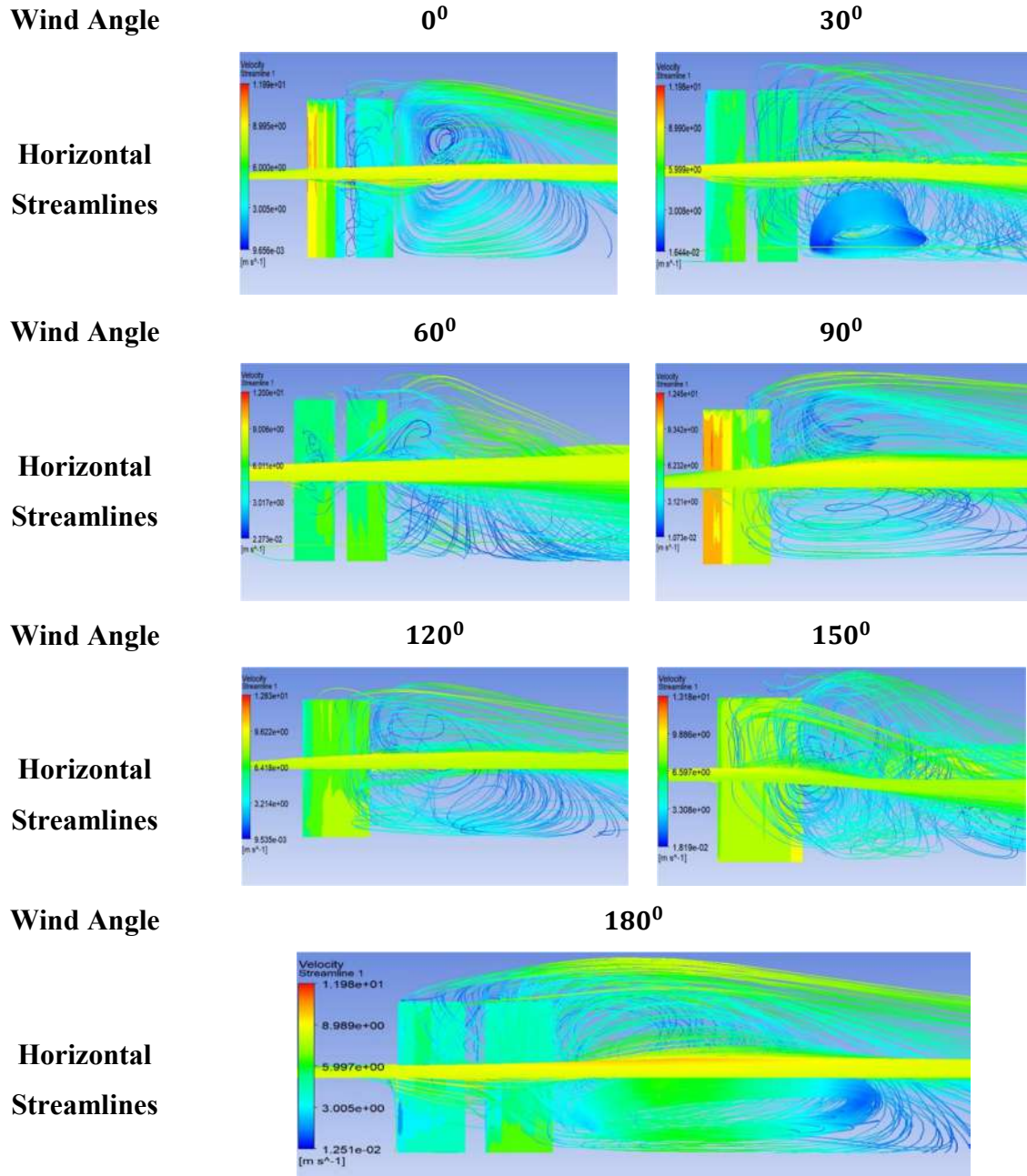
At 150 degrees, there is very little air congestion at the top and bottom, but there is a high radius swirling near the building that affects the model as the streamline crosses over the building. At 180 degrees, it is very similar to 0 degrees, with very little air density at the top and ground level.

However, the streamline passes through the edges and meets a fair distance away from the building, and less air passes towards the ground level. The implications of these findings

suggest that the angle of the model plays a critical role in the airflow and air density around the building. This can have significant implications for the design and performance of the building.

6.6.2 Back to Front Interference Condition

Table 6.51: Vertical velocity streamlines for Back to front interference for Wind incidence angle 0 to 180



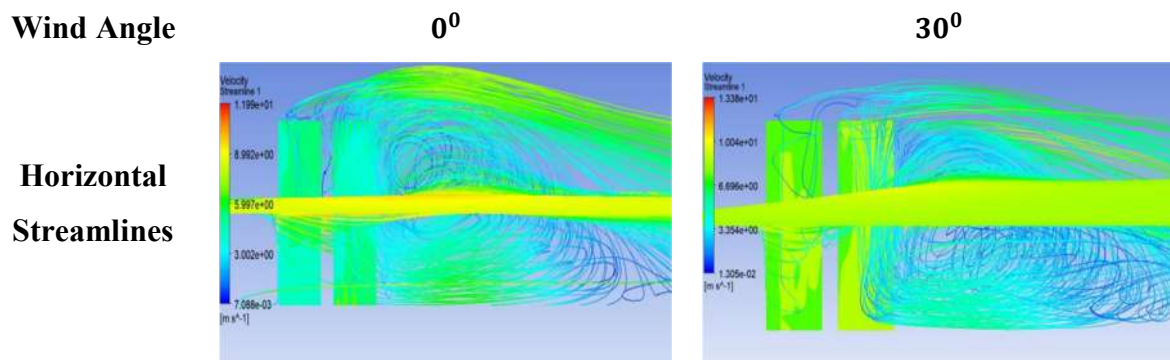
The results of the research indicate that wind inclination angle greatly affects the airflow and air density around the building model. At 60 degrees (**Table 6.51**), the research findings suggest that the middle part of the building experiences significant air congestion and density, while the top of the building is relatively unaffected by the wind. Furthermore, the air density is lower at the bottom of the building. These observations are attributed to the wind's interaction with the building and its shape, which creates a "wind shadow" near the top of the building and causes the wind to be deflected around it.

Similarly, at 150 degrees wind inclination, the research findings indicate a similar pattern of air congestion and density, with significant air congestion observed at the middle of the building and less air density at the top and bottom of the building. However, the air density is slightly higher compared to the results observed at 60 degrees.

6.6.3 Front-to-Back Interference Condition

The research findings reveal that at a wind inclination of 30 degrees, there is a noticeable formation of a large vortex at the bottom level of the building model, indicating a significant transfer of air towards the bottom. Furthermore, the streamlined analysis indicates that the air density is less congested at the top of the building, implying a smoother and less turbulent airflow. Similarly, at an inclination of 120 degrees (**Table 6.52**), the vertical streamline analysis shows the formation of a high-density swirling air near the model. The results further suggest that the streamlines at ground level are less congested, which indicates a smoother airflow around the building model.

Table 6.52: Vertical velocity streamlines for Front to back interference for Wind incidence angle 0 to 180

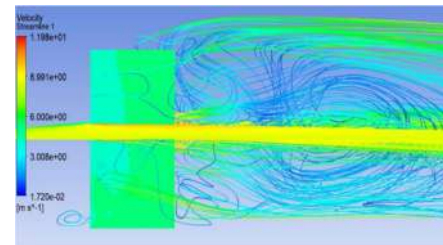
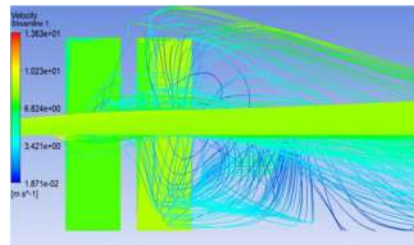


Wind Angle

60°

90°

Horizontal
Streamlines

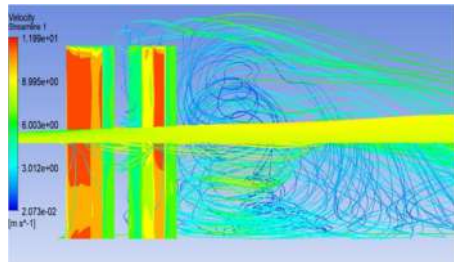
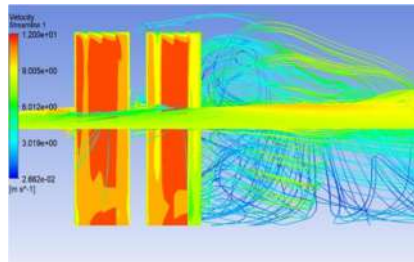


Wind Angle

120°

150°

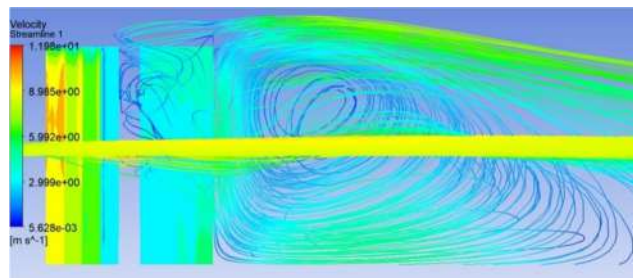
Horizontal
Streamlines



Wind Angle

180°

Horizontal
Streamlines



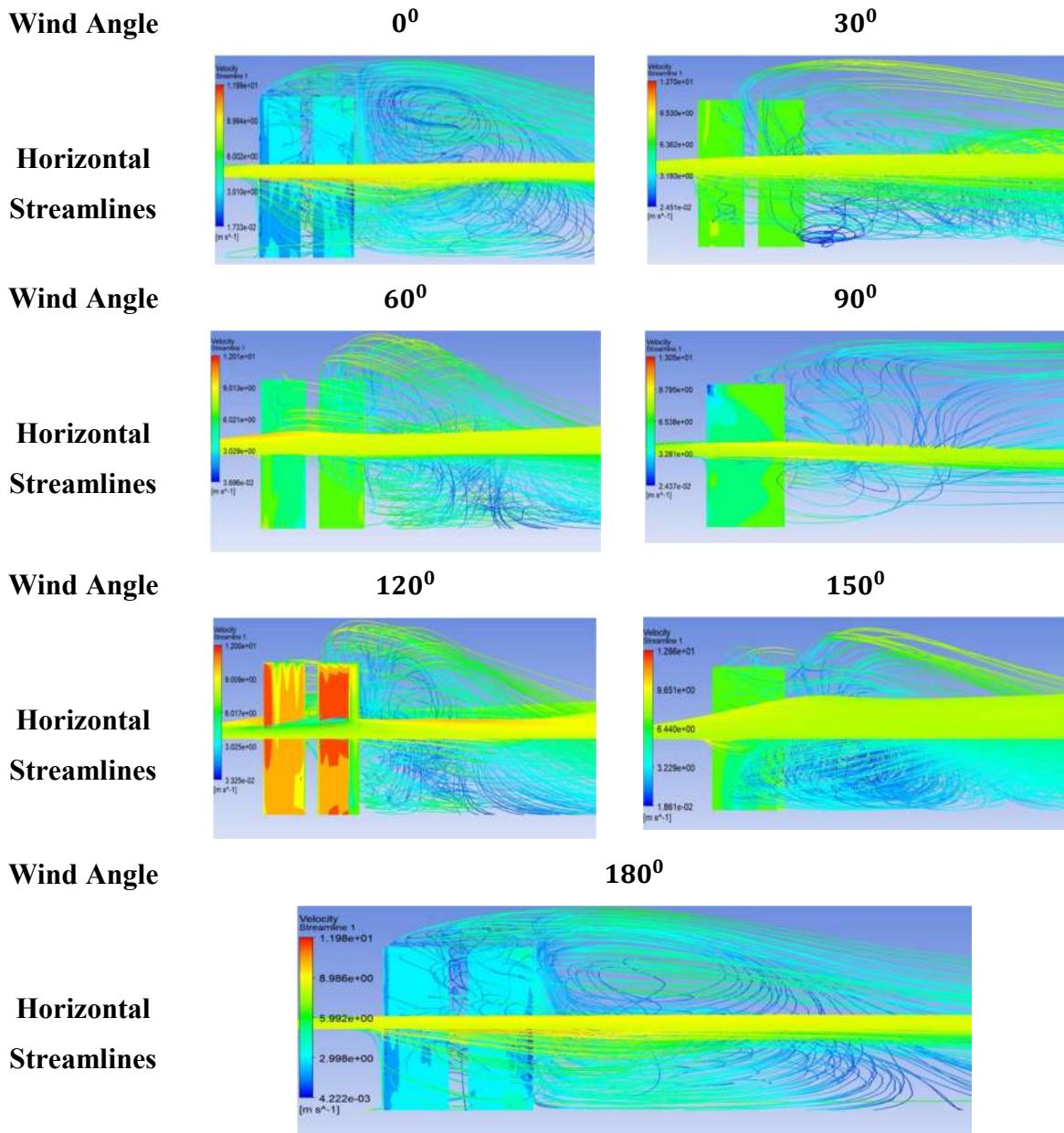
6.6.4 Front-to-Front Interference Condition

The wind flow behaviour around buildings is strongly influenced by the angle at which it approaches the building. In particular, the presence of vertical streamlines at both the top and bottom levels of the building model when subjected to a 60 degree (**Table 6.53**) wind incidence angle indicates that the effect of wind on the building varies depending on the location and angle of the building. These streamlines suggest that the wind flow is smoother at the top and bottom sections of the building, while the middle section may experience greater turbulence and pressure fluctuations due to the formation of large vortices.

Likewise, the observation of higher air congestion at the ground level when subjected to a 150-degree wind incidence angle emphasizes the importance of considering the angle of

incidence in building design and performance. This congestion can create areas of low pressure behind the building, which can lead to increased wind speeds and turbulence, potentially impacting the stability and comfort of the building's occupants. Therefore, it is essential to carefully consider the impact of wind incidence angles when designing buildings to ensure that they can withstand the expected wind conditions and provide optimal occupant comfort and safety.

Table 6.53: Vertical velocity streamlines for Front to front interference for Wind incidence angle 0 to 180



CHAPTER 7 - RESULTS AND ANALYSIS

CFD (Computational Fluid Dynamics) simulation results provide a detailed analysis of fluid flow behaviour around a body or a system. The results of a CFD simulation include data on pressure, velocity, temperature, and other fluid properties. The simulation results can be visualized in the form of contour plots, vector plots, streamlines, and other graphical representations. CFD simulations are used in a wide range of fields, including aerospace, automotive, energy, and civil engineering. For example, in building design, CFD simulation results can be used to analyse the wind loading on the building and optimize its design for better performance and safety. In automotive design, CFD simulation results can be used to analyse the aerodynamics of the car and optimize its design for improved fuel efficiency and performance.

Interpreting CFD simulation results requires a good understanding of the physics of fluid flow and the numerical methods used to solve the governing equations. It is important to validate the simulation results against experimental data to ensure their accuracy and reliability. CFD simulation results are also affected by the quality of the mesh used for the simulation, the choice of boundary conditions, and the accuracy of the physical models used to represent the fluid flow behaviour. Therefore, a thorough understanding of the underlying physics and numerical methods is essential for obtaining accurate and reliable CFD simulation results.

7.1 COMPARISON OF THE RESULTS FROM ISOLATED AND INTERFERENCE STUDY SIMULATION

The results of the isolated building simulation and the interference study simulation showed significant differences in the flow characteristics and forces acting on the building.

In the isolated building simulation, the flow was relatively undisturbed, resulting in a smooth and symmetrical flow around the building. The pressure distribution was also uniform across the building surface, with low-pressure regions on the windward side and high-pressure regions on the leeward side.

However, in the interference study simulation, the flow was highly distorted due to the presence of the adjacent buildings. The flow separation occurred on the windward side of the building, resulting in large vortices and turbulent flow patterns. The pressure distribution was also highly non-uniform, with high-pressure regions on the side of the building facing the adjacent buildings and low-pressure regions on the leeward side.

The forces acting on the building also showed significant differences between the two simulations. In the isolated building simulation, the forces were relatively small, with the maximum forces occurring on the roof of the building. However, in the interference study simulation, the forces were significantly larger, with the maximum forces occurring on the side of the building facing the adjacent buildings.

These results highlight the importance of considering the surrounding environment in the analysis and design of buildings, especially in urban areas with high building densities. The interference of adjacent buildings can significantly affect the flow characteristics and forces acting on a building, leading to potential structural issues and safety concerns.

7.2 DISCUSSION OF THE IMPLICATIONS OF THE FINDINGS ON BUILDING DESIGN

Based on the results obtained from the CFD simulations, several implications can be drawn that have practical significance for building design.

Firstly, it was found that the interference effects between adjacent buildings can have a significant impact on the flow patterns around the buildings. This implies that the placement of buildings in close proximity to each other should be carefully considered in order to minimize the adverse effects of the interference. Building spacing, height, and orientation should be optimized to minimize turbulence and maximize energy efficiency.

Secondly, the results suggest that the shape of the building can have a significant impact on the flow patterns around the building. Buildings with streamlined shapes tend to experience less drag and turbulence compared to buildings with complex shapes. Therefore, building designers should consider incorporating streamlined shapes and features that can optimize the flow patterns around the building.

Thirdly, the findings highlight the importance of considering the wind direction and velocity when designing buildings. Wind loads and flow patterns are highly dependent on the direction and velocity of the wind. Therefore, designers should conduct a thorough analysis of the wind conditions in the area where the building is to be constructed, and optimize the building design accordingly.

In conclusion, the implications of the findings from the study suggest that building design should be approached in a holistic manner that takes into consideration various factors such as building placement, shape, and wind conditions. By optimizing these factors, building designers can achieve buildings that are more energy-efficient, aesthetically pleasing, and functional.

CHAPTER 8 - CONCLUSION AND RECOMMENDATIONS

The present study analysed the aerodynamic behaviour of a building using CFD simulations. Two simulation scenarios were considered: an isolated building and a building surrounded by other buildings. The results showed that the presence of neighbouring buildings significantly affects the aerodynamic behaviour of the building, with increased turbulence intensity and vortex shedding observed in the interference case.

The comparison of the results obtained from the isolated building simulation and the interference study simulation revealed that the interference effect led to an increase in the overall lift and drag forces acting on the building. Additionally, the pressure coefficients were found to be significantly different for the two simulation scenarios, indicating that the presence of neighbouring buildings can lead to non-uniform pressure distributions on the building surface.

The implications of these findings on building design suggest that the design of buildings should take into consideration the aerodynamic effects of neighbouring buildings. This can be achieved through the use of wind tunnel testing and CFD simulations during the design phase, which can provide valuable insights into the aerodynamic behaviour of the building and its surrounding environment. By optimizing the building design to reduce the interference effect, it is possible to improve the building's structural stability and energy efficiency, while also enhancing the overall safety and comfort of the occupants.

In conclusion, the present study highlights the importance of considering the interference effects in the design of buildings, especially in areas with high wind loads. The results of this study provide a valuable contribution to the field of building aerodynamics and can be used as a basis for further research in this area.

8.1 RECOMMENDATIONS FOR FUTURE RESEARCH

Based on the findings of this study, some recommendations for future research and design considerations for building in windy environments can be made.

- Firstly, future studies should consider conducting more extensive wind tunnel experiments to investigate the effects of different wind directions and speeds on building aerodynamics. The use of computational fluid dynamics simulations can also be further improved and validated with experimental data.
- Secondly, building designers and engineers should consider the potential impact of neighbouring buildings and structures on the aerodynamics of their buildings, especially in urban environments where buildings are densely packed. Strategies such as building setbacks and staggered building heights can be used to mitigate the interference effects and improve building aerodynamics.
- Thirdly, it is recommended to use natural ventilation strategies, such as stack and cross ventilation, in building design. These strategies can not only improve indoor air quality but also reduce the reliance on mechanical ventilation systems, which can have high energy consumption and maintenance costs.

Lastly, the findings of this study can be used to inform building codes and regulations for buildings in windy environments. Guidelines on building height and shape, as well as setback requirements, can be developed to improve the safety and sustainability of buildings in these environments.

In conclusion, this study provides insights into the effects of building interference on aerodynamics and the potential implications for building design. The findings suggest that building designers and engineers should consider neighbouring structures and the potential interference effects on building aerodynamics. The recommendations made can be used to guide future research and inform building design considerations for buildings in windy environments.

REFERENCES

- [1] Y. L., Huang, M. L., & Zhang, C. Q. Xu, "Dynamic wind characteristics and wind-induced vibration analysis of a tall building," *Advances in Structural Engineering*, 17(5), pp. 695-707, 2014.
- [2] F. Farouk, "Wind effects on high-rise buildings: A review," *Ain Shams Engineering Journal*, 7(3), pp. 1053-1064, 2016.
- [3] "IS 875 (Part 3)," *Bureau of Indian Standards. IS 875 (Part 3): Wind loads on buildings and structures (3rd ed.)*, p. 72, 2015.
- [4] "AS/NZS: 1170.2," *Standards Australia/Standards New Zealand (2011), Structural design actions - Part 2: Wind loads*, p. 62, 2011.
- [5] "EN 1991-1 - 4," *European Committee for Standardization. (2005). Eurocode 1: Actions on structures - Part 1-4: General actions - Wind actions (EN1991-1-4)*, p. 97, 2005.
- [6] "BS 6399 - 2," *British Standards Institution. (1997). Loading for buildings - Part 2: Code of practice for wind loads (BS 6399-2)*, p. 66, 1997.
- [7] "GB 50009," *Ministry of Housing and Urban-Rural Development of the People's Republic of China. (2001). Technical code for the design of building structures (GB 50009)*, p. 188, 2001.
- [8] R., Bairagi, A., & Pal, A. Raj, "Importance of accurate wind load estimation for tall buildings," *Proceedings of the Institution of Civil Engineers-Structures and Buildings*, 173(1), pp. 3-10, 2020.
- [9] Y., Huang, J., & Li, Q. Xu, "Field measurement and analysis of wind-induced acceleration responses of a super-tall building," *Journal of Wind Engineering and Industrial Aerodynamics*, 125, pp. 141-152, 2014.
- [10] D., Chowdhury, S., & Mandal, S. Mallick, "Experimental investigation of wind-induced pressure coefficients on C-shaped buildings," *Journal of Wind Engineering and Industrial Aerodynamics*, 187, pp. 97-110, 2019.
- [11] Y., Wang, Y., & Chen, Y. Li, "Wind-induced torque on L-shaped tall buildings: A

- wind tunnel study," *Journal of Wind Engineering and Industrial Aerodynamics*, 168, pp. 114-124, 2017.
- [12] M., Hegazy, A. A., & Abdel-Kareem, H. El-Heweity, "Numerical simulation of buffeting longitudinal wind forces on buildings using ANSYS Fluent," *Alexandria Engineering Journal*, 58(3), pp. 753-760, 2019.
- [13] Y. L., Pan, C. B., Yang, J. L., & Wen, Y. Q. Xu, "Evaluating wind loads on super-tall buildings using field-measured wind-induced acceleration response," *Journal of Wind Engineering and Industrial Aerodynamics*, 126, pp. 124-139, 2014.
- [14] C., Luo, Y., & Xu, H. Zheng, "Wind-induced responses of tall buildings under combined aerodynamic control," *Journal of Wind Engineering and Industrial Aerodynamics*, 179, pp. 311-322, 2018.
- [15] A. M. Aly, "Prediction of wind-induced response of tall buildings using pressure integration technique," *Alexandria Engineering Journal*, 52(3), pp. 441-452, 2013.
- [16] B. A. Farouk, "CFD simulation of indoor thermal comfort in high-rise buildings," *Alexandria Engineering Journal*, 55(4), pp. 3769-3777, 2016.
- [17] S., Chattopadhyay, S., & Mandal, S. Chakraborty, "Effect of building shape on wind-induced loads: A CFD study," *Journal of Wind Engineering and Industrial Aerodynamics*, 130, pp. 85-97, 2014.
- [18] X., Zhu, X., & Letchford, C. W. Cheng, "Crosswind forces on a tall building with square and H-shaped cross sections using proper orthogonal decomposition analysis," *Journal of Wind Engineering and Industrial Aerodynamics*, 145, pp. 1-11, 2015.
- [19] S., & Dalui, S. K. Paul, "Wind effects on 'Z' plan-shaped tall building: A case study," *Alexandria Engineering Journal*, 55(3), pp. 2673-2683, 2016.
- [20] R. P., Montenegro, R., & Viana, F. A. Gomes, "An experimental and numerical study of wind pressures on irregular-plan shapes," *Journal of Wind Engineering and Industrial Aerodynamics*, 93(10), pp. 745-768, 2005.
- [21] R., & Ahuja, A. Amin, "Wind-induced pressures on buildings of various geometries: An experimental study," *Journal of Wind Engineering and Industrial Aerodynamics*, 99(11), pp. 1081-1089, 2011.

- [22] R., & Dalui, S. K. Bhattacharyya, "Experimental and numerical study of wind-pressure distribution on irregular-plan-shaped building," *Journal of Wind Engineering and Industrial Aerodynamics*, 197, p. 104105, 2020.
- [23] R., Dalui, S. K., & Paul, S. Bhattacharyya, "Wind-induced pressure on 'E' plan-shaped tall buildings: An experimental study," *Journal of Wind Engineering and Industrial Aerodynamics*, 129, pp. 23-33, 2014.
- [24] S. R., & Pandey, A. K. Telrandhe, "Dynamic wind effects on high-rise buildings with varying dimensions and height," *International Journal of Civil Engineering and Technology*, 10(2), pp. 354-360, 2019.
- [25] A., Rathish Kumar, B. V., & Pradeep Kumar, R. Ashok, "Numerical investigation of wind effects on buildings," *Journal of Wind Engineering and Industrial Aerodynamics*, 180, pp. 68-76, 2018.
- [26] A., Kumar, A., & Sarkar, S. Pal, "Experimental analysis of wind incidence on a Fish-plan building model," *Journal of Wind Engineering and Industrial Aerodynamics*, 215, p. 104940, 2021.
- [27] Y., Wang, Y., & Liu, H. Sun, "CFD simulation of the interference effects of wind pressures in building groups," *Journal of Wind Engineering and Industrial Aerodynamics*, 179, pp. 16-26, 2018.
- [28] S., Das, A., & Raj, P. Pal, "Evaluation of wind induced interference effects on shape remodeled tall buildings," *Journal of Wind Engineering and Industrial Aerodynamics*, 215, p. 104743, 2021.
- [29] A., Pal, S., & Raj, P. Anbukumar, "Bilateral interference of wind loads induced on duplicate building models of various shapes," *Journal of Wind Engineering and Industrial Aerodynamics*, 188, pp. 1-12, 2019.
- [30] R., Raj, P., & Goyal, M. Gaur, "Interference effects on corner configured structures with variable geometry and blockage configurations under wind loads using CFD," *Journal of Wind Engineering and Industrial Aerodynamics*, 211, p. 104651, 2021.
- [31] S. K., Raj, R., & Dev, N. Nagar, "Wind-induced pressure on twin tall buildings with recessed corners: An experimental study," *Journal of Wind Engineering and Industrial*

Aerodynamics, 193, p. 103976, 2019.

- [32] M., Singh, A., & Raj, P. Goyal, "Wind interference on a hexagonal-shaped high-rise building with different openings: A CFD approach," *Journal of Wind Engineering and Industrial Aerodynamics*, 212, p. 104659, 2021.
- [33] N. K., & Dalui, S. K. Bairagi, "Optimization of interference effects on high-rise buildings for different wind angles," *Journal of Wind Engineering and Industrial Aerodynamics*, 138, pp. 47-55, 2015.
- [34] S., & Raj, P. Kumar, "CFD study of flow characteristics and pressure distribution on re-entrant wing faces of L-shape buildings," *Journal of Wind Engineering and Industrial Aerodynamics*, 212, p. 104654, 2021.
- [35] Y., Wang, Y., & Liu, H. Sun, "CFD simulation of the interference effects of wind pressures in building groups," *Journal of Wind Engineering and Industrial Aerodynamics*, 165, pp. 21-30, 2017.
- [36] S. K., Raj, R., & Dev, N. Nagar, "Wind tunnel study on twin tall buildings with large recessed corners under interference conditions," *Journal of Wind Engineering and Industrial Aerodynamics*, 220, p. 104887, 2022.
- [37] N. J. Cook, "Wind effects on structures," *John Wiley & Sons*, 1985.
- [38] E. L., & Carruthers, D. J. Houghton, "Wind loads on structures," *John Wiley & Sons*, 1979.
- [39] M. R., & Ahuja, A. K. Amin, "Experimental study of wind-induced pressure coefficients on low-rise buildings with various roof configurations," *Journal of Wind Engineering and Industrial Aerodynamics*, 100(1), pp. 1-8, 2012.
- [40] S., & Dalui, S. K. Kar, "Interference effects on wind-induced responses of tall buildings: A CFD study," *Journal of Wind Engineering and Industrial Aerodynamics*, 151, pp. 1-16, 2016.